KINETIC AND MASS TRANSFER STUDIES OF OZONE DEGRADATION OF ORGANICS IN LIQUID/GAS-OZONE AND LIQUID/SOLID-OZONE SYSTEMS

ABSTRACT

Key words: Ozone; water-treatment; kinetics; mass-transfer; absorption; adsorption; reactive-dye; triclocarban; naphthalene; methanol.

This work was concerned with the determination of mass transfer and kinetic parameters of ozone reactions with four organic compounds from different families, namely reactive dye RO16, triclocarban, naphthalene and methanol. In order to understand the mechanisms of ozone reactions with the organic pollutants, a radical scavenger (t-butanol) was used and the pH was varied from 2 to 9.

Ozone solubility (C_{AL}^*) is an important parameter that affects both mass transfer rates and chemical reaction kinetics. In order to determine accurate values of the C_{AL}^* in the current work, a set of experiments were devised and a correlation between C_{AL}^* and the gas phase ozone concentration of the form $C_{AL}^*(\text{mol/L}) = 0.0456 \times C_{O3}$ (g/m^3 NTP) was obtained at 20°C. This work has also revealed that t-butanol did not only inhibit hydroxyl radical reactions but also increased mass transfer due to it increasing the specific surface area (a_L). Values of the a_L were determined to be 2.7 and 3.5 m^2/m^3 in the absence and presence of t-butanol respectively. It was noticed that the volumetric mass transfer coefficient (k_La) has increased following the addition of t-butanol.

Ozone decomposition was studied at pH values of 2 to 9 in a 500 mL reactor initially saturated with ozone. Ozone decomposition was found to follow a second order reaction at pH values less than 7 whilst it was first order at pH 9. When the t-butanol was added, the decomposition of ozone progressed at a lower reaction order of 1.5 for pH values less than 7 and at the same order without t-butanol at pH 9. Ozone

decomposition was found significant at high pHs due to high hydroxide ion concentration, which promotes ozone decomposition at high pHs.

The reaction rate constant (k) of RO16 ozonation in the absence of t-butanol was determined. The result suggests that RO16 degradation occurs solely by molecular ozone and indirect reactions by radicals are insignificant.

The chemical reaction of triclocarban with ozone was found to follow second order reaction kinetics. The degradation of naphthalene using the liquid/gas-ozone (LGO) system was studied. This result showed that hydroxyl radicals seemed to have limited effect on naphthalene degradation which was also observed when a radical scavenger (t-butanol) was used. Reaction rate constants were calculated and were found around 100 times higher than values reported in the literature due to differences in experimental conditions. From the results of the experimental investigation on the degradation of methanol by ozone it was found that the rate constant (k) of the degradation reaction increased at pH 9. The reaction stoichiometry was found to have a value of 1 mol/mol.

The two steps of the liquid/solid-ozone (LSO) system were studied on beds of silica gel and a zeolitic material (D915) and the ozone adsorption process was modeled and found that particle rate controls ozone adsorption step but liquid rate controls the water treatment step.

Ozone desorption with pure deionised water was studied. The water flow rate was found to accelerate the desorption rates but pH was found to decrease the desorption rates. In contrast, the effect of pH was insignificant in the presence of t-butanol.

Determination of the adsorption isotherms for RO16, naphthalene and methanol revealed that RO16 did not exhibit adsorption on silica gel, but both naphthalene and methanol showed adsorption on D915 described by Langmuir model.

DISCLAIMER

The work submitted in this thesis is genuinely carried out by me and has not been submitted to any other organization for any other degree.

The following publications have been based on this work:

- C. Tizaoui, N. M. Grima, J. K. Ephraim (Degradation of Triclocarban by Ozone), International Ozone Association Pan American Group (August 24-27, 2008) Orlando, Florida, USA, (Oral presentation, 35).
- N. M. Grima, C. Tizaoui, **(**Degradation of Naphthalene using a novel Liquid/Solid-Ozone (LSO) System), 5th International Conference (Oxidation Technologies for Water and Wastewater Treatment (March 30-April 1, 2009) Berlin, Germany, (Poster presentation, 251).
- C.Tizaoui, N. M. Grima, M. Z. Derdar, (Effect of the radical scavenger (t-butanol) on gas-liquid mass transfer), submitted for publication in Journal of Chemical Engineering Science.

ACKNOWLEDGEMENTS

I am very pleased to have carried out this research at Bradford University. Many people have contributed to its successful outcome to whom I would like to address my thanks.

Many Thanks to my supervisor Dr. C Tizaoui for everything; his encouragement, his help and support, his provision of his outstanding knowledge and his great experience. His kindness have created ideal conditions for carrying out this research.

I would like to thank the Education Service Department of the Libyan Government for sponsoring me for this PhD research study at the University of Bradford.

I would also like to thank all the technical staff in the School of Engineering, Design and Technology for their help and support. Special thanks to Mr. Ian Mackay, Mr. Arthur Kershaw, Mr. David Steele and Mr. Michael Cribb for their help. My thanks go to each of Dr. Jeya. Ephraim, Mr. John Purvis in EDT, Mr. Andrew Healey in the University Analytical Centre and Mr. Gream Dean and Mrs. Tracy Holmes in the School of Life Sciences for their valuable help.

I am deeply indebted to my family for their support and persistent encouragement. Lastly, I would like to thank a few of the many friends I made during my research.

INDEX

LIST OF FIGURES

LIST OF TABLES

CHAPTER 1: INTRODUCTION

1.1. General

Water is one of the essential elements on earth and is necessary for all life. A constant supply is needed to replenish the fluid lost through normal physiological activities such as respiration, sweating and urination, so proper care is needed to see if the water used is clean and pure for drinking purposes. Any contamination in water may lead to diseases, bacterial attack and fungal and sometimes even fatal consequences. For example, there are many sources of ground water pollution that can cause nasty tastes and odours and that may be a risk to human health. Contamination of the well water may occur naturally or as a result of human activity (Water Resources Act 1991). Examples of water contaminants follow:

Microorganisms: There are many types of microorganisms that can cause human illness or result in discolouration of water or produce nasty tastes and odours. Microorganisms include bacteria, viruses, algae and parasites. Shallow wells are most at risk from contamination by microorganisms, as are those located near farms, wildlife hotspots and high risk flood zones. Water run-offs from these areas are usually the cause of contamination (Water Resources Act 1991).

Nitrates and nitrites: High levels of nitrates are usually direct results of human activity, They are contained in fertilisers used on farms, with the potential to contaminate ground water. If large amounts are consumed this can be damaging to human health. Nitrates are linked to the blue baby syndrome (Water Resources Act 1991).

Heavy metals: Much of the underground rocks and soil contain heavy metals such as lead, chromium and many others. They can be damaging to human health but are not

usually found to contaminate wells that are properly constructed and maintained. As water moves through soil and rocks, it dissolves very small amounts of minerals and holds them in solution. Calcium and magnesium dissolved in water are the two most common minerals that make water hard. The degree of hardness becomes greater as the calcium and magnesium content increases (Hughes et al., 1996).

Water described as hard means it is high in dissolved minerals, specifically calcium and magnesium. Hard water is not a health risk but a nuisance because of its tendency to cause mineral build-up in water pipes and heating systems and poor soap and detergent performance when compared with soft water.

Water is a good solvent and picks up impurities easily. It combines with carbon dioxide in the air to form very weak carbonic acid, resulting in an even better solvent.

Many industrial processes generate wastewater streams contaminated with organic compounds harmful to human health and the environment. Water pollution by micro-pollutants such as pesticides, textile, dioxins, and organic compounds and so on is a worldwide problem at present (Mumma 1995, Hughes et al., 1996).

In order to solve this problem, many researchers are on track to develop new technologies capable of removing the chemicals from wastewater. One of these technologies is ozonation, which is the subject of this work. Ozone was found to be effective in removing a wide range of organic and inorganic compounds and has been applied successfully in treating both drinking and waste waters (Langlais et al., 1991). Ozone may react in water through two mechanisms (I) direct reactions involving molecular ozone and (II) indirect reactions involving secondary oxidants such as hydroxyl radicals (^{o}OH) formed following ozone decomposition in water, a reaction initiated by for example OH^- (Glaze et al., 1987). Knowledge of ozone reaction kinetics

parameters, such as reaction rate constant k, the reaction stoichiometry and the reaction order are essential to assess the feasibility of using ozone to treat the water and to design an appropriate reactor. The kinetic parameters are also important to understand the effects of operating parameters and to develop models capable of optimizing the treatment process. For these reasons, this work was concerned with the determination of the kinetics parameters of the ozone reaction with the RO16, triclocarban, naphthalene and methanol as organic pollutants. The reasons behind the selection of these compounds in this study are summarized in the following paragraphs.

In general, azo dyes are the most commonly used commercial dyes in the textile industry, accounting for over 50% of all commercial dyes (Waring et al., 1990). A large amount of azo dyes, however, remain in the factory effluent after the completion of the dyeing process and represent an environmental danger due to their refractory nature. azo-dyes contain azo groups (-N=N-) mainly bound to substituted benzene or naphthalene rings (Wu and Wang 2001a). Figure 1.1 shows the chemical structure of an azo-dye which contains sulphonic acid groups that ensure both its solubility in water and its ability to dye wool, silk, nylon (polymide), cotton, cellulose acetate and other kinds of fibres. However, the sulphonic acid group deactivates the structure with respect to an electrophilic attack and biological degradation that occur in common waste water treatment techniques (Liakou et al., 1997), (Muthukumar et al., 2001). Therefore, the treatment of textile wastewater by conventional methods such as biological, physical and chemical processes or a combination of each is inefficient for colour removal. A direct solution to this problem is treatment with advanced oxidation processes (AOP), such as O_3 + pH > 7; O_3+H_2O_2 or O_3+UV (J. Perkowski et al., 2000, (A. Balcioglu et al., 2001), (F. J Rivas et al., 2003), (A. Lo´pez-Lo´pez et al., 2004a). Studies on the degradation of azo-dyes using AOP is very important. It is in this wider context that a

reactive azo-dye (Reactive orange 16 RO16: $C_{20}H_{17}N_3Na2O_{11}S_3$) was chosen in this study (CAS Number: 12225-831-1 and Colour Index Number: 17757)

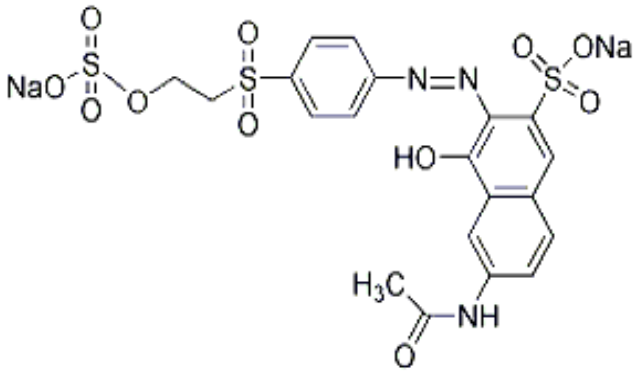

Figure 1.1: Molecular structure of dye (RO16)

Triclocarban or 3-(4-chlorophenyl)-1-(3,4-dichlorophenyl)urea (TCC) is a substance with antibacterial and antifungal properties (Triclocarban-Wikipedia 2009). Hence, it finds applications in disinfectants, detergents, cosmetics, soaps, etc. Although the disinfection mechanism is unknown, TCC may be involved in the inhibition of the enzyme enoyl-acyl carrier protein reductase (ENR). At lower concentrations, TCC provides a bacteriostatic effect by binding to ENR (Triclocarban-Wikipedia 2009). This enzyme is absent in humans but essential in building cell membranes of many bacteria and fungi. The data on the environmental impacts of using TCC is very scarce. However, few studies have shown that the chemical is toxic to humans and other animals (Halden and Paull 2005) since it increases methemoglobinemia. But still the use of TCC is not limited. For example, in 1998, according to the summary report which was submitted by the US Environmental Protection Agency (EPA), mentioned TCC production for the US market was estimated to approach one million pounds or about 454 metric tons per year, according to the summary report submitted by the industry to the US Environmental Protection Agency (EPA) in support of the ongoing risk evaluation for the antimicrobial compound; the maximum current use is estimated at 750 metric tons per year (Sapkota et al., 2007).

Researchers have already found that 75 % of triclocarban originates from anti-microbial soaps which had been washed down from household drains persists during wastewater treatment. The worse part is the accumulation of TCC at remarkable concentrations in the municipal sludge, which may be used as a fertilizer and soil conditioner for crops. It is already known from literature that TCC contained sludges treated biologically for an average period of three weeks showed negligible degradation, (Raabe E. W 1968). The continuous persistence of TCC in rivers and streams is really a major issue to the environment and mankind. TCC is a topical antiseptic but can end up in the food chain which is neither regulated nor monitored. The molecular structure of TCC is shown in Figure 1.2. Treatment studies to remove the compound from water are scares. In order to understand the behavioral degradation of TCC with ozone, this study was carried out.

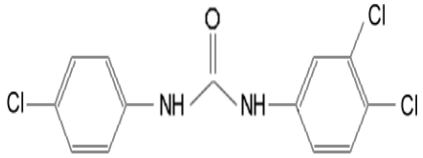

Figure 1.2: Molecular structure of triclocarban

Naphthalene (CAS number: 91-20-3: $C_{10}H_8$) is an aromatic compound widely used in a number of industrial applications such as the manufacturing of dyes, pesticides, polymers and many other products (Shiyun et al., 2002). Research studies have shown that naphthalene persists in effluents discharged from sewage treatment plants and is difficult to remove by conventional wastewater treatment processes due to the low solubility of this compound in water and as a result, it represents a long-term source of contamination. Naphthalene can contaminate surface waters since it persists in discharged waste waters or accumulate in biosolids that may be used as a fertilizer and soil conditioner for crops. Therefore, there is concern about the fate and potential impact of naphthalene released in the environment. Excessive exposure to naphthalene may affect the blood, breastfed babies, eye, lung and the unborn child (UK-

Environment-Agency 2008). Naphthalene is included in the UK Surface Waters (Dangerous Substances) (Classification) Regulations and the European Union Water Framework Directive (WFD) Priority list substances. The molecular structure of naphthalene is shown in Figure 1.3.

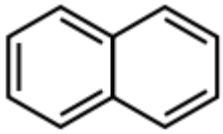

Figure 1.3: Molecular structure of naphthalene

Methanol is a type of alcohol, currently made from natural gas but which can also be made using biomass (wood waste or garbage) or coal. Methanol (CH_3OH) is a volatile organic compound commonly used in industry, which may have harmful effects on human health and the environment. Therefore, it has been listed as one of the 189 Hazardous Air Pollutants included in the 1990 Clean Air Amendment list in the US.

Although, methanol occurs naturally in the environment as a result of various biological processes in vegetation, microorganisms, and other living species, a large release of concentrated methanol to ground water, surface water, or soil has the potential to adversely impact the affected environment (Haward et al., 1991). Once released, the half-life of methanol depends on numerous factors including the nature of the release, quantity of the release, and physical, chemical and microbiological characteristics of the impacted media. Table 1.1 is a summary of the estimates of the range of probable methanol half-lives in various environmental media as documented from various reports, in comparison with the probable half-lives of benzene, a common gasoline constituent. Based on these data, regardless of the release scenario, methanol appears unlikely to accumulate in the groundwater, surface water, air, or soil. The physical and chemical properties of methanol help to further define the fate and transport of this chemical in the various environmental media in the context of each of the conceptual

release scenarios (Haward et al., 1991). The dominant mechanisms of methanol loss from subsurface soil and ground water are expected to be biodegradation and advection (dispersion and diffusion) with little loss from adsorption on soils due to its high solubility and low retardation factor. In surface water, the infinite solubility of methanol will result in rapid wave-, wind-, and tide enhanced dilution to low concentrations (< 1%). Once concentrations have been diluted below toxic levels, the dominant mechanism of methanol loss is expected to be biodegradation. Compared to other loss mechanisms identified, including volatilization and chemical degradation, biodegradation is expected to be the dominant process controlling the fate of methanol in the soil, groundwater, and surface water environments. In addition, the biodegradation of methanol can occur under both aerobic (oxygen present) and anaerobic (oxygen absent) conditions (Haward et al., 1991).

Table 1.1: Estimated Half-Lives of methanol and benzene in the Environment

Environmental medium	Methanol half- live (days)	Benzene half-live (days)
Soil (Based upon unacclimated grab sample of aerobic/water suspension from groundwater aquifers)	1-7	5-16
Air (Based on photooxidation half-life)	3-30	2-20
Surface water (Based upon unacclimated aqueous aerobic biodegradation)	1-7	15-16
Ground water (Based upon unacclimated grab sample of aerobic/water suspension from ground water aquifers	1-7	10-730

Therefore, following any of the three conceptual release scenarios presented, methanol is not likely to persist in soil or water due to its rapid biodegradation. Methanol is miscible in water and consequently will dissolve quickly and be diluted to low concentrations in the event of a surface water spill. In ground water, methanol concentrations are highly dependent on the nature and the magnitude of the release but are likely fall to low concentrations once complete dissolution has occurred. In both surface and ground waters, methanol is likely to be easily biodegraded under a wide range of possible water quality conditions (Raabe E. W 1968). Figure 1.4 shows the molecular structure of methanol. Methanol was used in this work simply to gain a better understanding of the processes used.

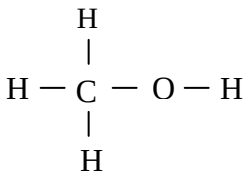

Figure 1.4: Molecular structure of methanol

Wastewater treatment becomes very essential, considering the widespread occurrence and toxicity profiles of some of the chemicals discussed.

Two systems were used in this research to study the degradation of four chemical compounds, which were described earlier. The two systems are: Liquid/Gas-Ozone (LGO) and Liquid/Solid-Ozone (LSO) system. In the (LGO) system: ozone was applied in the gaseous state and bubbled into water. Whereas, in the LSO system: ozone was adsorbed on particulate of silica-based adsorbents using a fixed bed reactor followed by water passing through the bed of the ozone loaded adsorbent. LSO technique was developed in the water laboratory at Bradford University in order to overcome some of the problems encountered in conventional ozone gas systems (i.e. Liquid/Gas-Ozone (LGO)), (Tizaoui 2001).

1.2. Aim and Objectives

The overall aim of this work is to investigate the oxidation of the compounds discussed earlier (reactive dye (RO16), triclocarban, naphthalene and methanol) in water using ozone. The two systems LGO and LSO were used for this purpose. It is expected that this investigation will reveal a better understanding of the kinetics and mass transfer processes that occur in both systems. The particular objectives of the study were:

- Determine ozone mass transfer parameters and discuss the effect of the operating conditions on their values and changes;
- Determine the effect of pertinent experimental parameters on the degradation rates of the compounds of interest;
- Study the effect of a radical scavenger (t-butanol) on both degradation rates and mass transfer;
- Study the feasibility of using the LSO system to remove RO16, naphthalene and methanol;
- Study gas ozone adsorption on two selected adsorbents;
- Study ozone desorption from the adsorbents using deionised water;
- Determine the effect of the experimental parameters such as liquid flow rate, pH, t-butanol on the performance of the LSO system.

1.3. Thesis Plan

A lengthy experimental study has been carried out to address the aims and objectives of this thesis. Results and discussions alongside conclusions and future work are presented in this thesis. The thesis is structured as follows:

Chapter 1 presents brief introduction on water and ozone importance and sets the scene for the work. The aim and objectives of this work have also been stated alongside the plan of the thesis in Chapter 1.

Chapter 2 provides the general background and shows an in depth literature review related to the topics of this work.

Chapter 3 presents the equations and mathematical models used in this work**.**

Chapter 4 is concerned with the equipments and experimental procedures that were used in the experimental work.

Chapter 5 & 6 includes the experimental results and their discussions.

Chapter 7 summarises the conclusions reached during the course of this work and proposes future work.

Chapter 8 comprises of appendices and references

CHAPTER 2: LITERATURE REVIEW

2.1. General

This chapter deals mainly with the general background and review past work on ozone, its physical properties and the brief description of the main applications of ozone.

2.2. Ozone

Ozone was discovered by van Marum in 1785, who noticed a peculiar odour developed by a machine producing static electricity but was not named until 1840. In 1801, Cruikshank observed that the electrolysis of sulphuric acid produced "oxygen" which had a peculiar "chlorine –like" smell. It is generally accepted, however; that the discovery of ozone was due to the observation of Schonbein. (Schonbien 1920) realized that (van Marum 1785) and Cruickshank 1801) had actually produced the same gas via different processes. It was Schonbein who named "ozone" from the Greek word (ozein), which means to smell. The true nature of ozone, however, was not agreed upon until 1865 when Soret claimed that ozone was a tri-atomic form of oxygen (Vosmaer 1916), (Ardon 1965). The ability of ozone to disinfect polluted water was recognized in 1886 by Meritens (Vosmaer 1916). A few years later, the German firm Siemens and Halske, manufacturers of electrical equipment, contacted local Prussian officials who were willing to test ozone's application for the disinfection of drinking water. The first full-scale application of ozone in drinking water treatment was in 1893 at Oudshoorn (Netherlands), Auer and (France 1909), (Madrid and Spain 1910) and (Vosmaea 1916) counted at least 49 European plants using Siemens, de Fries, Marmier, Abraham and Otto ozone generators by 1915. The construction of new ozone plants continued at a slow pace, especially in France. There was also some construction of ozone plants elsewhere, such as in the Belgian Congo, where 11 plants were built before 1939

(Pascal 1986). By 1936, there were close to 100 ozone plants in France and 30-40 in other parts of the world (Evans 1972). All of these were first generation plants. However, in the 1960s there were many new applications that required ozone to be added during the early stages of treatment, hence the term preozonation. Until this time, ozonation was, in most cases, the last stage of treatment. In France and Germany during the early 1960s, ozone was used specifically to oxidize iron and manganese. Some of the first applications for ozone were at Düsseldorf, Germany (1957 and 1980), Sitterdor, Switzerland (1963) and France (1974). At about this time, several Scottish and Irish plants that employed ozone for colour removal were designed and constructed (O'Donovan 1965, Greaves and Lowndes 1987). The most recent application of ozone are disinfection by-product (DBP) control and biological stabilization or minimization of microbiological growth potential of water. In 1990, there were close to 40 U.S. water treatment plants that were equipped with ozonation facilities. In addition, an increasing number of ozone facilities were being replaced by updated ozone equipment.

2.3. Ozone Properties

2.3.1. Solubility of ozone

The degree of solubility of ozone gas depends on the concentration in gas phase and thus is dependent on the partial pressure. Another important factor influencing the solubility is the temperature as shown in Table 2.1. Besides temperature, pH and ion concentration in the solution are the main factors influencing the solubility of ozone in water. In summary, ozone solubility can be increased by;(1) increasing the ozone concentration in air or oxygen;(2) increasing gas pressure;(3) decreasing the water temperature;(4) decreasing the amount of solutes;(5) decreasing the pH, **(**Stumm 1958).

Table 2.1: Effect of water temperatures and ozone concentration in the gas phase on ozone solubility in water (mg/L).

ozone gas %	ozone gas g/m^3	5 °C	10 °C	15 °C	20 °C
1.5	6.68	11.09	9.75	8.40	6.43
2	8.91	14.79	13.0	11.19	8.57
3	13.37	22.18	19.50	16.79	12.86

If oxidizable chemicals are present in the water, larger amounts of ozone will dissolve to satisfy the demand. One limiting factor is the efficiency of the mass transfer device used. When using ventury, more turbulence and smaller bubbles facilitate better mass transfer. When using bubble diffusers, the water column should be at least 4.804 m high. Higher concentrations of ozone in water cause more vigorous oxidation of even more resistant organic compounds. The solubility of ozone in water can be shown by the comparison of solubility values shown in Table 2.2 (Brink et al., 1991). This table shows that ozone is approximately 10 times less soluble than chlorine gas and 130 times less soluble than chlorine dioxide (the solubility of ozone is normally much less 10 mg/L because ozone is produced at low concentration 5-10% in air or oxygen).

Table 2.2: Solubility values for various pure gasses at (289k and partial pressure= 1 atm all gasses)

Gases	Formula	Solubility (mg/L)
Ozone	O_3	1.4
Oxygen	O_2	70
Carbon dioxide	CO_2	3.36
Chlorine	Cl_2	14.4
Chlorine dioxide	ClO_2	180

In addition, ozone solubility in water obeys Henry's Law (Gurol et at., 1982), (Sotelo et at., 1989), (Brink et at., 1991), (Degremont 1991b). Henry's Law may be described by Equation 2.1, where P_A is the vapour pressure of A, X_A the mole fraction of dissolved A and K_A is a constant (having units of pressure, sometimes expressed by the symbol H)

$$P_A = K_A X_A \tag{2.1}$$

If a component (solvent) is nearly pure, it behaves according to Raoult's Law and has a vapour pressure that is proportional to the mole fraction with a gradient P_A^*.

$$P_A = X_A P_A^* \tag{2.2}$$

When this component is the minor component (solute), its vapour pressure is proportional to the mole fraction but with a constant K_A (Henry's Law) (Atkins, 1990). As ozone is generally produced in small concentrations, we can say that the mole fraction of ozone in oxygen (or air) is small ($\rightarrow 0$) and that the relation between XO_3 and PO_3 is linear with a gradient K_A or H_A (known as the Henry's constant). Much work has been carried out on the estimation of Henry's Law constant for the solubility of ozone in water. (Sotelo et al., 1989) have carried out a literature survey of previous works and undertaken work on the variation of H_A with pH, temperature and ion strength. The outcome of their work is a set of equations showing the variation of H_A with the differing physical and chemical properties of the solutions.

$$H = f(T, pH) \tag{2.3}$$

2.3.2. Physical properties of ozone

The physical properties of ozone are somewhat different from those of dioxygen. It has a slightly bluish colour as both a gas and a liquid. It changes to a liquid at a temperature of -111.9 °C (± 0.3 °C) ≈ (-169.4 °F) and from a liquid to a solid at -192 °C (± 0.4 °C) ≈ (-135 °F). The density is 2.144 g/L. At typical ambient temperature, ozone is a blue coloured gas, but at low concentration this colour is not noticeable unless the gas is viewed through a considerable path length. At 112 ^{0}C, pure ozone condenses easily to a dark blue liquid that explodes readily. Less concentrated O_3/O_2 mixtures (above 20 % O_3) are also explosive, either in the vapour or liquid state. Such explosions may be initiated by small amounts of catalysts, organic matter, shocks, electrical sparks, or sudden changes in temperature or pressure (Sotelo et al., 1989).

2.3.2.1. Molecular ozone reactivity

The ozone molecule is angular in shape. Its shape has been accurately determined by microwave investigations (Trambraulo et al., 1953).

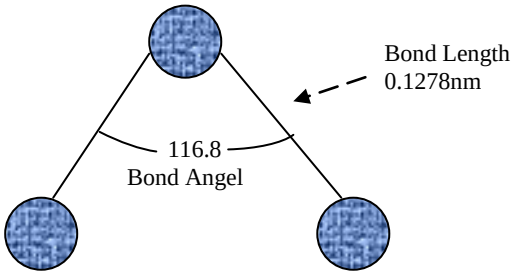

Figure 2.1: Molecular structure of ozone

The fact that the ozone molecule is angular became evident from the analysis of its infrared (IR) spectrum. The angle was first believed to be acute but interpretation of IR data showed it to be obtuse. Electron diffraction measurements assigned a length of 0.127(± 0.002 nm) to the O-O bond and angle of 116.8(± 0.2°C) between the central and outer atoms. The bond length (0.128 nm) is shorter than the single O-O bond in H-O-O-H (0.149 nm) and longer than in the oxygen (O_2) molecule (0.121 nm); thus, it is evident that this bond in ozone must have a considerable double bond character. The binding may be considered as consisting of two (σ) bonds between the central and the outer atoms and a delocalized (π) orbital spread over the whole molecule (Ardon 1965). The ozone molecule is described as a resonance structure Figure 2.2.

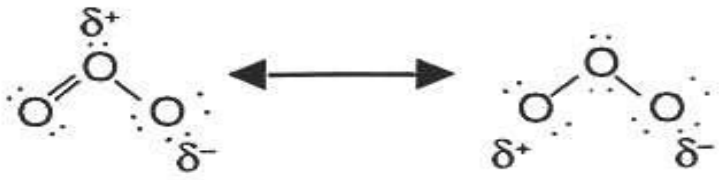

Figure 2.2: Ozone structure

2.3.2.2. Thermal and mechanical properties

The normal boiling point of liquid ozone is -111.9 °C; the critical temperature is -12.1 °C and critical pressure is 54.6 atm. The surface tension is 38.1 $mN.m^{-1}$ at -182.7 °C and the density is 1.5727 g cm^{-3} at -182.9 °C. The viscosity is 1.56 g/m.s at -183 °C and 4.14 at -195.6 °C. The specific heat of liquid ozone is 0.434 $cal.g^{-1}.°C^{-1}$ at -176.6 °C and that of gaseous ozone is 0.197 $cal.g^{-1}.°C^{-1}$ at 25 °C and 1 atm. The heat of formation of ozone is ΔH^0f =34.0 $kcal.mol^{-1}$ and the free energy of formation is ΔG^0f = 39.06 $kcal.mol^{-1}$, both at 1 atm and 25°C. The heat of vaporization of liquid ozone is 2.59 $kcal.mol^{-1}$ and the entropy of vaporization 15.92 $cal.mol^{-1}$, both at the normal boiling point. Above, -180 °C, liquid oxygen and ozone are miscible in all properties but below that temperature, two liquid phases appear over a certain range of concentrations. The relative permittivity of the gas ε_r =1.0019 at 0°C and 1 atm and in liquid ozone ε_r = 4.75 at -183°C. The solubility of ozone in water is higher than di-oxygen: 0.52 L will dissolve in 1 L of water at 0°C and 1 atm (Ardon 1965). Table 2.3 gives the solubility coefficient in relation to temperature (Stumm 1958).

Table 2.3: The solubility coefficient for ozone in water ($[O_3]$* water / $[O_3]$) at 1 atm Relative Ionic strangeth:I=0.05

Temperature (°C)	5	10	15	20	25
Solubility coefficient	0.45	0.41	0.37	0.34	0.30

Ozone is appreciably soluble in $CHCl_3$, CCl_4, CF_2Cl_2, CF_3Cl and other organic solvents shown in Table 2.4 (Gmelin 1960); however, at a temperature lower than -80 °C, ozone will react with CCl_4 and $CFCl_3$.

Table 2.4: Absorption of ozone in various solvents

Solvent	Temperature / (°C)	O_3/ solvent / ($g.L^{-1}$)
Acetic acid	18.2	5.40
Acetic acid	30.2	3.50
Acetic anhydride	0	4.60
Dichloroacetic acid	0	3.66
Propanoic acid	17.3	7.80

2.3.3. Chemical properties of ozone

2.3.3.1. Decomposition kinetics

Ozone is one of the most powerful oxidizing reagents known. Decomposition of ozone can produce an oxygen free radical, which has an even higher oxidizing capacity than that of ozone. Consequently, the oxidizing characteristics of ozone depend not only on the ozone molecule but also on its decomposition products. (Tomiyasu et al., 1985) studied the initial rate of ozone decomposition by the use of a scavenger, in this case Na_2CO_3, which removes any hydroxyl ions present in a solution. However, the kinetics studies and mechanistic descriptions of aqueous ozone have been investigated extensively in recent works (Tomiyasu et al., 1985), (Grasso 1987), (Gordon 1987a). The proposed mechanism involves a two electron transfer process or an oxygen atom transfer from ozone to hydroxide ion. The steps for the mechanism of ozone decomposition are described in the following section:

$$O_3 + OH^- \xrightarrow{k} HO_2^- + O_2 \qquad k = 40\ M^{-1}s^{-1} \qquad (2.4)$$

(Initiation step)

$$HO_2^- + O_3 \xrightarrow{k} O_3^- + HO_2^- \qquad k = 2.2 \times 10^6\ M^{-1}s^{-1} \qquad (2.5)$$

$$HO_2 + OH^- \xleftrightarrow{k} O_2^- + HO_2 \qquad k = 10^{-4.8} \qquad (2.6)$$

$$O_2^- + O_3 \xrightarrow{k} O_3^- + O_2 \qquad k = 1.6 \times 10^9\ M^{-1}s^{-1} \qquad (2.7)$$

$$O_3 + H_2O \xrightarrow{k} OH + O_2 + OH^- \qquad k = 20^{-30}\ M^{-1}s^{-1} \qquad (2.8)$$

$$O_3 + OH \xrightarrow{k} O_2^- + HO_2 \qquad k = 6 \times 10^9\ M^{-1}s^{-1} \qquad (2.9)$$

$$O_3^- + OH \xrightarrow{k} O_3 + OH^- \qquad k = 2.5 \times 10^9\ M^{-1}s^{-1} \qquad (2.10)$$

$$OH + O_3 \xrightarrow{k} HO_2 + O_2 \qquad k = 3 \times 10^9\ M^{-1}s^{-1} \qquad (2.11)$$

$$OH + CO_3^{-2} \xrightarrow{k} OH^- + CO_3^- \qquad k = 4.2 \times 10^8\ M^{-1}s^{-1} \tag{2.12}$$

$$CO_3^- + O_3 \rightarrow products\ (CO_2 + O_2^- + O_2) \tag{2.13}$$

The overall order of reaction for ozone decomposition in aqueous solution has still not been agreed. (Tomiyasu et al., 1985) have devised a rate Equation 2.14 for the decomposition of ozone. They propose that the system changes from a first order reaction (in ozone) in the presence of a radical scavenger; to one which has first and second order characteristics (in ozone) when a high hydroxyl ion concentration is present.

$$\frac{-d[O_3]}{dt} = k_{OH^-}[O_3][OH^-] + k_2[O_3][OH^-]^2 \tag{2.14}$$

They also state that the solution composition has marked effects on the magnitude of both K_{OH}- and K_2. (Gurol and Singer 1982) suggest that the overall order of reaction between pH values of 2 and 9.5 is second order with an expression for the decomposition of ozone shown in Equation 2.15.

$$-\frac{d[O_3]}{dt} = k_0[O_3]^2[OH^-]^{0.55} \tag{2.15}$$

It can be said with reasonable confidence that the description of ozone decomposition in solution is somewhat ambiguous when comparing works of different authors and that the order of ozone decomposition and its mechanism of decomposition may only be postulated and a dedicated study for ozone decomposition is essential. However, some conclusions may be drawn from the previous works; in that the pH of a solution has a marked effect on ozone decomposition and also that the presence of radical and ion scavengers will also markedly affect the rate of decomposition. Factors influencing the decomposition of ozone in water are temperature, pH, environment and concentrations of dissolved matter and UV light (Tomiyasu et al., 1985). Here, the main influencing factors for ozone decomposition will be discussed.

1. Temperature

Temperature has an important influence on the half-life of ozone (Stumm 1958). Table 2.5 shows the half-life of ozone in air and water. In water, the half-life of ozone is much shorter than in air, in other words ozone decomposes faster in water. On the other hand, the reaction speed increases with a factor 2 per 10 °C in complete. Principally, ozone dissolved in water cannot be applied when temperatures are above 40 °C because at this temperature the half-life of ozone is very short (Stumm 1958).

Table 2.5: Half -live of ozone in gas and water at different temperature

Air		Dissolved in water	
Temp. (^{0}C)	Half life	Temp. (^{0}C)	Half life
-50	3 months	15	30 min
-35	18 days	20	20 min
-25	8 days	25	15 min
20	3 days	30	12 min
120	1.5 hours	35	8 min

2. pH

As mentioned above, ozone decomposes partly into OH radicals. When the pH value increases, the formation of OH radicals increases. In a solution with a high pH value, there are more hydroxide ions present, see reaction equations below. These hydroxide ions act as an initiator for the decay of ozone (Stumm 1958).

$$O_3 + OH^- \rightarrow HO_2^- + O_2 \qquad k = 40 M^{-1}s^{-1} \qquad (2.16)$$

$$O_3 + HO_2^- \rightarrow O_3 + HO_2^- \qquad k = 2.2x10^6\ M^{-1}s^{-1} \qquad (2.17)$$

The radicals that are produced during reaction 2 can introduce other reactions with ozone causing more OH radicals to be formed and thus more ozone being decayed. In addition, the pH influences acid/base equilibriums of some compounds and also the reaction speed of ozone. This applies also to the reaction with scavenger CO_3^{2-}, which is also pH dependant (pKa HCO_3^{2-}/CO_3^{2-} = 10.3), (Stumm 1958). Figure 2.3 shows that the decay of ozone in a basic environment is much faster than in an acid environment.

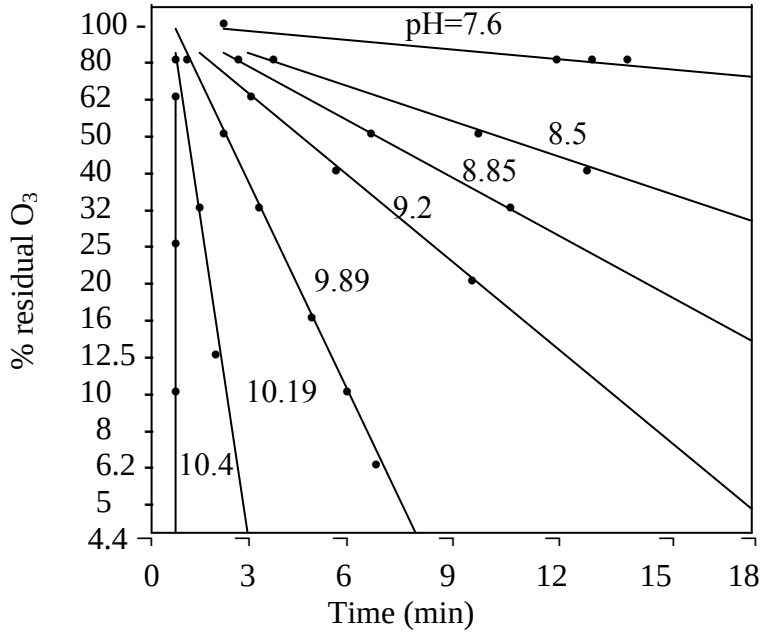

Figure 2.3: Effect of pH on the decay of ozone (T=15 °**C**) (Stumm 1958)

3. Dissolved Solids Concentration

Dissolved ozone can react with a variety of matter, such as organic compounds, viruses, bacteria, etc. As a result, ozone decomposes to other matter; see Figure 2.4. This Figure illustrates that the half-life of ozone in double distilled water is much higher, compared to tap-water, for example. However, once distilled water presented a shorter half-life compared to tap water. Depending on the nature of the dissolved matter, these can accelerate (chain-reaction) or slow down the decay of ozone. A substance that accelerates these reactions is called promoters. Inhibitors are substances that slow down the reaction (Stumm 1958).

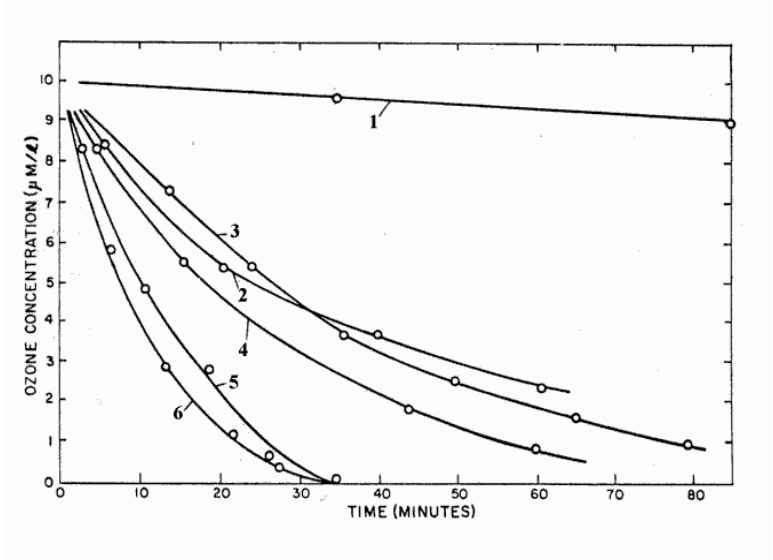

Figure 2.4: Ozone decomposition in different types of water at 20 °C (Stumm 1958)

1 = double-distilled water; 2 = distilled water; 3 = tap water; 4 = groundwater of low hardness; 5 = filtered water from Lake Zurich (Switzerland); 6 = filtered water from the Bodensee (Switzerland).

4. Carbonate and bicarbonate

Scavengers slow down the chain-reaction. This is because after the reaction of scavengers with OH radicals, the reaction products do not react with ozone any further. Carbonate is a scavenger with a strong effect. The addition of carbonate (CO_3^{2-}) can increase the half-life of ozone. The effect on the reaction speed is highest at low concentrations. Above 2 mmol L^{-1} for ozonisation and 3 mmol L^{-1} for advanced oxidation process (AOP), the decrease in the reaction rate is negligible (Stumm 1958).

5. Natural organic material

Natural organic material (NOM) exists in every kind of natural water and is often measured as dissolved organic carbon (DOC). NOM reduces the quality of the water with regard to colour and odour (Stumm 1958). Ozone can be used in water treatment for the reduction of the concentration of NOM. The concentration of NOM in natural waters can vary from 0.2 – 10 mg L^{-1}. The influence of NOM on ozone is twofold. Depending on the type of NOM, can be oxidized directly by NOM. This is the case for compounds which easily react with ozone, such as double bonds, activated aromatic

compounds, deprotonated amines and sulphides. On the other hand, OH radicals can react with NOM (indirect reaction) and act as a promoter or as a scavenger. In natural waters, it is difficult to determine the stability of ozone as a result of the indefinite effect of NOM. That means it is not possible to estimate the fraction that accelerates or slows down the reaction (Stumm 1958).

2.3.4. Ozone toxicity

Because ozone is found in so many places, its toxicity has been investigated extensively since the early 1900s. Experimentation has shown that the odour of ozone can be detected and identified by most people at a concentration of from 0.02 to 0.05 ppm (parts ozone per million parts air + ozone). As the concentration increases to a few tenths of a part per million, the first effect noted is likely to be a feeling of dryness in the back of the throat. If a concentration on the order of 0.2 or 0.3 ppm is inhaled more or less continuously for several hours to a few days, some lung irritation may result; however, in the air we breathe, ozone concentrations as low as 0.3 -0.5 mg/L provoke detrimental effects on the human respiratory tract. The atmospheric concentration at which ozone is dangerous is not well known but inhalation of 50 mg/L of ozone for half an hour would probably be fatal (Masschelein 1982).

2.3.5. Ozone and the environment

The effect of human activities on the level of ozone in our environment is under close scrutiny by environmentalists, politicians, and lawmakers. Ozone can be found in two very different layers of our atmosphere, the troposphere and the stratosphere. The environmental problems related to the levels of ozone in these two atmospheric layers are very different (Bunce 1991). In the troposphere, the level of the atmosphere that we live in, ozone is a component of the air pollution commonly referred to as "smog." The amount of ozone in our troposphere is increasing because of chemicals emitted

wherever natural gas, gasoline, diesel fuel, kerosene, and oil are combusted. Nearly 90% of our Earth's ozone is found in the atmospheric layer above ours, called the stratosphere. This layer extends from about 14.5 kilometres to 50 kilometres (9-31 miles) in altitude and is where aerplanes fly. The ozone layer is within the stratosphere, approximately 15-40 kilometres (10-25 miles) above the Earth's surface. This ozone is important for blocking the Earth from the Sun's harmful ultraviolet (UV) rays by absorbing the UV energy and keeping the rays from penetrating the Earth. The environmental problems related to stratospheric ozone result from the depletion of the ozone by reactions with man-made chemical compounds called chlorofluorocarbons or CFCs (Bunce 1991). These compounds are commonly used for refrigerants, solvents, and foam-blowing agents. Depletion of ozone causes ozone holes in our atmosphere that can be seen by modern detection equipment. Currently, two major holes exist; one over the Antarctic and another over Australia. The size of these holes in the ozone layer will continue to increase unless actions are taken to decrease the level of CFCs in our atmosphere (Bunce 1991). CFCs were discovered in the atmosphere in the early 1970s and subsequent studies showed increases in the ground level of CFCs from 50 ppt (parts per trillion) in 1971 to 150 ppt in 1979. CFCs may be decomposed photo chemically, giving rise to a free chlorine atom as in Equation 2.18, which can initiate the decomposition of ozone shown in Equation 2.19, (Bunce 1991).

$$CF_2Cl_2 \xrightarrow{h\gamma} {}^{\bullet}CF_2Cl + {}^{\bullet}Cl \qquad \text{h}\gamma,\ \lambda < 250\ \text{nm} \qquad (2.18)$$

$$X + O_3 \rightarrow XO + O_2 \qquad (2.19)$$

The ozone level in healthy outdoor environments is typically between 0.02 ppm and 0.04 ppm, which is the ozone level produced by Surround Air Ionizer purifiers. In most unhealthy indoor environments, the ozone level is virtually zero. In some unhealthy

indoor and outdoor environments, the ozone level may actually be well above 0.1 ppm, which is too high. However, this only happens when the hydrocarbon level (pollution from industrial smokestacks, vehicle emissions, etc.) rises to a very high concentration. It has been proven that ozone breaks down the hydrocarbon molecules. When the pollution is high enough though, the nature cannot help but to overcompensate under this strain. This is why indoor environments need a source of negative ions and ozone. In addition to being beneficial to your health when occurring at proper levels, they are highly effective at removing particles and contaminants from the air, which results in a much healthier environment by itself. In 1987, 27 nations signed a global environmental treaty, the Montreal Protocol to Reduce Substances that Deplete the Ozone Layer, that had a provision to reduce 1986 production levels of these compounds by 50 % before the year 2000. This international agreement included restrictions on the production of CFC-11, -12, -113, -114, -115 and the Halons (chemicals used as a fire extinguishing agents). An amendment approved in London in 1990 was more forceful and called for the elimination of production by the year 2000. The chlorinated solvents, methyl chloroform (CH_3CCl_3) and carbon tetrachloride (CCl_4) were added to the London Amendment. In Europe and North America, $CFCl_3$ and CF_2Cl_2 have been completely phased-out of production (Bunce 1991).

2.4. The Treatment of Water and Wastewater

All water used for supply originates from the atmosphere as precipitation (rain, snow and hail). This collects either above ground in rivers, natural lakes, man-made impounding reservoirs or below the ground in aquifers. Water rapidly absorbs both natural and man-made substances that generally make the water unsuitable for drinking prior to some treatment. The objective of water treatment is to produce an adequate and continues supply of water that is chemically, bacteriologically and aesthetically

pleasing. Water treatment plants must be able to produce a finished product of consistently high quality, regardless of how great the demand might be. Water treatment consists of a range of unit processes, usually used in series as shown in Figure 2.5, (Degremont 1991b). The cleaner the raw water, the fewer the treatment steps required and hence, the overall cost of water is less. The most expensive operations in conventional treatment are sedimentation and filtration, while water softening can also be very expensive, (Degremont 1991b). Ground water is generally much cleaner than surface waters so does not require the same degree or treatment, apart from aeration and disinfection before supply.

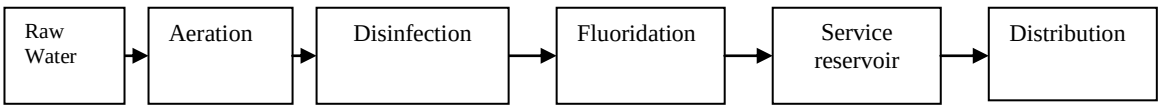

Figure 2.5: Typical water treatment process

Surface water requires more complex treatment due to poor quality, although the quality of surface waters can be very high, for example (upland reservoirs) as in Figure 2.6, (Degremont 1991b). The selection of water resources for supply purposes depends not only on the nature of the raw water and the ability of the resource to meet consumer demand throughout the year, but also on the cost of treating the water.

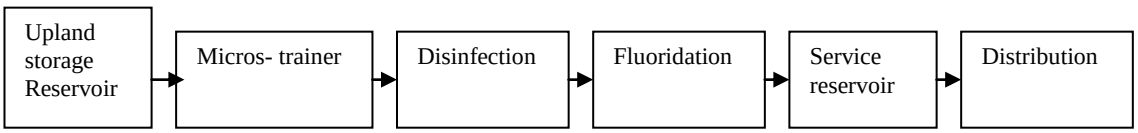

Figure 2.6: Typical sequence of unit treatment for water

Most plants treating variable surface water consist of at least two stages. The first is able to handle the very variable raw water quality, sometimes with high levels of suspended solids and as a results produce a reasonably consistent intermediate quality not normally good enough for supply but with most of the impurities removed and, by specification, good enough for filtration, (Degremont 1991b). In the industry, these primary processes are usually called clarification. The ultimate quality as far as

suspended solids and many other parameters are concerned is achieved by filtration. Most filters for water treatment are based on granular materials such as sand and because the solids being filtered out are retained within the voids in the sand bed, they have a limited capacity. They are able to produce a high quality filtrate when correctly operated, (Degremont 1991b). The clarification and filtration processes are therefore complementary. In some cases these stages are not able to remove all the undesirable species and activated carbon may be needed to adsorb pesticides, (Degremont 1991b). The required bacteriological quality of the water is achieved by a combination of the above, plus the addition of a specific disinfectant such as chlorine, which is usually applied at the last stage after most of the suspended solids have been removed. Filtered water will not be free of pathogenic organisms unless specifically disinfected in this way or else filtered through a membrane fine enough to remove them. The other important method used for treatment recently is ozonation, (Degremont 1991b). Ozone is widely used for drinking water treatment. It can be added at several points throughout the treatment system such as pre-oxidation, intermediate oxidation or final disinfection as shown in Figure 2.7. Usually, it is recommended to use ozone for pre-oxidation, before a sand filter or an active carbon filter General Activity Carbon (GAC). After ozonation, these filters can remove the remaining organic matter. This combination has several benefits:

- Removal of organic and inorganic matter;
- Removal of micro-pollutants, such as pesticides;
- Enhancement of the flocculation/coagulation decantation process;
- Enhanced disinfection and reduction of disinfection by-products;
- Odor and taste elimination.

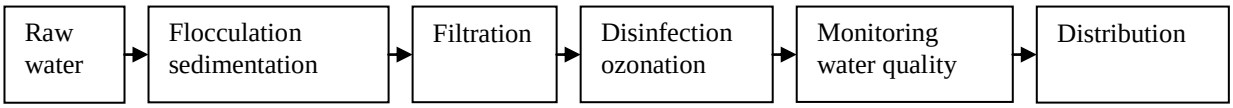

Figure 2.7: Water treatment by ozonation (Degremont 1991b).

2.4.1. Physical treatment of water

Physical treatment methods are used in both water treatment and wastewater processing. Except for preliminary steps, most physical processes are associated directly with chemical and biological operations. In water treatment, granular-media filtration (a physical method) must be preceded by chemical coagulation. In wastewater processing, the physical procedures of mixing and sedimentation in activated sludge are related directly to the biology of the system, (Degremont 1991a). However, a physical process usually treats suspended, rather than dissolved, pollutants. It may be a passive process, such as simply allowing suspended pollutants to settle out or float to the top naturally depending on whether they are more or less dense than water. The process may be aided mechanically, such as by gently stirring the water to cause more small particles to bump into each other and stick together, forming larger particles which will settle or rise faster a process known as flocculation. Chemical flocculants may also be added to produce larger particles, (Degremont 1991a). To aid flotation processes, dissolved air under pressure may be added to cause the formation of tiny bubbles which will attach to particles. Filtration through a medium such as sand as a final treatment stage can result in a very clear water. Ultrafiltration, nanofiltration and reverse osmosis are processes which force water through membranes and can remove colloidal material (very fine, electrically charged particles, which will not settle) and even some dissolved matter. Adsorption on activated charcoal is a physical process which can remove dissolved chemicals. Air or steam stripping can be used to remove pollutants that are gasses or low-boiling liquids from water and the vapours which are removed in this way

are also often passed through beds of activated carbon to prevent air pollution. These last processes are used mostly in industrial treatment plants, though activated carbon is common in municipal plants also, for odour control, (Degremont 1991a).

2.4.2. Biological treatment of water

Biological treatment of water has been in use since the beginning of time, (Degremont 1991a). Microorganisms can consume insoluble materials found in wastewaters for multiplication processes. Moreover, biological treatment plants are more commonly used to treat domestic or combined domestic and industrial wastewater from a municipality. They use basically the same processes that would occur naturally in the receiving water but give them a place to happen under controlled conditions, so that the cleansing reactions are completed before the water is discharged into the environment. Biological treatment is the most important step in processing municipal wastewaters. Physical treatment of raw wastewater by sedimentation removes only about 35% of the Biological Oxygen Demand (BOD), owing to the high percentage of non settleable solids (colloidal and dissolved) in domestic wastewaters. Chemical treatment is not favoured because of high chemical costs and inefficiency of dissolved BOD removal by chemical coagulation and precipitation. Advanced physical treatment method, such as carbon adsorption and reverse osmosis, can remove dissolved BOD and other contaminants but are very costly to construct, operate and maintain. A modern treatment plant uses a variety of physical, chemical, and biological processes to provide the best, most economical treatment, (Degremont 1991a).

2.4.3. Chemical treatment of water

Chemical treatment is the most important step in processing public water supplies (Tchobanoglous et al., 1991). Surface water normally requires chemical coagulation to

eliminate turbidity, colour, and taste-and odour-producing compounds, while well water supplies are commonly treated to remove dissolved minerals, such as iron, manganese and hardness. However, chemical treatment of water or wastewater involves the interaction or conversion of a pollutant with a chemical material. Some chemical processes such as adsorption, extraction and distillation may also be known as physico-chemical treatment, whereby there is no material conversion but physico-chemical interactions define the processes. Alternatively, there are many processes that use material conversion to remove pollutants from the source, such as; neutralization, precipitation, reduction, oxidation and ion exchange. (Tchobanoglous et al., 1991), propose that precipitation, adsorption and disinfection are the most common examples of chemical treatment processes.

2.4.3.1. Oxidation processes

Oxidation processes have in the last decade become very popular for treating refractory organic chemicals, due to their ability to oxidise chemicals that are otherwise difficult to remove from wastewaters. On-site oxidation processes have been integrated into wastewater treatment processes to increase the purity of effluent waste and make other processes, such as adsorption, more effective by increasing the polarity of some by-products formed (Degremont 1991a, b).

2.4.3.2. Hydrogen peroxide treatment

Hydrogen peroxide (H_2O_2) is used as a commercial oxidant and can be bought in solution of 35 %, 50 % and 70 % by weight. It is unstable under the effects of temperature, light, alkaline pH and certain metals. All materials used in conjunction with H_2O_2 should be stainless steel, due to the corrosive nature of peroxide. Equation 2.20 shows the dissociation of hydrogen peroxide in water.

$$H_2O_2 + H_2O \leftrightarrow HO_2^- + H_3O^+ \qquad K = 2.5\times10^{-12} \qquad (2.20)$$

One advantage of H_2O_2 is that it contains no halogen compounds, however, it is relatively expensive (Degremont 1991 a, b) and is difficult to transport or produce on site. H_2O_2 is used in conjunction with ozone as an Advanced Oxidation Process (AOP) since it aids the decomposition of ozone into highly reactive radicals in enough quantities via the reaction of ozone with hydrogen peroxide ions.

2.4.3.3. Ultraviolet treatment

Ultraviolet light has been used recently in the treatment of wastewater and is generally implemented as a tertiary process. This non-invasive process avoids the use of additional chemicals and also has the advantage over chlorine because chloro-compounds are not produced. The ultraviolet treatment process is defined by the excitation of molecules from their primary very short-lived single state to a longer-lived triplet state, with the transfer of energy to other molecules. These types of reaction maybe either type I, in which this triplet state photo sensitizer directly oxidizes the substrate, or type II, whereby the photosensitizer transfers energy to molecular oxygen, which then becomes excited to its singlet state ($1\Delta_g$). This may be depicted by Equations 2.21 to 2.23 (Halmann 1996) or by Figure 2.8 (Tchobanoglous et al., 1991).

$$^1S_0 + h_\gamma \rightarrow ^1 s_1 \qquad (2.21)$$

$$^1S_1 \rightarrow ^3S_1 \qquad (2.22)$$

$$^3S_1 + 3O_2 \rightarrow ^1S_0 + ^1O_2 \qquad (1\Delta_g) \qquad (2.23)$$

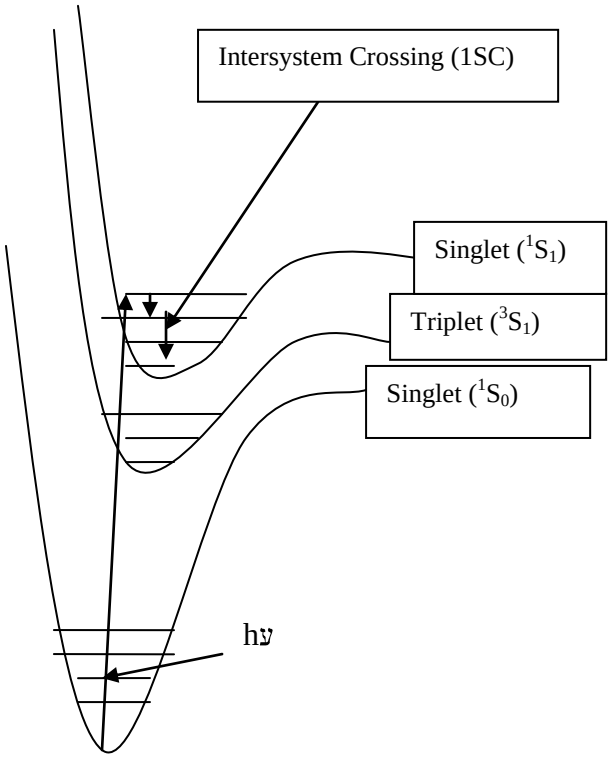

Figure 2.8: Energy diagram for the excitation of molecules

At present, low pressure mercury arc lamps are preferably used for generation of UV light. This type of lamp is preferred due to its ability to produce light at a wavelength of 253.7 nm .The lamp operates by striking an electric arc over the mercury vapour and the energy produced by the excitation of the mercury vapour is dissipated as UV light (Tchobanoglous et al., 1991). If the lamps are submerged within the solution, they are generally sealed within quartz tubing.

2.4.3.4. Ozonation

Ozonation is a water disinfection method first used in Nice, France in the early 20th century to improve drinking water taste and odour Vosmaer, (1916). It is now widely used in Western Europe, the United States and Japan. Ozonation is a clean and efficient alternative to chlorine-based water treatment. Ozone is not only a powerful disinfectant used to eradicate bacteria and viruses, it is also a highly effective oxidizing agent

(Coate 1997). Ozonation uses a four-step process. First, gas (air or oxygen) is cleaned, filtered, and dried. Then the dried gas is passed through electrodes to form ozone. The third step involves transferring ozone into water using gas/liquid type reactors (e.g. bubble columns). After bubbling, ozone off-gas is destroyed and the water flow is routed to the next treatment unit operation (Degremont 1991 a, b).

The numerous water-treatment applications for ozonation include:

* Water/wastewater disinfection and treatment;
* Bottled/drinking water disinfection;
* Industrial or commercial laundering;
* Aquaculture;
* Water treatment for commercial swimming pools and spas;
* Water treatment for cooling towers;
* Textile, pulp, and paper bleaching;
* Groundwater treatment;
* Industrial and oil refinery wastewater treatment;
* Aquarium water treatment;
* Colour and odour control;
* Creation of ultra pure water for the electronics industry.

2.5 Ozone Production

Because of its relatively short half-life, ozone is always generated on-site by an ozone generator. The two main principles of ozone generation are UV-light and corona-discharge. Ozone generation by corona-discharge is most common nowadays and has the most advantages. Advantages of the corona-discharge method are greater sustainability of the unit, higher ozone production and higher cost affectivity. UV-light can be feasible where production of small amounts of ozone is desired. In the ozone generator, the corona-discharge element is present, which provides a capacitive load. In the generator, ozone is produced from oxygen as a direct result of electrical discharge. This corona-discharge ruptures the stable oxygen molecule and forms two oxygen radicals. These radicals can combine with oxygen molecules to form ozone. To control and maintain the electrical discharge, a di-electric is present, carried out in ceramic or glass. The excessive heat of the electrodes is often cooled by cooling water or by air Figure 2.9, (Degremont 1991b).

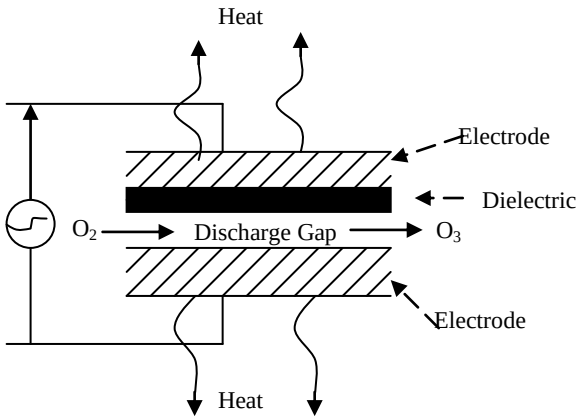

Figure 2.9: Outline of the corona-discharge generation of ozone

For the production of ozone, ambient air can be used (supplied by a compressor) or pure oxygen (supplied by an oxygen generator or sometimes by oxygen bottles). To condition this air, air dryers and dust filters are used. To break down the remaining ozone after use, ozone destructors are applied. The mechanism of an ozone destructor

can be based on different principles. Usually a catalyst is applied, which accelerates the decomposition of ozone into oxygen (e.g. magnesium oxide). The generation of ozone is very energy-intensive, with some 90 % of the power supplied to the generator being utilized to produce light, sound and primary heat (Degremont 1991b). Important factors that influence ozone generation are: oxygen concentration inlet gas, humidity and purity of inlet gas, cooling water temperature and electrical parameters. To minimize the energy that is used to produce a high ozone yield, it is important that these factors are optimal.

A) Cooling water temperature

The generation of ozone is accompanied by heat formation. This makes it important to cool the generator. An ozone reaction is reversible and this increases when temperatures rise. As a result, more oxygen molecules are formed.

$$-\Delta T \quad 3O_2 \leftrightarrow 2O_3 \quad +\Delta T \tag{2.24}$$

Figure 2.10 illustrates the relation between cooling water temperature and the yield of ozone generation. This Figure shows that an increasing cooling water temperature results in a decreasing ozone production. To limit the decomposition of ozone, the temperature in the discharge gap should not be higher than 25 °C. The general advice is that cooling water may increase 5 °C to 20 °C maximally. It is important that the temperature of the inlet air is not too high (Degremont 1991b).

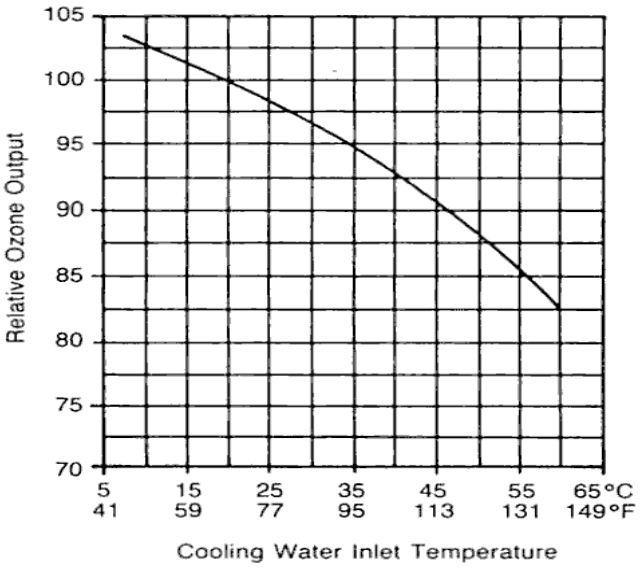

Figure 2.10: Influence of water cooling on ozone generator efficiency (Degremont 1991b)

B) Humidity inlet air

Before the feed gas enters the ozone generator, air dryers should dry the air. Ambient air contains moisture, which reacts with ozone. This leads to a reduction of the ozone yield per kWh. An additional problem of high humidity is that undesired reactions occur in the corona unit. When increased amounts of water vapour are present, larger quantities of nitrogen oxides are formed when sparks discharge occurs. Nitrogen oxide can form nitric acid, which can cause corrosion. Furthermore, hydroxyl radicals are formed that combine with oxygen radicals and with ozone. All these reactions reduce the capacity of the ozone generator. Figure 2.11 shows the influence of the humidity on the capacity of an ozone generator (Degremont 1991b). The two descending lines illustrate the capacity of the generator: 'oxygen' for an oxygen-fed generator and 'air' for an air-fed generator. At a dew point of -10 °C, the capacity of the air-fed generator is only 60 % of the total achievable capacity. For ozone generators that are oxygen-fed, this capacity is higher; about 85 %.

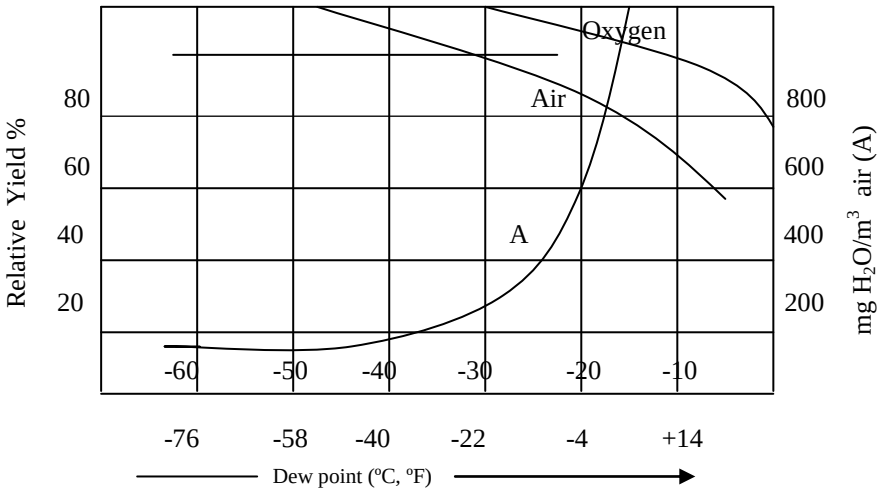

Figure 2.11: Influence humidity inlets on efficiency of ozone production

To prevent these side-reactions, inlet air first passes a drying chamber before ozone is generated. For drying, an aluminium compound can be used, comparable with silica gel. In an ozone generator, two or more drying chambers are used alternately. When a drying chamber is used for a certain period of time, humid air is led to the other drying chamber, while the first is regenerated (Degremont 1991b).

C) Purity of gas (inlet)

The presence of organic impurities in the gas feed must be avoided, including impurities arising from engine exhausts, leakages in cooling groups or leakages in electrode cooling systems. The gas supply of the generator must be very clean. An example is given in Figure 2.12, where the concentration of hydrocarbons is related to the ozone yield. This Figure shows that at a hydrocarbon concentration of about 1%, the ozone generation nearly approaches zero (Degremont 1991b).

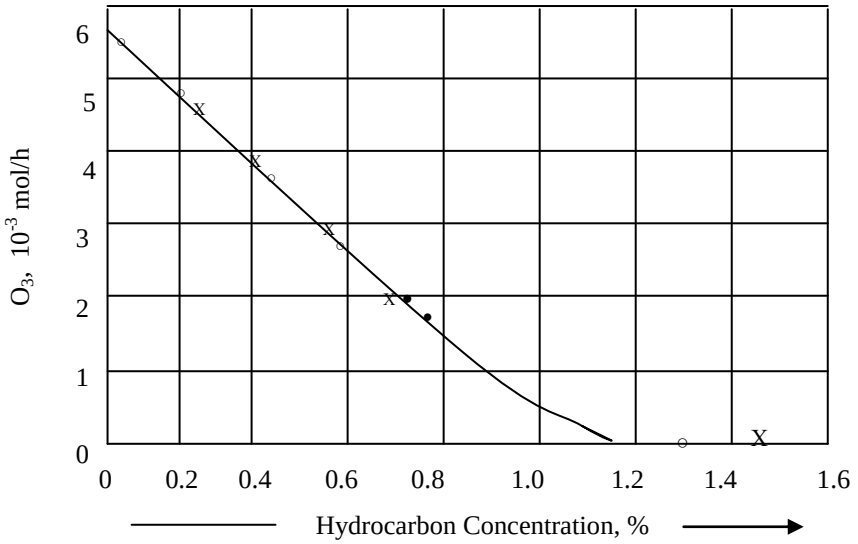

(○ = Cyclohexane, X = n- Heptane, ● = n- Hexane)

Figure 2.12: Influences of hydrocarbons on the generator yield of ozone

Produced amount of ozone versus oxygen concentration of inlet air ozone is produced from oxygen, so it can be produced from ambient air (21 % oxygen) or nearly pure oxygen (e.g. 95 %). Pure oxygen can be generated from ambient air by an oxygen generator. The ozone concentration an ozone generator delivers is dependent on the oxygen concentration (among other things). This is clarified by Figure 2.13, where the oxygen concentration is outline against the ozone concentration. The diverse lines demonstrate the ozone generators with different energy use. In summary, one can claim that the ozone production increases by a factor (1.7 to 2.5) when pure oxygen is used at constant electrical power (Degremont 1991b).

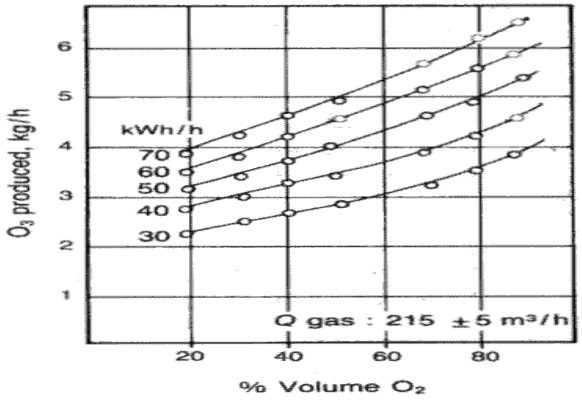

Figure 2.13: Influence of oxygen concentration on ozone production at different electrical current

2.6. Advantages & Disadvantages of Ozone

A) Advantages

Ozone has been shown to be the second most powerful oxidiser, after fluorine. Ozone can disinfect roughly 3000 times faster for Cryptosporidium removal than chlorine (DEL Industries 1997). This allows for either a lower concentration of the disinfectant or a faster travel time through the treatment system, whichever is more advantageous to the designer. As stated earlier, ozone reacts with almost anything it can. This provides ozone with strong taste and odour control as well as allowing it to oxidize many metals and organics. Lab results have shown that ozone can remove the following metals at 99.5% or above: aluminum, arsenic, cadmium, chromium, iron, nickel, cobalt, lead, zinc, copper, and manganese (Coate 1997). Ozone can completely oxidise mercury at pH 4 as well (Coate 1997). Ozonation changes nitrite ions to nitrate ions and has also been shown to be effective in treating the following: acetic acid, oxyethanol, isopropyl alcohol, methyl ethyl ketone, acetone, cetyl alcohol, glycerol, propylene glycol, n-butyl acetate, formaldehyde, methacrylic acid, benzene benzyl alcohol, resorcinol, n-butyl phthalate, camphor, para-phenylenediamine, styrene tricresyl-phosphate, xylene, butane, liquefied-petroleum-gas, mineral spirits, dichloromethane, perchloroethylene, trichloroethylene, hydrogen cyanide, ammonium hydroxide, ethanolamine, toluene,

isobutene, propane, methyl chloroform, aminophenol, ammonia, ammonium-persulfate-phenacetin, ethylene tetracetic acid (EDTA), alkylated silicates and non-ionic detergents (Coate 1997).

B) Disadvantages

The primary drawback to the use of ozonation is the cost. Not only are capital costs significantly higher than its chlorinated alternatives but the maintenance and daily operation costs also tend to be higher. Some have estimated that ozonation can cost up to eight times more than disinfection (EPRI 1996). Although this may be true in certain cases if only disinfection is considered, the total cost benefit will largely depend on the water being treated. As stated earlier, ozone provides numerous other advantages besides disinfection: ozone can reduce treatment needed for taste, odour, manganese and iron control and aid in coagulation. Table 2.6 shows the advantages and disadvantages of ozone for water treatment (Coate 1997).

Table 2.6: Advantages and disadvantages an ozone for water treatment

ADVANTAGES	DISADVANTAGES
More powerful disinfectant than chlorine compounds (more effective at Cryptosporidium removal).	Tends to cost more than traditional chlorinated disinfection techniques.
Has no negative residual such as trihalomethane production.	Does not produce a disinfection residual that would prevent bacterial regrowth.
Does not alter the pH of the water.	Forms nitric oxides and nitric acid which could lead to corrosion.
Increases coagulation.	
Helps with the removal of iron and manganese.	
Has taste and odour control properties.	

2.7. Ozone Analysis

2.7.1. Aqueous phase ozone analysis

2.7.1.1. Acid chrome violet K method

This method has been used by the Tailfer- Water – Utility since 1968, which supplies water to the city of Brussels. This procedure shows a linear relationship of

decolonization to ozone concentration at λ = 548 nm with its upper limit of detection being ~ 25 ug O_3/L. It has the advantage that it is free from interferences (as it is selective to ozone) involved in water treatment, such as chlorine, chloramines, chlorite and chlorate ions (Brink et al., 1991), (Masschelein et al., 1989).

2.7.1.2. Iodometric method

This method is used extensively in ozone analysis due to its simple procedure. However, it is used more frequently in gas phase measurement of ozone concentration. The principle behind this method may be described by the Equations (2.25 and 2.26). On oxidation of potassium iodide with ozone, the liberated iodine is titrated with a solution of sodium thiosulphate and the colour change (blue/black to yellow to clear) is observed using starch as an indicator (Brink et al., 1991).

$$O_3 + 2I^- + H_2O \rightarrow I_2 + 2OH^- + O_2 \quad (2.25)$$

$$I_2 + 2S_2O_3^{-2} \rightarrow 2I^- + S_4O_6^{-2} \quad (2.26)$$

2.7.1.3. Indigo trisulphonate batch method

This method had been devised from previous methods of residual chlorine analysis. The authors (Barder and Hoigne 1982) propose that this method has greater selectivity to ozone than most other aqueous phase analytical methods. In their paper, they describe the method for ozone determination using potassium indigo trisulphonate for various concentration of ozone. The authors also provide a list of manufacturers that supply potassium indigo trisulphonate. (Kerc and Saatci 1996) describe a method for continuous monitoring of ozone in solution using the indigo method combined with UV-spectrophotometer, suggesting that their method is advantageous due to it having a response time of only a few seconds. The principle of this method is that in acidic solution, ozone rapidly decolorizes indigo. The decrease in absorbance is liner with

increasing concentration over a wide range. (Gordon et al., 2000a, 2000b) provides details of the indigo method; the method is based on a change in absorbance (600 nm wavelength) of indigo between an unreacted blank solution and an ozone-reacted sample solution.

2.7.2. Gaseous phase ozone analysis

2.7.2.1. Direct UV ozone analysis

Gaseous ozone absorbs light in a short- UV wavelength region with a maximum absorption at 253.7 nm. Instruments for measuring ozone by the absorption of UV radiation are supplied by several manufactures for gas concentration below 1 g/m^3 NTP (0.076 % by weight). In general, these instruments measure the amount of light when no ozone is present and the amount of light when ozone is present. The meter output is the difference between the two readings or the actual ozone concentration. This method of gas phase analysis is one of the most favourable as it can give continuous real time measurements without interference. Ultraviolet absorption has been specified by the U.S. Environmental Protection Agency (EPA) as the method to be used for calibrating atmospheric ozone monitors and analyzers (Brink et al., 1991). (Gordon et al., 1992) have made the comparison of wet chemistry measurements (Iodometric) with those of UV measurements. They suggested that the two methods of measurement gave a 0.54 % difference in ozone concentration. Data collected over a period of nine years (1985 – 1994) from various commercial ozone UV- meters was compared to KI wet chemistry ozone measurements by (Rakness et al., 1996). Their results showed that the difference in ozone concentration produced by the two methods (UV-spectrophotometer and KI wet chemistry ozone analysis), for ten of the fifteen meters tested gave a percentage difference of ± 2 %. (Kenly 1996) suggests that the UV-ozone

monitoring system is a robust and reliable measurement device, with the most commonly replaced component being the UV – lamp (1-2 years).

2.7.2.2. Iodometric ozone analysis

Iodometric methods have been used for all of the ozone concentration ranges encountered in water treatment plants. This includes the measurement of ozone directly from the generator and the measurement of ozone as stripped from aqueous solution. For the Iodometric method, the ozone containing gas is based into an aqueous solution containing excess potassium iodide, in which the ozone oxidizes iodide ion Maier and (Kurzmznn 1977). However, this method may be used in the measurements of gaseous ozone but the method is prone to problems that arise due to changes in the pH of the solution.

2.8. Current Ozone Technology

2.8.1. Liquid/Gas-Ozone (LGO) Process

The heterogeneous liquid/gas-ozone process is the technique most used for ozone transfer to the water. The kinetics of heterogeneous reactions is governed by absorption theories of gases in liquids accompanied by chemical reactions. The fundamental of these theories are necessary to understand the phenomena developing during the ozonation of compounds in water. (Astarita 1967) and (Danckwerts 1970) both gave extensive treatment to the subject developing expressions for the gas absorption rate at various reaction rates. These expressions have been experimentally applied in chemical techniques for the determination of physical mass transfer coefficient. The liquid/gas-ozone system falls into two major categories; physical absorption method and chemical method. Both techniques offer advantages and disadvantages.

2.8.1.1. Physical absorption reaction

The physical absorption system normally consists of a gas absorbing into water, possibly with some additives, to change the physical properties. In a general case, when gas and liquid phases are in contact, components can be transferred from one phase to the other until equilibrium is reached. The transfer of a component from one phase to another, across a separating interface, is due to a concentration gradient, caused by a resistance to the mass transfer developed in each phase. The resistance in one phase is the contribution of the diffusion resistance in the laminar film and the resistance in the bulk fluid. The latter resistance is usually considered negligible compared to the diffusion resistance (Astarita 1967) and (Danckwerts 1970). The film mass transfer coefficient is proportional to the molecular diffusion coefficient (D) at a certain power n (D^n). The value of n depends on the turbulence of the system; n = 0.5 for sufficiently turbulent conditions and n =1 for laminar conditions.

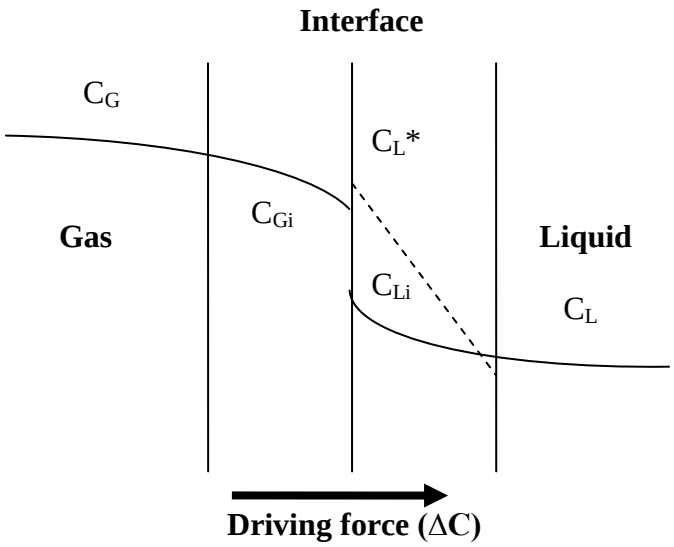

Figure 2.14: Mass transfer between two phases (double-film theory)

The mass transfer flux N is the product of the film coefficient and the concentration gradient in the film.

$$N = k_G (C_G - C_{Gi}) = k_L (C_{Li} - C_L) \quad (2.27)$$

In reality, both resistances (in the two phases) affect the mass transfer rate. An overall mass transfer coefficient can be defined relative to the liquid phase (k_L) or relative to the gas phase (k_G). Each coefficient is based on a calculated overall driving force (DC), defined as the difference between the bulk concentration of one phase (C_L or C_G) and the equilibrium concentration (C_L* or C_G*) corresponding to the bulk concentration of the other phase Equation. 2.27. Since ozone is only slightly soluble in water, the mass transfer is controlled by the liquid phase ($K_L = k_L$; $C_{Gi} = C_G$; $C_{Li} = C_L$*) Equation 2.28 (Van Krevelen and Hoftijzer 1954).

$$N = k_G (C_G - C_{Gi}) \cong k_L (C_{Li} - C_L) \cong K_G (C_G - C_G^*) \cong K_L (C_L^* - C_L) \quad (2.28)$$

$$N = k_L (C_{Li} - C_L) = K_L (C_L^* - C_L) \quad (2.29)$$

By introducing the specific surface area, a (m^2/m^3), the specific mass transfer rate is written in this form:

$$N_a = k_L a \left(C_L^* - C_L\right) \quad (2.30)$$

Where: k_La is the volumetric mass transfer coefficient relative to a controlling resistance in the liquid phase, it depends on the hydrodynamic conditions in the liquid phase (s^{-1}), (C_L^*) is the liquid concentration in equilibrium with the bulk gas concentration (mol/m^3). The liquid equilibrium concentration (C_L^*) is given by the modified Henry's law Equation 2.31 (Van Krevelen and Hoftijzer 1954).

$$C_L^* = \frac{C_G}{H_C} \quad (2.31)$$

H_C dimensionless modified Henry's law constant, which is the inverse of ozone solubility ratio in water (at 20^{o}C and 1 atm).

2.8.1.2. Chemical absorption reaction

Gas-liquid mass transfer with chemical reaction has been the focus of a great deal of investigation, both theoretically and experimentally (Astarita 1967) and (Danckwerts 1970). Film theory with slow chemical reaction is the most popular chemical technique employed for k_La measurement. This slow reaction regime assumes negligible reaction in the liquid film and the conditions approximate a physical absorption. When reaction in film can no longer be neglected, the system enters the fast reaction regime. The concentration gradient at the gas-liquid interface is increased, thereby increasing the rate of absorption. When ozone is transferred to aqueous solutions containing ozone consuming species, the mass transfer is enhanced due to the chemical reaction, as compared to physical absorption alone. In order to account for this, an enhancement factor E is defined Equation 2.32, (Van Krevelen and Hoftijzer 1954).

$$E = \frac{rate\ of\ ozone\ transfer\ with\ reaction}{rate\ of\ physical\ mass\ transfer\ alone} = \frac{N_A}{k_L a\left(C_{AL}^{*} - C_{AL}\right)} \tag{2.32}$$

When the gas absorption is accompanied by the chemical reaction, the reaction will occur in one of the following places (Figure. 2.15) (Van Krevelen and Hoftijzer 1954).

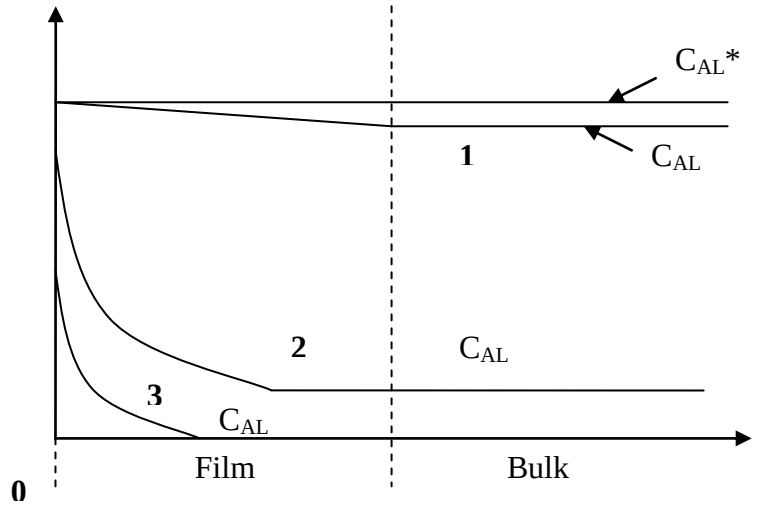

Figure 2.15: Different kinetic regimes for mass transfer with chemical reaction

(1)- In the liquid bulk (slow kinetic regime), (2) - In both (intermediate kinetic regime)

(3)- In the liquid film (fast kinetic regime).

First-order or pseudo first-order reactions

The concentration profile of A at a distance x from the interface is given by equation 2.33, (Van Krevelen and Hoftijzer 1954).

$$C_{Af} = C_{AL}^{*}\frac{\sinh\left[\left(1-\frac{x}{\delta}\right)Ha_1\right]}{\sinh Ha_1} + C_{AL}\frac{\sinh\left[\frac{x}{\delta}Ha_1\right]}{\sinh Ha_1} \tag{2.33}$$

And the absorption rate of A is given by either of the similar equations, Equation. 2.34 or Equation. 2.35:

$$N_{A0} = -D_A\frac{dC_A}{dx}\Big|_{x=0} = M_1\frac{Ha_1}{\tanh Ha_1}\left[1-\frac{M\dfrac{Ha_1}{\sinh Ha_1 \cosh Ha_1}}{R_{b\max} + M_1\dfrac{Ha_1}{\tanh Ha_1}}\right] \tag{2.34}$$

$$N_{A0} = -D_A \frac{dC_A}{dx}\Big|_{x=0} = M_1 \frac{Ha_1}{\sinh Ha_1}\left[\cosh Ha_1 - \frac{1}{\cosh Ha_1 + \frac{\beta}{a\delta} Ha_1 \sinh Ha_1}\right] \quad (2.35)$$

Where: Ha_1 is the Hatta number for first-order or pseudo first-order reaction defined by Equation. 2.36

$$Ha_1 = \frac{\sqrt{k_1 D_A}}{k_L} \quad (2.36)$$

M_1 is the maximum physical absorption rate at the interface, Equation. 2.37

$$M_1 = k_L C^*_A \quad (2.37)$$

R_{bmax} is the maximum chemical reaction rate in the bulk liquid (mol/m^2.s), Equation 2.38

$$R_{b\max} = \frac{\beta}{a} k_1 C_{AL} \quad (2.38)$$

β is the liquid hold-up, that is the ratio of liquid to (liquid + gas) volumes; a is the specific interfacial area (m^2/m^3); δ is the liquid film thickness (m); k_1 is the rate constant (s^{-1}); k_L is the mass transfer coefficient (m/s); D_A is the gas (ozone) diffusivity in water (m^2/s). If we consider the various kinetic regimes in which the absorption rate develops, simplified equations can be obtained as shown in Table 2.7, (Van Krevelen and Hoftijzer 1954).

Table 2.7: First or pseudo first-order kinetic regimes

Kinetic Regime	Condition	N_{A0} (mol/m^2.s)
Fast	$H_{a1}>3$, $C_{AL}=0$	$N_{A0}=M_1H_{a1}$
Moderate	$0.3<H_{a1}<3$	E.q 2.30 or E.q 2.31
Diffusion	$H_{a1}<0.3$, $C_{AL}=0$	$N_{A0}=M_1$
Slow	$H_{a1}<0.3$, $C_{AL}>0$	E.q 2.30 or E.q 2.31
Very slow	$H_{a1}<0.01$	$N_{A0}=R_{bmax}$

Second-order reactions

The case of second-order reactions is more complex than first-order reactions. There are no general analytical solutions to give the concentration profiles for A and B or to give flux equations (Van Krevelen and Hoftijzer 1954). Usually simplified equations and graphical curves, obtained depending on the kinetic regime, are used. The Hatta number for second-order reactions is given by Equation. 2.39.

$$Ha_2 = \frac{\sqrt{k_2 D_A C_{BL}}}{k_L} \tag{2.39}$$

Where: k_2 is the second-order reaction rate constant (mol/L.s); D_A is diffusivity of ozone in water (m^2/s); C_{BL} is the bulk liquid concentration of compound B (mol/L); k_L is the film mass transfer coefficient (m/s). Table 2.8 summarises the various kinetic regimes obtained in a second-order reaction system, (Van Krevelen and Hoftijzer 1954).

Table 2.8: Second-order kinetic regimes

Kinetic Regime	Condition	Observation	E	Equation
Very slow	H_{a2}<0.02	Reaction takes place into the bulk of the liquid.	1	$C_{AL} = \frac{C_{AL}}{1+\frac{k2C_{BL}}{k_L a}} + \frac{1}{k_L a \tau}$
Too slow	0.02< H_{a2}<0.3	Reaction takes place into the bulk of the liquid.	1	C_{AL}=0 if $\frac{k_2 C_{BL}}{k_L a} + \frac{1}{k_L a \tau} >> 1$
Moderate	0.3< H_{a2}<3	Reaction takes place into both the bulk of the liquid and the liquid film.	>1	-
Very fast	3< H_{a2}	Reaction occurs entirely in liquid film , no gas reaches the bulk liquid.	>1	C_{AL}=0 $N_{A0} = Ek_L C^*_{AL}$
2nd order °R=pseudo 1st order °R	3< H_{a2} <E/2	$C_{\delta L}$ is considered constant Everywhere.	E= H_{a2}	$N_{A0} = Ek_L C^*_{AL}$
Instantaneous	3< H_{a2} and H_{a2}>10E1	Mass transfer controls via Diffusion of A and B through the liquid film.	E=E1	$N_{A0} = Ek_L C^*_{AL}$
Very high	3< H_{a2}	Reaction ozone at the interface, gas phase resistance controls the absorption rate.	-	-

(Van Krevelen and Hoftijzer 1954) have reported in a curve values for E as a function of Ha_2 and E_i (Figure 2.16).

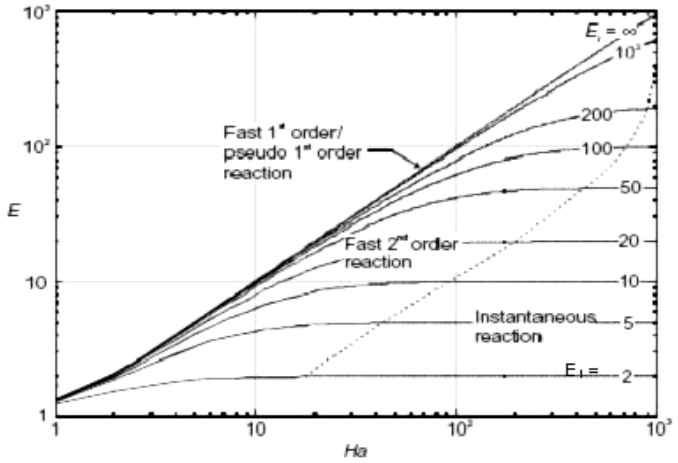

Figure 2.16: Enhancement factor for second-order reaction For $Ha_2>2$, the curve can be approximated by Equation. 2.40.

$$E = \frac{Ha_2\sqrt{\frac{E_i - E}{E_i - 1}}}{\tanh\left[Ha_2\sqrt{\frac{E_i - E}{E_i - 1}}\right]} \tag{2.40}$$

Where: k_La is the volumetric mass transfer coefficient (s-1); τ is hydraulic residence time of the liquid inside the contactor; E_i is the instantaneous enhancement factor. Equation 2.41.

$$E_i = 1 + \frac{D_B C_{BL}}{z D_A C^*_{AL}} \tag{2.41}$$

D_B is the diffusivity of compound B (m^2/s) and z is the stoichiometric coefficient

2.8.2. Liquid/Solid-Ozone (LSO) Process

Figure 2.17 shows the basic stages of the liquid/solid-ozone process used for quantifying ozone adsorption in liquid/solid-ozone (LSO) system. LSO system is a technique developed in the water laboratory at Bradford University in order to overcome some of the problems encountered in conventional gas/liquid-ozone (LGO)

systems (Tizaoui 2001). The principle behind this system is described in the following paragraphs.

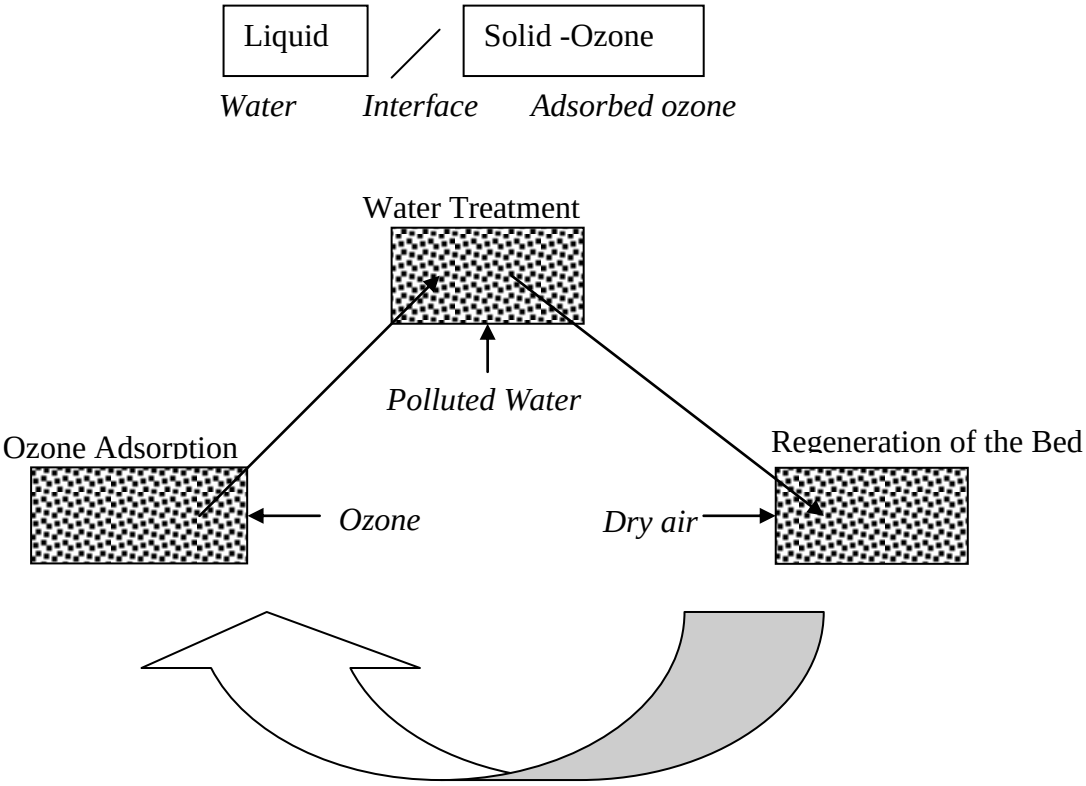

Figure 2.17: Basic stages of the Liquid/Solid-Ozone process

The LSO consists of three steps: (a) loading ozone on a bed of an adsorbent (b) passing polluted water through the ozone-saturated bed and (c) regenerating the bed using dry air. By doing this, it is expected that kinetics are enhanced due to the high ozone concentration in contact with pollutants. In addition, better control over the contact time of ozone with pollutants may also prove beneficial for pollutants that react only slowly with ozone; this can be achieved by using a packed bed and water flow rates to match reaction rates. With direct gas/liquid systems, long contact times require a stirred or loop reactor in which gravity does not control gas bubble relative velocities and in that case, back mixing is deleterious compared to a plug flow reactor or counter-current contact system. The counter-current flow of adsorbent is possible but not usually an attractive proposition, so a fixed bed system operating cyclically is used. Any pollutant

residues on the dry adsorbent may be oxidized during ozone re-loading. Since the LSO system involves adsorption processes, the theory of adsorption will be presented in the following paragraphs (Tizaoui 2001).

2.8.2.1. Adsorption theory

The solid that takes up the gas is called the adsorbent and the gas or vapour taken up on the surface is called the adsorbate. It is not always easy to tell whether the gas is inside the solid or merely at the surface because most practical adsorbents are very porous bodies with large internal surfaces. It is not possible to determine the surface areas of such materials by optical or electron microscopy because of the size and complexity of the pores and channels of the material (Atkins 1990). The gas adsorption itself, however, can be used to determine the accessible surface area of most molecules and atoms can attach themselves onto surfaces in the following two ways. In physisorption (physical adsorption), there is a weak van deer Walls attraction of the adsorbate to the surface. The attraction to the surface is weak but long ranged and the energy released upon accommodation to the surface is of the same order of magnitude as an enthalpy of condensation on the order of 20 kJ/mol, (Atkins 1990). During the process of physisorption, the chemical identity of the adsorbate remains intact, i.e. no breakage of the covalent structure of the adsorbate takes place. For physisorption to be a spontaneous thermodynamic process, it must have a negative ΔG. Because translational degrees of freedom of the gas phase adsorbate are lost upon deposition onto the substrate, ΔS is negative for the process. Since $\Delta G = \Delta H - T\Delta S$, ΔH for physisorption must be exothermic. In chemisorptions (chemical adsorption), the adsorbate sticks to the solid by the formation of a chemical bond with the surface. This interaction is much stronger than physisorption and, in general, chemisorptions have more stringent requirements for the compatibility of adsorbate and surface site than physisorption. The

chemisorptions may be stronger than the bonds internal to the free adsorbate, which can result in the dissociation of the adsorbate upon adsorption (dissociative adsorption). In some cases, ΔS for dissociative adsorption can be greater than zero, which means endothermic chemisorptions, although uncommon, are possible. The energy of adsorption depends on the extent to which the available surface is covered with adsorbate molecules. This is because the adsorbents can interact with each other when they lie upon the surface (in general they would be expected to repel each other). The fractional coverage of a surface is defined by the Equation 2.42 (Atkins 1990).

$$\theta = \frac{Number\,of\ adsorption\,sites\ occupied}{Number\,of\ \ adsorption\,sites\ available} = \frac{A}{N} \tag{2.42}$$

The rate of adsorption is the rate of change of an increase in coverage with time. Processes which allow adsorption to be monitored include; Flow methods, whereby the rates of flow of a gas into and out of the system are monitored (integration of this rate gives the fractional coverage at any time), Flash desorption, where the adsorbate and adsorbent are suddenly heated and the increase in pressure is interpreted as the amount adsorbed, Gravimetric, where the adsorbents weight is monitored using a microbalance with time (Atkins 1990). At this point it is useful to distinguish between physical and chemical adsorption. These terms may be loosely distinguished through physical adsorption involving only relatively weak intermolecular forces and chemisorptions, involving essentially the formation of a chemical bound between the sorbate molecule and the surface adsorbent. However, these definitions are not unequivocal as there are many intermediate cases which describe the two different types of adsorption processes Table 2.9 (Ruthven 1984).

Table 2.9: Differences between physical and chemical adsorption

Physical adsorption	Chemical adsorptions
Low heat of adsorption < 40 KJ.mol^{-1}	High heat of adsorption > 100KJ.mol^{-1}
Non specific	High specific
Monolayer or multilayer	Monolayer
No dissociatation of adsorbed species	May involve dissociation
Only significant at relatively low temperatures	Possible over a wide range of temperature
Rapid, non-activated, reversible	Activated, may be slow and irreversible
No electron transfer although polarization of sorbate my occur	Electron transfer leading to bond formation between sorbate and surface

At a constant temperature, the dependence of θ on pressure or concentration at equilibrium may be plotted. The graphs that show these relationships are collectively known as isotherms. The Figure 2.18 has shown the Brunaure classification of isotherms (Ruthven 1984).

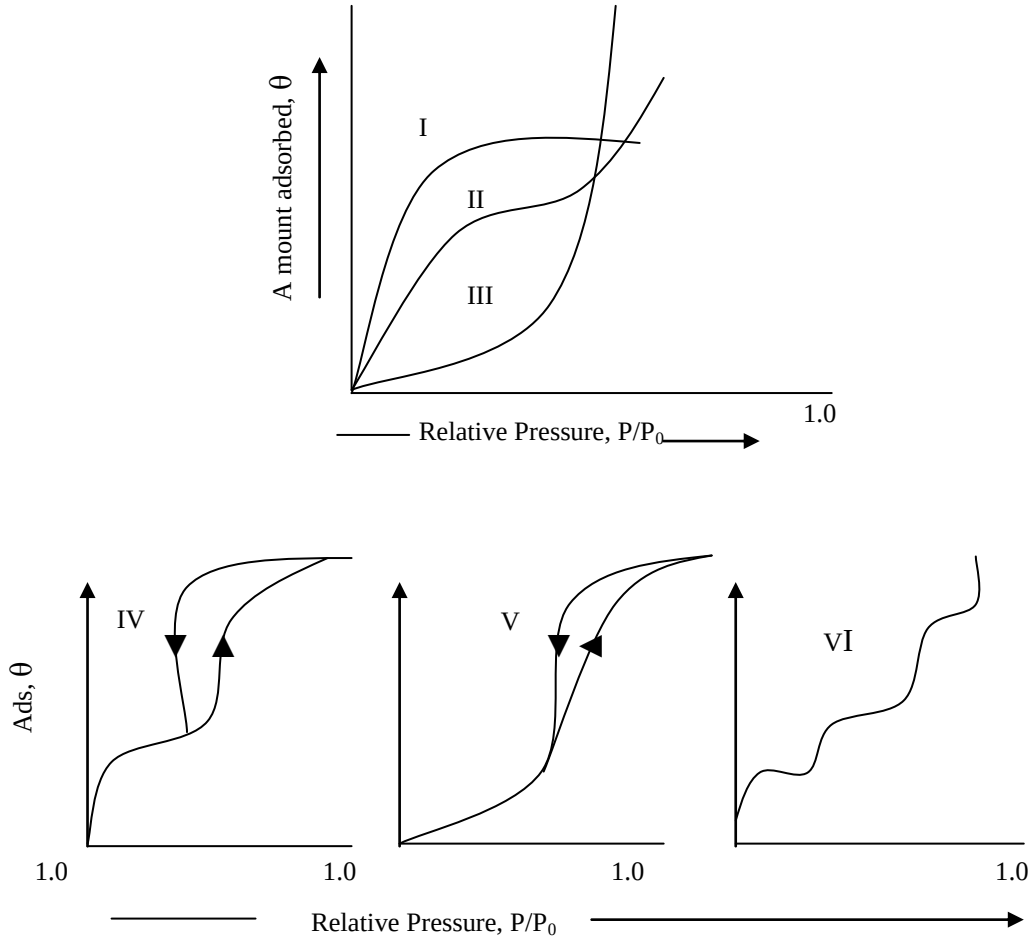

Figure 2.18: Brunauer classifications of isotherms

(I-V) (Ruthven 1984) and an additional stepped isotherm (VI) (Gregg and Sing 1982)

The types of solids that will exhibit isotherms of the type I-V may be characterised by the type of pores contained in the solid. A type VI isotherm may be observed by the adsorption of a gas on a non-porous solid, which has a uniform or near uniform surface (Gregg and Sing 1982).

2.8.2.2. Ozone adsorption

A few researchers have studied selective oxidation using adsorbed ozone (Cohen et al., 1975), (Avzyanova et al., 1996). However, a substantial amount of work has been carried out by infrared (IR) spectroscopy on the study of ozone adsorption onto various solids to establish the type of bonding involved in the system (Bulanin et al., 1994, 1995a, 1995b, 1997), (Thomas et al., 1997). (Mangnus and Grahling 1929) attempted quantifying the amount of ozone adsorption on silica gel at reduced temperatures (204 K to 224 K).To compensate for oxygen adsorption on the silica gel, they compared the results of oxygen adsorption isotherm on silica with that of the oxygen/ozone adsorption isotherm and by subtracting the two isotherm, they arrived at an isotherm for the adsorption of ozone onto silica gel. (Briner and Lachman 1943) carried out work initially on the oxidation of sulphur dioxide on the surface of silica gel using ozone. They also carried out work to quantify the amount of ozone adsorption, using potassium iodide to monitor ozone concentrations in di-oxygen and followed the adsorption of ozone by monitoring the weight increase of the gel. These authors suggest that partially dehydrated silica gel (5-7 % by weight moisture, achieved by heating silica gel at 200°C for 2 hours) increases the amount of ozone adsorption by the gel. Table 2.10 shows their results for ozone adsorption at various temperatures, (Briner and Lachmann 1943).

Table 2.10: Adsorption of ozone on silica gel

Temperature (°C)	0	0	-30	-45	-80	-80
Circulation time (h)	5	8	3.3	7	1.5	0.5
Amount of Silica (g)	18.1	18.1	18.1	1.46	1.96	1.46
Amount of O_3 adsorption (g)	0.073	0.12	0.11	0.12	0.11	0.05
Weight adsorption %	0.40	0.66	0.60	8.22	5.61	3.42
Q(mg/g)	4.03	6.6	6.0	82.2	56.1	34.2

The method which (Cook et al., 1959) implemented, to characterise the amount of ozone adsorbed, was achieved by passing a mixture of O_2/O_3 through a vessel immersed in a cooled bath containing silica gel until the outlet concentration of ozone equalled the input concentration of gas. At this point, the experiment was stopped and the adsorbed ozone was swept off the adsorbate with an inert gas into a solution of potassium iodide. The liberated iodine was then titrated with a standard sodium thiosulphate solution. Their results are shown in Table 2.11, (Cook et al., 1959).

Table 2.11: Adsorption of ozone on silica gel (* = partial pressure of ozone in oxygen)

Temperature (^{0}C)	Weight adsorption of ozone %	
	10.3 mmHg*	15.9 mmHg*
25.0	0.042	0.068
0.0	0.092	0.146
-10.0	0.13	0.21
-40.0	0.45	0.72
-78.5	3.0	4.5
-90.0	6.0	8.0

Tizaoui and Slater (2003) studied ozone adsorption on a range of materials using silica gel of a mean particle size of 1.5 mm. They established the process of mass transfer loading for ozonation treatment technique, which followed by water treatment. From their research, it was concluded that the estimated cost of ozone treatment was acceptable for wastewater in industrial plants.

Recently, (Tizaoui et al., 2007) investigated the degradation of reactive orange (RO16) and 2- chlorophenol using, ozone loading on silica gel in liquid/solid - ozone (LSO) system. They proved that this method was technically useful instead of conventional

method (LGO). In addition; they concluded that the LSO technically was producing a better performance for removal rates and ozone operation.

Ozone adsorption on anatase (TiO_2) was also studied by (Bulanin et al., 1995b) at three different stages of surface dehydration; 1) completely dehydrated, 2) evacuated at 300K, 3) evacuated at 773 K. Sites of varying Lewis acidity gave rise to four different types of ozone bonding mechanisms with TiO_2; 1) physical adsorption, 2) hydrogen bonding, 3) molecular adsorption via coordinative bonding to weak Lewis sites, 4) dissociative adsorption on interaction with strong Lewis acid sites, resulting in the formation of atomic oxygen. A Lewis acid may be described as a substance that will accept a pair of electrons; conversely a Lewis base is a substance that is able to donate a pair of electrons. (Bulanin et al., 1997) proposed that ozone adsorption on basic sites would reveal acidic properties of ozone and yield species different to those found on SiO_2 or on TiO_2. They found that ozone bonded weakly causing a shift in the hydroxyl wave number, different to the shift found in ozone adsorbed on silica or titanium oxides. They proposed a coordinative bond between the oxygen atom of the hydroxyl and the central atom of the ozone molecule Figure 2.19.

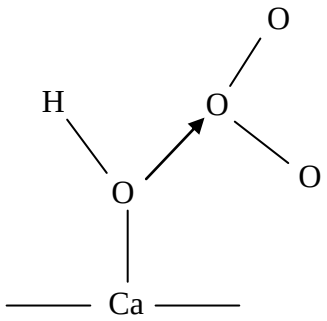

Figure 2.19: Coordinative bond of calcium oxide with ozone

(Thomas et al., 1997) shows that ozone decomposition occurs even at liquid nitrogen temperatures when alumina is subjected to ozone. The authors claim that the strong Lewis acid sites (Al^{+3}) are responsible for the catalytic decomposition of ozone. They

confirmed their hypothesis by selectively poising these strong Lewis acid sites with pyridine. When ozone was passed through the cell, they claimed that almost no oxygen was formed, indicating no catalytic decomposition of ozone.

2.8.2.3. Silica gel (SG)

Silica gel (Formula, SiO_2; molecular weight, 60.08; boiling point, 2230 °C; melting point, 1610°C) is used in various fields of our daily life as a high adsorbent of high safety. Silica gel (SG) has excellent adsorption capacities at low relative humidity for keeping materials dry. Current uses as desiccant include the following; pharmaceutical stoppers, laboratory desiccators, diagnostic and medical equipment, transformer tank breathers, drying flower, packaging during transportation and storage, gas drying and refining, as well as protection of the electronic and telecommunications equipment, photographic and optical equipment, engines, clothing and leather goods and food(especially dried seaweed). Other uses of silica gel are aromatics, gas absorbent, hydro gel and so on. Silica gel is a form of silicon dioxide, SiO_2; the material that occurs in nature as sand. The difference between silica gel and sand is that sand is a crystalline, non-porous form, whereas silica gel is a non-crystalline and highly porous form. Silica gel is an amorphous adsorptive substance with stable chemical properties and has a highly complicated porous structure. It is odourless, tasteless non-toxic and offers an excellent capacity for physical and chemical dehumidification because of its good absorbability, chemical stability, wide surface area and higher mechanical strength. Therefore, silica gel is used for packing food, pharmaceuticals, goods for export and precision instruments. Silica gel is easy to handle and silica gel saturated with moisture can be regenerated to afford new moisture protection by simply reheating under a specified condition. In the current study silica gel is used mostly in the study of ozone adsorption as it has been shown that it shows favorable adsorption

characteristics towards ozone (Magnus and Grahling 1929), (Edgar and Paneth 1941), (Briner and Lachmann 1943), (Cook et al., 1959). Silica gel is used along with activated alumina as a sorbent for drying because of its high surface areas and favourable surface properties. Silica gel is prepared by mixing a solution of sodium silicate (sometimes known as water glass) with a mineral acid such as sulphuric acid or hydrochloric acid. Equation 2.43 shows the reaction for the formation of silica hydrosol (silica acid).

$$Na_2SiO_3 + 2HCl + nH_2O \rightarrow 2NaCl + SiO_2 \bullet NH_2O + H_2O \quad (2.43)$$

Polymerisation occurs when the molecular weight of the hydrosol reaches about six million and on standing, produces a jelly-like precipitate; silica gel in its `raw` form. Silica concentration, temperature, pH and soluble additives affect the gelation time of the solution. At pH 7, the gelation is almost instantaneous. However, in dilute solution maximum stability occurs at pH2, with the longest set times for acid gelation occurring approximately at pH of 1.5. It is important to note that the sequence of adding either sodium silicate to a stirred acid (acid gelation) or the reverse (alkaline-set gelation) changes the effects of pH, temperature and silica concentration on silica gel produced. (Winyally 1984) discusses the differences in both types of gel. The gel is then washed, dried and activated before use. Amorphous silica consists of silica micelles in a random arrangement and these micelles may vary in size and arrangement or packing. The surface of these micelles in pure silica consists primorily of two groups, either silanol (SiOH) or siloxane (Si-O-Si). Silica is manufactured as either regular density silica or low-density silica. However, the densities are the same. The main differences are shown in Table 2.12, (Winyally 1984).

Table 2.12: Different between regular and low-density silica gel

Silica	Surface area ($m^2.g^{-1}$)	Pore volume ($m1 . g^{-1}$)	Average pore diameter Å (Angstroms)
Regular Density	600 – 900	0.35 – 042	22 – 26
Low Density	255 – 375	1.05 – 1.30	100 -150

Regeneration of silica may be achieved by heating. The temperature to which the gel is heated may affect its re-use, as activation at 200 °C, removes adsorbed water but very few silanol groups. If activation temperatures are kept below 450 °C the two silanol can be regenerated from each siloxane (created by activation) by re-hydration. If the temperatures exceed 450°C, siloxane bond formation is extensive and the regeneration of silanol groups is irreversible (Winyall 1984, Yang 1987).

2.8.2.4. Zeolite

Zeolites are widely used as ion-exchange beds in domestic and commercial water purification, softening and other applications. ZSM-5, a zeolite used in this study, is a typical high silica zeolite with MFI-type structure, which makes ZSM-5 widely useful as catalysts in petroleum and petrochemical industry. ZSM-5 type is a zeolite with high silica to alumina ratio. The substitution of an aluminium ion (charge 3^+) for a silicon ion (charge 4^+) requires the additional presence of a proton. This additional proton gives the zeolite a high level of acidity, which causes its activity. ZSM-5 is a highly porous material and throughout its make-up, it has an intersecting two-dimensional pore structure (Fujita et al., 2004a).

In recent years, the application of ZSM-5 is expanding into the synthesis fields of speciality and fine chemicals (Davis 1998), such as the preparation of ethylene amines. The excellent catalytic performance of ZSM-5 was noted by (Hua and Hu 2001). In most cases, the synthesis of ZSM-5 is achieved by hydrothermal synthesis. The crystallization process and final product are sensitively dependent on the composition of source materials, temperature, time, template agents and other initial conditions of the reaction system. As the crystallisation time is relatively long (usually over 3 days), the rapid synthesis of ZSM-5 zeolite in a system containing simple amines holds researchers' interests (Hu et al., 2001), (Liu and Xiang 2001). In order to prepare

ZSM-5 for amination of ethanolamine, the authors investigated the effect of pre-treatment of silicate source and alkalinity on synthesis of ZSM-5 zeolite, and found a new method with which the crystallization time in ethylenediamine-containing system was shortened greatly.

2.8.2.4.1. Adsorbent characterisation

Surface area

Surface area is an important property for many types of advanced materials such as nanomaterials, pharmaceutical materials, powder metallurgy materials, battery active materials, fibres, pigments, thermal spray powders, minerals and additives. BET stands for Brunauer, Emmett and Teller, the three scientists who optimized the theory for measuring surface area. Clear Science has the capability to measure surface area by the BET method and the Langmuir surface area method. In addition, the BET surface area instrument can also be used to determine other information such as gas uptake, micropore volume (t-plot method) and pore size distribution via adsorption and desorption isotherms (BET Therory-wikipedia 2008).

BET theory is a rule for the physical adsorption of gas molecules on a solid surface and serves as the basis for an important analysis technique for the measurement of the specific surface area of a material. In 1938, Stephen Brunauer, Paul Hugh Emmett and Edward Teller published an article about the BET theory in a journal for the first time; "BET" consists of the first initials of their family names. The concept of the theory is an extension of the Langmuir theory, which is a theory for monolayer molecular adsorption, to multilayer adsorption with the following hypotheses: (a) gas molecules physically adsorb on a solid in layers infinitely; (b) there is no interaction between each

adsorption layer; (c) the Langmuir theory can be applied to each layer. The resulting BET equation is expressed by Equation 2.44 (BET Theory-Wikipedia 2008).

$$\frac{1}{z\left[\left(P_0/P\right)-1\right]}=\frac{x-1}{z_m x}\left(\frac{P}{P_0}\right)+\frac{1}{z_m x} \tag{2.44}$$

P and P_0 are the equilibrium and the saturation pressure of adsorbate at the temperature of adsorption; z is the adsorbed gas quantity (for example, in volume units); z_m is the monolayer adsorbed gas quantity; x is the BET constant, which is expressed by Equation 2.45.

$$x=\exp\left(\frac{H_1-H_L}{RT}\right) \tag{2.45}$$

H_1 is the heat of adsorption for the first layer; H_L is that for the second and higher layers and is equal to the heat of liquefaction.

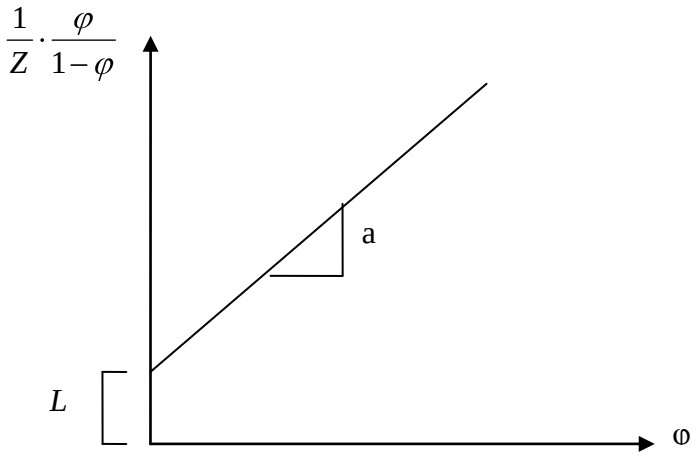

Figure 2.20: BET plot

Equation 2.44 is an adsorption isotherm and can be plotted as a straight line with $1 / z[(P_0 / P) - 1]$ on the y-axis and $\varphi = P / P_0$ on the x-axis according to experimental results. This plot is called a BET plot. The linear relationship of this equation is maintained only in the range of $0.05 < P / P_0 < 0.35$. The value of the slope a and the

y-intercept I of the line are used to calculate the monolayer adsorbed gas quantity z_m and the BET constant x. The following equations can be used:

$$z_m = \frac{1}{a + i} \tag{2.46}$$

$$x = 1 + \frac{a}{i} \tag{2.47}$$

The BET method is widely used in surface science for the calculation of surface areas of solids by physical adsorption of gas molecules. A total surface area S_{total} and a specific surface area S are evaluated by the following equations:

$$S_{BET,total} = \frac{\text{[illegible]}_m N_\delta}{Z} \tag{2.48}$$

$$S_{BET} = \frac{S_{total}}{e} \tag{2.49}$$

Where: N is Avogadro's number; S is adsorption cross section; Z is molar volume of adsorbent gas; e is molar weight of adsorbed species (BET Theory-Wikipedia 2008).

CHAPTER 3: MODELLING AND REACTION KINETICS

3.1. General

In this chapter, the modelling of experimental data and the reaction kinetics of ozone with water and organic compounds are described.

3.2. Mass transfer Coefficient (k_La)

3.2.1. Modelling of mass transfer

Double film theory was used in this work to describe the gas/liquid mass transfer. The reactor was a glass semi-batch type reactor. The reactor can be represented by Figure 3.1 (Lewis and Whitman 1924):

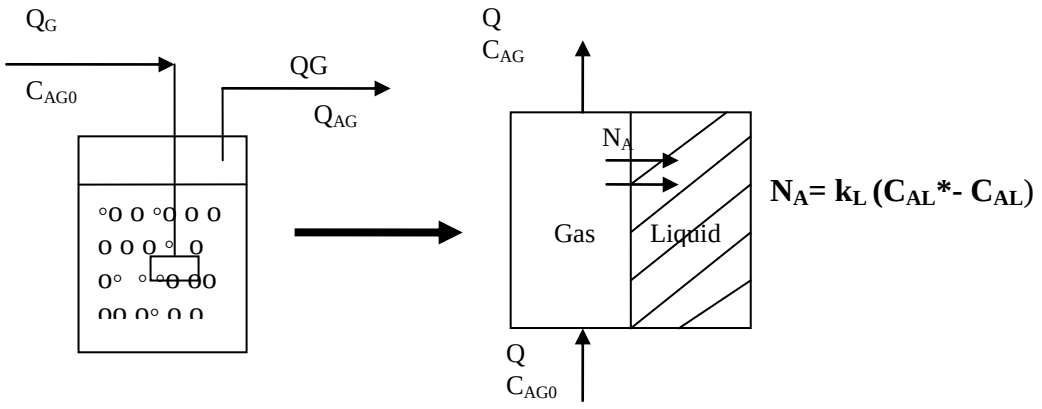

Figure 3.1: Semi -batch gas/liquid reactor

3.2.1.1. Oxygen absorption

The governing equations for oxygen absorption in water were deserved from mass balance equations coupled with physical absorption equation for a gas in a liquid. The mass balance in liquid phase was integrated by the following equations (Lewis and Whitman 1924):

Mass balance over the liquid phase

$$k_L a(C_{AL}^* - C_{AL})V_L = \frac{dc_{AL}}{dt}V_L \qquad (3.1)$$

$$\frac{dC_{AL}}{dt} = k_L a \left(C_{AL}^{*} - C_{AL}\right) \tag{3.2}$$

$$\int_{C_{AL0}}^{C_{AL}} \frac{dC_{AL}}{C_{AL} - C^{*}_{AL}} = \int_{0}^{t} k_L a \; dt \tag{3.3}$$

$$\int_{C_{AL0}}^{C_{AL}} \frac{dC_{AL}}{C_{AL}^{*} - C_{AL}} = -k_L a \; dt \tag{3.4}$$

$$\ln\left(\frac{C_{AL} - C_{AL}^{*}}{C_{AL0} - C_{AL}^{*}}\right) = -k_L a \; t \tag{3.5}$$

$$\frac{C_{AL} - C_{AL}^{*}}{C_{AL0} - C_{AL}^{*}} = \exp\left(-k_L a \; t\right) \tag{3.6}$$

$$C_{AL} = C_{AL}^{*} + \left(C_{AL0} - C_{AL}^{*}\right)\exp\left(-k_L a \; t\right) \tag{3.7}$$

Where: C_{AL0} is the initial liquid concentration; C_{AL}* the saturation liquid concentration; k_La the volumetric mass transfer coefficient. Experimental data were then fitted with the model using the least square method and the solver tool available in Microsoft office Excel spreadsheet. Values for k_La and C_{AL}* were then determined. It is noteworthy that a plot of $\ln\left(\frac{C_{AL} - C_{AL}^{*}}{C_{AL0} - C_{AL}^{*}}\right)$ as function of time would give a straight line of slope-k_La (Lewis and Whitman 1924).

3.2.1.2. Ozone absorption

When ozone is absorbed into water, it undergoes a slow decomposition reaction assumed of first order in this work. The mass balance for ozone absorption on the liquid phase can then be written as follows:

$$k_L a V_L \left(C_{AL}^{*} - C_{AL}\right) = V_L \frac{dC_{AL}}{dt} + V_L \; k_d C_{AL} \tag{3.8}$$

$$k_L a C_{AL}^{*} - \left(k_L a + k_d\right) C_{AL} = \frac{dC_{AL}}{dt} \tag{3.9}$$

$$\frac{dC_{AL}}{dt} = -(k_L a + k_d)\left(C_{AL} - \frac{k_L a}{k_L a + k_d} C_{AL}^{*}\right) \tag{3.10}$$

Assume that:

$$K = k_L a + k_d \text{ and, } \alpha = \frac{k_L a}{k_L a + k_d} C_{AL}^{*}$$

Equation 3.10 can be rewritten as:

$$\frac{dC_{AL}}{dt} = -K(C_{AL} - \alpha) \tag{3.11}$$

$$\int_{C_{AL0}}^{C_{AL}} \frac{dC_{AL}}{C_{AL} - \alpha} = \int_{0}^{t} -K\, dt \tag{3.12}$$

$$\ln \frac{C_{AL} - \alpha}{C_{AL0} - \alpha} = -K\, t \tag{3.13}$$

If $C_{AL0} = 0$

$$\frac{C_{AL} - \alpha}{-\alpha} = \exp(-K\, t) \tag{3.14}$$

$$C_{AL} = \alpha(-\exp(-K\, t)) \tag{3.15}$$

or can be rewritten as:

$$C_{AL} = \frac{k_L a}{K} C_{AL}^{*}(1 - \exp(-K\, t)) \tag{3.16}$$

Where: k_d is the rate constant of ozone decomposition; $K = k_L a + k_d$, k_d was determined from a separate experimental study; C_{AL}^{*} was determined from the equation presented in Section (5.4.2) Chapter 5 (Lewis and Whitman 1924).

3.3. Models used for the Determination of Stoichiometry and Rate Constant

3.3.1. Stoichiometry

The direct reaction of ozone with a compound can be expressed by the following equation:

$$A + zB \rightarrow products \quad (3.17)$$

The stoichiometric ratio, z, was determined in a homogeneous system by measuring the change of concentration of compound (B) in excess of ozone (10-20 times) after reaction with a given initial concentration of ozone (A). Assuming the volume of the initial ozone solution is V_A at concentration C_A, the volume of the solution of compound B is V_B at a concentration C_{B0} and the final concentration of compound B after complete reaction is C_{Bf}, the stoichiometric ratio is then calculated by Equation 3.18, (Hoigne and Bader 1983).

$$z = \frac{n(B)_{initial}\, mol - n(B)_{final}\, mol}{n(A)_{initial}\, mol} = \frac{C_{B0}V_B - C_{Bf}(V_B + V_A)}{C_A V_A} \quad (3.18)$$

Where: A is the ozone molecule; B the compound (RO16 or triclocarban or naphthalene or methanol); z is the stoichiometric ratio; n is number of moles.

3.3.2. Rate constant

Three methods are tested to determine the rate constant of compound B with molecular ozone ($k_{B/A}$). The methods are: ozone bubbling; heterogeneous competitive kinetic; homogenous kinetics. The rate constant of compound (B) with molecular ozone can be expressed by the following equation:

$$-\frac{d[B]}{dt} = k_{B/A}[A][B] \quad (3.19)$$

In order to determine $k_{B/O3}$, all experiments were conducted at pH 2. Under this pH it is assumed that no radical chain reactions occur and the only oxidant is molecular ozone. The reaction equation can be solved by the integration below: (Hoigne and Bader 1983).

$$Ln\left(\frac{[B]_t}{[B]_0}\right) = -k_{B/A}\int_0^t [A]\,dt \quad (3.20)$$

Where: $k_{B/A}$ is the reaction rate constant for compound B degradation by ozone.

3.3.2.1. Heterogeneous (ozone bubbling in the solution of compound B)

In this experiment, ozone gas was bubbled in solution of compound B at different concentrations as described in ozonation experiments for each compound. The following model was used to calculate the rate constant assuming fast reaction between ozone A and the compound of intcest B. The double film theory suggests that for a second order reaction and with the assumption of fast regime, the change of the concentration of B is given by Equation 3.22. Integrating of Equation 3.22 yields Equation 3.23: (Hoigne and Bader 1983).

$$A + zB \xrightarrow{k} products \tag{3.21}$$

$$-\frac{dC_B}{dt} = C_{AL}^{*} a_L z \sqrt{kD_A C_B} \tag{3.22}$$

$$C_{B0}^{0.5} - C_B^{0.5} = z\frac{\sqrt{kD_A}a_L C_{AL}^{*}}{2}t \tag{3.23}$$

A plot of the left hand side of Equation 3.23 as function of time would lead to a straight line with a slope (s) given by:

$$s = z\frac{\sqrt{kD_A}a_L C_{AL}^{*}}{2} \tag{3.24}$$

From the slope, the rate constant k can be determined if the other parameters are known.

$$k = \frac{1}{D_A}\left(\frac{2\times s}{z\ a_L C_{AL}^{*}}\right)^2 \tag{3.25}$$

Where: z is stoichiometry factor of compound (B); D_A is diffusivity of ozone 1.74×10^{-9} m^2s^{-1} (Roustan et., 1987); Johnson and (Davis 1996); a_L specific surface area (m^2/m^3); C_{B0}, C_B are initial and final concentrations (mol/L) of B respectively. In Equation 3.24, all parameters for computation of k are known except a_L. Experiments were carried out to determine a_L in the liquid /gas- reactor used in this study. The

method involved bubbling ozone in a solution of indigo. The change of indigo concentration can also be described by Equation 3.23, in which k represents the rate constant of ozone reaction with indigo, which has value of 9.4×10^7 $m^{-1}s^{-1}$; a_L is determined using Equation 3.26.

$$a_L = \frac{2s}{z\ C_{AL}^{*}\sqrt{k_{indigo/O3}D_A}} \tag{3.26}$$

3.3.2.2. Heterogeneous competitive kinetics

The heterogeneous competitive kinetics system consists of bubbling ozone (A) in a solution containing two compounds B_1 and B_2. The reaction between ozone and one of the two compounds (e.g. B_1) is known and the values of its rate constant, k_1, and stoichiometry, z_1, are known. The rate constant of B_2 using this method can be calculated using the following Equations: (Hoigne and Bader 1983).

$$A + z_1 B_1 \xrightarrow{k_1} products_1 \tag{3.31}$$

$$r_{A_1} = -\frac{dC_{B1}}{dt} = k_1 C_A C_{B1} = -\frac{1}{z_1}\frac{dC_{B1}}{dt} \tag{3.32}$$

$$\frac{dC_{B_1}}{dt} = -z_1 k_1 C_A C_{B_1} \tag{3.33}$$

$$A + z_2 B_2 \xrightarrow{k_2} products_2$$

(3.34) $$r_{A_2} = -\frac{dC_{B2}}{dt} = k_2 C_A C_{B2} = -\frac{1}{z_2}\frac{dC_{B2}}{dt} \tag{3.35}$$

$$\frac{dC_{B_2}}{dt} = -z_2 k_2 C_A C_{B_2} \tag{3.36}$$

By dividing Equation 3.33/3.36

$$\frac{\frac{dC_{B_1}}{dt}}{\frac{dC_{B_2}}{dt}} = \frac{z_1 k_1}{z_2 k_2}\left(\frac{C_{B_1}}{C_{B_2}}\right) \tag{3.37}$$

From Equation 3.37, the change of the left hand side of the equation as function of C_{B1}/C_{B2} would lead to a straight line of slope z_1k_1/z_2k_2. However, the calculation of the

derivatives in the left hand side of the equation was tedious and Equation 3.38 derived from Equation 3.23 was used instead. The use of Equation 3.23 is valid here as we assume that fast regime prevails.

$$C_{B_1}{}^{0.5} - C_{B_{0_1}}{}^{0.5} = \left(\frac{z_1}{z_2} \sqrt{\frac{k_1}{k_2}} \right) \left(C_{B_2}{}^{0.5} - C_{B_{0_2}}{}^{0.5} \right) \tag{3.38}$$

A plot of the left hand side of Equation 3.38 (i.e. $C_{B_1}{}^{0.5} - C_{B_{0_1}}{}^{0.5}$) as function of ($C_{B_2}{}^{0.5} - C_{B_{0_2}}{}^{0.5}$) would lead to a straight line of slope s given by $s = \frac{z_1}{z_2} \sqrt{\frac{k_1}{k_2}}$.

From this equation the rate constant of the ozone reaction with compound B_2 can then be calculated by the following equation:

$$k_2 = \left(\frac{z_1}{s z_2} \right)^2 k_1 \tag{3.39}$$

Where: z_1 is the stoichiometric ratio of compound B_1; k_1 is the rate constant of the reaction ozone with compound B_1; z_2 is stoichiometric ratio of compound B_2 (either known or can be determined by the method presented in 3.3.1).

3.3.2.3. Homogenous kinetics

In this method, ozone mother solution was prepared by bubbling ozone gas in deionised water until saturation then a solution of compound (B) of known concentration and volume was injected by a syringe into the ozone solution. The content of the reactor was mixed very well. The rate constant (k) of B can be calculated as discussed below.

$$A + zB \rightarrow \text{Products} \tag{3.40}$$

$$\frac{dC_B}{dt} = -k C_A C_B \tag{3.41}$$

$$= -k \left[C_{A0} - \frac{C_{B0} - C_B}{z} \right] C_B \tag{3.42}$$

Integration of Equation 3.41 leads to:

$$C_B = \frac{\left(C_{A0}C_{B0} - C_{B0}^{\,2}\right)\exp\left(-zk\left(C_{A0} - \frac{C_{B0}}{z}\right)t\right)}{zC_{A0} - C_{B0}\exp\left(-zk\left(C_{A0} - \frac{C_{B0}}{z}\right)t\right)} \tag{3.43}$$

Where: C_{A0} is initial ozone concentration in liquid (mol/L); C_{B0}, C_{Bf} are initial and final concentration of B (mol/L) respectively; z is stoichiometric ratio. The rate constant k can be determined by best fitting experimental data to Equation 3.43, which was developed by (Tizaoui, un-published, University of Bradford 2008).

3.4. Modelling used for Liquid/Solid-Ozone (LSO)

Ozone adsorption (gas phase)

The mathematical model used to describe ozone adsorption on the fixed bed reactor was given in (Tizaoui and Slater 2003):

$$\frac{C_{AG}}{C_{AG_0}} = 0.5\left(1 - erf\left(\frac{1}{2}N_p^{0.5} - \frac{1}{2}\left(N_p\tau\right)^{0.5}\right)\right) \tag{3.44}$$

$$\text{Where } \tau = \frac{t - \frac{L}{u}}{K_{vb}\frac{1-\varepsilon}{\varepsilon}\frac{L}{u}} \tag{3.45}$$

$$\text{and } N_p = \frac{60(1-\varepsilon)LK_{vb}}{d_p^2\,\varepsilon\,u}D_e \tag{3.46}$$

Where: C_{AG} is ozone concentration in gas exiting bed at any time (g/m^3) NTP; C_{AG0} ozone concentration in feed gas (g/m^3) NTP; N_P is number of particle mass transfer units, τ is dimensionless time; De Effective ozone diffusivity in the adsorbent (m^2/s); L total packed bed length (m); d_p average particle diameter (m); K_{vp} equilibrium constant based on particle volume; u gas interstitial velocity (m/s); ε is bed voidage.

Ozone desorption by a liquid flow

A simple equation was used to model ozone desorption from the fixed bed reactor which is given by:

$$\frac{C_{ALout}}{C_{AL0}} = \exp(-K_{des}t) \tag{3.47}$$

Where: $C_{AL0,}$ C_{ALout} are initial and final concentration of ozone (mol/L) respectively; K_{des} is an effective desorption rate constant; t is time

Ozone adsorption isotherms

Ozone adsorption isotherms were described by the two well known Langmuir and Freundlich models which are described below.

Langmuir:

The relationship between the adsorbent equilibrium capacity, q, and the fluid concentration, C, is given by Equation 3.48. The parameters A and B can be determined by plotting 1/q as function of 1/C Equation 3.49.

$$q = \frac{AC}{1+BC} \tag{3.48}$$

$$\frac{1}{q} = \frac{1}{AC} + B \tag{3.49}$$

Where: q is adsorbent capacity at equilibrium (mg/g); C is the compound concentration (mg/L); A and B are two constants.

Freundlich:

Equation 3.50 gives the Freundlich relationship between the equilibrium capacity, q, and the fluid concentration, C. The parameters k and n can be determined by plotting Ln(q) as function of Ln(C) Equation 3.51.

$$q = kc^{\frac{1}{n}} \tag{3.50}$$

$$\ln(q) = \ln(k) + \frac{1}{n}\ln(c) \tag{3.51}$$

CHAPTER 4: MATERIALS AND EXPERIMENTAL METHODS

4.1. General

In this chapter, the materials and methods used for the study are described. The instruments used for the studies are also described.

4.2. Materials

Oxygen (O_2) of high purity (> 99 %) was used in all experiments to feed the ozone generator. Pure oxygen was purchased from BOC. Polytetrafluoroethylene (PTFE) tube of OD 3.18 mm x ID 1.6 mm (1/18″ x 1/16″) was used for connecting the system. The gas diffuser type used in all experiments is fritted glass of Grade 1 as shown in Appendix A3 (Figure 19). A bubble column glass was used as the ozone reactor having holding capacity of 1000 mL but 500 mL of the volume was used in this work (Figure 4.1). Thermocouple was fitted to the reactor for the purpose of measuring the solution temperature. A Manometer model R200 UL (Digitron, England) was used for measuring gas pressure. General laboratory glassware was used in this work. Chemicals utilised in this research work include HPLC grade acetonitrile (99 %), methanol (CH_3OH) (99 %) obtained from Fisher Scientific UK Ltd, dye reactive orange (RO16): $C_{12}H_{19}O_{11}S_3.2Na$ (617.54 AMU)(Sigma Aldrich), triclocarban ($C_{13}H_9Cl_3N_2O$) and naphthalene ($C_{10}H_8$) were purchased from Sigma Aldrich, all solutions were prepared with deionised water as described in Section (4.3.).

Stock pH 2 buffer solution was obtained by dissolving 10 g of analytical grade NaH_2PO_4 and 7 mL analytical grade H_3PO_4 (85 %) in 1L Milli-Q pure water (Xiong and Graham 1992). Stock buffer solutions of higher pH ranging from 7 to 9 were prepared by appropriate quantities of 2 M sodium hydroxide solution to the stock pH 2 buffer solution. Concentrated phosphoric acid H_3PO_4 (85 %), potassium indigo trisulfonate:

$C_{16}H_7N_2O_{11}S_3K_3$ and sodium dihydrogen phosphate NaH_2PO_4 were used to prepare the indigo reagent for ozone analysis. t-butanol: $C_4H_{16}O$ was used as radical scavenger. Two types of ozone adsorbents (silica gel and a zeolite D915) were also used in this work to study the performance of the LSO system.

Figure 4.1: Reactor of ozone experiments

4.3. Preparation of Samples

4.3.1. Water samples

Deionised water of pH between of 5.5-6.5 was used to prepare all solutions that were used in this work. This water was produced from Millipore- Direct- Q 3 System as shown in Appendix A3 (Figure 10). It has been used to produce water quality that has (Resistivity 18.2 MΩ, Conductivity 0.056 µS/cm at 25 °C). The equipment has a water storage tank of 6 L, a production capacity of 3-4 L/h and the drain capacity of this equipment is 30 L/h. A water pre-filtration unit was fitted at the inlet of the equipment to remove any suspended solids in the feed tap water. 500 mL of deionised water was used as a sample to make experiments for ozone reactions.

4.3.2. Dye samples

The dye samples were prepared by dissolving the dye in deionised water. The concentrations of samples were 25, 50, 75 and 100 mg/L. In order to prepare dye solutions, calculations were made to arrive at the mass of dye needed to make a solution at a given concentration. The following steps show the calculation was made to prepare 500 mL of solution with 100 mg/L concentration of dye:

Concentration = Mass (M) / Volume (V)

Mass = Concentration x Volume. The Mass = 100 x 0.5 = 50 mg.

The next step was to weigh 50 mg of dye using the analytical scale (Mettler, AE 200, precision 00.0001). The dye was transferred to a volumetric flask. Then 500 mL of deionised water was poured slowly into the volumetric flask. It is worth mentioning here that special care was taken to prepare accurate concentrations of the dye solutions.

4.3.3. Triclocarban samples

Since the solubility of TCC is very low in water (~ < 2 mg/L) (Chun-Yu Chiu et al., 2007), a mixture of 70 % acetonitrile and 30% Milli-Q high purity water (> 18 MΩ cm) was prepared for dissolving the TCC. TCC was initially dissolved in pure acetonitrile to prepare a stock solution at 1 g/L. Solutions at desired concentrations were prepared by diluting a given volume of the stock solution with 70 % acetonitrile + 30 % water.

4.3.4. Naphthalene samples

Because naphthalene also has low solubility in water (less than 3 mg/L) (Chun-Yu Chiu et al., 2007), a mixture of 50 % methanol and 50 % water was used to prepare the naphthalene solutions.

4.3.5. Methanol samples

Since methanol is a miscible compound in all proportions, the solutions of methanol at 0.2 to 5 mol/L were prepared by directly mixing pure methanol with water. It was

assumed that the final volume of the solution equals to the sum of water volume and methanol volume. The concentration of methanol in mol/L was calculated by Equation 4.2 which was derived from Equation 4.1:

$$C_M = \frac{m}{v} = \frac{m_M}{V_W + V_M} = \frac{m_M}{M_M (V_M + V_W)} = \frac{\rho_M \times V_M}{M_M (V_M + V_W)} \qquad (4.1)$$

Knowing that the density (ρ) of methanol is 791 g/L and its molecular mass (M_M) is 32 g/mol.

$$C_M = \frac{791}{32}\left(\frac{V_M}{V_M + V_W}\right) \qquad \text{in mol/L} \qquad (4.2)$$

4.4. Equipment

The ozone generator used in this work is Triogen, LAB2B laboratory ozone generator and PC/ 230 V-1 PH-50 HZ, as shown in Appendix A3 (Figure 2). The generator can produce ozone either from dry air or oxygen operating at either negative or positive pressure. The maximum ozone production of the generator is 10 g/h at flow rate 2-5 L/min feed gas (100% oxygen) and pressure of 0.7 bar (max), whereas ozone production drops to 4.0 g/h at flow rate 4-10 L/min feed gas (dry air at 60 °C dew point) and pressure 0.7 bar (max). The ozone variable output control is 15-100 %. The ozone analyser type (BMT963) was used to measure the ozone concentration in the gas phase. The instrument electronics compensate for temperature and pressure and displays ozone concentration in g/m^3 NTP (NTP: $0^{\circ}C$ and 1 atm). The pH meter (Inolab, Terminal level 3, WTW) and conductivity meter (Omega, CDB-92) were used in this study see Appendix A3 (Figure 7 and 8) respectively.

4.5. Analysis Techniques

4.5.1. Ozone analysis in gas phase

Once ozone gas is generated from pure oxygen by (Lab2b Laboratory ozone generator), the ozone concentration in output gas of ozone generator is measured by the ozone analyser (BMT963VNT g/Nm^3, 0^{o}C and 1 atm). Dasylab software was used to collect the data provided by the gas analyser at 2 sampling rate. The data was converted to Excel spreadsheet format and processed using in house written Excel macros.

4.5.1. Ozone analysis in liquid phase

In this work, two methods were used to determine ozone concentration in liquid phase. They are the standard indigo method developed by (Hoigne and Bader 1982) and the spectrophotometric method as described below.

a. Indigo method

Ozone concentration in water was determined using the indigo method (Standard method 4500-Ozone 1998). The indigo trisulfonate method is quantitative and selective. The indigo method presumes use of high-quality indigo trisulfonate. The principle of this method is that in acidic solution, ozone rapidly decolorizes indigo. The decrease in absorbance is linear with increasing concentration over a wide range. The proportionality constant at 600 nm is 0.42 ± 0.01cm^{-1}mg^{-1} L ($\Delta\varepsilon$ =20,000 M^{-1}cm^{-1}). A stock solution of indigo is made up with 770 mg potassium indigo trisulfonate, $C_{16}H_7N_2O_{11}S_3K_3$, which has a molecular mass of 616.74 gmol^{-1}, giving a molar concentration of (1.248x10^{-3} M). A 1:100 dilution exhibits an absorbance of approximately 0.20± 0.01cm^{-1} at 600 nm. In the event of absorbance lowering of a (1:100 dilution) falls below 0.16 cm^{-1}, the stock solution should not be used. The stock solution is stable for about 4 months when stored in dark place. Reagent II is a 10:1 dilution of stock solution and is used to measure ozone concentration greater than

0.1 mgL^{-1}. Reagent II includes chemicals to prolong stability, namely 10 g sodium dihydrogen phosphate (NaH_2PO_4) and 7 mL concentrated phosphoric acid in 1000 mL of deionised water. This solution should be prepared fresh when its absorbance decreases to less than 80% of its initial value (Typically within a week). Reagent II solution is designated as the blank solution and has a molar concentration of $1.248x10^{-4}$ M. The absorbance measurements are preferably carried out in 4 or 5 cm cuvettes. (Gordon et al., 2000a, 2000b) provide additional details of indigo method; the method is based on a change in absorbance (600 nm wavelength) of the indigo between the unreacted blank solution and an ozone-reacted sample solution. The ozone concentration can be calculated using Equation 4.3.

$$CO_3 (mg/L) = \frac{(Abs_B \times V_B - Abs_A \times (V_B + V_A))}{f \times b \times V_A} \quad (4.3)$$

Where: Abs_B is absorbance of indigo stock solution (blank solution); V_B is volume of indigo blank solution; mL, Abs_A is absorbance of the mixture sample + indigo solution; V_A is volume of sample (V_{O3}) mL; f is sensitivity coefficient of 0.42 $mg^{-1}cm^{-1}$ L; b is path length of cell, cm. (1cm and 5 cm cells were used in this work). The molar absorbance of indigo solution can be determined using Equation 4.4. Gordon and co-workers (Gordon et al., 2000a) measured molar absorbance for seven indigo trisulfonate product samples and found ε to vary from 15,800 to 20,355 M^{-1} cm^{-1}.

$$\varepsilon = \frac{Abs}{M} \quad (4.4)$$

Where: Abs is absorbance cm^{-1}; ε is Molar absorbance M^{-1} cm^{-1}; M is Molar concentration, mol/L. In this work, the molar absorbance for the indigo solution was found to be within the molar absorbance specification, which is 20,000 M^{-1} cm^{-1}.

b. Spectrophotometric method

The indigo method can be tedious to apply. The spectrophotometric method, which is simple, was thus used in this work to measure ozone concentration in "pure" water. The maximum absorption of ozone occurs at 262 nm as shown in Figure 4.2, which is in agreement with literature. Using the Beer Lambert law (Equation 4.5), ozone concentration in liquid can be calculated by knowing the Abs_{262}.

$$Abs = \varepsilon LC \tag{4.5}$$

$$C(mol/L) = \frac{Abs}{\varepsilon L} \tag{4.6}$$

$$CO_3(mg/L) = \frac{48 \times 1000 \times Abs_{262}}{2900 \times L} \tag{4.7}$$

Where: Abs is (absorbance at 262 nm; ε is Molar absorbance that was taken equal 2900 M^{-1} cm^{-1}; C is concentration mol/L); L is path length of cell cm. A UV/Vis spectrophotometer Agilent HP8453 was used to measure the absorbance of ozone solutions in pure water.

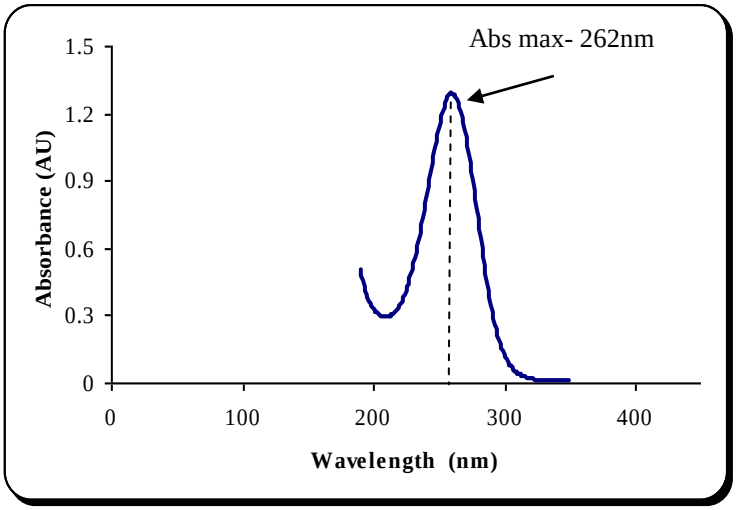

Figure 4.2: Full spectrum of ozone at 262nm

4.5.2. UV/VIS Spectroscopy

The UV/Vis spectroscopy was used to measure the absorbance of light of a chemical at given wavelength. The value of the absorbance is proportional to the chemical concentration (Beer Lambert law), thus concentrations may be measured through

absorbance measurement and a calibration curve. In this study, a diode array Agilent 8453 UV-visible Spectrophotometer (190 to 1100 nm) was used. It is fitted with a general purpose Agilent ChemStation software for UV-visible spectroscopy running on PC with the supported Microsoft operating system. These two components are linked together by a network connection. All of the data display, evaluation and long-term storage are done under software control on the PC.

4.5.3. High-performance liquid chromatography (HPLC)

HPLC is a separation technique which has the facility to separate highly complex mixtures. HPLC (Waters 2695) with UV detection (Waters 2487 Dual λ) was used in this work to analyse triclocarban and naphthalene. The mobile phase used for triclocarban analysis was 70 % acetonitrile + 30% water mixture and for naphthalene was 75 % methanol + 25 % water. The sample was injected at one end of the column (C18 Hypersil Gold column (150 × 4.6 mm, 5 μm - Thermo Scientific) and carried through the column by a continuous flow of the mobile phase.

The principle of HPLC is that a liquid mobile phase transports a sample through a column containing a liquid stationary phase. The interaction of the sample with the stationary phase selectively retains individual compounds and permits separation of sample components. Detection of the separated sample compounds is achieved mainly through the use of absorbance detectors for organic compounds and through conductivity and electrochemical detectors for metal and inorganic components (R.M.Smith 1988).

$$A_{mobile} \leftrightarrow A_{stationary}$$

Equilibrium constant $$K = \frac{[A]_{stationary}}{[A]_{mobile}} \quad (4.8)$$

The chromatogram is a record of the detector response as function of time and indicates each separate eluted component as peak. In quantitative measurement, the area under these peaks is directly proportional to the amount of sample. With the integrator calculating the area under each peak, a calibration plot can be achieved by measuring the different areas of the same compound at different concentrations (R.M. Smith 1988).

4.5.4. Gas chromatograph (GC/FID)

GC/FID, type (PYE, UNICAM, PU 4500 gas chromatograph) was used in this work for the analysis of methanol in water. The column used in this work was a 104-Polyethylene glycol (PEG) column installed in an oven with the inlet attached to a heated injector block and the outlet attached to a Flame Ionisation Detector (FID). The carrier gas used in this work was nitrogen (1 mL/min flow rate, column length was 1.524 m, oven temperature 250 °C injector temperature 130 °C and column (initial and final) temperature 95 °C). The injection volume of methanol sample was 1µL.

The principle of gas chromatography is that the mobile phase is a carrier gas and a stationary phase is a liquid. For packed columns, the stationary phase is a liquid that has been coated on an inert granular solid, called the column packing, which is held in borosilicate glass tubing. Precise and constant temperature control of injector block, oven and detector is maintained. Stationary-phase material and concentration, column length and diameter, oven temperature, carrier-gas flow, and detector type are the controlled variables. When the sample solution is introduced into the column, the organic compounds are vapourised and moved through the column by the carrier gas. They travel through the column at different rates, depending on differences in partition coefficients between the mobile phase and stationary phases. Figure 4.3 shows a diagram of a gas chromatograph (R.M. Smith 1988).

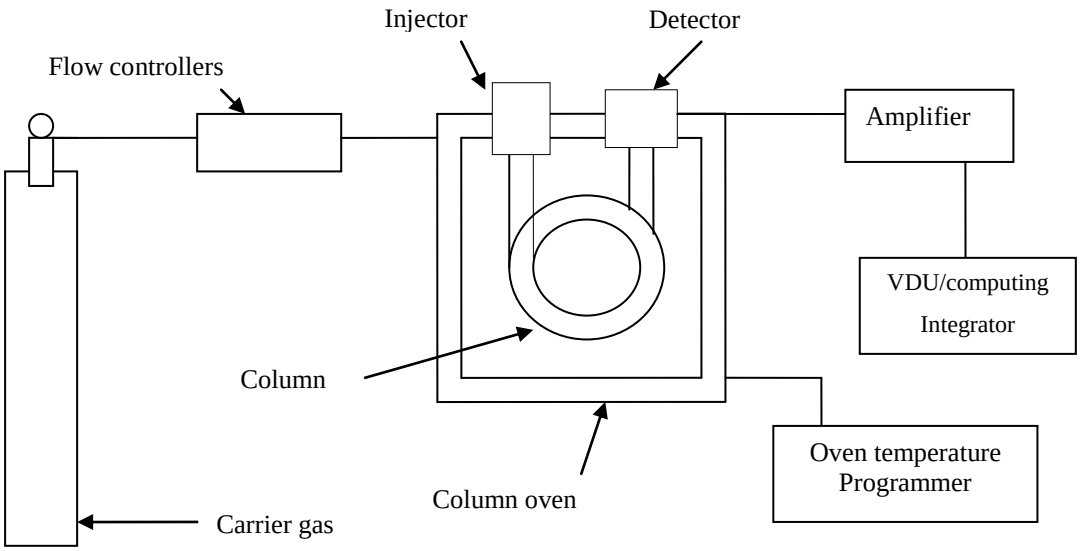

Figure 4.3: Diagram of Gas Chromatograph. (R.M. Smith 1988)

4.6. Experimental set-up and Procedures of LGO and LSO Systems

This subsection provides the principle of the experimental procedure and experimental set-up used in this work.

4.6.1. Liquid/Gas-Ozone (LGO) System

4.6.1.1. Principle of experimental set-up of LGO system

Figure 4.4 shows a diagram of the experimental apparatus used for studying ozone reactions with the compounds and also was used for studying ozone absorption in pure water. The method is based on the flow analysis of the input and output gas concentrations with time. PTFE tube was used for all piped connections carrying ozone/oxygen gas as it is suitably resistant to ozone in high and low concentrations. Oxygen gas was passed through the PTFE tube to the ozone generator which generated ozone gas.

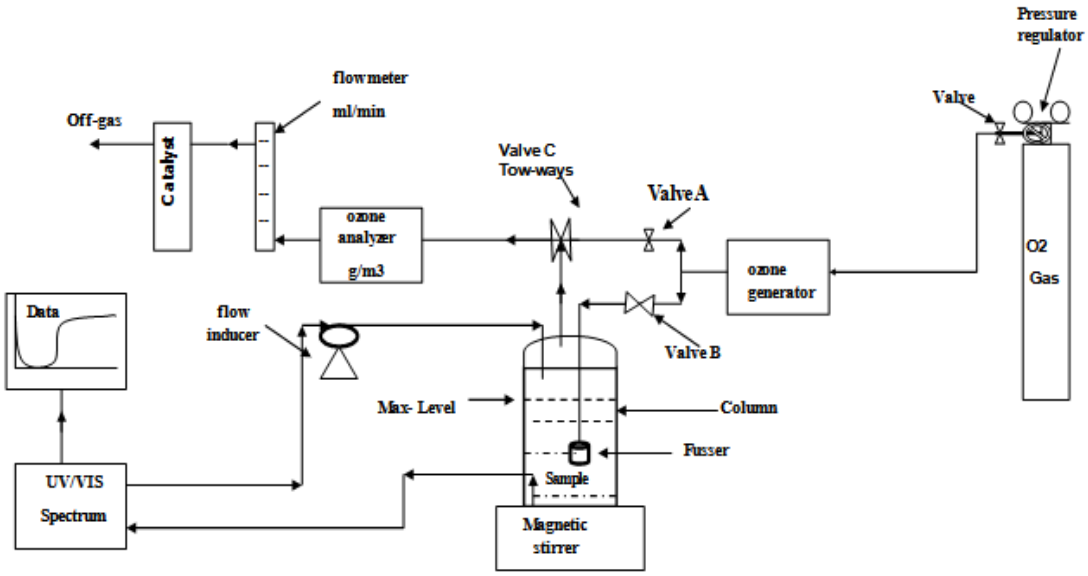

Figure 4.4: Liquid / gas -ozone (LGO) system set-up

Variable measurement flow meter of (100-1200 mL/min) was installed to control the flow rate; 400 mL/min was used as flow rate and kept constant in all experiments. The valves for switching the ozone gas were 2-ways, one way direct to the ozone analyzer, another way direct to the reactor, then to ozone analyzer. 500 mL of sample (pure water or solutions of dye or triclocarban or naphthalene or methanol) was used in this study. A Grade 1 (pore index 90-150 μm) Pyrex@ sintered glass gas distribution sparger was used to disperse the gas into bubbles.The ozone was measured by UV/Vis Spectrophotometer using 1cm flow through quartz cell. Ozone concentration was measured using the solution absorption at 262 nm at which maximum absorbance was obtained. pH was taken during the experiment at different times. The temperature of the reactor was measured using a thermocouple (COMARK, Pocket Digital Thermometer Model 314).

4.6.1.2. Experimental procedures conditions of LGO system

All experiments were carried out with the following conditions: gas flow rate 400 mL/min; with and without 0.2 M t-butanol; temperature (20±1 °C); pressure that was slightly higher than the atmospheric pressure by about 0.1 bar. The aqueous ozone

concentration was measured either by UV/Vis spectrophotometer (ג =262 nm) or by the indigo method.

4.6.1.3. Experimental procedure of mass transfer parameters using LGO system

The mass transfer parameters were determined using two methods. Method 1 involved bubbling O_2 in water then the concentration of oxygen (O_2) was measured with time using an oxygen probe (WTW – CellOx 325). The 2nd method involved bubbling ozone (O_3) of known concentration in water. The O_2 experiments were conducted at 7 gas flow rates (100-700 mL/min); the operating conditions for all experiments of oxygen absorption are shown in Appendix A1 Table A1.1. The ozone absorption experiments were conducted under the following conditions: gas flow rates (200-800 mL/min) and gas concentration (20, 40, 60 and 80 g/m^3 NTP). The determination of mass transfer, self-decomposition and solubility parameters for ozone were carried out using deionised water at various pH values (2, 7 and 9), different gas flow rates (200- 800 mL/min) and in the presence or absence of 0.2 M t-butanol. Four ozone gas concentrations were also used (20, 40, 60 and 80) g/m^3 (NTP). The volume of the reactor was 500 mL and all experiments were carried out at 20 ± 2 $^\circ$C. The operating conditions for all experiments of ozone absorption are shown in Appendix A1 Table A1.2 and A1.3.

4.6.1.4. Experimental procedure of ozone decay using LGO system

As described earlier in section (2.3.2.2), when ozone is dissolved in water it will decay rapidly because ozone is an unstable compound with a relatively short half-life time (Tomiyasu et al., 1985). Therefore ozone decomposition was studied in this work to determine the rate constants and reaction orders as function of pH and t-butanol concentration applicable to this work. The ozone decomposition was studied at pH values of 2, 5, 7 and 9 in a 500 mL reactor initially saturated with ozone of 40 g/m^3. At each pH value, the experiment was either carried out in the absence or presence of

t-butanol at 0.2 mol/L. With the aid of a peristaltic pump, the aqueous solution was pumped in a closed loop through a 1-cm quartz UV/VIS spectrophotometer flow-through cell, in the same fashion as for the other experiments. Values of the ozone decay constant, k_d, and ozone decay reaction order, n, were determined using the objective function shown in Equation 4.9.

$$objective\ function = \sum \frac{\left| C_{AL\,\exp} - C_{AL\,\mathrm{mod}\,el} \right|}{C_{AL\,\exp}} \tag{4.9}$$

The operating conditions for all experiments are shown in Appendix A1 Table A1.4. Once the gas concentration is stable, the stream of ozone in oxygen was directed to the reactor then to the ozone analyzer until saturation. In order to measure the absorbance of ozone decay solution, the maximum absorbance was monitored at λ_{max} = 262 nm.

4.6.1.5. Experimental procedure of ozone absorption in water using LGO system

Several experiments were carried out on ozone absorption/desorption, under conditions as described in section (4.6.1.2). These experiments were carried out by bubbling ozone at a known concentration of 20, 40, 60 and 80 g/m^3 NTP in the semi-batch reactor containing 500 mL of deionised water. Figure 4.4 shows the diagram of the experimental apparatus used for quantifying ozone absorption in the liquid/gas-ozone (LGO) system.

4.6.1.6. Experimental procedure of RO16 degradation using LGO system

In this study the ozonation of reactive orange 16 (RO16) dye was investigated. The molecular structure of the azo-dye reactive orange (RO16) is shown in Figure 1.1. It presents environmental concerns since it is a persistent organic that can not be removed by conventional treatment processes. This study of RO16 degradation is novel, since no other work has attempted to investigate its ozonation. RO16 concentrations of 25, 50, 75 and 100 mg/L were used in this study at various pH values (2, 7 and 11), different

ozone concentrations (20, 40, 60 and 80 g/m^3 NTP), in addition to the conditions in section (4.6.2). A mass of dye was dissolved in deionised water, as described early in section (4.3.2). This procedure was repeated with all concentrations. The solutions were stored in cool dark place. The operating conditions for experiments are shown in Appendix A1, Table A1.5, A1.6 and A1.7. The dye concentration was measured continuously using a peristaltic pump that pumped the solution through the UV/Vis spectrophotometer in a closed loop.

4.6.1.7. Experimental procedure of triclocarban (TCC) degradation using LGO system

In these experiments, the stock solution of TCC at 100 mg/L was prepared by directly dissolving solid TCC in a mixture made of 70 % acetonitrile and 30 % Milli-Q high purity water (>18 MΩ cm), due to the low solubility of TCC in water < 2 mg/L (Lgnasi Sires et al., 2007). Reaction solutions were buffered using phosphoric acid and concentrated sodium hydroxide solutions. The pH values were measured before and after ozonation of the solutions. In some experiments, before bubbling ozone, t-butanol (0.2 M) was added into the TCC solution to act as scavenger of hydroxyl radicals. The experiments were performed at a constant temperature of 20 ± 1 °C. Experiments were carried out in a semi batch gas/liquid reactor filled with 500 mL of TCC solution of known concentration. The operating conditions of TCC experiments are shown in Appendix A1.3 Table A1.8, A1.9 and A1.10. Three different ozone gas concentrations 10, 20, 60 g/m^3 NTP were used in this work. Once the gas concentration is stable, the stream of ozone in oxygen was directed to the reactor. The gas is then diffused into water through a sintered glass diffuser and further dispersed within the volume of the reactor using a magnetic stirrer. Water sampling with a syringe (glass) was carried out manually at different time intervals. The content of the syringe was quickly transferred

to initially prepared vials containing a known volume of 0.005 M sodium thiosulphate ($Na_2S_2O_3.5H_2O$) solution to quench the aqueous ozone remaining in the reaction solution and thus stopping the reaction before analyzing for TCC concentration with HPLC. Because of the dilution effect, due to the addition of sodium thiosulphate to the sample, the effective concentration of TCC was corrected using the mass method. The method consists of taking the glass vial mass (m_v), the previous and sodium thiosulphate quenching solution mass (m_{vq}) and the previous and the sample mass (m_{vqs}). The analysis made by the HPLC results in an intermediate concentration of TCC (C_i) and the effective concentration (C) is given by Equation 4.10.

$$C = \frac{m_{vq} - m_v}{m_{vqs} - m_{vq}} C_i \tag{4.10}$$

The HPLC conditions used for TCC analysis were isocratic mobile phase 70 % acetonitrile: 30 % water at 1 mL/min, UV detection at a wavelength of 265 nm, the injection volume was 20 μL and the retention time for TCC was 4.82 minutes, as shown in Figure (4.5). The column used was (C18 Hypersil Gold column (150×4.6 mm, 5 μm - Thermo Scientific).

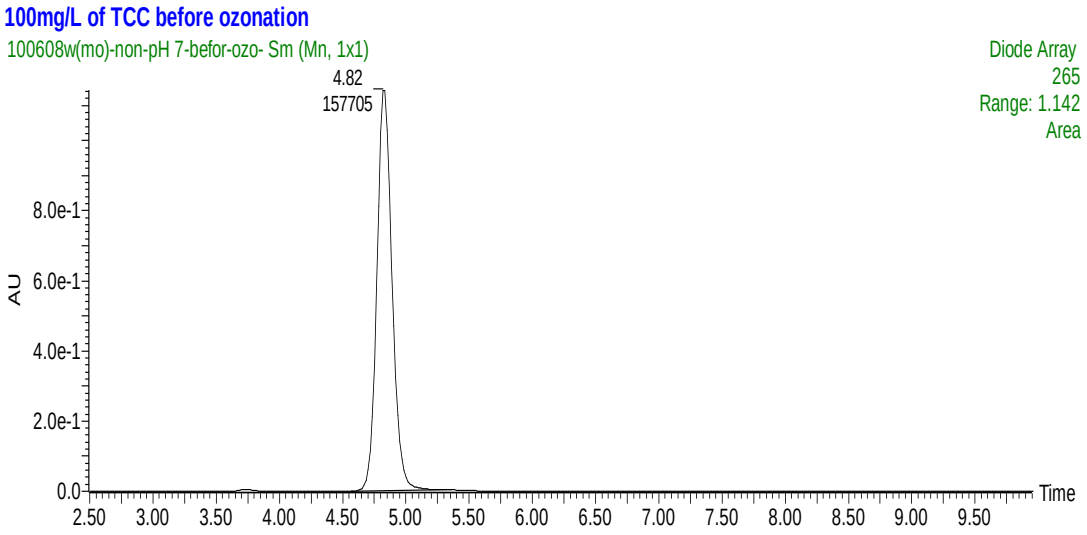

Figure 4.5: Peak area and retention time of TCC

4.6.1.8. Experimental procedure of naphthalene degradation using LGO system

Several experiments of naphthalene degradation by ozone were carried out in a semi-batch (LGO) reactor (Figure 4.4). Ozone gas concentration 40 g/m^3 NTP was used in this work to degrade 100 mg/L of naphthalene in 50% methanol: 50% water at pH of 2, 5, 7 and 9 and water flow rate 10 mL/min. In order to study the effect of t-butanol as a scavenger on naphthalene degradation, 0.2 M of t-butanol was added. The samples of naphthalene were injected in HPLC. Isocratic mobile phase (75 % methanol: 25 % water) at 1 mL/min was used to elute naphthalene, which is detected at a wavelength of 269 nm. 10 μL volume was injected and the retention time for naphthalene was obtained at 4.68 minutes as shown in Figure 4.6. The same column (C18 Hypersil Gold column (150 × 4.6 mm, 5 μm - Thermo Scientific) was also used here.

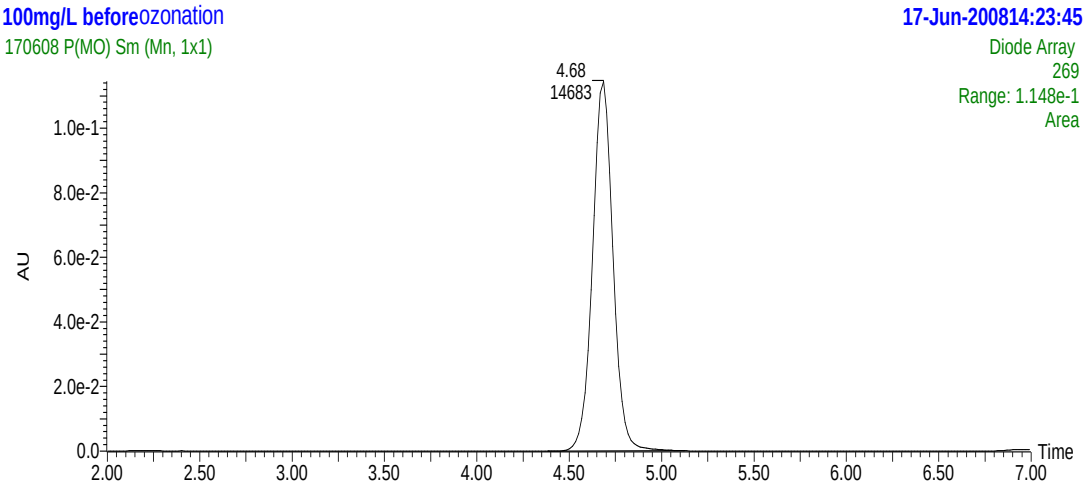

Figure 4.6: Peak area and retention time of naphthalene

4.6.1.9. Experimental procedure of methanol degradation using LGO system

Several experiments were carried out to study the degradation of methanol. Ozone gas concentrations of 10 to 80 g/m^3 were used in this study at the pH of 2, 5 and 9, in the presence and absence of t-butanol as hydroxyl radicals scavenger. Samples at high methanol concentrations were analysed by HPLC and those at low concentrations were analysed with GC/FID. For HPLC analysis, isocratic mobile phase (70 % acetonitrile: 30 % water) at 1 mL/min was used to elute methanol, which was detected at a

wavelength of 195 nm. The injection volume was 10 μL and the retention time for methanol was obtained at 1.27 minutes as shown in Figure 4.7. The Hypersil Gold column was also used here. The GC/FID analysis was carried out as described in 4.5.4.

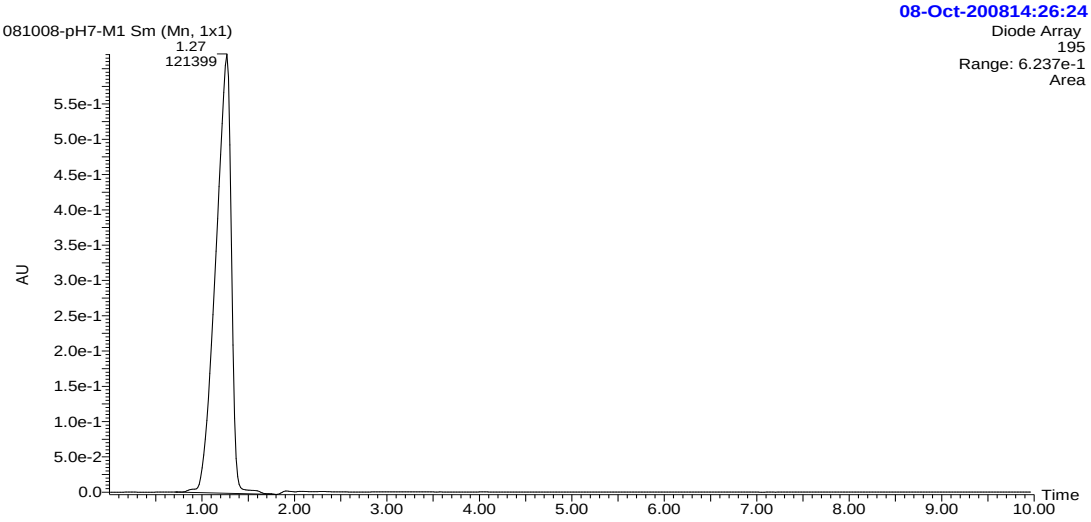

Figure 4.7: Peak area and retention time of methanol

4.6.2. Liquid/Solid-Ozone (LSO) System

4.6.2.1. Experimental set-up of LSO system

As described earlier in Section 2.8.2, the LSO system consists of three steps: (a) loading ozone on a bed of an adsorbent; (b) passing polluted water through the ozone-saturated bed; (c) regenerating the bed using dry air. By doing this, it is expected that kinetics are enhanced due to the high ozone concentration in contact with pollutants (Tizaoui 2001). Figure 4.8 shows a diagram of LSO system. In LSO, ozone is adsorbed in a selective adsorbent of (silica gel or zeolite (D915)) and then in the second step, the polluted water (RO16 or naphthalene or methanol solution) passes through the adsorbent loaded with ozone. The ozone adsorption experiments were conducted under the conditions described in section (4.6.1.2) at 10 mL/min of water flow rate and the ozone concentrations were determined by the indigo method. To determine pollutants concentration at any given time, sodium thiosulphate at a known volume and concentration was added to stop the chemical reaction between ozone and the pollutant.

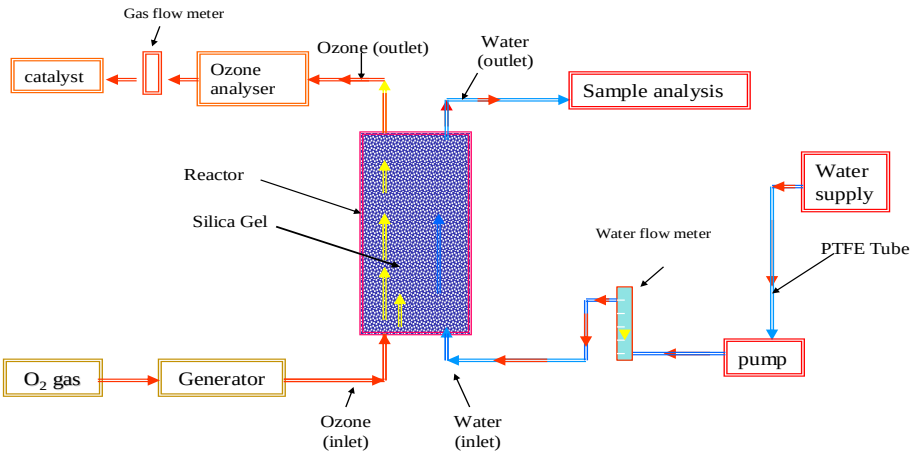

Figure 4.8: Liquid /solid -ozone (LSO) system set-up

4.6.2.2. Reactor scale

In order to easily obtain the volume of the adsorbent loaded in the reactor, a scale was developed on the reactor wall. The scale divided the total length of the reactor (160 mm) into a succession of 1-cm lengths (Figure 4.9). Figure 4.10 shows the relationship between the scale and the reactor volume. The slope of the line in Figure 4.10 gave the cross section area of the reactor which was found equal to approximately 1 cm^2, giving a reactor diameter of about 10 mm id.

Figure 4.9: LSO reactor

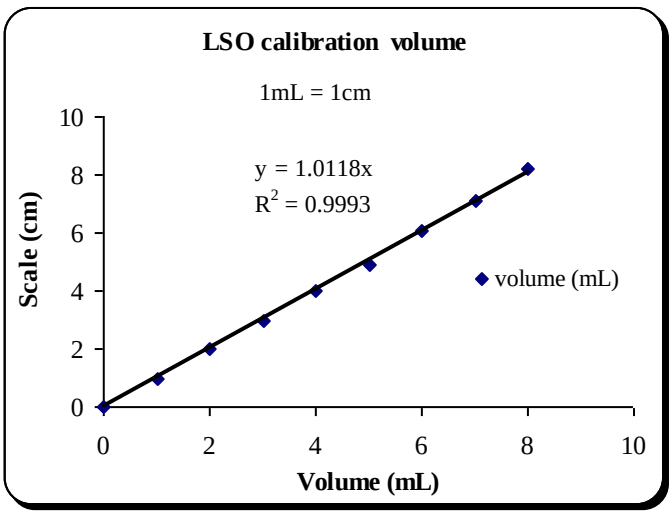

Figure 4.10: Calibration volume of the reactor in LSO system

4.6.2.3. Experimental procedure of RO16 degradation using LSO system

The degradation of RO16 using the LSO system was studied by passing a solution of RO16 at 50 mg/L through 80 g bed of silica gel initially loaded with ozone, at a known gas concentration 60 g/m^3 NTP. The RO16 solution liquid flow rate was 10 mL/min and the pH was 7.

4.6.2.4. Experimental procedure of naphthalene degradation using LSO system

High purity naphthalene: $C_{10}H_8$ (99+%), was used to prepare a stock solution of naphthalene at 100 mg/L by directly dissolving solid naphthalene in a mixture made of 50 % Methanol and 50 % water (see section 4.3.4.). Reaction solutions were buffered using phosphoric acid and concentrated sodium hydroxide solutions. The pH values were measured before and after ozonation of the naphthalene solutions. In some experiments, t-butanol (0.2 M) was added into naphthalene solution before bubbling ozone as scavenger for hydroxyl radicals. The experiments were performed at room temperature 20 ± 1°C. Experiments were carried out in the liquid/solid-ozone (LSO) reactor filled with 2 g of the zeolitic adsorbent D915 (Figure 4.8) and all the operating conditions of naphthalene experiments are shown in Appendix A1.4 Table A1.11 to A1.16. Ozone gas concentration 40 g/m^3 NTP was used in this work. Once the gas concentration is stable, the stream of ozone in oxygen was directed to the reactor. Samples were collected at different times, quenched with 0.005 M sodium thiosulphate solution and analysed by HPLC as describe in section (4.6.1.8).

4.6.2.5. Experimental procedure of methanol degradation using LSO system

Methanol solutions at 0.2 to 5 mol/L were prepared by directly diluting liquid methanol 99 % with Milli-Q high purity water (>18 MΩ cm). Reaction solutions were buffered to keep the pH constant during the experiments. The pH values were measured before and after ozonation of the solutions. In this study pH levels of 2, 5, 7 and 9 were used and

all the operating conditions of methanol experiments are shown in Appendix A1.5, Table A1.17 to A1.24. Ozone gas concentrations of 10, 30, 60 and 80 g/m^3 NTP were used in this work. Once the gas concentration is stable, the stream of ozone in oxygen was directed to the reactor. In the LSO system, ozone was adsorbed in 6g of the selective adsorbent zeolite (D915), then in the second step the methanol solution passed through the adsorbent loaded with ozone. Again here samples of methanol solutions were collected with time, quenched with sodium thiosulphate and analysed as described in section (4.6.1.9).

4.6.2.6. Determination of BET surface area

BET surface areas of the silica gel and the zeolite material D915 were determined by liquid nitrogen. Degassed samples of silica gel (0.9960 g) and the zeolite material D915 (0.5320 g) were placed in the automated gas adsorption apparatus (Micromeritics ASAP, 2000) Accelerated Surface Area and Porosimetry as shown in Figure 4.11. The results were compared with other silica as shown in Table 4.1.

Table 4.1: BET surface area of different types of silica

Adsorbent	mass (g)	BET surface area (m^2/g)
Zeolite D915	**0.5320**	**238.6 ± 3**
Silica gel	**0.9960**	**490.9 ± 3**
Silica Alumina	0.2750	232.3 ± 7
Silica gel grad 40	0.7650	643.3 ± 1
Silica gel 100 g	1.2900	268.7 ± 1
Silica gel tablet	0.8650	108.4 ± 0.2
Silica 85330	0.4760	728.2 ±4

Figure 4.11: Micromeritics ASAP 2000

CHAPTER 5: RESULTS OF THE LIQUID/GAS-OZONE (LGO) SYSTEM

This chapter will present and discuss the experimental results obtained in this work.

Mass transfer Studies

5.1. Mass transfer Studies in the Liquid/Gas-Ozone (LGO) System

5.1.1. Ozone absorption

These experiments were carried out under 400 mL/min oxygen gas flow rate and the aqueous ozone concentration was measured by a UV/Vis spectrophotometer ג =262 nm.

5.1.2. Ozone liquid concentration: calibration curve

In these experiments, ozone solutions were prepared by bubbling ozone gas at concentrations of (20, 40, 60 and 80 g/m^3 NTP) into deionised water for about one hour for each concentration. After having the ozone concentration stable in water, the absorbance at 262 nm was measured and a sample was taken by a syringe and added to 10 mL of indigo until the blue solution turned to a light blue colour, then the absorbance of the sample was measured by the spectrophotometer at 600 nm. Table 5.1 shows the experimental conditions and results obtained by using Equation 4.3 (indigo method).

Table 5.1: Experimental conditions and results calculation of ozone in liquid

$C_{A\ inlet}$ g/m^3	Abs 262nm	Abs_{blank} 600nm	V_{indigo} (mL)	$V_{sample + indigo}$ (mL)	V_{Sample} (mL)	$Abs_{Sample + indigo}$ 600nm	C_{AL} (mg/L)
20	0.2133	2.42	10	18.8	8.8	0.25	5.26
40	0.4169	2.41	10	15.1	5.1	0.140	10.21
60	0.6404	2.33	10	13.6	3.6	0.179	13.46
80	0.9704	2.37	10	12.7	2.7	0.197	18.64

Each experiment was repeated three times and average values were taken. The relationship between ozone liquid concentration (C_{AL}) and Abs_{262} is then determined by plotting C_{AL} as function of Abs_{262} as shown in Figure 5.1. The theoretical relationship between C_{AL} and Abs_{262} is given in Figure 5.2 when ε = 2901 M^{-1} cm^{-1}. It can be seen

from Figure 5.1 that a linear relationship between ozone concentration in liquid and absorbance was achieved though the slope of the experimental line is slightly higher than that obtained for $\varepsilon = 2900\ M^{-1}cm^{-1}$ (Figure 5.2).

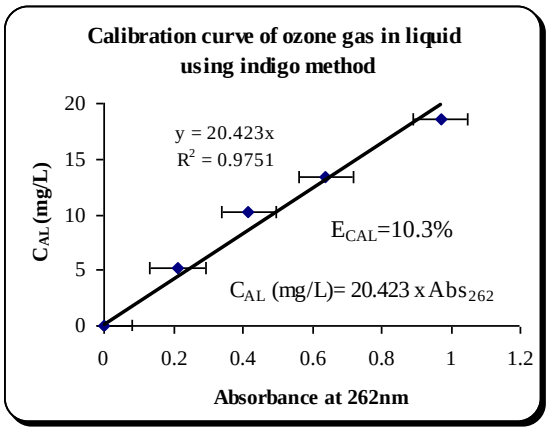

Figure 5.1: Ozone gas concentration versus absorbance, experimental

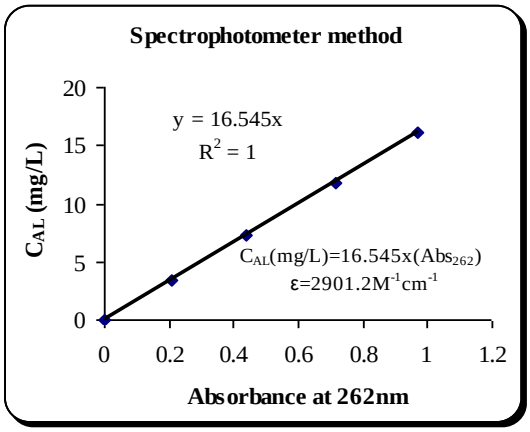

Figure 5.2: Ozone gas concentration versus absorbance theoretical

5.2. Experimental Results of Ozone Decay

Ozone decay experiments were carried out as described earlier in section 4.6.1.4.

5.2.1. Effect of pH on ozone decay

pH is one of the parameters that affects ozone decay significantly. In order to understand the effect of pH on ozone decay, several experiments were carried out at different pH values of 2, 5, and 7. Figure 5.3 shows the effect of pH on ozone decay when the experiments were conducted in the absence of scavenger (t-butanol). From Figure 5.3, it can be seen that the ozone decay rate is slow at low pH and increases when pH increases; that means at the half-life time $t_{1/2}$ of ozone is pH-dependent; an increase in pH leads to a decrease of $t_{1/2.}$

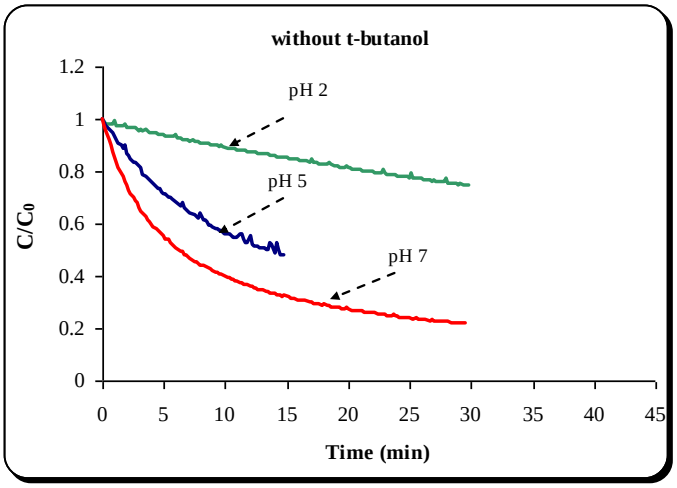

Figure 5.3: Liquid ozone concentration versus time

5.2.2. Effect of scavenger (t-butanol) on ozone decay

Several experiments were carried out to study the effect of t-butanol on ozone decay by bubbling ozone at known concentration 40 g/m^3 in a semi-batch reactor using 500 mL of deionised water with conditions as described earlier in section 4.6.2 and presented in Table A1.4 in Appendix A1. The values of the order and rate constant of ozone decay reaction are shown in Table 5.8. Ozone decomposition was found to follow a second order reaction at pH values less than 7 whilst it was first order at pH 9. When the scavenger t-butanol was added, the decomposition of ozone progressed at lower reaction order of 1.5 for pH values less than 7 and at the same order in the absence of t-butanol at pH 9. Table 5.2 shows significant increase of the ozone decomposition rate constant with pH, merely due to the increase of hydroxide ion concentration, which promotes ozone decomposition. The results also show that although t-butanol was used as a radical scavenger, ozone decomposition was not fully inhibited.

Table 5.2: Rate constant and order of the ozone decay reaction

	Non [t-butanol]		[t-butanol] = 0.2 (mol/L)	
pH	n	$k_d(M^{1-n}s^{-1})$	n	$k_d(M^{1-n}s^{-1})$
2.2	2	1.02	1.5	0.182
5.0	2	10.44	1.5	0.222
7.3	2	18.51	1.5	0.359
9.0	1	0.030	1	0.023

5.2.3. Summary

From ozone decay experiments, it can be summarised that the ozone decomposition was found to follow a second order reaction at pH values less than 7, whilst it was first order with respect to ozone at pH 9. When the scavenger t-butanol was added, the decomposition of ozone progressed at lower reaction order of 1.5 for pH values less than 7 and at the same order when without t-butanol at pH 9. The ozone decay rates have also increased when pH increased due to increased hydroxide ion concentration, which promotes ozone decomposition.

5.3. Ozone Absorption and Desorption in Water

Several experiments were carried out on ozone absorption/ desorption in order to study ozone mass transfer in water. Appendix A1, Table A1.2 shows the conditions for these experiments. Experiment number oz3 was chosen as a typical an example to show here. This experiment was carried out by bubbling ozone at a known concentration of 60 g/m^3 NTP. The reactor contained 500 mL of deionised water. Table 5.3 shows the operating conditions for this experiment.

Table 5.3: Values of the variable for typical experiment of ozone absorption

Exp No	Sample (mL)	Flow rate (mL/min)	Ozone conc. inlet (g/m^3) NTP	Ozone conc. at end of experiment (g/m^3) NTP	Initial pH	Final pH
oz3	500	400	60	58.5	5.195	5.022

Figure 5.4 shows a relationship between ozone gas concentration (g/m^3 NTP) and time (minutes) during the experiment. As seen from Figure 5.4 the ozone gas concentration increases gradually with time. This Figure shows that the steady state ozone gas concentration 58.5 g/m^3 NTP reached at the end of the experiment is less than the inlet ozone concentration 60 g/m^3 NTP. This is due to ozone decay in water, which is a well established phenomenon when ozone dissolves in water.

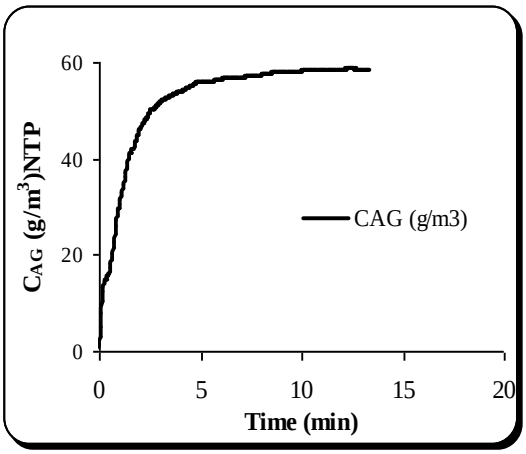

Figure 5.4: Gas ozone concentration versus time

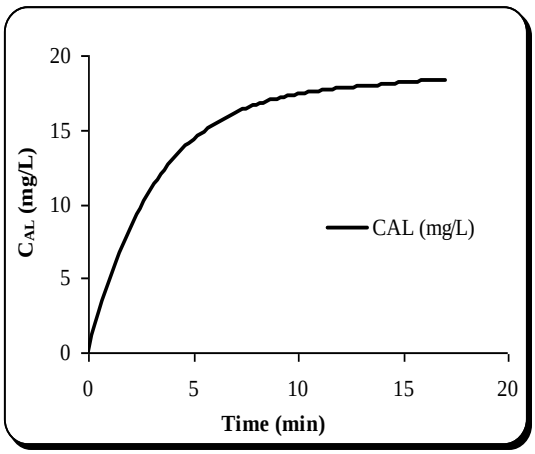

Figure 5.5: Liquid ozone concentration versus time

Figure 5.5 illustrates the change of liquid ozone concentration as a function of time. It can be seen from Figure 5.5 that liquid ozone concentration increases with time until it reaches almost a steady-state that marks the saturation point. Following ozone absorption, experiments of desorption were also carried out. A typical absorption and desorption curve for liquid ozone concentration is shown in Figure 5.6; whereas Figure 5.7 explains changes points of gas.

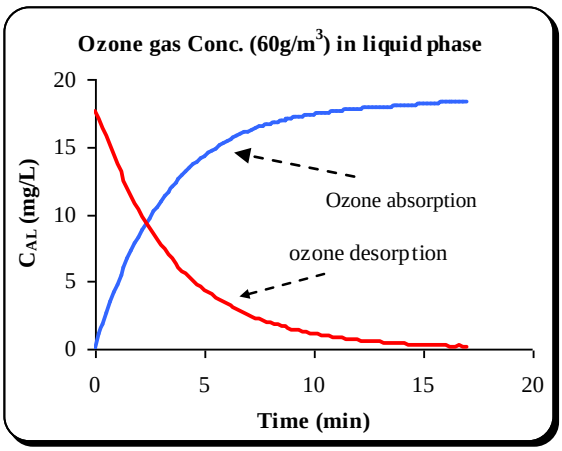

Figure 5.6: Liquid ozone concentration versus time

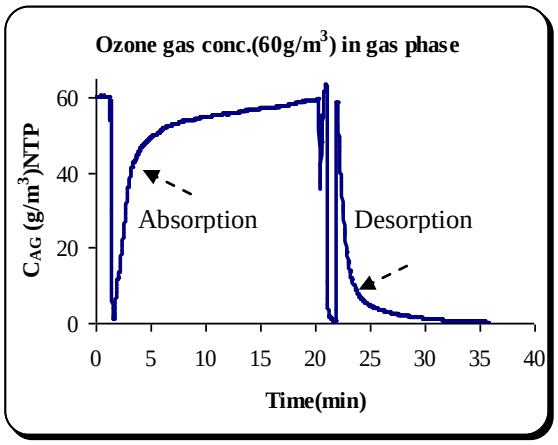

Figure 5.7: Gas ozone concentration versus time

5.4. Experimental Results of Mass transfer Coefficient (k_La)

5.4.1. Oxygen experiments

Mass transfer coefficient (k_La) was studied with pure oxygen (O_2) at different flow rates of (100 – 600 mL/min) by using dissolved oxygen meter (DO_2) type (handy lab ox12), pH and temperature were 7±0.2 and 20±2 °C respectively. Experimental conditions and

results for all experiments are shown in Table 5.4 and Figures 5.8 and 5.9 show typical example model results of experiment ox4. Figure 5.8 shows excellent agreement between experimental results and the model which is also reflected in excellent linear relationship ($R^2 = 0.9996$) between $\ln = \left(\frac{C_{AL} - C_{AL}^*}{C_{AL_0} - C_{AL}^*} \right)$ as function of time (Figure 5.9).

Table 5.4: Experimental operating condition and results calculated of k_La (O_2)

Exp No	Gas flow rate (mL/min)	Pressure (mbar)	$k_La(s^{-1})$ $x10^3$	C_{AL}^* (mg/L)	C_{AL0} (mg/L)
ox1	100	171.9	2.95	44.0	10.84
ox2	200	182.2	4.05	46.0	11.71
ox4	400	186	5.76	50.8	7.73
ox5	500	186.3	6.66	47.4	8.67
ox6	600	186.8	7.47	46.3	7.147

Where: k_La is the volumetric mass transfer coefficient; C_{AL0} the initial oxygen liquid concentration; C_{AL}* the saturation oxygen concentration.

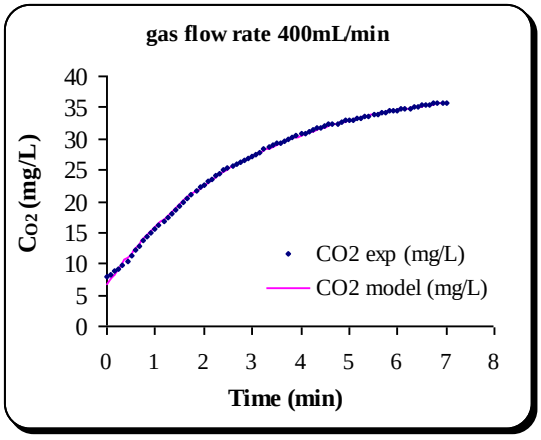

Figure 5.8: Oxygen Concentration versus time

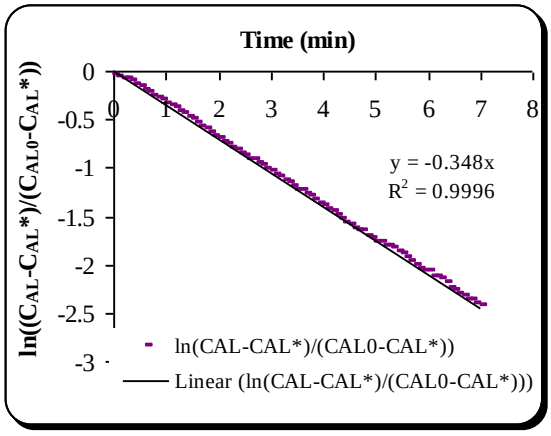

Figure 5.9: Model results

The slope of the line shown in Figure 5.9 is equal to the value of k_La. In this particular experiment, a value of 5.8×10^{-3} s^{-1} was obtained for a flow rate equal to 400 mL/min. Once k_La oxygen was determined, k_La ozone may be calculated as shown in Section 5.4.3. Figure 5.10 shows the relationship between k_La and gas flow rate of oxygen. It can be seen from the Figure that the values of k_La increased by increasing the oxygen gas flow rate.

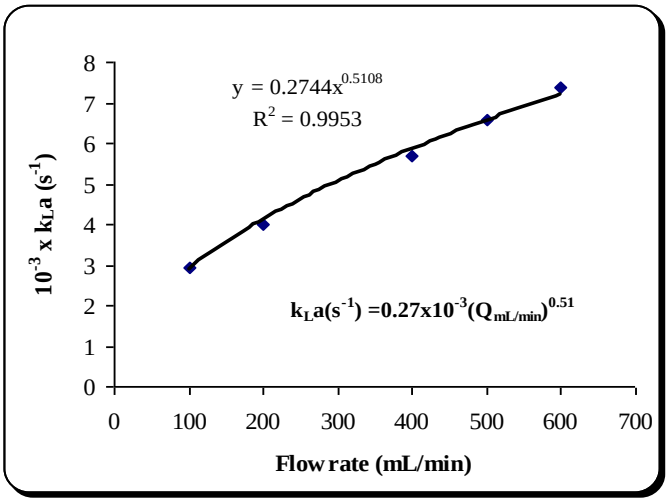

Figure 5.10: Relationship between k_La and oxygen gas flow rate at pH 7

5.4.2. Ozone experiments

Mass transfer of ozone gas/liquid was studied at different ozone gas concentrations (20, 40, 60 and 80 g/m^3), different flow rates of (200, 400, 600 and 800 mL/min) and different pH (2, 7 and 9) in the presence and absence of t-butanol and temperature 20±2 °C. The experimental operating conditions and results calculated k_La of ozone in water are shown in Table 5.5. Figure 5.11 and 5.12 show typical graphs in liquid and gas phases respectively. The observation from Figure 5.11 is that C_{AL} at flow rate 800 mL/min took less time to reach saturation point (8 minutes) as compare to the C_{AL} at 200 mL/min (15 minutes), due to increasing in mass transfer.

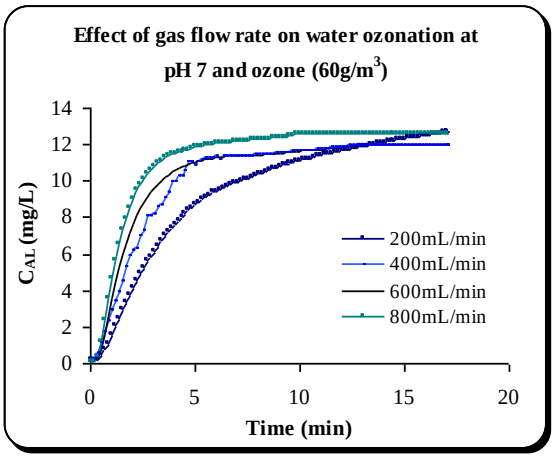

Figure 5.11: Ozone conc. versus time (liquid phase)

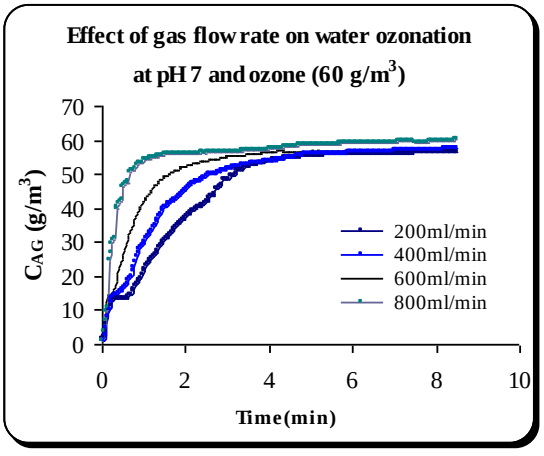

Figure 5.12: Ozone Conc. versus time (gas phase)

Figure 5.13 shows the relationship between k_La and the gas flow rate. It can be seen from the Figure that k_La values were increased by increasing the gas flow rate. Again a power relationship between k_La and flow rate was found.

Table 5.5: Operating conditions and results calculated k_La of ozone in water

Exp No	Q (mL/min)	pH	C_{O3} (g/m^3)	$(k_La)_{O3}$ s^{-1} x10^3	k_d s^{-1}x10^3	C_{AL}* (mg/L)	$(k_La)_{O2}$ s^{-1} x10^3	$(k_La)_{O3}/(k_La)_{O2}$
Without t-butanol								
1	200	7.2	60	2.38	1.1	0.924	4.05	0.58
2	400	7.0	60	3.4	2.5	0.924	5.76	0.58
3	600	7.2	60	6.3	3.8	0.924	6.66	0.94
4	800	7.2	60	7.09	3.5	0.924	7.47	0.94
5	200	4.3	20	3.2	0	0.301	4.05	0.79
6	200	4.2	40	3.4	0	0.61	4.05	0.83
7	200	4.1	60	3.5	0	0.91	4.05	0.86
8	200	4.2	80	3.7	0	1.21	4.05	0.91
9	400	5.3	20	5.3	0.13	0.318	5.76	0.92
10	400	5.2	40	5.7	0.72	0.614	5.76	0.98
11	400	5.1	60	6.5	0.65	0.908	5.76	1.1
12	400	5.2	80	6.8	0.41	1.23	5.76	1.1
13	400	2	20	4.7	0	0.31	5.76	0.81
14	400	2	80	6.1	0	1.23	5.76	1
15	400	7	20	4.8	1.6	0.309	5.76	0.83
16	400	7	80	6.6	1.2	1.22	5.76	1.1
17	400	9	80	1.5	0.52	1.23	5.76	0.29
With t-butanol (0.2M)								
18	400	2	20	6.3	0	0.307	5.76	1.1
19	400	2	80	6.3	0	1.23	5.76	1.1
20	400	7	20	5.1	0.37	0.306	5.76	0.88
21	400	7	80	7.5	2.9	1.23	5.76	1.3
22	400	9	80	1.8	1.06	1.23	5.76	0.31

Where: C_{AL}* is the saturation liquid concentration (mg/L) calculated by the following Equation.

$$C_{AL}^* = \alpha\, C_{AG} \qquad (5.1)$$

Where: α is the slope of the relationship between C_{AL}* and C_{AG} determined experimentally (Figure 5.14); C_{AG} is ozone gas concentration. The value of slope was obtained to be 0.0456, 0.0514 for without t-butanol and with-butanol respectively.

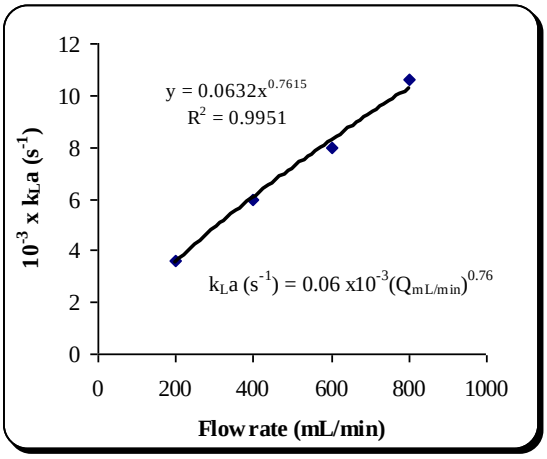

Figure 5.13: Relationship between k_La and ozone gas flow rate at pH 7

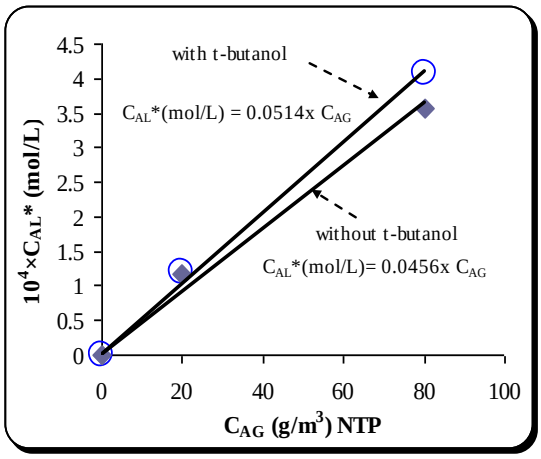

Figure 5.14: C_{AL}* versus ozone gas conc. at pH 2

5.4.3. Relationship between $k_La_{(O2)}$ and $k_La_{(O3)}$

Theoretically, the relationship between k_La values for absorption of two different gases (e.g. ozone and oxygen) is given by $k_La_{(O3)}=(D_{O3}/D_{O2})^n\ k_La_{(O2)}$. Where: n is a factor that depends on the hydrodynamics of the system ($0.5\leq n\leq 1$) D_{O3}; D_{O2} are ozone and oxygen diffusivities respectively. The ratio of $k_La_{(O3)}$ /$k_La_{(O2)}$ for all experiments are shown in Table 5.5, whereas Table 5.6 shows only ratio for experiments run at three different flow rates. Knowing that the diffusivities of ozone and oxygen in water are $1.7x10^{-9}m^2s^{-1}$ and $2.5x10^{-9}$ m^2s^{-1} respectively and taking n=1, theoretically the ratio $(k_La)_{O3}$ / $(k_La)_{O2}$ should equal to 0.68. The theoretical value is slightly lower than the experimental values due to experimental errors and possible variation in the values of diffusivities used in the calculation.

Table 5.6: Ratio between $k_La(O_2)$ and $k_La(O_3)$

Exp-No	Flow rate (mL/min)	k_La (O_2) (s^{-1})	k_La (O_3) (s^{-1})	$(k_La)_{O3}/(k_La)_{O2}$
1	200	$4.1x10^{-3}$	$3.7x10^{-3}$	0.9
2	400	$5.7x10^{-3}$	$5.9x10^{-3}$	1
3	600	$7.5x10^{-3}$	$8.1x10^{-3}$	1

5.4.4. Effect of the radical scavenger t-butanol and pH on ozone absorption in deionised water

pH plays an important role in ozone reaction pathway. Free-radical oxidation is favoured at higher pH while molecular ozone oxidation tends to dominate at acidic conditions.

This is because the production of hydroxyl radicals (OH°) is enhanced by alkaline conditions. The free radicals are more powerful oxidants than molecular ozone (Hoigne and Bader 1983). In this study, t-butanol was used as an OH° scavenger to assess the contribution of OH° to the oxidation of compounds studied in this work. It is believed that addition of t-butanol to the water will affect the mass transfer parameters (i.e. k_La, gas hold-up etc.). For this reason, the effect of t-butanol on mass transfer was studied separately and presented in this section. The same is also true for pH. The study was conducted for pH values of 2, 7 and 9 with and without t-butanol. The pH was adjusted as described earlier in section (4.2). These experiments were run with 0.2 M t-butanol and without it at 20±1°C as shown in Table 5.7.

Table 5.7: Operating conditions for pH and scavenger effect on ozone absorption in deionised water

Experimental No	pH	Ozone concentration (g/m^3)NTP	t-butanol (mol/L)
oz9	2	80	0.2
oz10	2	80	0
oz11	7	80	0.2
oz12	7	80	0
oz13	9	80	0.2
oz14	9	80	0

Experiments with and without t-butanol and at different pH were carried out in order to understand and assess the scavenger effect. From the results shown in Figures 5.15, 5.16 and 5.17, two interesting observations can be made. First, by adding t-butanol, mass transfer coefficient k_La has increased as shown in Table 5.8. The percentage of k_La increase was calculated by Equation 5.4. Second, significant effect of t-butanol is observed at higher pH values.

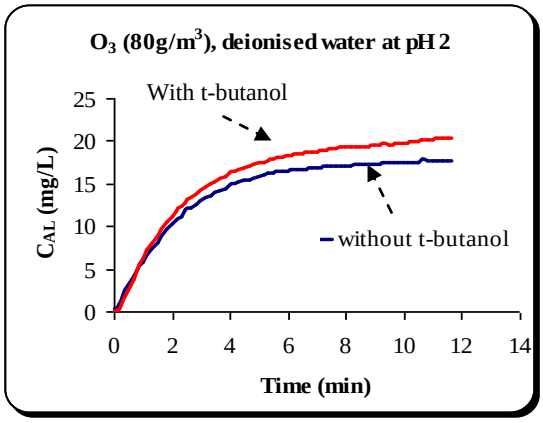

Figure 5.16: water ozonation at pH 2 with and without t-butanol

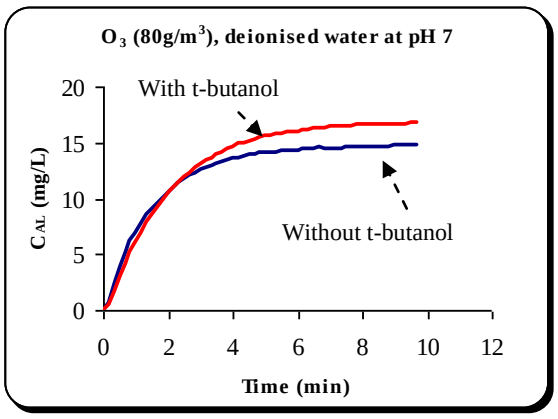

Figure 5.17: water ozonation at pH 7 with and without t-butanol

In Figure 5.17, it can be seen the effect of pH 9 on water ozonation in the presence and absence of t-butanol. The profile of liquid ozone concentration in Figure 5.17 is different from those obtained at lower pHs than 9. This may be attributed to ozone decomposition in the presence of hydroxide ions (OH^-). The observation from all experiments is that the bubble size decreased due to the addition of t-butanol, hence the volumetric mass transfer coefficient (k_La) increased following increase of the specific surface area (a).

$$O_3 + OH^- \xrightarrow{K} O_2 + HO_2^- \qquad k = 40\ M^{-1}s^{-1} \tag{5.2}$$

$$^{\circ}OH + C(CH_3)_3OH \xrightarrow{K} {}^{\circ}CH_2C(CH3)_2OH + H_2O \tag{5.3}$$

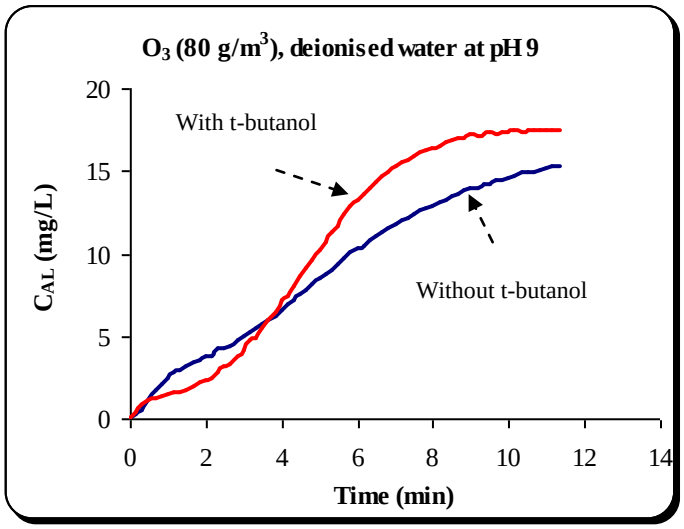

Figure 5.17: Water ozonation at pH 9 with and without t-butanol

$$\% \text{ increase } k_La = \frac{(k_L a)_{with} - (k_L a)_{without}}{(k_L a)_{without}} \times 100 \quad (5.4)$$

Table 5.8: Values of mass transfer coefficient (k_La) at different pH value in the presence and absence of t-butanol.

pH	2	7	9
k_La (without t-butanol) $x10^3(s^{-1})$	7.58	8.12	1.89
K_La (with t-butanol) $x10^3$ (s^{-1})	7.83	9.81	7.90
Increases **%**	3%	20%	316%

5.5. Summary

Ozone decay was studied at different pH values and in the absence and presence of t-butanol (0.2 M). As can be expected, ozone decay rates have increased as the pH increased and the presence of t-butanol has lowered the decay of ozone. Ozone mass transfer parameters were also determined and compared to those of pure oxygen. The ratio of the volumetric mass transfer coefficients obtained by ozone and oxygen have been compared to the ratio of their diffusivities and reasonable agreement have been obtained with the theoretical ratio (Dankckwerts PV 1970).

Degradation Studies

Degradation of Dye RO16

5.5. Degradation of Dye RO16 by Ozone using (LGO) System

Figure 5.18 shows a full spectrum of the dye RO16. From that graph, it can be seen the maximum absorbance of dye RO16 occurs at λ_{max} = 496 nm. Thus, all subsequent analyses of the dye were made by measuring the absorbance at λ_{max} = 496 nm.

5.5.1. RO16 UV/Vis Spectrum

Figure 5.18 shows a full spectrum of the dye RO16. From that graph, it can be seen the maximum absorbance of dye RO16 occurs at λ_{max} = 496 nm. All subsequent analysis of the dye were made by measuring the absorbance at λ_{max} = 496 nm.

5.5.2. Calibration curve of dye (RO16)

As shown earlier, the concentration of the dye RO16 was determined using the maximum absorbance at 496 nm. The relationship between RO16 concentration and absorbance at 496 nm is determined here. Figure 5.19 shows that RO16 concentration follows a linear relationship with Absorbance 496 nm as described by the Beer-Lambert Law, Section (4.5.1).

Table 5.9: Absorbance at λ = 496 for different concentrations of dye (RO16)

Dye (RO16)concentration (mg/L)	Absorbance at 496nm
0	0
25	0.61767
50	1.1987
75	1.7967
100	2.3918

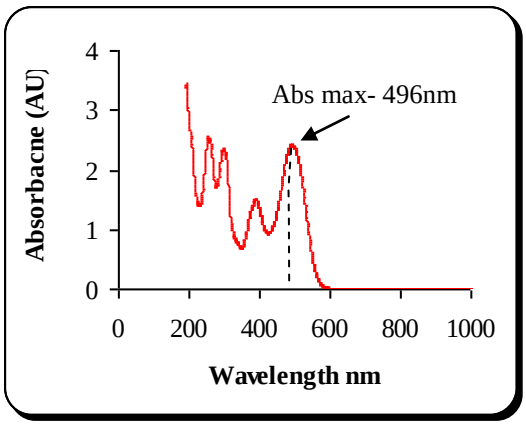

Figur 5.19: Full spectrum of dye RO16

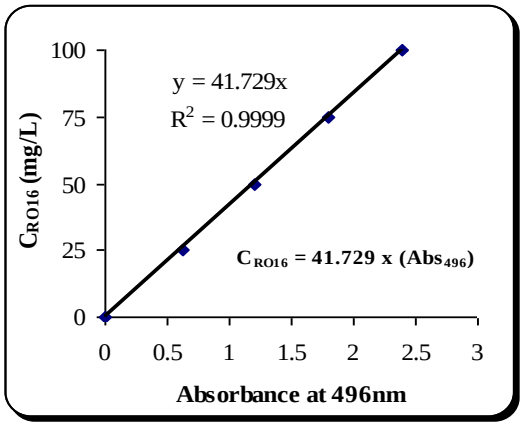

Figure 5.20: Dye RO16 conc. versus absorbance

5.5.3. Results of dye (RO16) ozonation experiment

Gas ozone at different concentrations (20, 40, 60 and 80 g/m^3 NTP) was bubbled into dye solutions at different concentrations (25, 50, 75 and 100 mg/L), as described in Section (4.6.2.6). Typical operating conditions for an experiment are shown in Table 5.10 and typical results are shown in Figure 5.20 and 5.21. Appendix A1.2 and A2.2 shows all experimental conditions and results of RO16 degradation.

Table 5.10: Experiment operating condition of dye typical experiment

Exp No	Sample (mL)	(Q)O_2 (mL/min)	Ozone (g/m^3)NTP	Dye(RO16) (mg/L)	Initial pH	Final pH
D12	500	400	60	100	5.304	3.533

Figure 5.20 shows the change of ozone gas concentration as a function of time. The ozone concentration tends to reach a plateau after about 5 minutes at a value which is less than the initial concentration; this proves that ozone reactions with by-products continue to take place even though dye decolourisation is completed. It is also noticeable that at the end of the experiment, the dye was totally removed and the water becomes colourless, as shown in Figure 5.21 and 5.22. Figure 5.21 shows the change of dye concentration as function of time. The Figure shows that total dye decolourisation occurred in about 8 minutes. The efficiency of ozone to decolourise the RO16 solution was measured by considering the time at which 95% of the initial colour was removed. This time was noted by $t_{0.95}$.

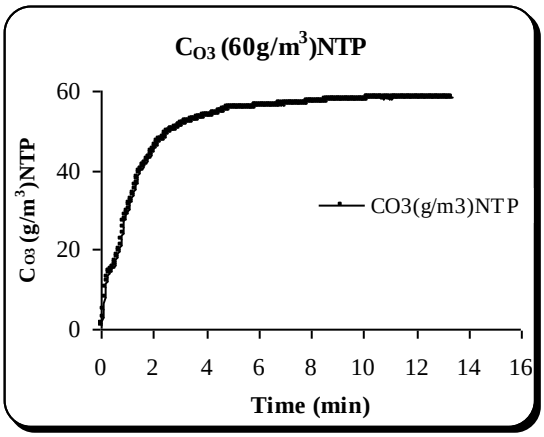

Figure 3.20: Ozone gas concentration versus time

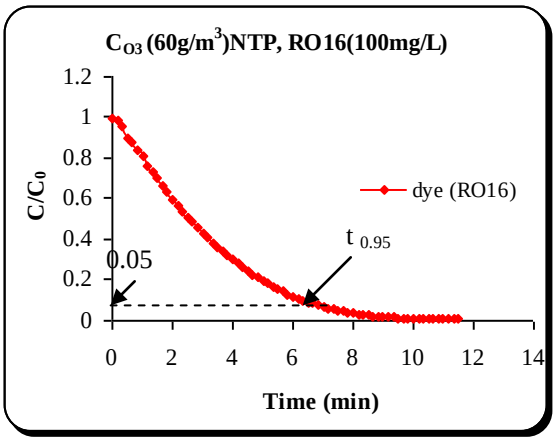

Figure 5.21: Concentration of RO16 versus time

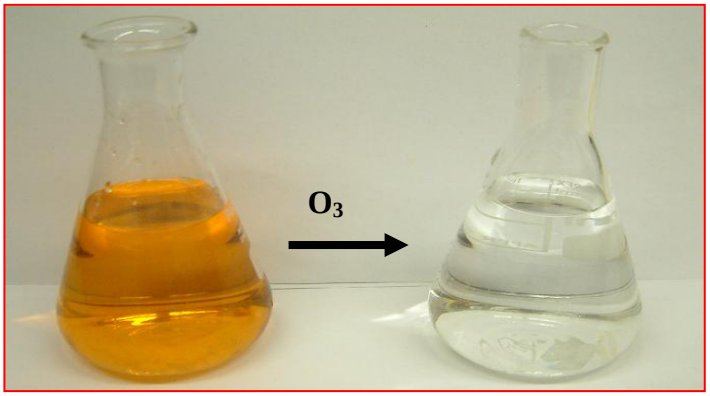

Figure 5.22: Dye (RO16) before and after ozonation

5.5.4. Effect of the Ozone Gas Concentration and Initial Dye Concentration on RO16 Decolourisation

In order to study the ozone effect on RO16 decolourisation, ozone was applied to dye solutions at different concentrations using different ozone gas concentrations. It has been noticed that the time required to remove RO16 decreases with the increase of ozone gas concentration applied, as shown in Figure 5.23. Figures 5.24 to 5.27 show the change of dye concentration as function of time for various dye and ozone concentrations. Table 5.11 provides the parameters of all experiments and the time required to remove 95 % of the dye, $t_{0.95}$. By simply following the figures obtained, it is clear that the time required decolourise 100 mg/L of dye by 20 g/m^3 NTP is about 27 minutes. On the other hand, only about 5.5 minutes were needed to decolourise 100 mg/L of dye by applying an ozone gas concentration of 80 g/m^3 NTP, as shown in Figure 5.23. Also from Figure

5.27, it can be observed that the RO16 solution, which had the concentration of 25 mg/L, decolourised effectively within 1.25 minutes. But from Figure 5.23, higher dye concentration required more time for decolourization (6 minutes). So it could be concluded that as the concentration of dye increased, the time required for ozonation is also increased. Figure 5.28 shows that $t_{0.95}$ increases linearly with the dye concentration for a given ozone gas concentration. The time $t_{0.95}$ can the be calculated using an equation of the form $t_{0.95}$ = S (C_{AGi}) x C_{B0} ; where S (C_{AGi}) is the slope of the lines shown in Figure 5.28, which is function of the inlet gas ozone concentration C_{AGi}; C_{B0} is the initial dye concentration. A plot of S as function of C_{AGi} is shown in Figure 5.29, which gives a linear relationship between S and C_{AGi}, that can be written as S = a× C_{AGi}. From this analysis, it was deduced that $t_{0.95}$ may be simply calculated using Equation 5.5.

$$t_{0.95} = a \times C_{AGi} \times C_{B0} \tag{5.5}$$

Table 5.11: Parameters of all experiments of RO16

Experimental No	Ozone Concentration inlet (g/m^3)NTP	Dye Concentration (mg/L)	$t_{0.95}$ (min)
D1	20	25	5.46
D2	20	50	10.12
D3	20	75	15.31
D4	20	100	20.33
D5	40	25	2.96
D6	40	50	5.62
D7	40	75	8.60
D8	40	100	10.97
D9	60	25	2.20
D10	60	50	4.15
D11	60	75	5.66
D12	60	100	7.35
D13	80	25	1.25
D14	80	50	2.33
D15	80	75	3.87
D16	80	100	5.49

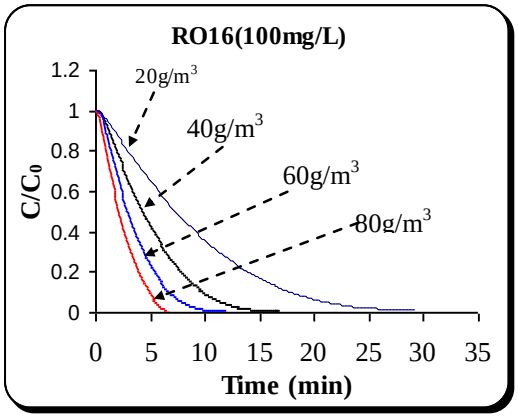

Figure 5.23: Effect of ozone concentration on RO16 decolourisation

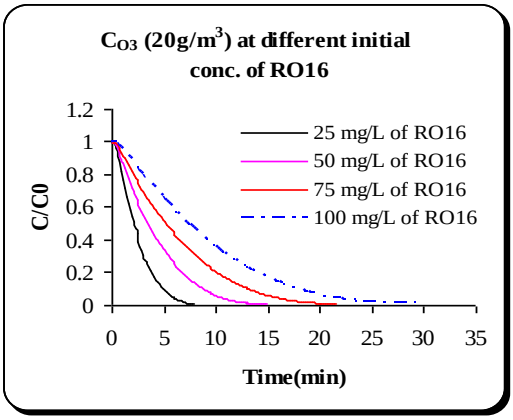

Figure 5.24: RO16 decolourisation with 20g/m^3 of ozone at different initial dye concentrations

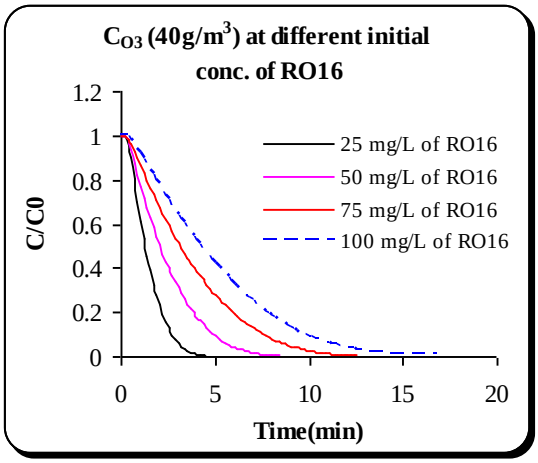

Figure 5.25: RO16 decolourisation with 40g/m^3 of ozone at different initial dye concentrations

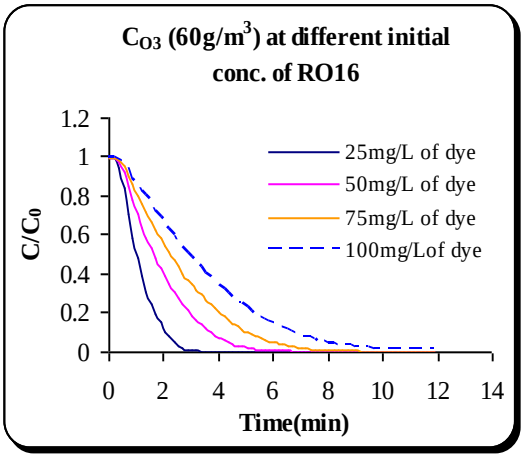

Figure 5.26: RO16 decolourisation with 60g/m^3 of ozone at different initial dye concentrations

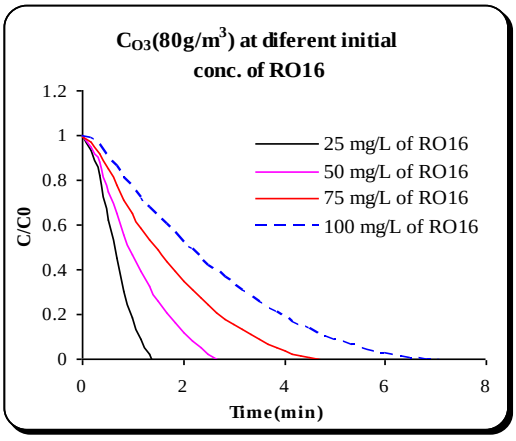

Figure 5.27: RO16 decolourisation with 80g/m^3 of ozone at different initial dye concentrations

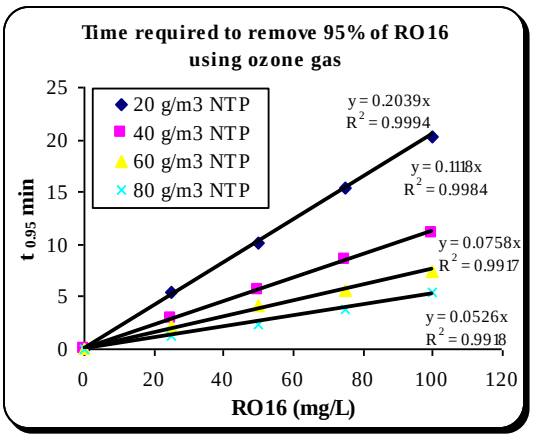

Figure 5.28: Effect of initial RO16concentration and ozone concentration on $t_{0.95}$

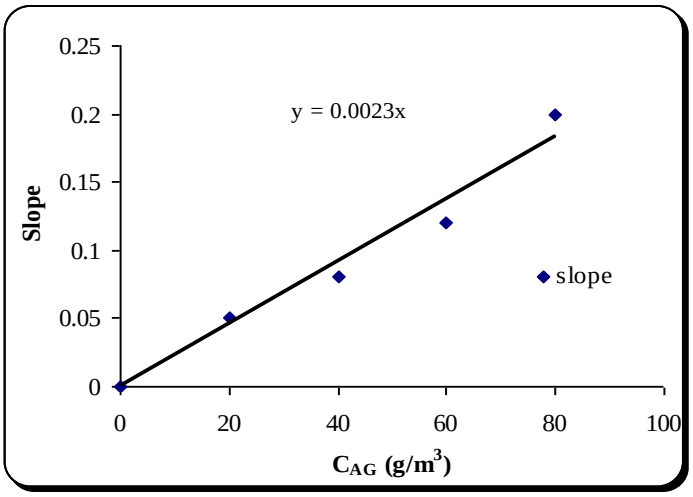

Figure 5.29: Effect of C_{AG} on the slope in Figure 5.28

5.5.5. Determination of the reaction stoichiometry and rate constant of RO16 ozonation

5.5.5.1. Stoichiometric ratio

The direct reaction of ozone with dye RO16 can be expressed by the following equation:

$$A + zB \rightarrow products \qquad (5.6)$$

The stoichiometric factor (z) was determined as described in Section (3.3.1). In most cases, the stoichiometric ratio of the reaction between ozone and dyes is in the order of 1 to 4 mol/mol (Hoigne and Bader 1983a). According to the experimental results of this work and knowing that the purity of the dye is 50 %, approximately 3 mol of ozone are required to decolourise one mol of RO16, which is in close agreement with literature. The experiments were conducted at pH 2 and flow rate 400 mL/min. The operating conditions and calculated results are shown in Table 5.12

Table 5.12: Operating conditions and calculated results of stoichiometric factor (z)

CO_3_gas (g/m^3)	v(reactor) (mL)	v(RO16) (mL)	n(ozone) $_{initial}$ (mol)	Δn(RO16) n(init)-n(final) (mol)	CO_3_L (mg/L)	z(RO16/O_3) (mol/mol)	1/z (mol O_3/mol RO16)
41.3	350	2.5	4.8×10^{-5}	1.85×10^{-5}	10.94	0.39	2.59
40.0	500	5.0	6.1×10^{-5}	2.40×10^{-5}	9.57	0.39	2.54
39.1	500	2.5	6.6×10^{-5}	1.85×10^{-5}	10.34	0.28	3.57
					Average	0.35	2.90

5.5.5.2. Rate constant

The rate constant of dye RO16 with molecular ozone was determined at different pH values, as described in section (3.3.2) and the results are shown in Table 5.13.

5.5.5.2.1. Heterogeneous (ozone bubbling in RO16)

The determination of the rate constant was made using Equation 3.25, assuming fast kinetics. Because the specific surface area, a_L, was required for the calculation of k, a preliminary study was made to determine its value under the experimental conditions used in this work. The experimental procedure was described in Section 3.3.2.1 and Equation 3.26 was used for the calculation of a_L. Results of this work are presented in Table 5.13 and the effect of gas flow rate on a_L is shown in Figure 5.30. By replacing a_L value in Equation 3.25, the rate constant k of RO16 degradation was determined. Results are shown in Table 5.13.

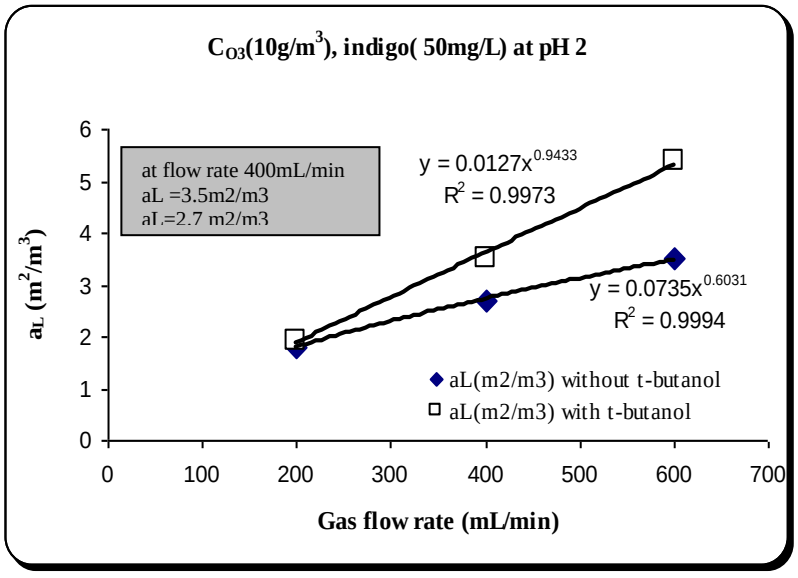

Figure 5.30: Surface area versus gas flow rate

Table 5.13: Experimental operating conditions and calculated results of a_L and k

Exp No	Q_G (mL/min)	a_L (m^2/m^3)	C_{AG} (g/m^3)	C_{AL}* (mol/L)	CB_0 (mg/L)	pH	slope	Rate constant k ($M^{-1}s^{-1}$)
Indigo & ozone (without t-butanol)								
In1	200	1.780	10.6	$5.62x10^{-5}$	50	2.2	$2.0x10^{-5}$	$9.4x10^{7}$
In2	400	2.749	10.3	$5.46x10^{-5}$	50	2.2	$3.0x10^{-5}$	$9.4x10^{7}$
In3	600	3.523	10.7	$5.68x10^{-5}$	50	2.2	$4.0x10^{-5}$	$9.4x10^{7}$
Indigo & ozone (with t-butanol)								
In4	200	1.900	10.1	$5.36x10^{-5}$	50	2.2	$2.09x10^{-5}$	$9.4x10^{7}$
In5	400	3.500	10.7	$5.68x10^{-5}$	50	2.2	$3.90x10^{-5}$	$9.4x10^{7}$
In6	600	5.400	104	$5.52x10^{-5}$	50	2.2	$5.65 x10^{-5}$	$9.4x10^{7}$
RO16 & ozone (without t-butanol)								
D1	400	2.749	20	$1.06 x10^{-4}$	25	4.74	$1.0 x10^{-3}$	$1.2x10^{7}$
D2	400	2.749	20	$1.06 x10^{-4}$	50	4.69	$8.0 x10^{-4}$	$7.4x10^{6}$
D3	400	2.749	20	$1.06 x10^{-4}$	75	4.71	$6.0 x10^{-4}$	$4.2x10^{6}$
D4	400	2.749	20	$1.06 x10^{-4}$	100	4.74	$5.0 x10^{-4}$	$2.9x10^{6}$
D5	400	2.749	40	$2.12 x10^{-4}$	25	4.68	$1.8 x10^{-3}$	$1.9 x10^{7}$
D6	400	2.749	40	$2.12 x10^{-4}$	50	4.72	$1.3 x10^{-3}$	$9.7x10^{6}$
D7	400	2.749	40	$2.12 x10^{-4}$	75	4.78	$1.1 x10^{-3}$	$7.0x10^{6}$
D8	400	2.749	40	$2.12x10^{-4}$	100	4.74	$9.0x10^{-4}$	$4.7x10^{6}$
D9	400	2.749	60	$3.19 x10^{-4}$	25	4.72	$2.4 x10^{-3}$	$2.2 x10^{7}$
D10	400	2.749	60	$3.19 x10^{-4}$	50	4.77	$1.7 x10^{-3}$	$1.1 x10^{7}$
D11	400	2.749	60	$3.19 x10^{-4}$	75	4.7	$1.6 x10^{-3}$	$9.8x10^{6}$
D12	400	2.749	60	$3.19 x10^{-4}$	100	4.71	$1.3 x10^{-3}$	$6.5x10^{6}$
D13	400	2.749	80	$4.20 x10^{-4}$	25	4.69	$3.2 x10^{-3}$	$2.9 x10^{7}$
D14	400	2.749	80	$4.20 x10^{-4}$	50	4.72	$2.9 x10^{-3}$	$2.4 x10^{7}$
D15	400	2.749	80	$4.20 x10^{-4}$	75	4.69	$2.2 x10^{-3}$	$1.4 x10^{7}$
D16	400	2.749	80	$4.20 x10^{-4}$	100	4.7	$1.8 x10^{-3}$	$9.3x10^{6}$
D17	400	2.749	20	$1.06 x10^{-4}$	25	2	$2.3x10^{-5}$	$6.1 x10^{3}$
D18	400	2.749	20	$1.06 x10^{-4}$	100	2	$1.37x10^{-5}$	$2.2 x10^{3}$
D19	400	2.749	80	$4.20 x10^{-4}$	25	2	$6.9x10^{-5}$	$1.4 x10^{4}$
D20	400	2.749	80	$4.20 x10^{-4}$	100	2	$7.09x10^{-5}$	$1.1 x10^{4}$
D21	400	2.749	20	$1.06 x10^{-4}$	25	7	$2.35x10^{-5}$	$6.4 x10^{3}$
D22	400	2.749	20	$1.06 x10^{-4}$	100	7	$1.34x10^{-5}$	$2.1 x10^{3}$
D23	400	2.749	80	$4.20 x10^{-4}$	25	7	$4.49x10^{-5}$	$5.8 x10^{3}$
D24	400	2.749	80	$4.20 x10^{-4}$	100	7	$3.46x10^{-5}$	$3.4 x10^{3}$
D25	400	2.749	20	$1.06 x10^{-4}$	25	11	$2.37x10^{-5}$	$8.6 x10^{3}$
D26	400	2.749	20	$1.06 x10^{-4}$	100	11	$2.07x10^{-5}$	$4.9 x10^{3}$
D27	400	2.749	80	$4.20x10^{-4}$	25	11	$5.29x10^{-5}$	$8.1 x10^{3}$
D28	400	2.749	80	$4.2 x10^{-4}$	100	11	$6.25x10^{-5}$	$1.1 x10^{4}$
RO16 with t-butanol								
D29	400	3.5	20	$1.06 x10^{-4}$	25	2.05	$2.0x10^{-5}$	$3.6 x10^{3}$
D30	400	3.5	20	$1.06 x10^{-4}$	100	2.05	$3.0x10^{-5}$	$8.1 x10^{3}$

D31	400	3.5	80	4.20×10^{-4}	25	2.17	7.0×10^{-5}	1.1×10^{4}
D32	400	3.5	80	4.20×10^{-4}	100	2.18	8.0×10^{-5}	1.4×10^{4}
D33	400	3.5	20	1.06×10^{-4}	25	7.08	4.0×10^{-5}	1.4×10^{4}
D34	400	3.5	20	1.06×10^{-4}	100	7	2.0×10^{-5}	3.6×10^{3}
D35	400	3.5	80	4.20×10^{-4}	25	7.01	8.0×10^{-5}	1.1×10^{4}
D36	400	3.5	80	4.20×10^{-4}	100	7.01	1.0×10^{-5}	2.3×10^{2}
D37	400	3.5	20	1.06×10^{-4}	25	11.01	3.0×10^{-5}	8.1×10^{3}
D38	400	3.5	20	1.06×10^{-4}	100	11.1	5.0×10^{-5}	2.3×10^{4}
D39	400	3.5	80	4.2×10^{-4}	25	11.01	5.0×10^{-5}	5.6×10^{3}
D40	400	3.5	80	4.2×10^{-4}	100	11.1	7.0×10^{-5}	1.1×10^{4}

Figure 5.31 and Figure 5.32 show the change of $C_B^{0.5}$-$C_{B0}^{0.5}$ as function of time for RO16 ozonation without and with t-butanol respectively. The figures show linear relationship, which proves the applicability of the model discussed in section (3.3.2.1).

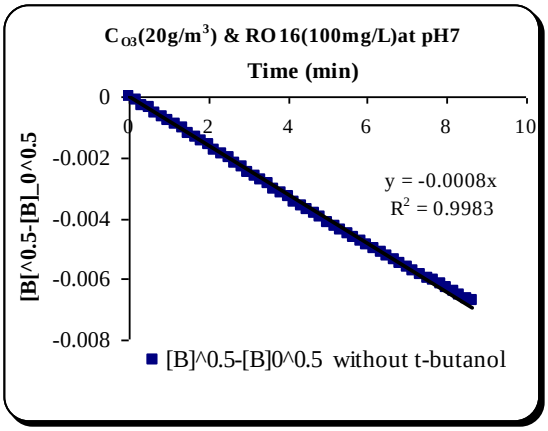

Figure 5.31: [B]^0.5-[B]_0^0.5 versus time (without t-butanol) at pH 7

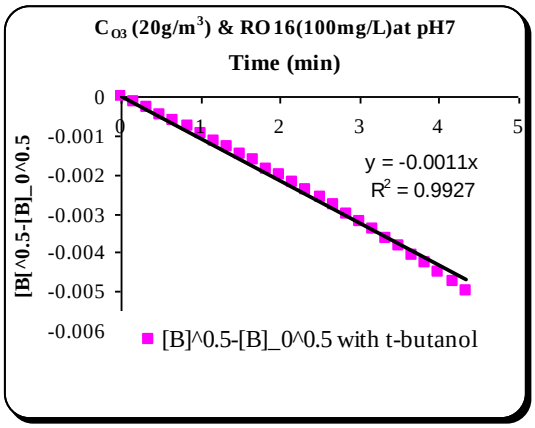

Figure 5.32: [B]^0.5-[B]_0^0.5 versus time (with t-butanol) at pH 7

5.5.5.2.2. Heterogeneous competitive kinetics

The rate constant of RO16 was studied as described in section (3.3.2.2). A UV/Vis spectrum for 50:50 % of RO16 at 100 mg/L and indigo at 100 mg/L is shown in Figure 5.33. From Figure 5.33, when the indigo and RO16 are mixed, there was no absorbance interference at the wavelength 600 nm, whereas at wavelength 496 nm it can be seen clearly there was interference. In order to take into account of the contribution of indigo in absorbance at 496 nm, a method was developed to remove such interference as described below.

First, the relationship between abs_{600} and abs_{496} using indigo solutions was determined and resulted in a straight line of slope (β), as shown in Figure 5.36. Second, the interference of indigo at 496 nm is removed as follows:

$$(Abs)_{measurement} = Abs_{B1} + Abs_{B2} \quad (5.7)$$

$$(Abs_{496})_{measurement} = (Abs_{496})_{B2} + (Abs_{496})_{B1} \quad (5.8)$$

$$(Abs_{496})_{measurement} = (Abs_{496})_{B2} + \beta * (Abs_{600})_{measurement} \quad (5.9)$$

$$(Abs_{496})_{B2} = (Abs_{496})_{measurement} - \beta (Abs_{600})_{measurement} \quad (5.10)$$

Where: β is the slope of line in Figure 5.37, B_1 is indigo and B_2 is RO16.

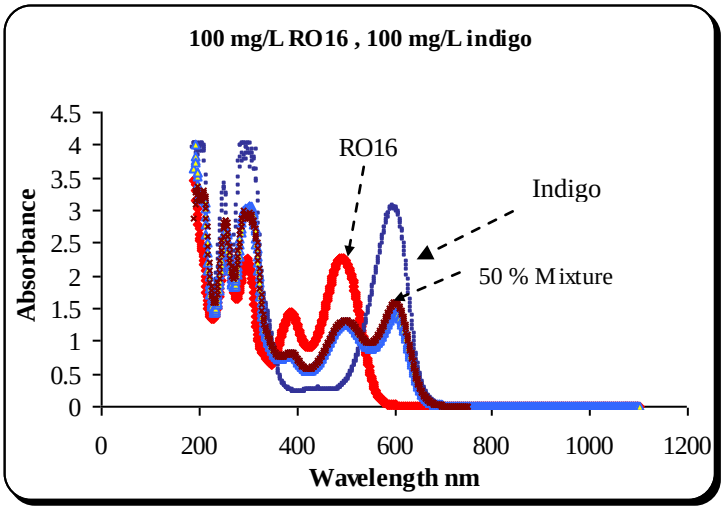

Figure 5.33: Full spectrums of (RO16 + indigo)

Once the interference at 496nm was removed, it was not possible to determine the rate constant of RO16 because the indigo reaction with ozone is very fast as compared to RO16 reaction with ozone; this can be seen from corrected graphs Figure 5.34 and Figure 5.35.

Table 5.14: Operating conditions of all experiments rate constant using competitive method

Exp No	Flow Rate (mL/min)	C_{O3} (g/m^3)	C_{RO16} (mg/L)	C_{Indigo} (mg/L)	$V_{(dye: indigo)}$ mL (50:50)%	Rate(k) ($M^{-1}.s^{-1}$)
D29	400	20	100	100	500	Cannot be determined
D30	400	15	100	100	500	
D31	400	10	100	100	500	

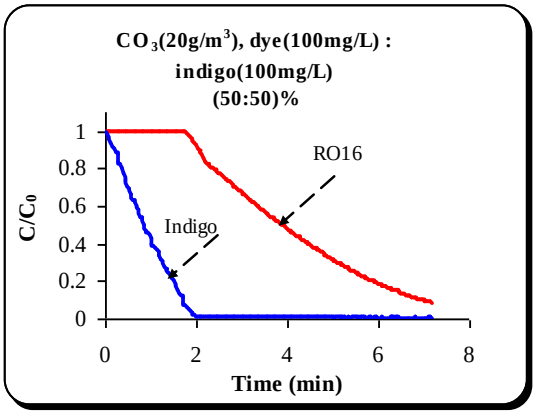

Figure 5.34: Concentrations versus time

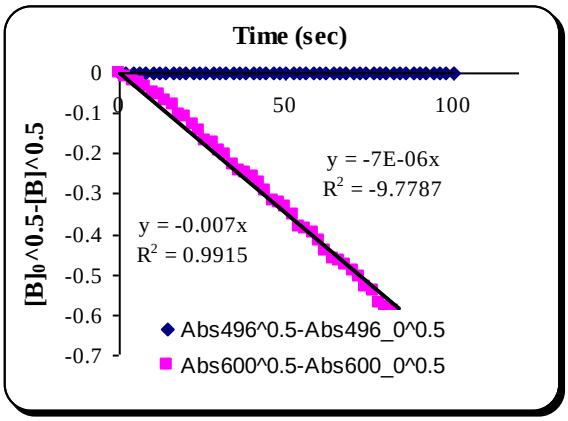

Figure 5.35: $[B]_0$^0.5-[B]^0.5 versus time

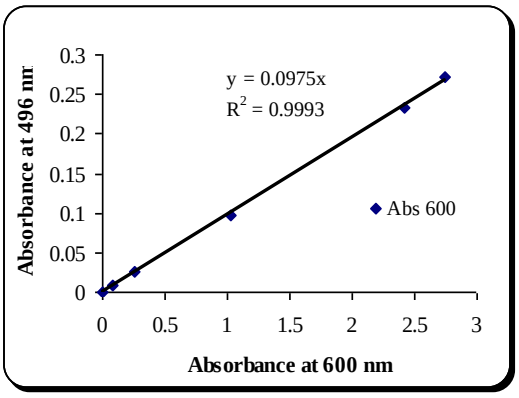

Figure 5.36: Relationship between Abs 496 and Abs 600

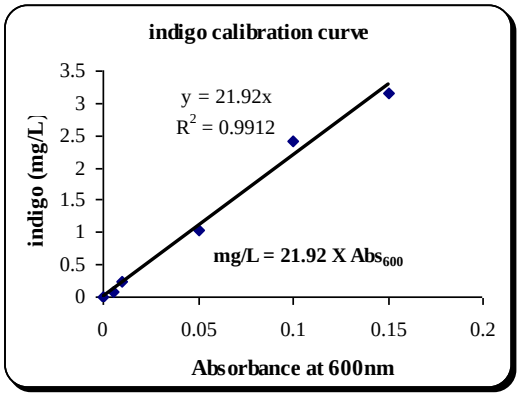

Figure 5.37: Calibration curve of indigo

It is to note that a calibration curve for indigo was determined as shown in Table 5.15 and Figure 5.37 to calculate indigo concentrations from absorbance values at 600 nm.

Table 5.15: Maximum absorbance for different concentration of indigo solution

Indigo (mg/L)	Absorbance at 600nm
0	0
0.005	0.08185
0.010	0.25140
0.050	1.02770
0.100	2.42550
0.150	3.15380

5.5.5.2.3. Homogenous kinetics

In this experiment, ozone mother solution was prepared by bubbling ozone gas in deionised water, then a solution of RO16 of known concentration and volume was injected by a syringe into the ozone solution as described in Section (3.3.2.3) and the rate constant of RO16 (k) was determined using Equation 3.43. Table 5.16 shows the rate constant of RO16 obtained by this method. The rate constant at pH 7 was obtained equal to 4.4×10^{-3} $M^{-1}s^{-1}$, which is in agreement with values of the rate constant obtained

with the heterogeneous method at pH7 as shown in Table 5.13. Moreover, this rate constant was compared to literature and again, good agreement was obtained with (Lopez 2007) who used a reactive Red 120 (RR120) at pH 7 (Table 5.16).

Table 5.16: Rate constant value of RO16

Compound	Rate constant of RO16, this work ($M^{-1}s^{-1}$)	Rate constant of (RR120), (Lopez, 2007) ($M^{-1}s^{-1}$)
Dye	$4.4x10^3$	$4.6x10^3$

5.5.6. Change of pH and conductivity RO16 ozonation experiment

The pH of the solution before and after ozonation was measured by the pH meter. Figure 5.38 shows the change of pH before letting the mixture of ozone in the reactor and at the end of the experiment, after around 5 minutes at (20 g/m^3 ozone gas and 25 mg/L RO16). From this graph, the pH level was reduced by 1.3 to 1.4 less than the initial pH. In addition to pH, the conductivity of the solution was also measured before and after ozonation. Figure 5.39 shows the change of conductivity as function of the initial dye concentration. Noticeable in this graph is that the conductivity values at the end of experiments have increased by 2 to 2.5 μs/cm more than the initial conductivity of the solution. The change of conductivity of the solution after ozonation is an indication of the formation of ions such as Na^+ and SO_4^{-2} following the degradation of the dye molecule (see molecular structure, Figure 1.1). In contrast, no significant changes of pH and conductivity occurred when ozone was simply bubbled in pure deionised water, indicating that ozone dissolution in water does not significantly change pH and conductivity of the solution. The reason behind the noticeable reduction of pH value in dye experiments is the formation of carboxylic acid following dye oxidation.

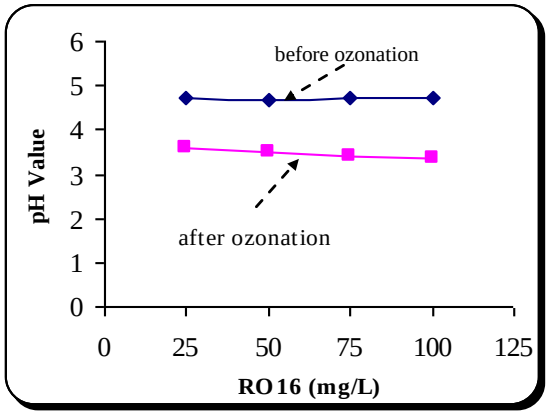

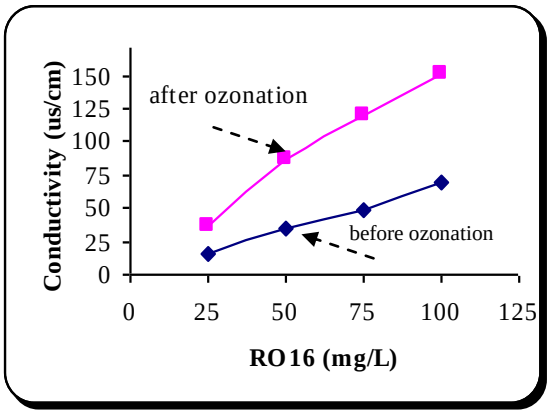

Figure 5.38: pH vs. initial RO16 concentration **Figure 5.39: C**onductivity vs. RO16 concentration

5.5.7. Effect of pH and Radical Scavenger on RO16 Ozonation

In order to study the effect of pH and radical scavenger on RO16 ozonation, experiments were carried out in the 500 mL- semi-batch reactor as previously described. The experiments were run without and with 0.2 M t-butanol (as radical scavenger) at different controlled pH values (2, 7 and 11). The temperature was kept constant at 20 ±1 ºC. The experiments numbers DS1-DS6 were made at dye concentration 100 mg/L and 20 g/m^3 of ozone concentration and were chosen as typical examples to present here. Table 5.17 shows the operating conditions for those experiments.

Table 5.17: Conditions of experiments (1-6) of dye ozonation

Exp. No	pH	Ozone conc. (g/m^3)	Dye conc. (mg/L)	t-butanol (mol)	$t_{0.95}$ (min)
DS1	2	20	100	0.2	6.41
DS2	2	20	100	0	11.16
DS3	7	20	100	0.2	2.71
DS4	7	20	100	0	4.46
DS5	11	20	100	0.2	4.08
DS6	11	20	100	0	9.83

Figure 5.40, 5.41, and 5.42 show the effect of addition of 0.2 M t-butanol on 100 mg/L of dye (RO16) with 20 g/m^3 of ozone gas at different pH. The observation from all experiments is that the bubble size decreased due to the addition of t-butanol, hence the volumetric mass transfer coefficient (k_La) increased following increase of the specific surface area (a). The increase in mass transfer is reflected in faster decrease of the dye concentration when t-butanol was added.

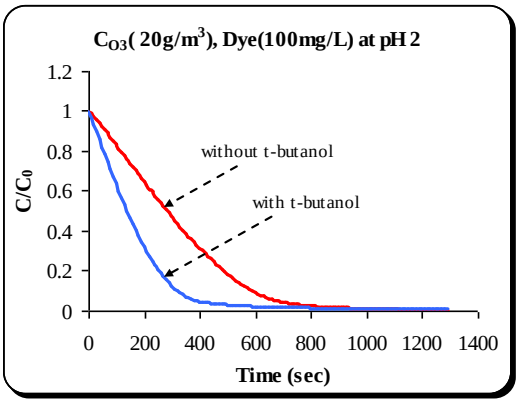

Figure 5.40: RO16 ozonation at pH 2 with and without t-butanol

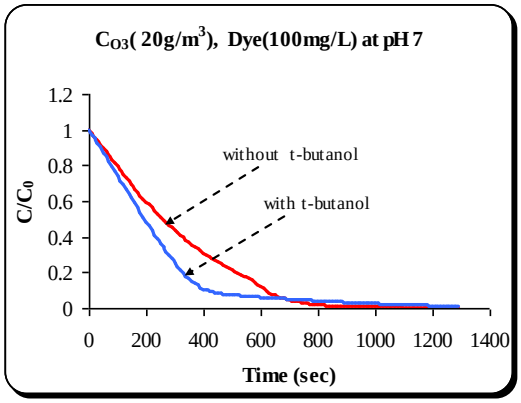

Figure 5.41: RO16 ozonation at pH 7 with and without t-butanol

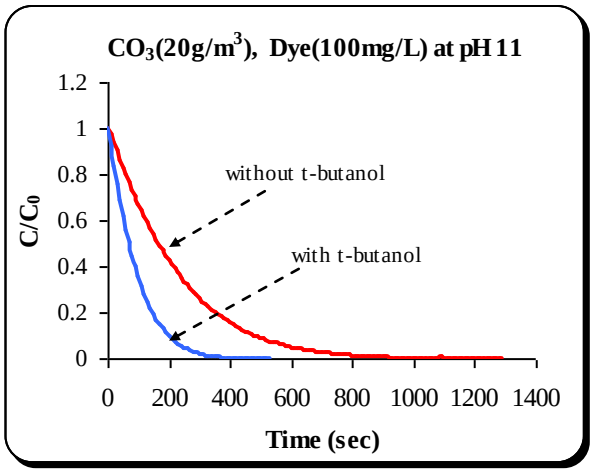

Figure 5.42: RO16 ozonation at pH 11 with and without t-butanol

On the other hand, dyes are more prone to reactions with molecular ozone as compared to indirect reactions with hydroxyl radicals, which also explains the enhanced rates obtained when t-butanol (a radical scavenger) was added (Lopez 2007).

5.5.8. Summary

From the above study, it was found that RO16 degradation increased by increasing the concentration of ozone. This degradation reaction was further increased by the addition of t-butanol. Rate constant (k) of RO16 ozonation in absence t-butanol was determined to be 9.1×10^3, 4.4×10^3 and 8.2×10^3 $M^{-1}s^{-1}$ at pHs (2, 7 and 11) respectively, whereas when the t-butanol was added to the solution of RO16, the values of k almost doubled at high pH but remained unchanged at low pH. These results indicate that molecular ozone reactions prevail those of radical reactions to degrade RO16.

Degradation of Triclocarban (TCC)

5.6. Degradation of Triclocarban (TCC) by Ozone using (LGO) System

As presented in the Introduction, there are environmental concerns regarding the presence of the widely used antiseptic TCC in water. Results on degradation of TCC in water using ozone are presented in this section.

5.6.1. Analysis of TCC

The analysis of TCC was made using the HPLC/UV methodology. In order to determine the maximum absorbance wavelength of TCC, initially a solution of the compound was analysed with a UV/Vis spectrophotometer (HP8453). 70 % acetonitrile: 30 % water was used as blank solution and TCC was used at a concentration of 100 mg/L. The full spectrum is presented in Figure 5.43. As can be seen from Figure 5.43, a maximum absorbance occurred at 265 nm. Based upon this result, subsequent analysis of the TCC using the HPLC/UV detector was carried out at a wavelength of 265 nm.

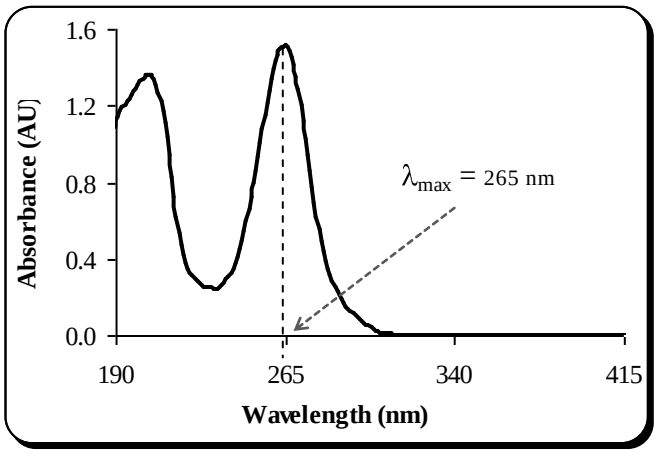

Figure 5.43: UV absorption spectrum of TCC (λ_{max} = 265 nm)

Six standard solutions of TCC in 70 % acetonitrile: 30 % water were prepared and injected in the HPLC system. Peak areas were correlated to the injected TCC

concentration and a plot was obtained as shown in Figure 5.44. The result was a straight line having an equation $C_{TCC}(mg/L) = 3.6 \times 10^{-4} \times$ (Peak area).

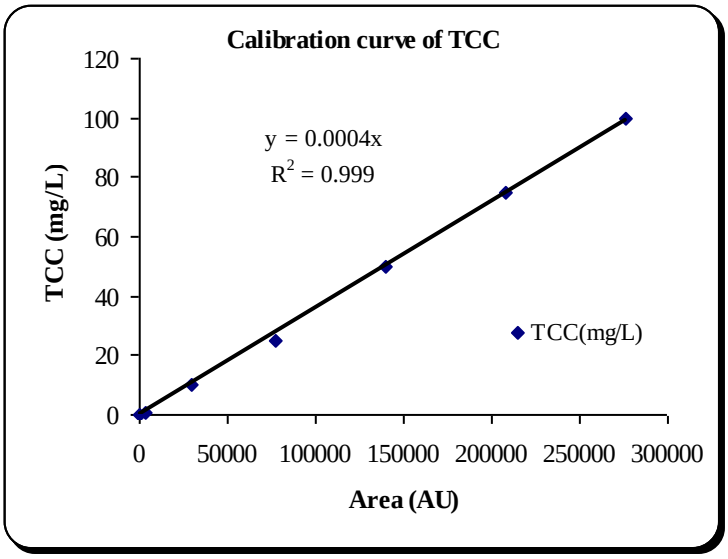

Figure 5.44: Calibration curve of TCC

5.6.2. Determination of ozone mass transfer parameters

5.6.2.1. Saturation ozone concentration in (70% acetonitrile: 30% water)

It was important for calculating the kinetics parameters to determine the saturation ozone concentration in the solvent used in this work (i.e. 70 % acetonitrile: 30 % water), which is different from pure water. Ozone gas concentration was fixed at a given value and the gas was bubbled in the liquid phase until saturation was reached. A UV spectrophotometer flow through cell was used in this work. Ozone concentration in the liquid phase was measured at the maximum absorbance λ_{max} = 262 nm, using an extinction coefficient ε = 3000 L/mol.cm. The values of molar ozone liquid concentrations were then correlated to the gas concentration. Linear relationship was obtained. The work was carried out for both solutions with and without t-butanol and the results are shown in Figure 5.45.

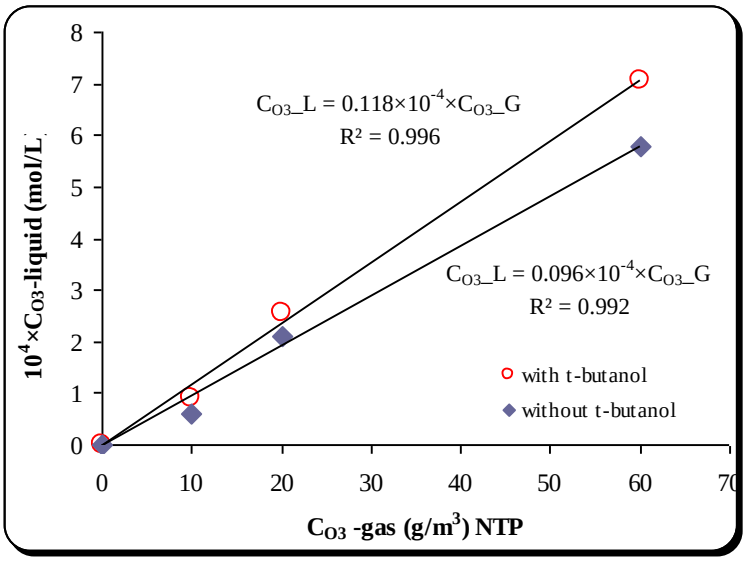

Figure 5.45: Correlation between ozone saturation concentration in 70%acetonitrile: 30%water and ozone gas concentration

5.6.2.2. Mass transfer specific surface area

The mass transfer specific surface area (a_L) was determined in this work using the fast kinetics method. The method involved bubbling ozone in a solution of indigo thrisulfonate, which reacts very fast with ozone at a rate constant of 9.4×10^7 $m^{-1}s^{-1}$ and the stoichiometric ratio is z = 1.

The specific area, a_L, was calculated as discussed in section 3.3.2.1, Equation 3.26. Results of this work gave values for a_L as presented in Table 5.18. It is obvious from Table 5.18 that t-butanol has increased a_L, due to reduction in the bubble sizes following the addition of t-butanol.

Table 5.18: Specific surface area for solvent (70%acetonitrile: 30% water)

Liquid phase	t-butanol (mol/L)	a_L (m^2/m^3)
70 % acetonitrile: 30 % water	0	7.0
70 % acetonitrile: 30 % water	0.2	11.6

5.6.3. TCC ozonation experiments

Different ozone gas concentrations (10, 20 and 60 g/m^3) NTP were used in this study to degrade a 100 mg/L TCC in 70 % acetonitrile: 30 % water solution. The change in ozone gas concentration at the outlet of reactor is shown in Figure 5.46 and the change in TCC concentration as function of time is shown in Figure 5.47.

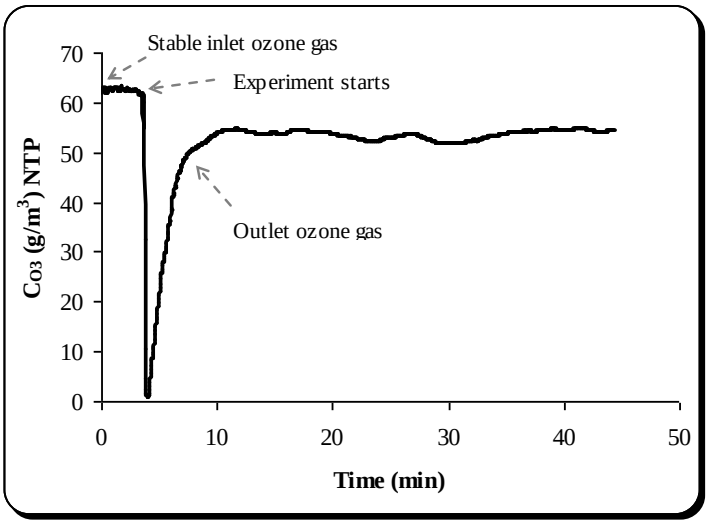

Figure 5.46: Ozone gas concentration versus time

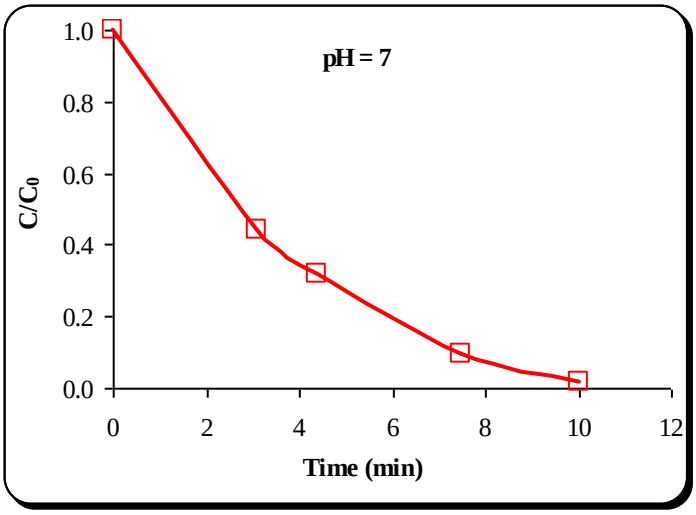

Figure 5.47: Degradation of TCC by ozone

The ozone gas concentration tends to reach after about 10 minutes a stable concentration lower than the inlet gas concentration. This may be due to ozone reactions with oxidation products, which may take place even though TCC degradation is completed. Figure 5.47 shows that within about 10 minutes, TCC degradation was almost completed. This result shows that ozone is effective in degrading TCC. Direct ozone and indirect (i.e. radical) reactions may be contributed to the degradation process. The trend of the relative concentration change with time, shown in Figure 5.47, seems to be described by a second order reaction kinetics, as will be demonstrated in the following sections.

5.6.4. Effect of ozone gas concentration on TCC degradation

In order to study the effect of ozone concentration on TCC degradation, ozone was bubbled into the TCC solution at different gas concentrations and the experiments were carried out as described previously. Figure 5.48 shows that the degradation of TCC increases with increasing ozone concentration. From the graph, it could be seen that when the ozone concentration was around 10 or 20 g/m^3 NTP, the time required to degrade TCC was around 60 minutes but when the ozone concentration increased to 60 g/m^3 NTP, the TCC degradation was very fast reaching zero in almost 10 minutes. In order to understand the effect of pure oxygen (O_2) on TCC degradation, control experiments using O_2 without ozone were carried out. In addition, experiments with nitrogen (N_2) were also carried out to asses the volatilization of TCC. Figure 5.49 shows the results obtained when O_2 and N_2 were used and for comparison purposes, results obtained when ozone was used is also shown in the figure. The Figure clearly shows that neither O_2 nor N_2 affect the degradation or removal of TCC and only the presence of ozone was capable to degrade TCC.

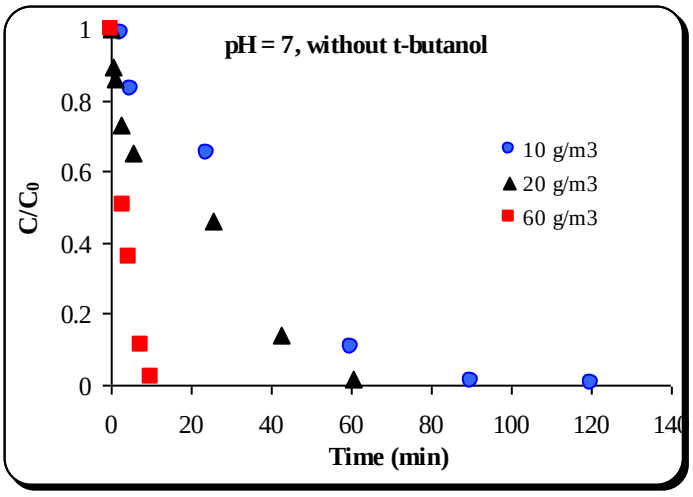

Figure 5.48: Concentration of TCC versus time at various inlet ozone gas concentrations

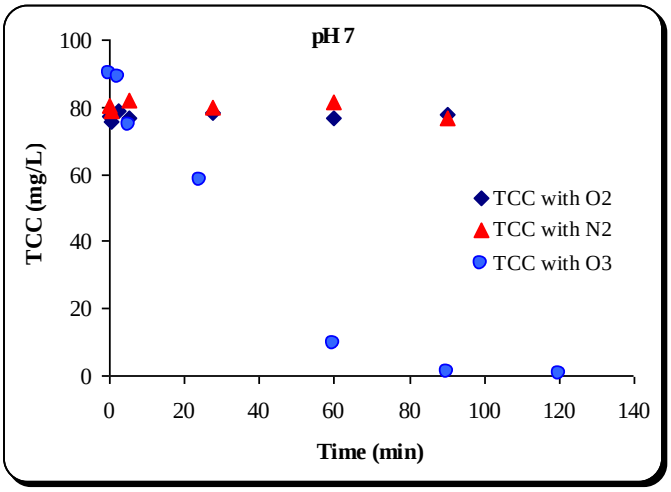

Figure 5.49: Concentration of TCC versus time

5.6.5. Effect of pH on TCC degradation

In order to determine the optimum pH at which the maximum degradation of TCC may occur, experiments were carried out at different controlled pH values of 2, 7 and 9. The temperature was kept constant at 20±1 ºC. The TCC concentration of the solution was 100 mg/L and an ozone concentration of 60 g/m^3 NTP was used. Figure 5.50 depicts the change in TCC concentration at different pH values. It is clear as long as the pH increased from 2 to 7, the rate of TCC degradation increased significantly. This may be due to increased hydroxyl radical concentrations, as consequence of ozone decomposition, which is promoted at high pH values by hydroxide ions. However, when the pH further increased to 9, a slight decrease in TCC degradation rate occurred as compared to pH 7, possibly due to competitive reactions between ozone and hydroxyl radicals with hydroxide ions, TCC and its degradation products and the solvent medium. Therefore, optimum pH needs to be obtained. Under the conditions of this study, pH 7 gave the best results for TCC degradation.

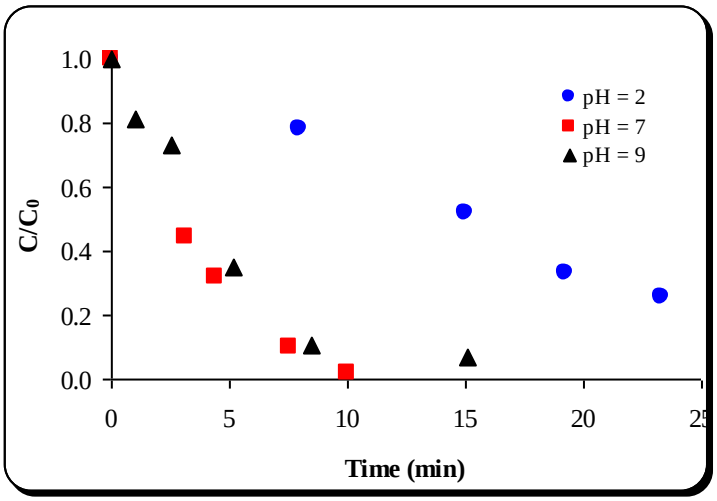

Figure 5.50: Effect of pH on TCC degradation

5.6.6. Effect of t-butanol as scavenger on TCC degradation

In order to study the effect of t-butanol as scavenger on TCC degradation, experiments were carried out with and without 0.2 M t-butanol at pH 7 and 20 ^{o}C. Figure 5.51 shows that at low ozone gas concentrations, t-butanol seems to have an insignificant effect on the degradation rates of TCC. However, for higher ozone concentration 60 g/m^3 NTP, the addition of t-butanol showed a significant decrease in the rate and extent of TCC degradation. This may be explained by the fact that t-butanol scavenges hydroxyl radicals, thus reducing their oxidation potential. During ozone bubbling, it was observed that the bubble size decreased due to the addition of t-butanol, thus increasing the specific surface area (Table 5.18), which in its turn increased the volumetric mass transfer coefficient, k_La. Increasing the specific surface area would also increase ozone mass transfer, thus would affect the degradation rate and this effect will be analysed in the following section.

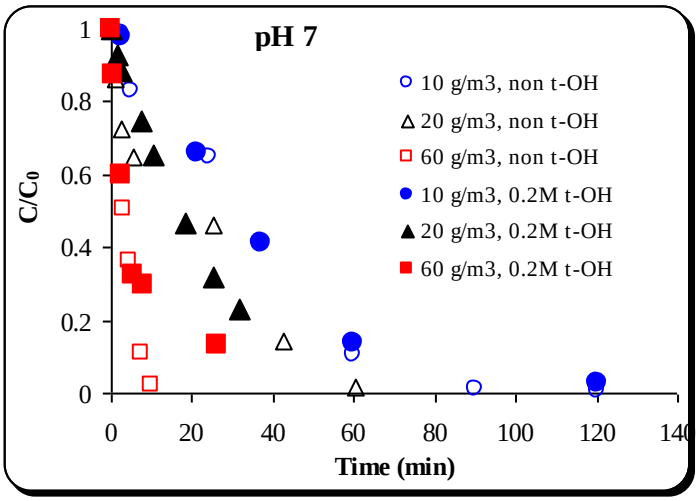

Figure 5.51: Effect of t-butanol (0.2 M) as scavenger on TCC degradation

5.6.7. Effect of Temperature on TCC Degradation

The effect of temperature on TCC degradation was also studied at three different temperatures of (10, 20 and 30 °C) in absence and presence of t-butanol. The results are shown in Figures 5.52 and 5.53 in the cases without and with t-butanol respectively. From Figure 5.52, it can be seen that at temperature 30 °C, 95 % of TCC was achieved in 60 minutes but at 10 and 20 ^{o}C, times of over 75 minutes were required. This result clearly shows that temperature increases the rate of the reaction between TCC and ozone. This effect was also noticed when t-butanol was added.

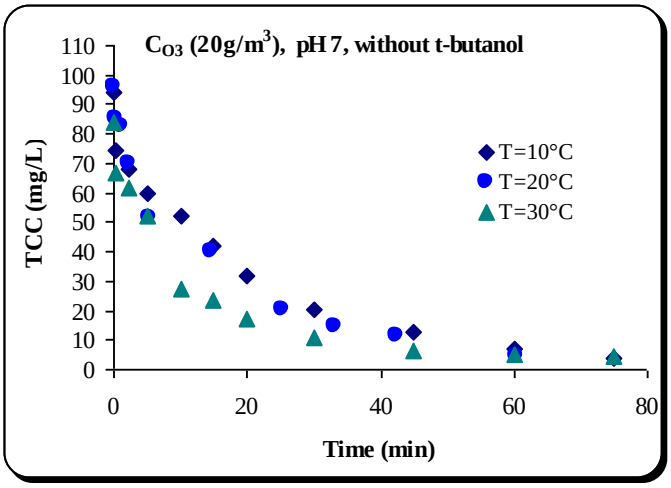

Figure 5.52: Effect of temperature on TCC degradation "non t- butanol"

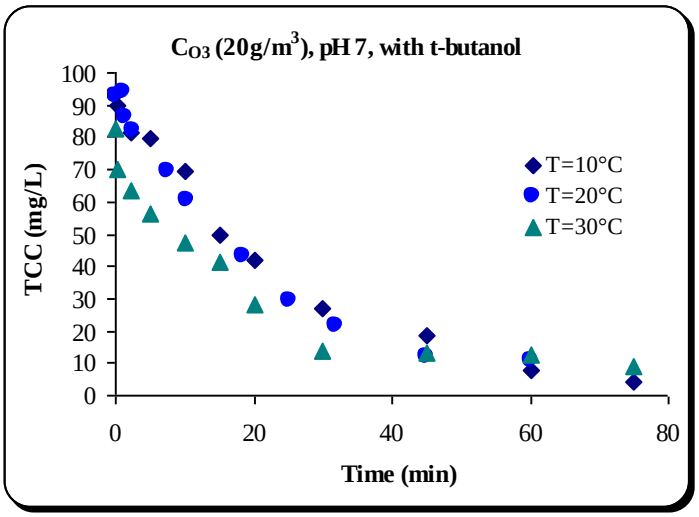

Figure 5.53: Effect of temperature on TCC degradation "with t-butanol"

5.6.8. Determination of the Stoichiometric Coefficient

The chemical reaction between ozone and TCC can be represented by the equation:

$$O_3 + zTCC \xrightarrow{k} \text{Products} \qquad (5.11)$$

The stoichiometry coefficient of TCC was determined in homogeneous system by measuring the change of TCC concentration after reaction, with a given initial concentration of ozone, as described earlier in Section 3.3. An average value of z equal to 1mol was obtained. The reaction rate constant of TCC oxidation with ozone at different pHs was determined using Equation 3.43, as discussed in the following section.

5.6.9. Determination of the Reaction Rate Constant at Different pHs

The three pH values of 2, 7 and 9 were studied in this work. For each pH value, the rate constant k was determined using an ozone gas concentration of 60 g/m^3 NTP, without the addition of t-butanol. The change of $\log_{10}$ (k) with pH is shown in Figure 5.54. It is clear that higher pH values gave higher rate constant. This may be explained by the presence of higher concentrations of hydroxyl radicals generated by ozone decomposition at higher pHs. The Figure also shows that an optimum pH should be determined since the rate constant did not increase substantially after pH7.

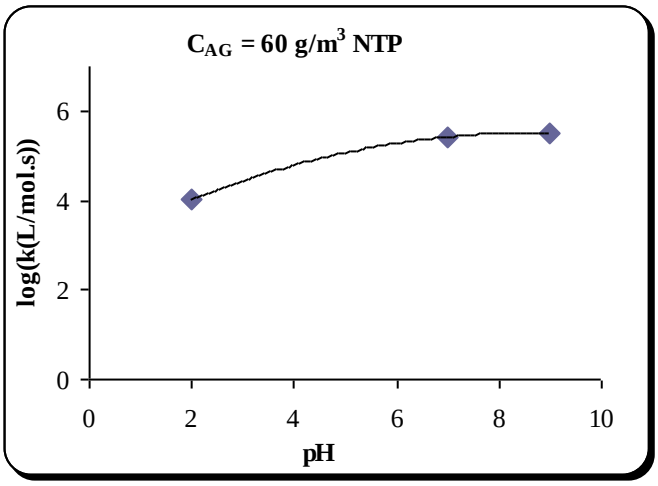

Figure 5.54: Effect of pH on TCC degradation rate constant

5.6.10. Effect of t-butanol on rate constant (k)

In the same fashion as previously presented, rate constants for different ozone gas concentrations 10, 20, 60 g/m^3 NTP and in the absence and presence of 0.2 M t-butanol were determined. Average values of rate constants are presented in Table 5.19. It can be seen that the addition of t-butanol has caused a substantial decrease in the rate constant by almost 78 %. Indeed the presence of t-butanol would scavenge hydroxyl radicals, thus reducing the rate constant (Glaze et al., 1987). Generally the rate constant is the result of the molecular ozone and °OH reactions as given below:

$$r = \frac{dc}{dt} \tag{5.12}$$

$$r = k_d [O_3][TCC^-] + k_i [OH^-][TCC^-] \tag{5.13}$$

$$r = (k_d + \alpha k_i)[O_3][TCC^-] = k[O_3][TCC^-] \tag{5.14}$$

Where; $\alpha = \frac{[OH^-]}{[O_3]}$

Table 5.19: Reaction rate constant of TCC

pH	[t-butanol] (mol/L)	k (L/mol.s)	k_d (L/mol.s)	α k_i
7	0	5.4×10^4	9.3×10^3	4.5×10^4
7	0.2	9.3×10^3	9.3×10^3	0

5.6.11. Summary

The degradation of TCC with ozone at different experimental conditions was studied using solutions of TCC in 70 % acetonitrile: 30 % water. From these degradation experiments it can be concluded that the chemical reaction of triclocarban with ozone was found to follow second order reaction kinetics. As the pH increased, the rate constant also increased but an optimum pH has to be obtained. The addition of t-butanol decreased the rate of reaction, due to inhibition of radicals that contribute to the overall degradation reaction. The stoichiometry was found to be 1 mol/mol and the rate constant at pH 7 was 5.4×10^4 L/mol.s but dropped to 9.3×10^4 L/mol.s when t-butanol was added to the solution.

Degradation of Naphthalene

5.7. Degradation of Naphthalene using LGO System

The degradation of naphthalene with ozone at various experimental conditions was studied using solutions of naphthalene in 50 % methanol: 50 % water. The results obtained are presented and discussed in this section.

5.7.1. Naphthalene analysis

The maximum absorbance wavelength was determined using a 1-cm cell placed in an HP8453 UV/Vis spectrophotometer. 50 % methanol: 50 % water was used as a blank solution and naphthalene was used at a concentration of 100 mg/L. The spectrum is shown in Figure 5.55, from which the maximum absorbance wavelength was determined to be 269 nm. Based upon this result, subsequent analysis of the naphthalene using the HPLC/UV detector was carried out at a wavelength of 269 nm.

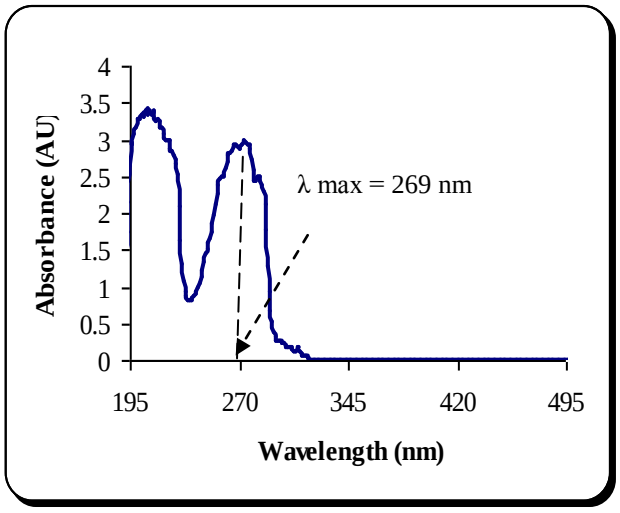

Figure 5.55: Absorption spectrum of naphthalene (λ_{max} = 269 nm)

Six standard solutions of naphthalene in 50 % methanol: 50 % water were prepared and injected in the HPLC system. Peak areas were correlated to the injected naphthalene concentration and a plot was obtained as shown in Figure 5.56. The result was a straight line having an equation $C_{Naph\text{-}}(mg/L) = 1.8x10^{-3} \times$ (Peak area).

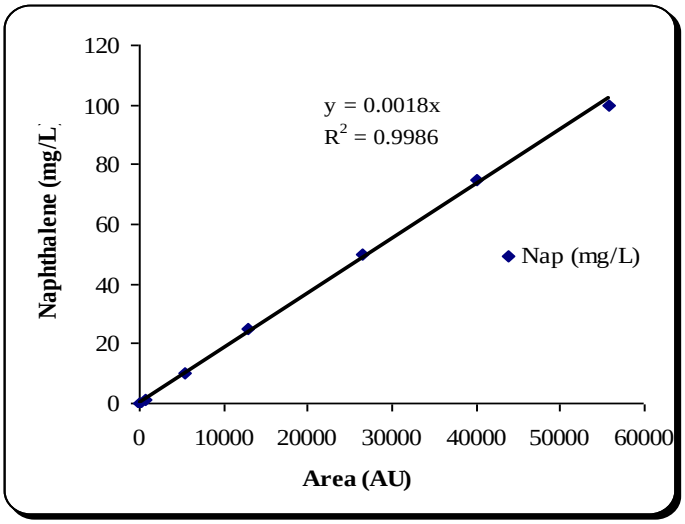

Figure5.56: Calibration curve of naphthalene

5.7.2. Determination of ozone mass transfer parameters

5.7.2.1. Saturation ozone concentration in 50%methanol: 50%water

The saturation of ozone gas concentration in solvent used in this work (50 % methanol: 50 % water) was determined by similar procedure in section 5.6.2.1. The results are shown in Figure 5.57. From Figure 5.57, a linear relationship was obtained. The work was carried out for both solutions with and without t-butanol.

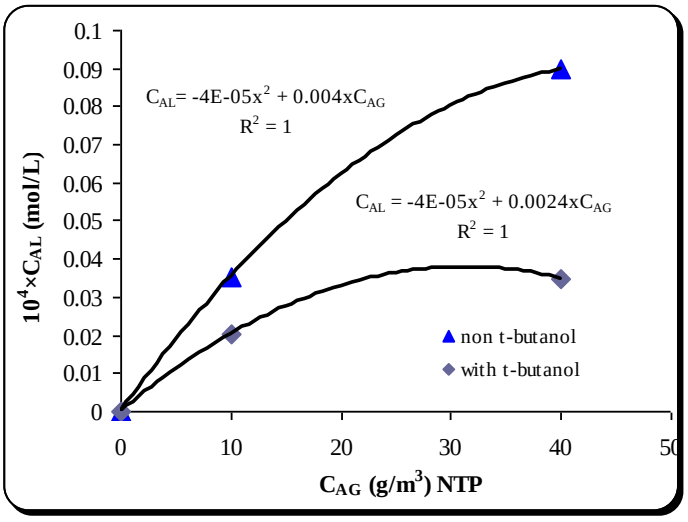

Figure 5.57: Correlation between ozone saturation concentrations in 50%methanol: 50%water and ozone gas concentration

5.7.2.2. Mass transfer specific surface area (a_L)

The mass transfer specific surface area (a_L) was determined in this work using the fast kinetics method. The method involved bubbling ozone in a solution of indigo

thrisulfonate at pH 2. Results of this work gave values for a_L, as presented in Table 5.20. It is obvious from Table 5.20 that t-butanol has increased a_L, due to changes in the liquid physico-chemical properties (e.g. surface tension), following the addition of t-butanol.

Table 5.20: specific surface area

Liquid phase	t-butanol (mol/L)	a_L (m^2/m^3)
50%methanol:50%water	0	148
50%methanol:50%water	0.2	342

5.7.3. Naphthalene ozonation experiments

Ozone gas concentration 40g/m^3 NTP was used in this study to degrade 100 mg/L naphthalene in 50 % methanol: 50 % water solution. The change in ozone gas concentration at the outlet of reactor is shown in Figure 5.58 and the change in naphthalene concentration as function of time is shown in Figure 5.59.

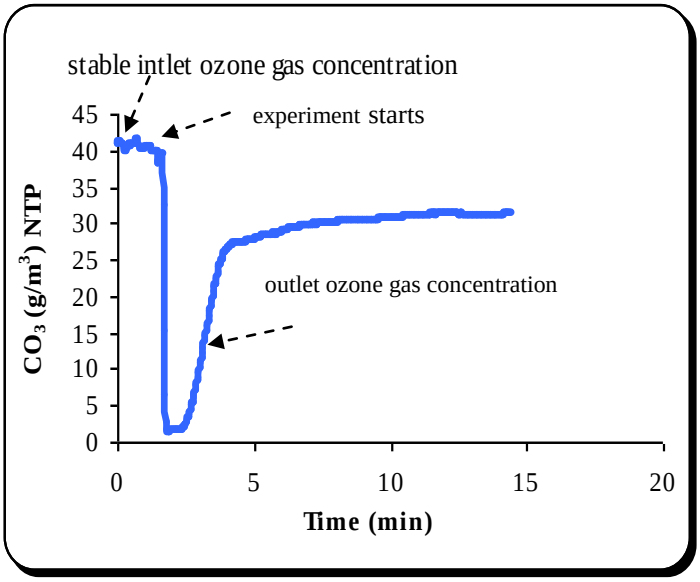

Figure 5.58: Ozone gas concentration versus time

The ozone gas concentration tends to reach a stable concentration lower than the inlet gas concentration after about 8 minutes. The ozone concentration did not reach the inlet concentration due to the ozone reactions with oxidation products and with methanol, which was present in large concentration in the solution. As shown in Figure 5.59, naphthalene concentration deceases with time and the total time required to remove 100mg/L of naphthalene was about 10 minutes from the beginning of bubbling. Figure

5.60 shows a linear relationship between $[naphthalene]^{0.5}$ - $[naphthalene]_0^{0.5}$ as function of time.

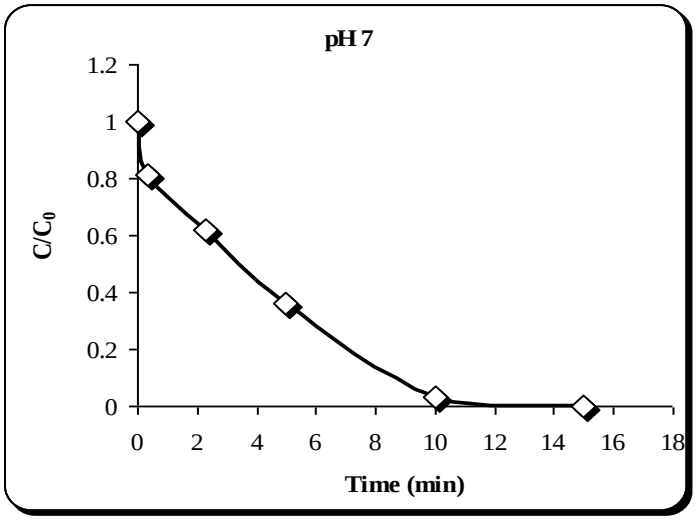

Figure 5.59: Concentration of naphthalene versus time

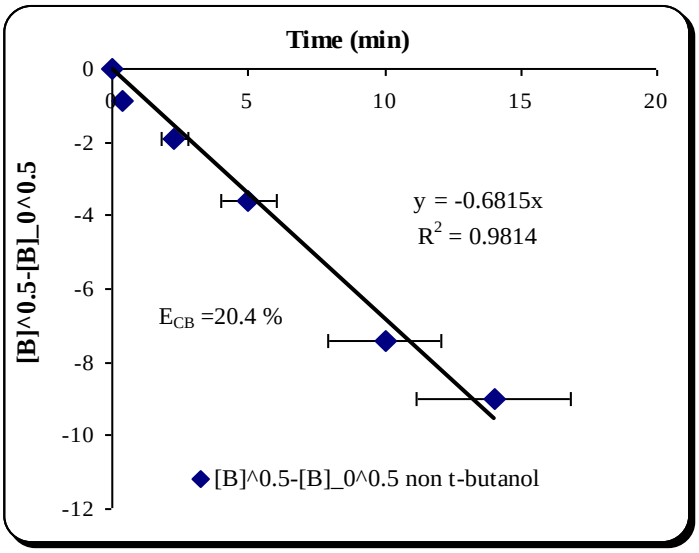

Figure 5.60: [B] ^0.5-[B] _0^0.5 versus time

The rate constant was then calculated and the value of 1.4×10^5 L/mol.s was obtained. This value was compared with the literature value ($1.5x10^3$ L/mol.s), which was obtained by (Legube et al., 1986) when the reaction was carried out at 20 °C and pH 6.5. The mechanism of naphthalene degradation with ozone was proposed by (Legube et al., 1986) and is shown as follows:

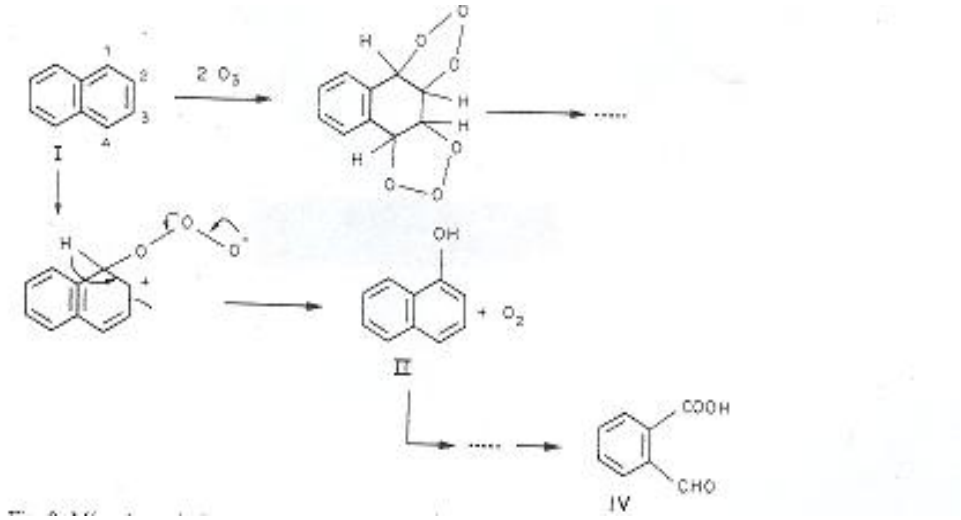

A: ozonation pathway of naphthalene: other possible initial attacks.

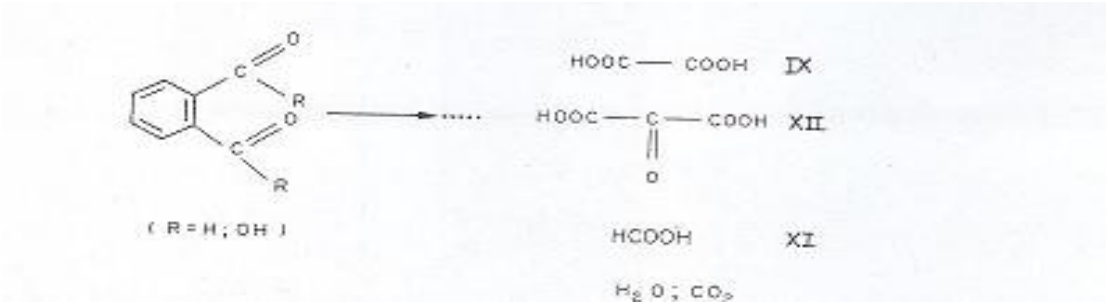

B: ozonation pathway of naphthalene: breakdown products from aromatic ring.

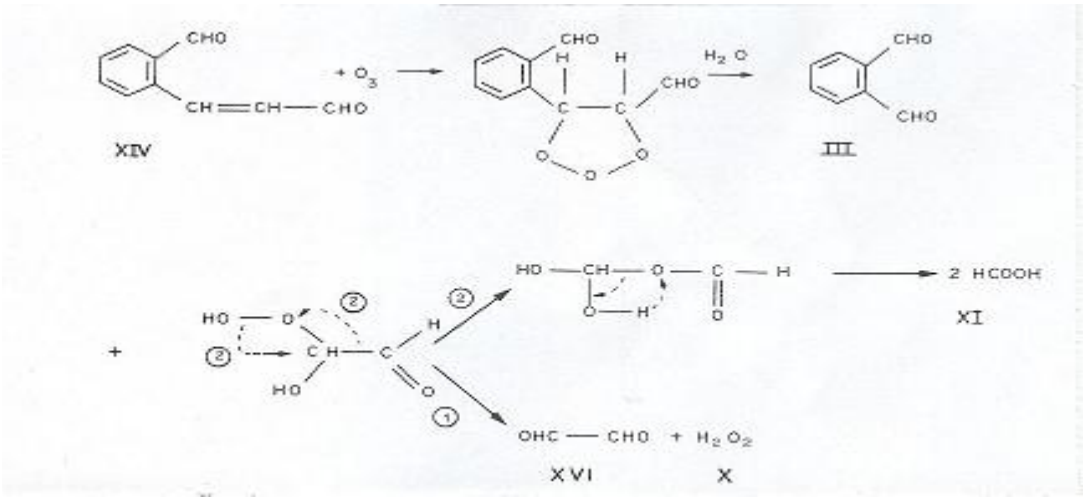

C: ozonation pathway of naphthalene: formation of formic acid.

5.7.4. Effect of pH and t-butanol on naphthalene degradation

In order to determine the optimum pH at which the maximum degradation of naphthalene may occur, experiments were carried out at different controlled pH values of 2, 7 and 9. The temperature was kept constant at 20±1 ºC. The naphthalene

concentration of the solution was 100 mg/L and an ozone concentration of 40 g/m^3 NTP was used. Figure 5.61 depicts the change in naphthalene concentration at different pH values. The Figure shows that the degradation rate of naphthalene increases as the pH decreases. Figure 5.62 depicts the change of [naphthalene]$^{0.5}$ - [naphthalene]$_0^{0.5}$ as function of time, which gives good linear relationship. From the slopes of the lines in Figure 5.62, the rate constants at different pHs were calculated and their values were obtained equal to 1.73x10^5, 1.4x10^5 and 0.15x10^5 L/mol.s at pH 2, 7 and 9 respectively.

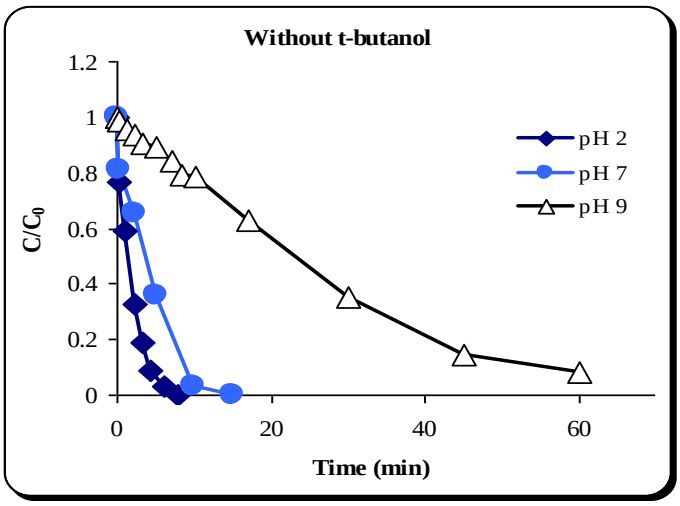

Figure 5.61: Effect of pH on naphthalene degradation

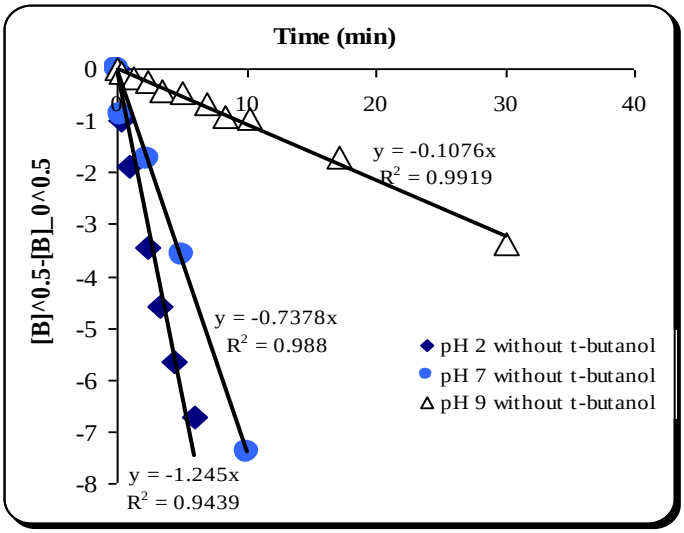

Figure 5.62: [B] ^0.5-[B] _0^0.5 versus time

In order to study the effect of t-butanol as scavenger on naphthalene degradation, experiments were carried out with and without 0.2 M t-butanol at pH value 7 and 20 ^{o}C

by mixing a solution of naphthalene with ozone saturated solution at 40 g/m^3 gas concentration. Figure 5.63 shows the change of naphthalene concentration with time in presence and absence of t-butanol. The Figure shows that t-butanol had no effect on the degradation rates of naphthalene, which proves that the main pathway of the oxidation of naphthalene is by molecular ozone.

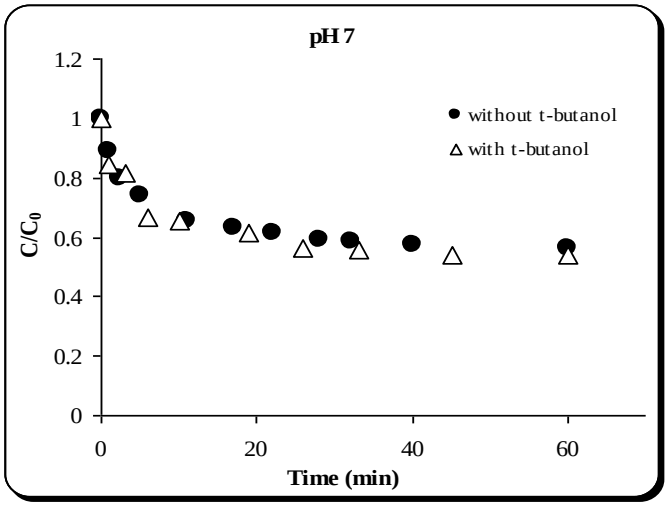

Figure 5.63: Effect of t-butanol on naphthalene degradation (homogenous)

5.7.5. Determination of the stoichiometric coefficient and reaction rate constant

The chemical reaction between ozone and naphthalene can be represented by the following equation:

$$O_3 + zNaph \xrightarrow{k} \text{Products} \qquad (5.15)$$

It was assumed that this reaction is of second order, (i.e. first order with respect to O_3 or ^oOH and first order with respect to naphthalene). The stoichiometry was determined in homogeneous system by measuring the change of naphthalene concentration after reaction with a given initial concentration of ozone as discussed in Section 3.3.1 (Equation 3.18). An average value of 1 mol per mol was obtained as shown in Table (5.21) and the worksheet of this calculation is shown in Appendix A2.4. The reaction rate constant was determined using Equation 3.25. The values of stoichiometry z and rate constant k of naphthalene degradation with ozone were compared to the literature as

shown in Table 5.22. The values of the rate constant that were obtained by (Hoigne 1983a, b) and (Legube et al., 1986) were found to differ from those obtained in this work by a factor of about 100 times, due to differences in the experimental conditions used in each study; in particular the solvent used in this work is by far different from the two past works. On the other hand, the stoichiometric ratios were found to be almost similar in all studies.

Table 5.21: Calculation of the stoichiometric ratio (z) of naphthalene

C_A Initial (mol/L)	C_B Initial (mol/L)	C_B final (mol/L)	n_A (mol)	n_B initial (mol)	n_B Final (mol)	D_n B (mol)	z (B/A)
$2.3x10^{-4}$	$3.9x10^{-4}$	$1.4x10^{-4}$	$4x10^{-5}$	$7.8x10^{-5}$	$3x10^{-5}$	4.810^{-5}	1.1

A: ozone; B: naphthalene

Table 5-22 Comparison of stoichiometric ratio and the rate constant values of naphthalene degradation with ozone

Parameter	This work	(Hoigne and Bader 1983a,b)	(Legube et al., 1986)
Stoichiometric ratio, z	1	1	2
Rate constant, k ($M^{-1}s^{-1}$)	$1.4 - 1.6 \times10^5$ (non t-butanol) 1.5×10^5 (with t-butanol)	$3 - 3.6 \times10^3$	1.5×10^3
Experimental Conditions	- pH 7 - temp- 20±1°C - ozone liquid concentration $1.12x10^{-2}$ mol/L - Napht- (100 mg/L) - Solvent: 50% methanol: 50% water	- pH 2 - temp- 20°C - ozone (10^{-5} mol/L) - Napht- (192 mg/L) Solvent: methanol 50%: 50 water	- pH 5.6 - temp 20°C - ozone ($0.6\text{-}1.1x10^{-5}$) mol/L - Napht-(51-89) mg/L - Solvent: methanol 50% : 50 water

5.7.6. Effect of pH and t-butanol on the reaction rate constant, (k)

Three pH values 2, 7 and 9 were studied in this work. For each pH value, the rate constant k was determined using an ozone gas concentration of 40 g/m^3 NTP without the addition of t-butanol. A typical curve for the change of naphthalene concentration with time is shown in Figure 5.64 and the change of k with pH is shown in Figure 5.65. From Figure 5.65, it is clear that the rate constants of naphthalene decrease as pH values increase.

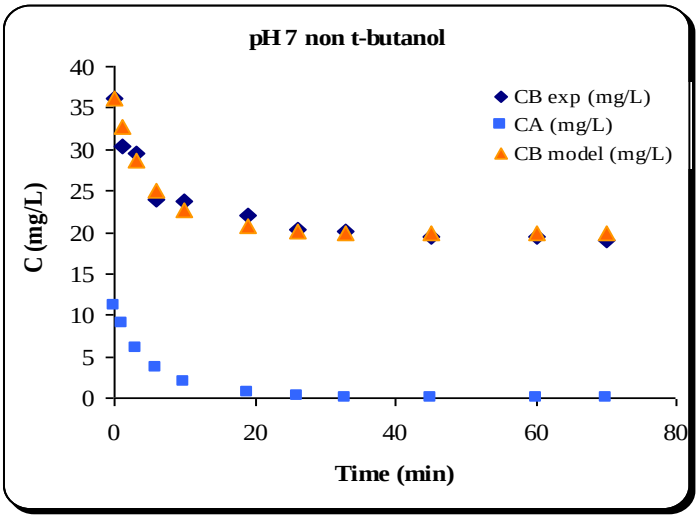

Figure 5.64: Modeling of determination of rate constant and stoichiometry of reaction between ozone and naphthalene at pH 7 "non t-butanol"

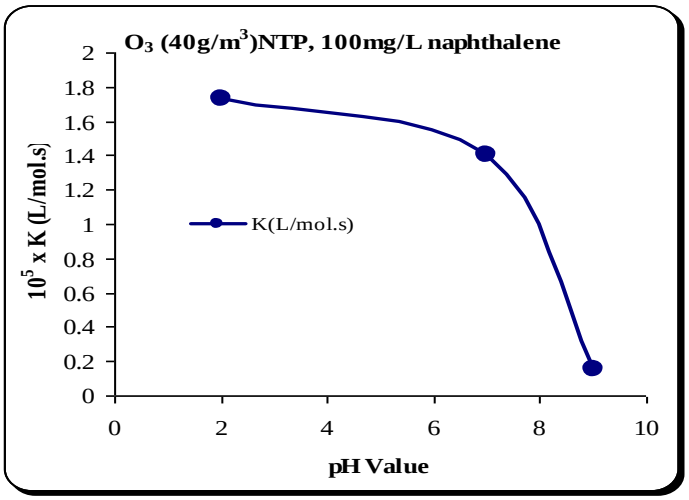

Figure 5.65: Effect of pH on naphthalene degradation rate constant

In the same way as previously presented, rate constants for ozone gas concentration 40 g/m^{3}NTP and in the absence and presence of t-butanol were determined (Figure 5.66). The values of rate constant are presented in Table 5.23. It can be seen that the addition of t-butanol has slightly increased by about 14 %, the rate constant from 1.4×10^5 to 1.6×10^5 L/mol.s.

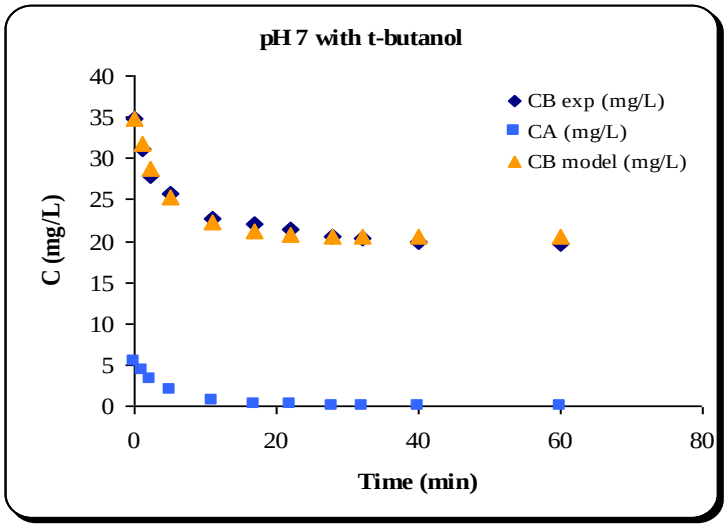

Figure 5.66: Modeling of determination of rate constant and stoichiometry of reaction between ozone and naphthalene at pH 7 "with t-butanol"

Table 5.23: Reaction rate constant of naphthalene without and with t-butanol

pH	t-butanol (mol/L)	k (L/mol.s)
7	0	1.4×10^5
7	0.2	1.6×10^5

5.7.7. Summary

The degradation of naphthalene using liquid /gas-ozone (LGO) system was studied. From naphthalene degradation experiments, it can be summarised, that the pH had a substantial effect on the degradation rate of naphthalene. Reaction rate constants were in the order of 1.4×10^5 and 1.6×10^5 L/mol.s in absence and presence of t-butanol as radical scavenger respectively**.** The reaction stoichiometry was found to have a value of 1mol/mol.

Degradation of Methanol

5.8. Degradation of Methanol by Ozone Using LGO System

The degradation of methanol was studied in this section using different experimental conditions. The aim here was to provide information on methanol degradation with ozone that is useful not only to enhance our understanding of the ozone reaction with methanol but also to provide base data useful to gain further understanding of the LSO system.

5.8.1. Degradation of methanol using (LGO) system

A literature search revealed that there is not enough studies on methanol degradation by ozone, except the work carried out by (Hoigne and Bader 1983a, b) and (Hoigne et al., 1985), who presented some kinetic data of the ozone reaction with methanol amongst other alcohols such as propanol, tert-butanol, and ethanol. In their studies, they found that ozone reacts with these alcohols at slow rates as shown in the Table (5.24) (Hoigne and Bader 1983a, b) and (Hoigne et al., 1985).

Table 5.24: Rate of reaction for some alcohols with ozone gas

Compound	Substituted Alkanes	pH	Rate constant ($M^{-1}.s^{-1}$)
Propanol	$O_3 + C_3H_7OH \rightarrow product$	2	0.37 ± 0.04
Ter-butanol	$O_3 + C(CH_3)_3OH \rightarrow product$	2/6	≈ 0.003
Methanol	$O_3 + CH_3OH \rightarrow product$	2/5	≈ 0.024
Ethanol	$O_3 + C_2H_5OH \rightarrow product$	2	0.37 ±0.04

For this reason, this study was important to add more information on methanol degradation using LGO system. In this work, several experiments were carried out to study the degradation of methanol using LGO system taking into account the effect of the mass transfer parameters such as ozone gas concentration, specific surface area, pH and scavenger (t-butanol).

5.8.1.1. Analysis of methanol

Methanol concentrations were determined using HPLC/UV or GC/FID techniques. The maximum absorbance wavelength was determined using a 1-cm cell placed in an HP8453 UV/Vis spectrophotometer. 100 % of deionised water was used as blank solution and methanol was used at known concentrations. The spectrum is shown in Figure 5.67 from which the maximum absorbance wavelength was determined to be 195nm. Based upon this result, subsequent analysis of the methanol using the HPLC/UV detector was carried out at a wavelength of 195 nm.

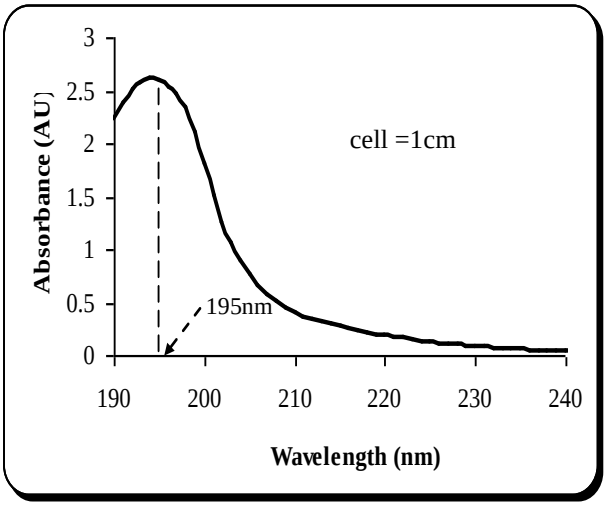

Figure 5.67: Absorption spectrum of methanol

Five standard solutions of methanol were prepared and injected in the HPLC system and the operating conditions of calibration curve of methanol are shown in Appendix A1.5 Table A1.17. Peak areas were correlated to the injected methanol concentration and a plot was obtained as shown in Figure 5.68. The result was a straight line having an equation: C_{MeOH}-(mol/L) = (Peak area) / 5348.9

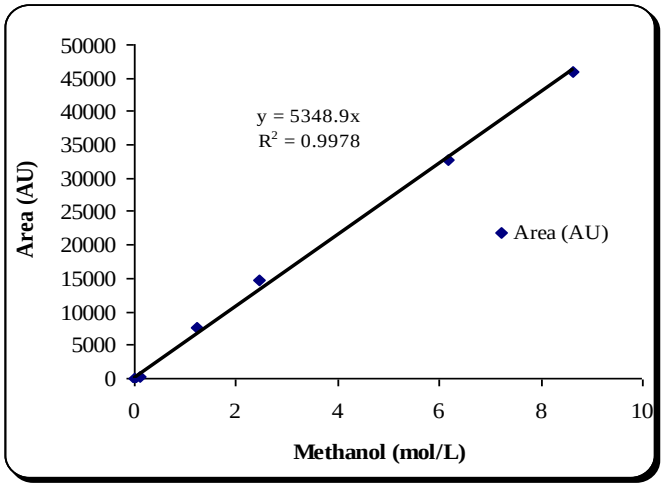

Figure 5.68: Calibration curve of methanol using (HPLC)

5.8.1.2. Methanol and GC/FID calibration curve

Methanol at low concentration was analysed with a GC/FID because simple HPLC/UV is not capable to detect methanol at low concentrations. In order to obtain a calibration curve of methanol in GC/FID, six standard solutions of methanol in water were prepared and injected in the GC/FID system and the data is shown in Appendix A1.5 Table A1.20. Peak areas were correlated to the injected methanol concentration and a plot was obtained as shown in Figure 5.69. The result was a straight line having an equation $C_{MeOH\text{-}}$(mol/L) = (Peak area) / 98224.

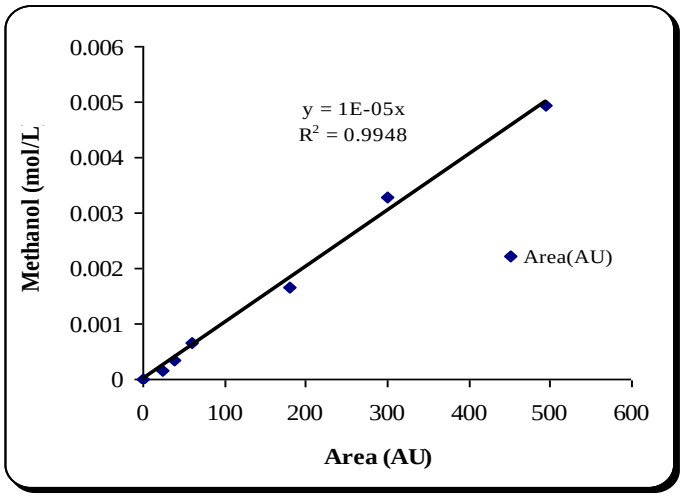

Figure 5.69: Calibration curve of methanol using (GC/FID)

5.8.1.3. Determination of ozone mass transfer parameters

5.8.1.4. Saturation ozone concentration in water

The saturation of ozone concentration in the solvent used in this work (i.e. deionised water) was determined as describe earlier in Section 5.4.2.

$$C_{AL}^{*} = 0.0456 \times C_{AG} \tag{5.16}$$

5.8.1.5. Mass transfer specific surface area (a_L)

The mass transfer specific surface area (a_L) was determined in this work using the fast kinetics method. The method involved bubbling ozone in a solution of indigo thrisulfonate at pH 2, as described earlier in Section 5.7.2.2. Results of this work gave values for a_L as presented in Table 5.25. It is obvious from Table 5.23, that t-butanol has increased a_L, due to reduction in surface tension following addition of t-butanol.

Table 5.25: Specific surface area of indigo solution without and with t-butanol

Liquid phase	t-butanol (mol/L)	a_L (m^2/m^3)
Indigo solution	0	2.74
Indigo solution	0.2	3.52

5.8.1.6. Methanol ozonation experiments

Ozone gas concentrations of 10 to 80 g/m^3 NTP were used in this study to degrade methanol in water. The operating conditions for the experiments are shown in Appendix A2.5.1.1. The change in ozone gas concentration at the outlet of the reactor is shown in Figure 5.70 for a typical experiment and the change in methanol concentration as function of time is shown in Figure 5.71.

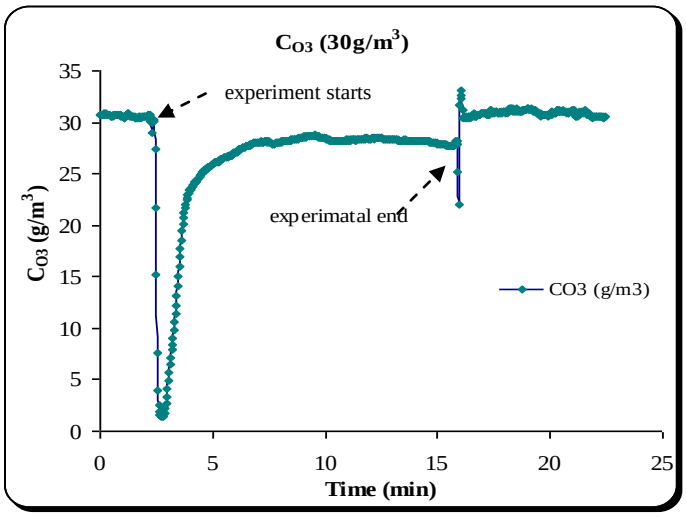

Figure 5.70: Ozone gas concentration versus time

The ozone gas concentration tends to reach a stable concentration lower than the inlet gas concentration after about 3 minutes from the start of the experiment. This was due to ozone reactions with oxidation products which take place even though methanol degradation is completed. As shown in Figure 5.71, methanol concentration decreased with time and reached lower values after about 3 minutes.

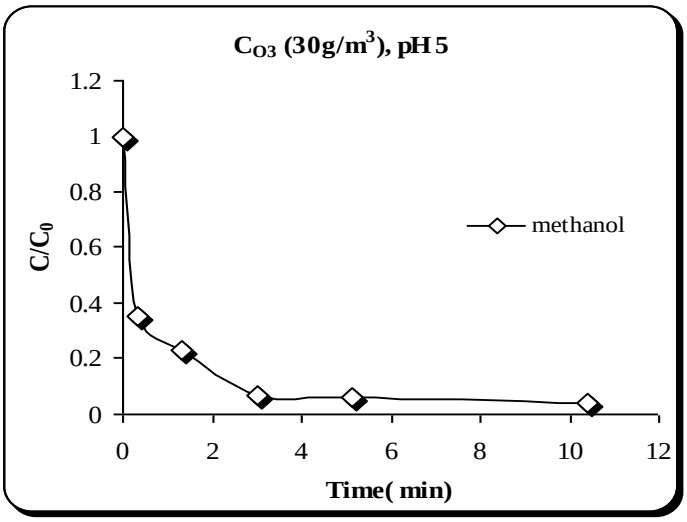

Figure 5.71: Concentration of methanol versus time

5.8.1.7. Effect of ozone gas concentration on methanol degradation

In order to study ozone effect on methanol degradation, ozone was bubbled into the methanol solution at different gas concentrations of 10, 30, 60 and 80 g/m^{3}NTP and the experiments were carried out as described previously. Figure 5.72 shows that the degradation of methanol increases with increasing ozone concentration. From the graph,

it could be seen that when the ozone concentration was around 30 g/m^{3}NTP, the time required to degrade methanol took around 15 minutes but when the ozone concentration increased to 80 g/m^{3}NTP, the methanol degradation was faster reaching zero in almost 3 minutes, whereas at 10 g/m^3, the degradation time took more than 60 minutes as shown below in Figure 5.72.

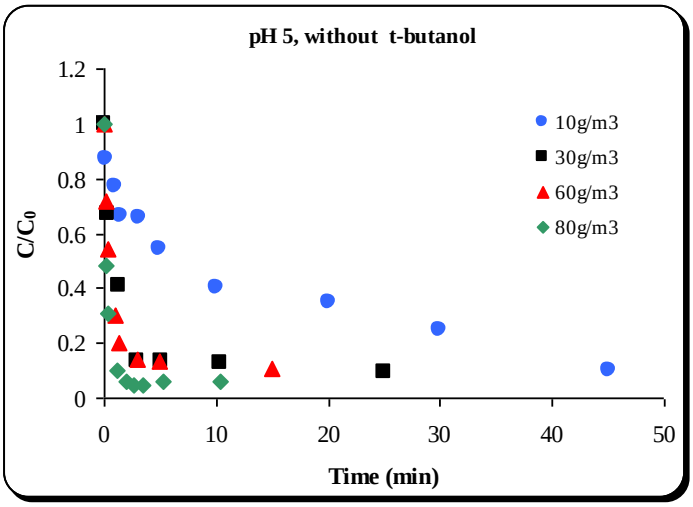

Figure 5.72: Concentration of methanol versus time at various inlet ozone gas concentrations

5.8.1.8. Effect of pH and t-butanol as scavenger on methanol degradation

In order to determine the optimum pH at which the maximum degradation of methanol may occur, experiments were carried out at different controlled pH values of 2, 5 and 9. The methanol concentration of the solution was 1.3 mol/L and an ozone concentration of 30 g/m^{3}NTP was used. Figure 5.73 depicts the change in methanol concentration at different pH values. The Figure shows that initially (within the first 1.5 minutes), the degradation rates were not significantly affected by changes in pH. However, when the pH increased from 2 to 5, appreciable enhancement in the degradation of methanol occurred but further increase of pH to 9 resulted in slowing down of the degradation rate and the methanol concentration leveled off at values higher than zero. This indicates that complete degradation of methanol at higher pHs is very difficult. The reason for this is that at high pH, ozone reaction with hydroxide ions prevail over that with methanol, due to the fact that the rate constant of ozone reaction with OH^- is much higher (around 3000

times) than with methanol (70 $M^{-1}.s^{-1}$ as compared to only 0.024 $M^{-1}.s^{-1}$). The rapid drop of methanol concentration observed at the beginning of the experiment may be due to the high concentration of methanol present initially, which gave high reaction rates within the first few minutes.

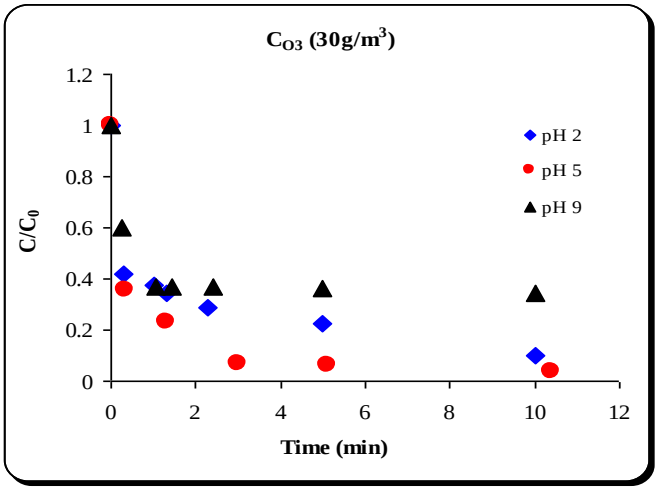

Figure 5.73: Effect of pH on methanol degradation

In order to study the effect of t-butanol as scavenger on methanol degradation, experiments were carried out with and without 0.2 M t-butanol at pH 2, 5 and 9. Figure 5.74 shows that at ozone gas concentrations 30 g/m^{3}NTP, t-butanol seems to have a complex effect on the degradation rates of methanol.

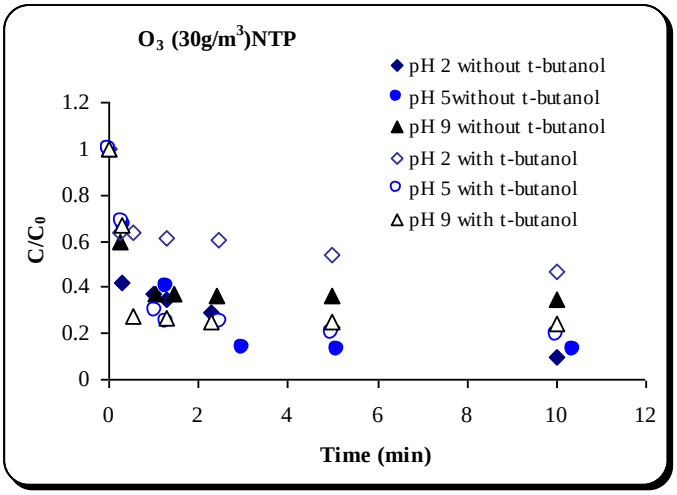

Figure 5.74: Effect of t-butanol on methanol degradation

5.8.1.9. Determination of the stoichiometric ratio and reaction rate constant

The chemical reaction between ozone and methanol can be represented by the equation:

$$O_3 + zMeOH \xrightarrow{k} \text{Products} \quad (5.17)$$

Again here, it was assumed that this reaction is of second order and the stoichiometric ratio was determined in homogeneous system by measuring the change of methanol concentration after reaction with a given initial ozone concentration (details can be found in Section 3.3.1 Equation 3.18). The average value of z was found to be 1 mol per mol and this value is in agreement with literature (Hoigne and Bader 1983a) and (Hoigne et al., 1985). The reaction rate constant was determined using Equation 3.43. The values of the rate constant of methanol with ozone are presented in Table 5.26 and compared to literature. Good agreement with literature was also obtained. It is clear that the degradation of methanol is highest at pH 9.

Table 5.26: Values of the rate constant of methanol with ozone

Property	Rate constant this work ($M^{-1}s^{-1}$)	Rate constant (Hoigne1983a) ($M^{-1}s^{-1}$)
2/5	2.62	2.40
7	2.85	-
9	4.15	-

5.8.1.10. Effect of pH on the reaction rate constant (k)

Three pH values (2, 7 and 9) were studied in this work. For each pH value, the rate constant k was determined using an ozone gas concentration of 60 g/m^3 NTP, without the addition of t-butanol. The operating conditions for all experiments are shown in Appendix A1.5 Table A1.21. A Figure 5.75 shows the modeling of determination of the rate constant and the stoichiometry of the reaction between ozone and methanol at pH 7 using equation (3.43). The change of k with pH is shown in Figure 5.76. It can be seen that the rate constant of reaction between ozone and methanol has increased when the pH value was increased and the highest value of the rate constant was observed at pH 9. This can be explained by ozone decomposition at high pH that leads to the formation of hydroxyl radicals which are highly reactive species.

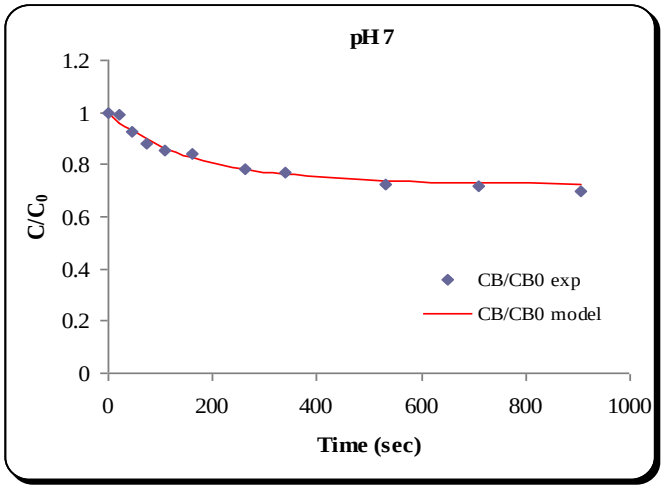

Figure 5.75: Determination of the rate constant and the stoichiometry of the reaction between ozone and methanol at pH 7

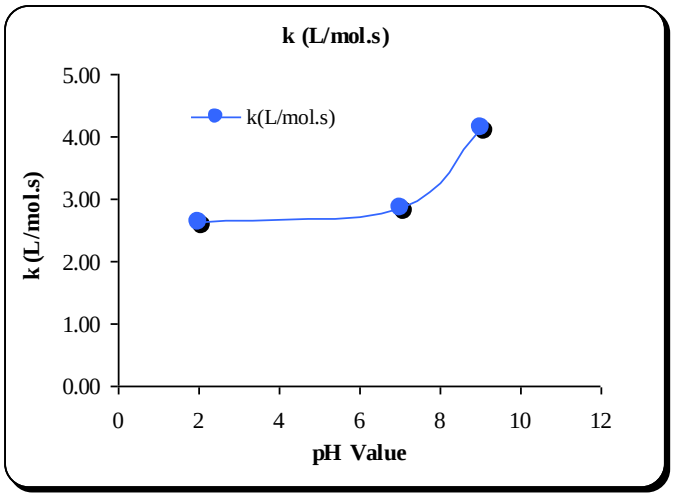

Figure 5.76: Effect of pH on methanol degradation rate constant

5.8.1.11. Summary

From the results of the experimental investigation on the degradation of methanol by ozone, it was found that the rate constant (k) of the degradation reaction increased when the pH was increased and the highest value of the rate constant was obtained at pH 9**.** The reaction stoichiometry was found to have a value of 1 mol/mol.

CHAPTER 6: EXPERIMANTAL RESULTS & DISCUSSIONS FOR THE LIQUID/SOLID-OZONE (LSO) SYSTEM

The degradation studies carried out with the Liquid/Solid-Ozone (LSO) system are presented and discussed in this chapter. Three model compounds, namely the reactive dye RO16, naphthalene and methanol, were used to test the performance of the LSO system under different conditions and to study its feasibility of removing these compounds.

6.1 Ozone Adsorption

The adsorbents used in this study were a commercial silica gel obtained from Gjay Ciba Specialty Chemicals and a zeolytic material (D915) manufactured in a previous project by Catal Ltd. The characteristics of both adsorbents are presented in Table 6.1.

Table 6.1: Adsorbents characteristics

Adsorbent	Particle size (mm)	BET surface area (m^2/g)	Average Pore diameter (4V/A by BET) (cm^3/g)
Silica gel	1.5	490 ± 3	20.1
Zeolite D915	2	238 ± 3	36.1

Several experiments were carried out to study ozone adsorption (i.e. phase 1 of the LSO system) on both adsorbents. The experiments were carried out using a fixed bed of adsorbent by passing a stream of oxygen containing ozone at various known concentrations (10, 20, 60 and 80 g/m^3 NTP) and a known gas flow rate (400 mL/min) at a temperature of 20±1 ^oC. Two Pyrex glass reactors were used: one for silica gel experiments (31.24 mm ID and contained 80 g of silica gel) and a smaller reactor for D915 experiments (10 mm ID and contained 2 g of D915). Table 6.2 shows the operating conditions for these experiments and Figures 6.1 and 6.2 show typical breakthrough curves obtained for ozone adsorption on silica gel and D915 respectively.

Table 6.2: Operating conditions of ozone adsorption

Exp-No	Gas flow (mL/min)	C_{O3} (g/m^3)	Silica (g)	m_{O3} (mg)	Water flow (mL/min)	pH	Abs_0	C_{AL0} (mg/L)
1si	400	20	80	31.40	10	5	1.060	17.55
2si	400	10	80	7.16	10	7	0.898	14.87
3si	400	20	80	45.80	10	7	1.186	10.96
4si	400	20	80	41.28	10	9	1.213	20.07
5si	400	60	80	76.40	10	5	2.144	35.49
6si	400	60	80	111.56	10	7	2.467	40.84
7si	400	60	80	144.30	10	9	2.903	48.06
8si	400	80	80	172.80	10	5	3.179	52.61
9si	400	80	80	104.42	10	7	2.836	46.94
10si	400	80	80	159.76	10	9	3.452	57.13

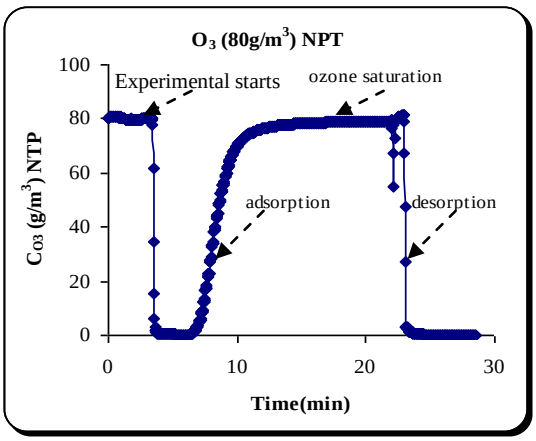

Figure 6.1: Ozone adsorption on silica gel

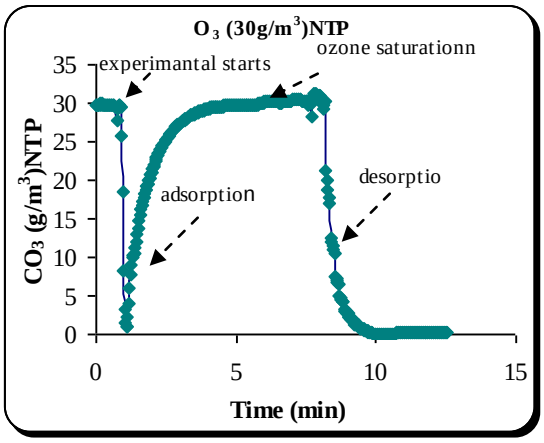

Figure 6.2: Ozone adsorption on D915

The mass of ozone adsorbed on the bed, m_{O3}, was calculated by integration as shown in Chapter 3 and the bed capacity, q_b, was calculated by Equation 6.1, where; m_{ad} is the adsorbent mass. Figure 6.3 and 6.4 show plots of the bed ozone capacity as function of the ozone gas concentration for silica gel and D915 respectively. From Figures 6.3 and 6.4, it can be seen that the relationship between bed capacity and ozone gas concentration is linear with an equilibrium constant, K_{vb}, equal to 11.47 for silica gel and 56.34 for D915 respectively. This clearly indicates that D915 has a higher ozone capacity than silica gel by about five times under the experimental conditions used in this work.

$$q_b = \frac{m_{O3}}{m_{ad}} \tag{6.1}$$

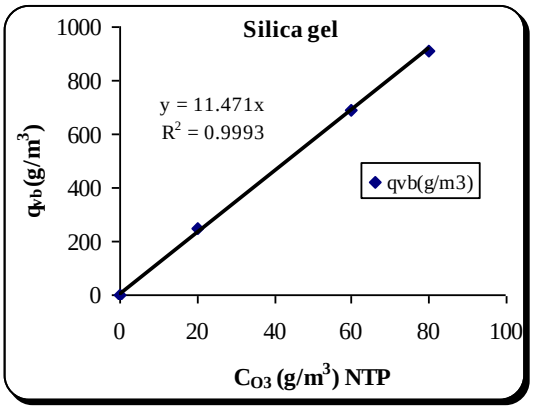

Figure 6.3: bed ozone capacity versus ozone gas concentration (for silica gel)

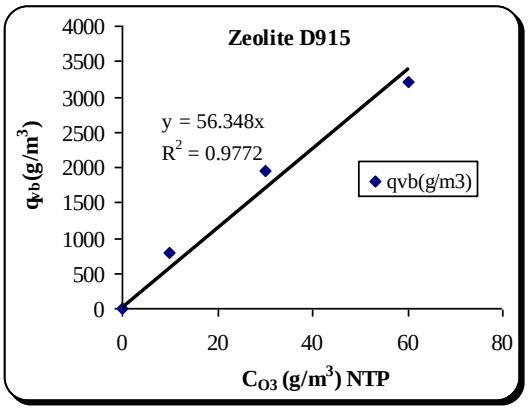

Figure 6.4: bed ozone capacity versus ozone gas concentration (for D915)

The model presented in (Tizaoui and Slater 2003) was used to predict the breakthrough curves obtained in this work. The breakthrough curves were characterized by constant pattern behavior and the mass transfer was controlled by resistance in the particle side Equation 6.2. This equation was derived with the following assumptions (Slater 1991): particle rate controls mass transfer, linear equilibrium, plugs flow (i.e. no axial dispersion), constant flow velocity, constant effective diffusivity and isotherm conditions.

$$\frac{C_{AG}}{C_{AG_0}} = 0.5\left(1 - erf\left(\frac{1}{2}N_p^{0.5} - \frac{1}{2}\left(N_p\tau\right)^{0.5}\right)\right) \tag{6.2}$$

Where $\tau = \dfrac{t - \dfrac{L}{u}}{K_{vb}\dfrac{L}{\varepsilon u}}$ (6.3)

and $N_p = \dfrac{60LK_{vb}}{d_p^2 \varepsilon u} D_e$ (6.4)

Tizaoui and Slater (2003) gave a value of the diffusivity of ozone equal to 25×10^{-9} m^2/s.

6.2. Desorption of Ozone from Deionised Water

Once ozone has been adsorbed on the bed, desorption experiments were carried out using different flow rates of deionised water. The water flow meter was initially

calibrated as shown in Table 6.3. A calibration curve was then plotted (Figure 6.5) and served to subsequently determine the water flow rate for a given scale reading. The ozone concentration at the outlet of the fixed bed column was measured using the spectrophotometric method by measuring the light absorbance at 262 nm. Values of absorbance were then converted to concentrations using an emissivity of 2900 $M^{-1}.cm^{-1}$.

Table 6.3: Calibration of the water flow meter

Flow meter scale	100	200	400	600	800	1000	1100
Water flow rates (mL/min)	1.5	3.9	7.9	12.5	16.2	19	21.9

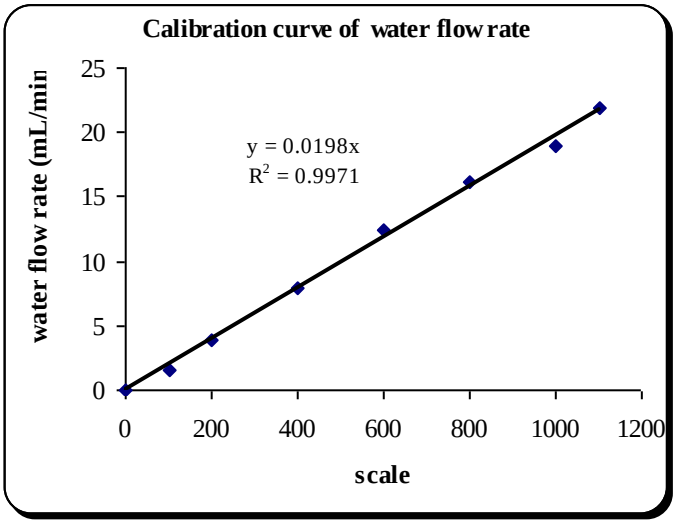

Figure 6.5: Calibration curve of the water flow meter

Ozone desorption was modelled with an exponential model described by Equation 6.5.

$$\frac{C_{ALout}}{C_{AL0}} = \exp\left(-K_{des}t\right) \tag{6.5}$$

Where K_{des} depends on the water flow rate, bed volume, bed voidage, and desorption mass transfer coefficient.

Results of the model are shown in Figures 6.6 to 6.15. These Figures show very good agreement between the experimental data and the proposed model. Values of K_{des} are shown in Table 6.4.

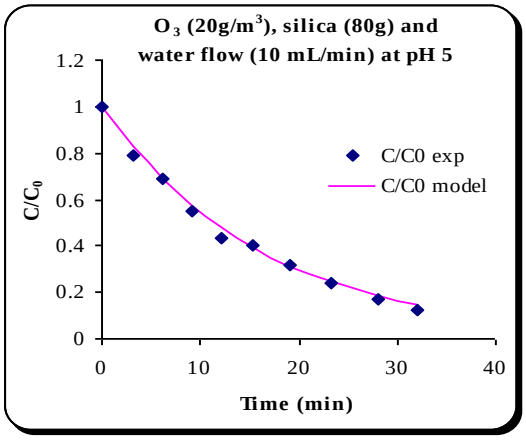

Figure 6.6: Model results at pH 5

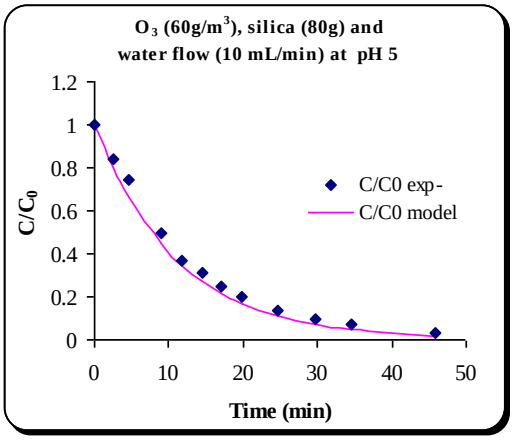

Figure 6.7: Model results at pH 5

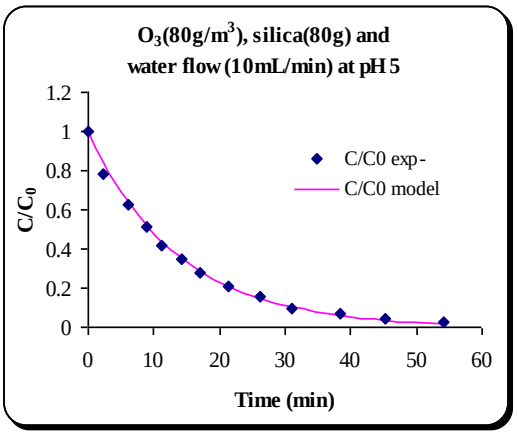

Figure 6.8: Model results at pH 5

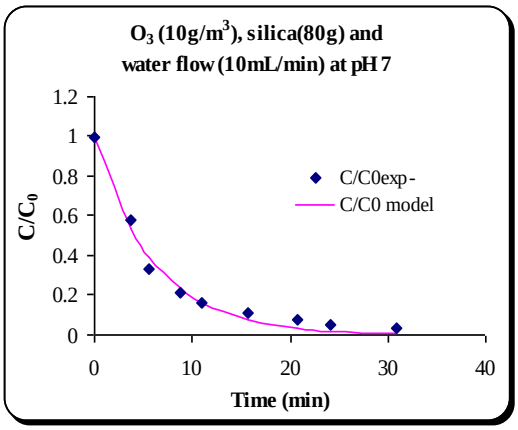

Figure 6.9: Model results pH 7

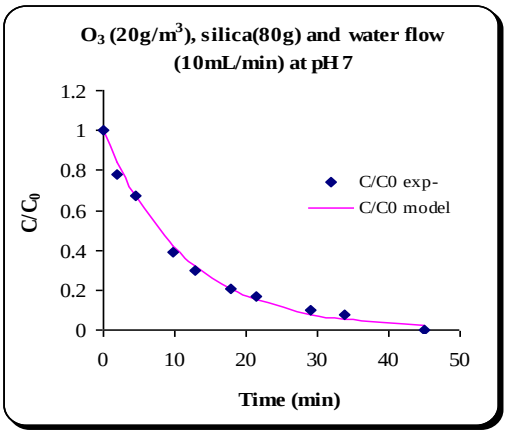

Figure 6.10: Model results at pH 7

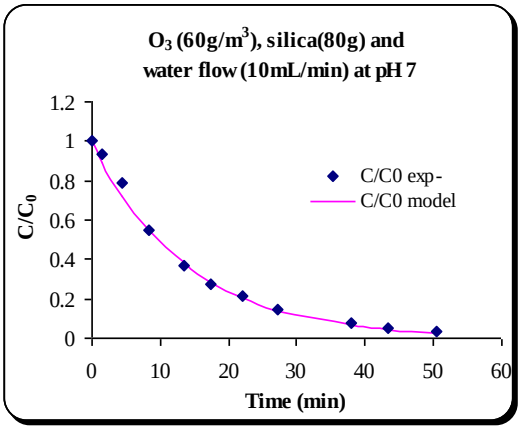

Figure 6.11: Model results at pH 7

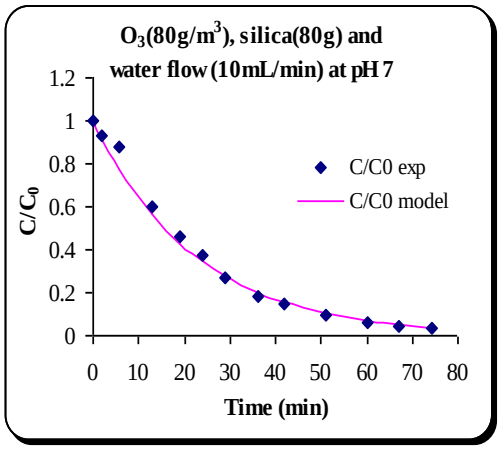

Figure 6.12: Model results at pH 7

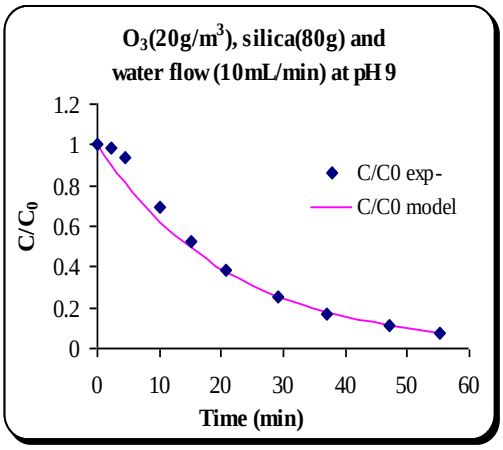

Figure 6.13: Model results at pH 9

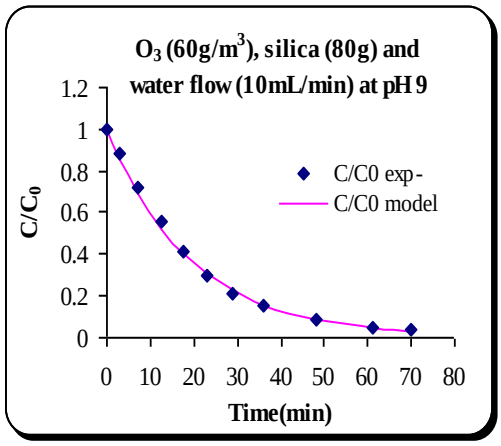

Figure 6.14: Model results at pH 9

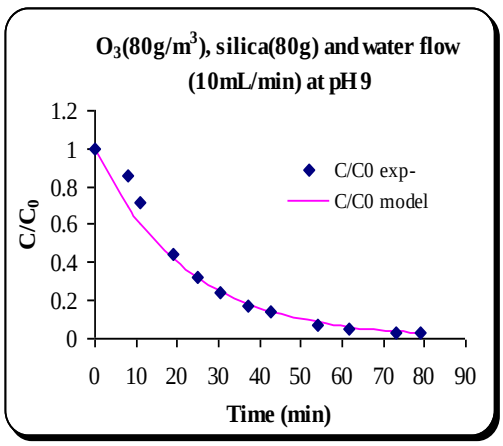

Figure 6.15: Model results at pH 9

6.2.1. Effect of water flow rate on ozone desorption

The effect of the water flow rate on ozone desorption was studied at different ozone gas concentrations used in the adsorption step. Table 6.4 shows the operating conditions used in these experiments alongside the values of K_{des} obtained by fitting the experimental data with Equation 6.5.

Table 6.4: Operating conditions for water flow rate effect experiments

Exp-No	Gas flow (mL/min)	C_{O3} (g/m^3)	Silica (g)	m_{O3} (mg)	Water flow (mL/min)	pH	Abs_0	C_{AL0} (mg/L)	K_{des}
Fw1	400	20	80	33.65	5	7	0.696	11.52	0.045
Fw2	400	20	80	45.8	10	7	1.186	10.96	0.087
Fw3	400	20	80	34.12	20	7	0.763	12.64	0.128
Fw4	400	60	80	101.30	5	7	1.579	26.13	0.017
Fw5	400	60	80	111.56	10	7	2.467	40.84	0.072
Fw6	400	60	80	98.45	20	7	1.638	27.11	0.080

Figures 6.16 and 6.17 show the effect of water flow rate on the exit ozone concentration. It can be observed that slower desorption rates are obtained at low water flow rates and an increase in the water flow rate resulted in rapid desorption of ozone. The water flow rate showed significant effect on desorption process. The relationship between water flow rate and desorption rate is shown in Figure 6.18. From Figure 6.18, it can be noticeable that K_{des} has increased when the water flow rate increased; it can thus be concluded that the mass transfer limiting step is in the liquid film.

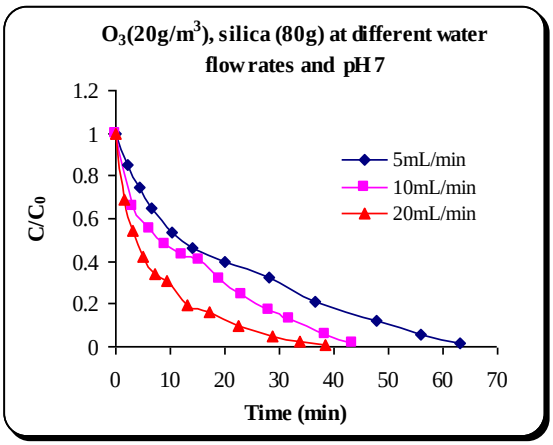

Figure 6.16: C/C_0 at ozone gas conc. ($20g/m^3$)

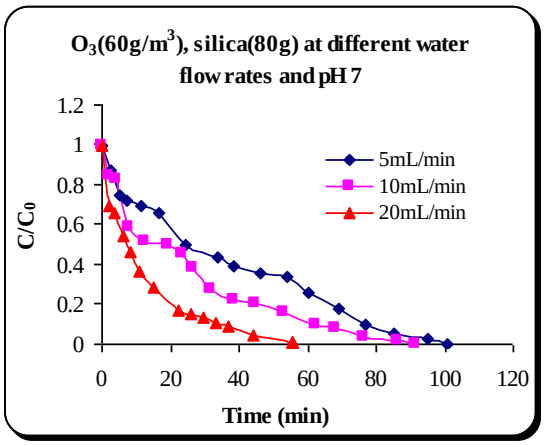

Figure 6.17: C/C_0 at ozone gas conc. ($60g/m^3$)

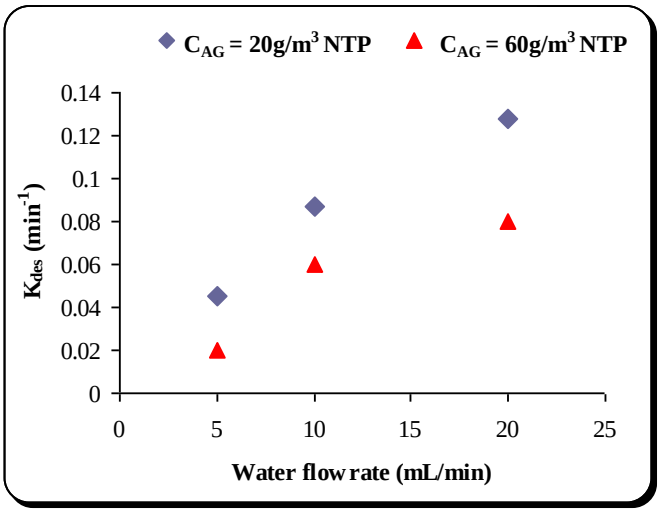

Figure 6.18: Relationship between water flow rate and K_{des}

6.2.2. Effect of pH on ozone desorption

The effect of pH (5, 7, 9) on ozone desorption was studied using a water flow rate of 10 mL/min. The temperature was kept constant at 20 ±1ºC and the gas ozone concentration was also kept constant at 60 g/m^3, (Table 6.5).

Table 6.5: Operating condition for effect of pH on ozone desorption experiments

Exp-No	Gas flow (mL/min)	C_{O3} ($g/m^{3)}$	Silica (g)	m_{O3} (mg)	Water flow (mL/min)	pH	Abs_0	C_{AL0} (mg/L)	K_{des}
11si	400	60	80	76.40	10	5	2.144	35.49	0.089
13si	400	60	80	111.56	10	7	2.467	40.84	0.072
15si	400	60	80	144.30	10	9	2.903	48.06	0.051

Figure 6.19 shows the change of the exit ozone concentration with time at different pH values. From Figure 6.20, it can be noticed that ozone desorption rate (K_{des}) decreases as pH increases. Although it is not clear why K_{des} decreased at high pH values, one might expect the decrease was due to reduction in ozone mass transfer.

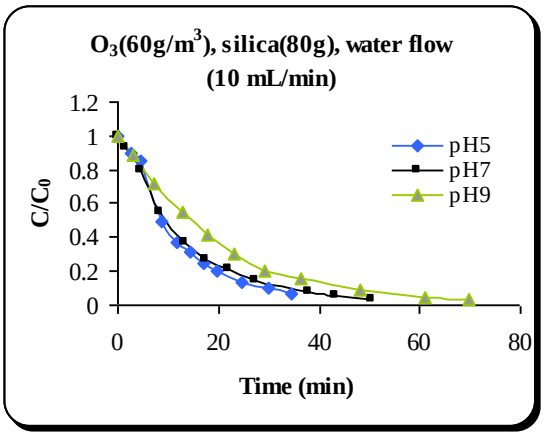

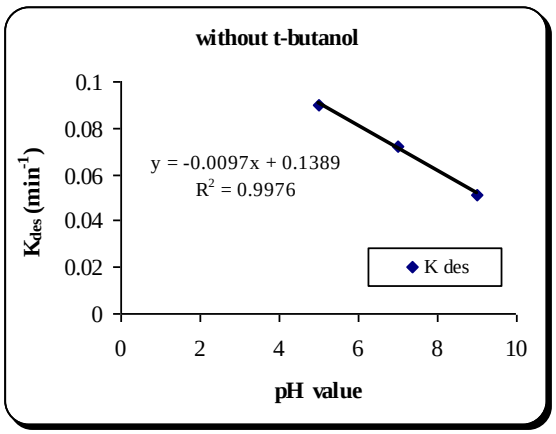

Figure 6.19: Liquid ozone concentration vs. time **Figure 6.20:** Relationship between K_{des} and pH

6.2.3. Effect of t-butanol radical scavenger on ozone desorption

The effect of the radical scavenger (0.2M t-butanol) on ozone desorption was studied at different pH values using a water flow rate of 10 mL/min. The temperature was kept constant at 20 ±1 ºC and the gas ozone concentration was also kept constant at 60 g/m^3, (Table 6.6).

Table 6.6: Operating condition for effect of t-butanol on ozone desorption experiments

Exp-No	Gas flow (mL/min)	C_{O3} (g/m^3)	Silica (g)	m_{O3} (mg)	Water flow (mL/min)	pH	t-butanol (mol)	Abs_0	C_{AL0} (mg/L)	K_{des}
12si	400	60	80	174.2	10	5	0.2	2.821	46.70	0.030
14si	400	60	80	160.8	10	7	0.2	2.958	48.97	0.041
16si	400	60	80	137.6	10	9	0.2	3.511	58.11	0.051

Figures 6.21 to 6.23 show a comparison between the results obtained in the presence and absence of t-butanol at different pHs. It can be seen that t-butanol has an effect on ozone desorption at pH 5 and 7, whereas at pH 9 no significant effect was observed. Figure 6.24 shows the change of the exit ozone concentration with time for all pH values in the presence of the scavenger. The Figure shows that all curves are almost similar, which indicates that in the presence of t-butanol, pH has small effect on the desorption of ozone.

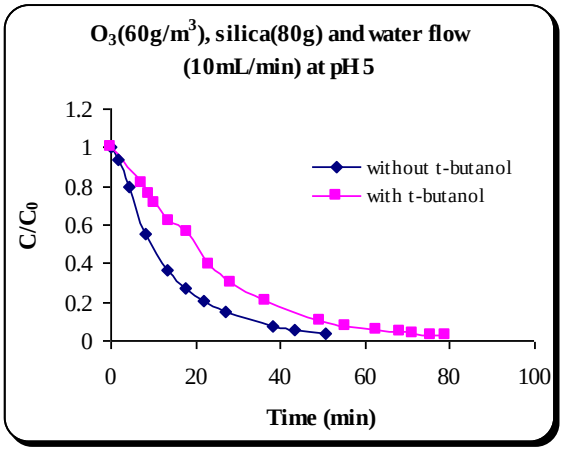

Figure 6.21: Concentration versus time at pH 5

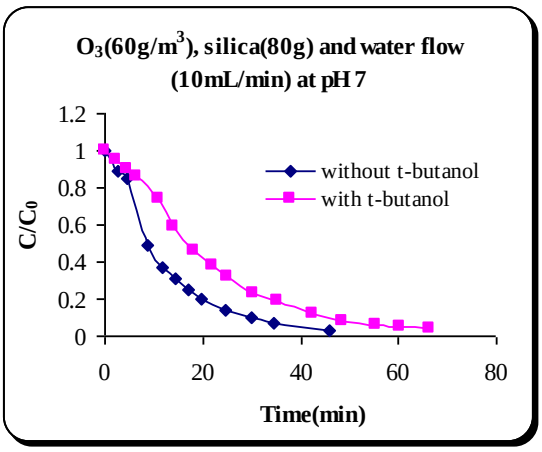

Figure 6.22: Concentration versus time at pH 7

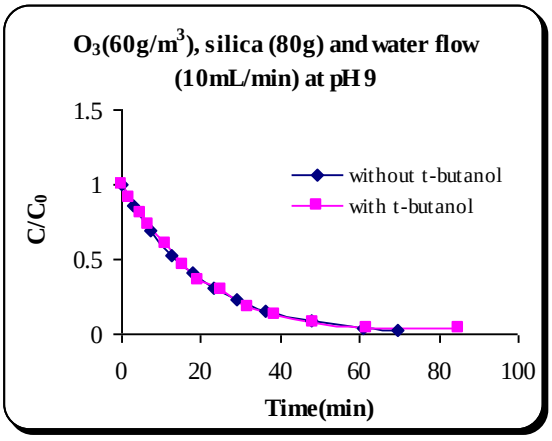

Figure 6.23: Concentration versus time at pH 9

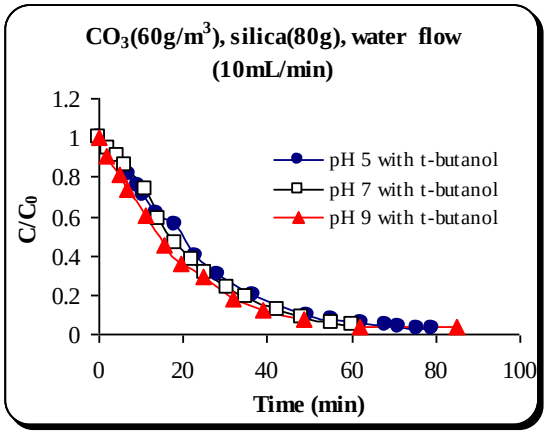

Figure 6.24: Concentration versus time at different pH

6.2.4. Summary

Ozone adsorption and desorption studies were carried out using silica gel. The experiments were validated with models developed in the literature and found to agree

well. The desorption rate of ozone depended mainly on the water flow rate and pH, whereas in the presence of t-butanol, pH was found to have only little effect.

6.3. Degradation of Dye (RO16) by Ozone Adsorbed on Silica Gel

The degradation of RO16 with LSO system was studied here. Experiments were carried out by passing ozone at a known concentration of (60 g/m^3) NTP, known oxygen flow rate (400 mL/min) until saturation of the bed of silica gel. A water flow rate 10 mL/min contains RO16 at 50 mg/L at pH 7 and temperature 20±1°C was passed through the fixed bed of adsorbent loaded ozone in absence and presence of t-butanol. The reactor contained 80 g of silica gel. In order to measure the absorbance of dye (RO16) solution, the maximum absorbance was monitored at λ_{max} = 496 nm see (Figure 5.19). Table 6.7 shows the operating conditions for these experiments and the results are shown in Figure 6.25; whereas Figure 6.26 shows the breakthrough curve of ozone adsorption.

Table 6.7: Operating conditions for ozone adsorption effect on RO16 Decolourization

Exp-No	Gas flow (mL/min)	Ozone conc. (g/m^3)	Silica (g)	m_{O3} (mg)	Ro16 Conc. (mg/L)	Sample flow (mL/min)	PH	t-butanol (mol/L)
1si/d	400	60	80	92.62	50	10	7	0
2si/d	400	60	80	98.45	50	10	7	0.2

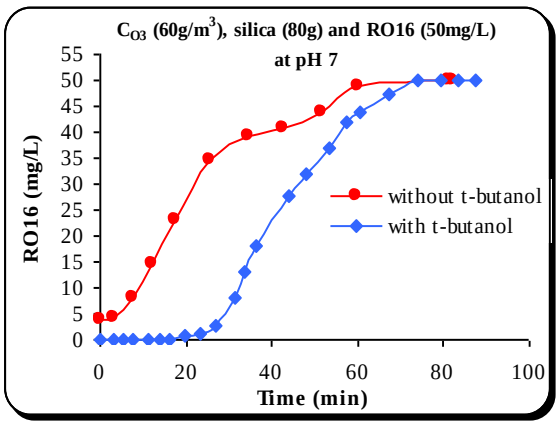

Figure 6.25: Outlet dye concentration versus time

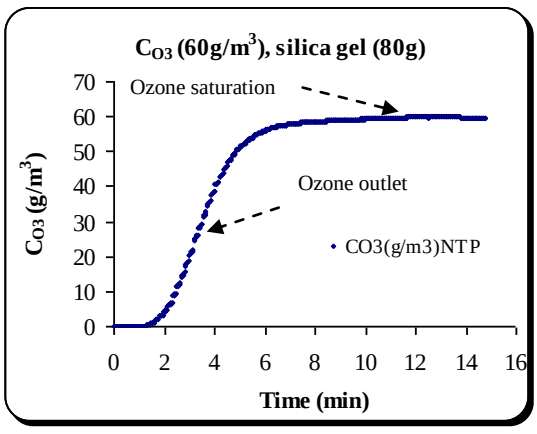

Figure 6.26: Outlet ozone gas concentration versus time

As can be seen from Figure 6.25, that in the absence of t-butanol, the concentration of the dye dropped initially to lower values of about 5 mg/L and then started increasing

slowly with time until reaching a concentration approaching the inlet concentration. Though if the experiment continued for longer periods of time, the concentration at the outlet of the reactor would reach the inlet concentration. The reduction in dye concentration was due to its oxidation with ozone and it was established by experiment that adsorption of the dye on silica gel would not take place (Figure 6.27). Surprisingly, when t-butanol was added to the solution, a significant improvement in the dye oxidation took place. On the one hand, the presence of t-butanol in the solution causes inhibition of hydroxyl radicals to decompose ozone, thus ozone availability in the solution increases at on the other hand dyes are more prone to molecular ozone reactions as compared to hydroxyl radicals. Putting together these two arguments, the better performance obtained in the presence of t-butanol is explained.

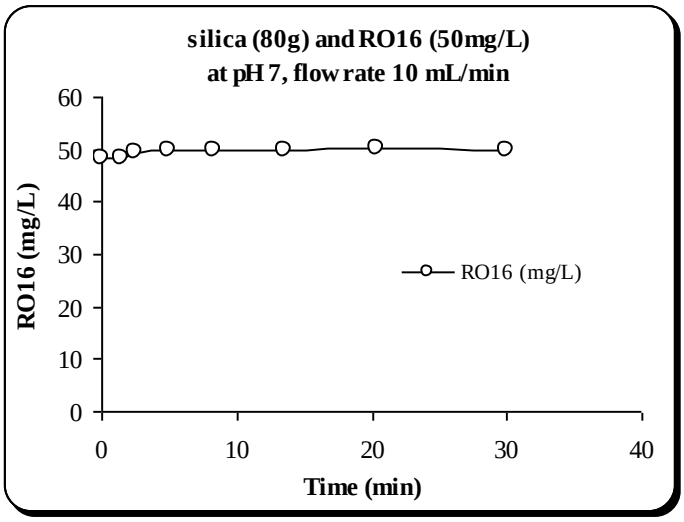

Figure 6.27: Outlet dye concentration versus time (without ozone)

As can be seen from Figure 6.25, initially the dye concentration reached zero and remained at the zero value for a longer period of time (about 30 minutes) before it started to slowly increase again. The concentration would also reach the inlet concentration if the experiment is left to run for a longer period of time.

Tizaoui and Slater (2003) developed a model to describe the profile of concentrations similar to those observed in Figure 6.25. Their model was applied in this work and good

agreement was obtained between experimental and the model data. The rate constant, K_{dd}, was calculated by fitting the experimental data to the model.

6.4. Degradation of Naphthalene Using the (LSO) System

The degradation of naphthalene was studied using the LSO system. Because of the high adsorption capacity of the zeolite D915, the experiments in this section were carried out on the fixed bed column of D915. Ozone was adsorbed on the selective adsorbent zeolite (D915), as described earlier in section 4.6.2.4. In this study, the experiments were performed at room temperature (20 ± 1°C). Experiments were carried out in (LSO) reactor containing 2 g of D915. The ozone gas concentration (30 g/m^3 NTP) was passed through the reactor until saturation point, then a flow of 10 mL/min of naphthalene solution made in (50 % methanol : 50 % water) at 100 mg/L, was passed through the reactor and the samples were taken by syringe at different times. Sodium thiosulphate (0.005 M) was added to the sample to stop the reaction between ozone and naphthalene prior to analysis by HPLC.

6.4.1. Calibration curve for naphthalene analysis with HPLC

Four standard solutions of naphthalene in 50 % methanol: 50 % water were prepared and injected in the HPLC system. Peak areas were correlated to the injected naphthalene concentration and a plot was obtained as shown in Figure 6.28. The results gave a straight line having an equation C_{Naph}(mg/L) = 0.0028 × (Peak area).

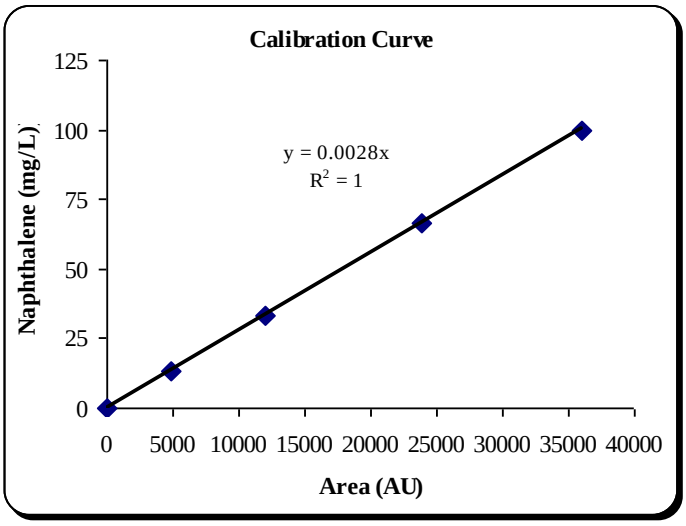

Figure 6.28: Calibration curve of naphthalene solution

6.4.2. Ozone adsorption and desorption on zeolite D915

Figure 6.29 shows typical graphs of the experiment carried out by passing 30 g/m^{3}NTP of ozone gas concentration in the 2 g of D915, until the concentration of ozone is stable (adsorption). Then, in the second step the ozone generator was stopped and the oxygen gas passed through the adsorbent loaded with ozone until the ozone gas was totally removed (desorption).Table 6.8 shows the operating conditions of ozone adsorption on zeolite D915.

Table 6.8: Operating conditions of ozone adsorption on D915

Exp-No	Gas flow (mL/min)	C_{O3} (g/m^3)	D915 (g)	m_{O3} (mg)	Water flow (mL/min)	pH	C_{B0} (mg/L)
1	400	10	2	3.13	10	7	55.35
2	400	30	2	7.77	10	7	29.55
3	400	60	2	12.89	10	7	13.60
4	400	30	2	7.77	10	2	27.51
5	400	30	2	8.77	10	7	29.55
6	400	30	2	5.71	10	9	50.32

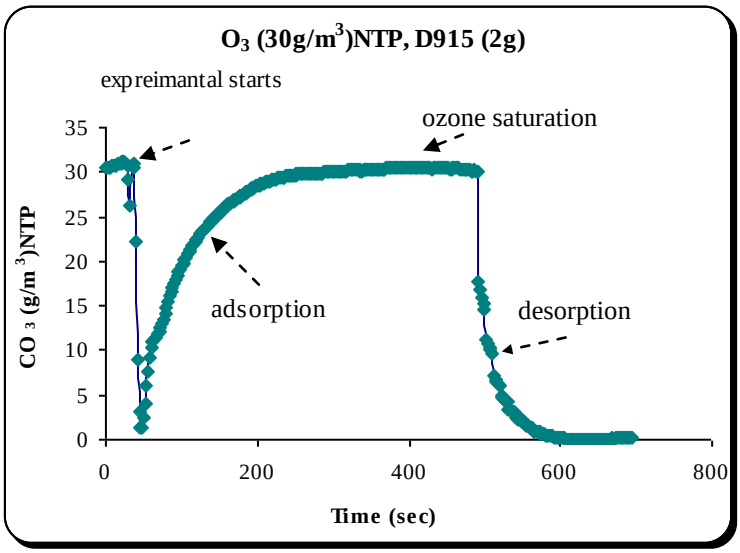

Figure 6.29: Ozone adsorption and desorption on zeolite D915

6.4.3. Adsorption of naphthalene on zeolite D915

In this experiment, 50 mL of naphthalene solution in (50 % methanol: 50 % water) at 80 mg/L and pH 7 was added to five different quantities of zeolite D915 (0, 0.5, 1, 1.5 and 2 g) without ozone loading and mixed well by magnetic stirrer over night. Then, the samples were taken and injected in the HPLC. The results are shown in Table 6.9.

Table 6.9: results calculation of bed capacity for naphthalene adsorption

Mass adsorbent (g)	V solution (mL)	C final (mg/L)	q (mg/g)
0	50	79.7	-
0.5	50	51.8	2.8
1	50	20.8	2.9
1.5	50	18.3	2.0
2	50	15.1	1.6

(Freundlich (Equation 6.6 and 6.7)) and (Langmuir (6.8 and 6.9)) adsorption isotherms were used to describe the results. Figures 6.30 and 6.31 show the linearised plots of the Freundlich and Langmuir models respectively. From the values of R^2, it is clear that the Langmuir model was slightly better than the Freundlich model to fit the experimental results.

$$q = kc^{\frac{1}{n}} \tag{6.6}$$

$$\ln(q) = \ln(k) + \frac{1}{n}\ln(c) \tag{6.7}$$

$$q = \frac{Ac}{1 + Bc} \tag{6.8}$$

$$\frac{1}{q} = \frac{1}{Ac} + B \tag{6.9}$$

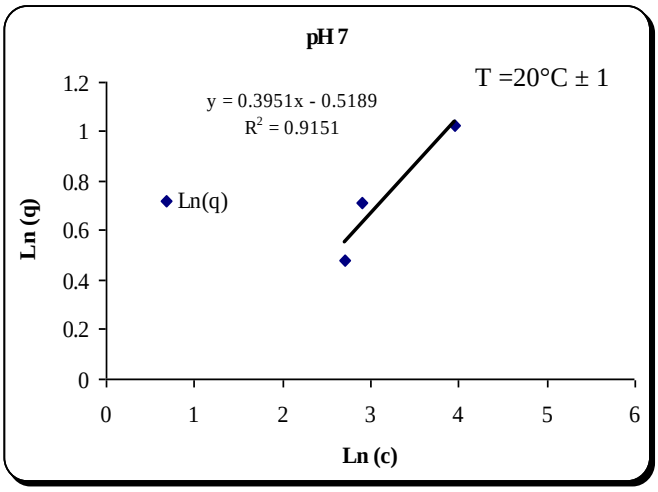

Figure 6.30: Naphthalene adsorption (model experimental results)

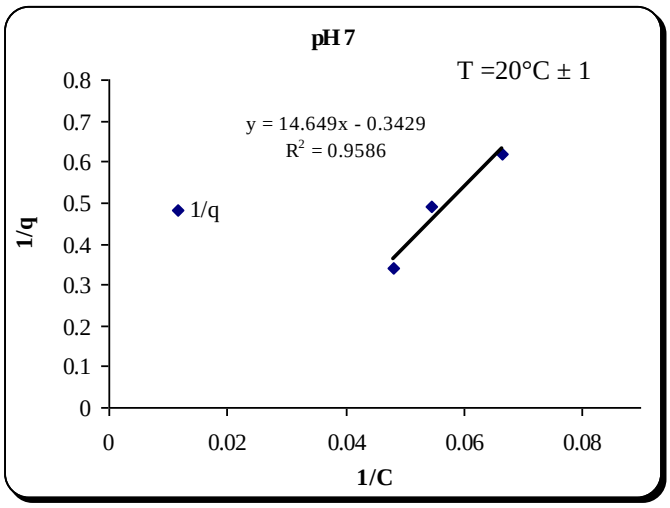

Figure 6.31: Naphthalene adsorption (model experimental results)

6.4.4. Effect of flow rate on naphthalene removal

Three different flow rates of 5, 10 and 20mL/min were used to study the effect of flow rate on naphthalene removal on 2 g bed of D915. Figure 6.32 shows the effect of flow rate on naphthalene removal at pH 7 when the ozone gas concentration was 30 g/m^{3}NTP. It is clear that the LSO system showed naphthalene removal up to 9 minutes from the start of the experiment, after which the exit column concentration

almost reached the inlet concentration and did not change much with time. Figure 6.32 shows also as the flow rate decreased, the performance of the system enhanced. The breakthrough curves did not reach zero due to the small quantity of adsorbent used and the relatively high solvent flow rate. That means if the solvent flow rate was much smaller than the one used in this work, or the mass of adsorbent was higher, a clear breakthrough curve should be seen. It was not feasible to carry out experiments under these conditions, due to time constraints and cost of materials. The current results, however, indicate that the LSO system can be used to effectively degrade naphthalene if the operating conditions are optimised.

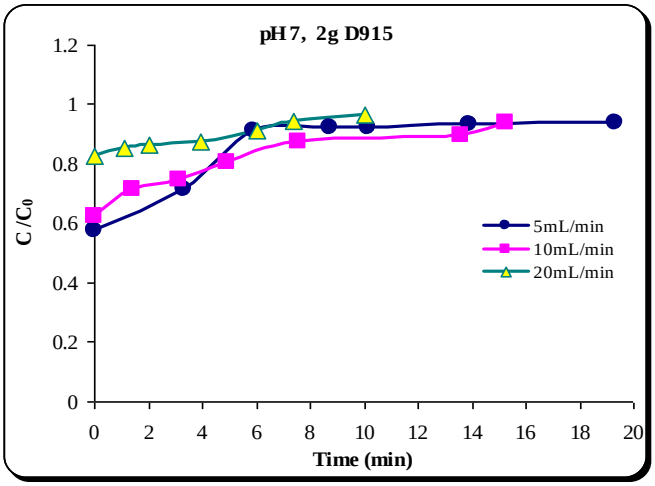

Figure 6.32: Effect of flow rate on naphthalene removal on D915

6.4.5. Effect of ozone concentration on naphthalene removal

The effect of the ozone gas concentration on naphthalene removal using D915 as ozone adsorbent was studied. Experiments were run at three different ozone gas concentrations of 10, 30 and 60 g/m^3 NTP, in addition to a control experiment without ozone (0 g/m^{3}NTP) at pH 7. The results are shown in Figure 6.33. From Figure 6.33, the lowest naphthalene concentrations measured at the outlet of the reactor exit for the different ozone concentrations are shown in Table 6.10. This Table shows that the removal of naphthalene increased by increasing the ozone gas concentration. For ozone gas concentrations of 10, 30 and 60 g/m^3 NTP, the exit lowest naphthalene concentration

reached 55 %, 30 % and 12 % of the inlet concentration respectively, before starting to increase almost linearly for about 2 minutes, followed by a gradual increase to almost the inlet concentration.

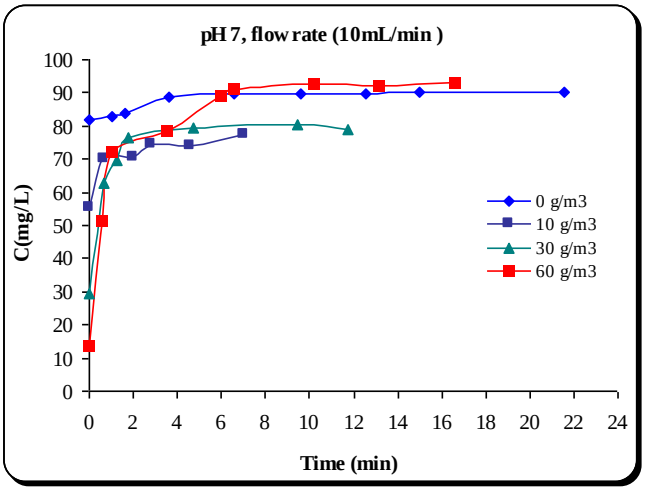

Figure 6.33: Effect of ozone gas concentration on naphthalene removal

Table 6.10: Effect of ozone concentration on the lowest exit naphthalene concentration

C_{O3} (g/m^3) NTP	q (mg/g)	Lowest exit concentration (mg/L)
0	0	82.94
10	3.13	55.35
30	7.77	29.55
60	12.89	13.60

6.4.6. Effect of pH and t-butanol on naphthalene removal

The effect of pH and t-butanol on naphthalene removal was also studied here. Experiments were carried out at different controlled pH values of 2, 7 and 9 and the temperature was kept constant at 20±1 ºC. The naphthalene concentration of the solution was 100 mg/L and the ozone concentration was 30 g/m^3 NTP. Several experiments were carried out with and without t-butanol in order to understand the effect of t-butanol on naphthalene removal. Figure 6.34 shows the effect of pH on naphthalene removal and Table 6.11 shows the lowest exit concentration as function of pH. As can be seen from the Table and the Figure, the lowest pH values gave better performance of the system.

Figure 6.35 shows the effect of t-butanol as scavenger when the experiment was run at pH 7. From Figure 6.35, it can be concluded that t-butanol decreased the performance of

the system, indicating that the degradation of naphthalene occurs by both direct molecular ozone and indirect hydroxyl radical reactions.

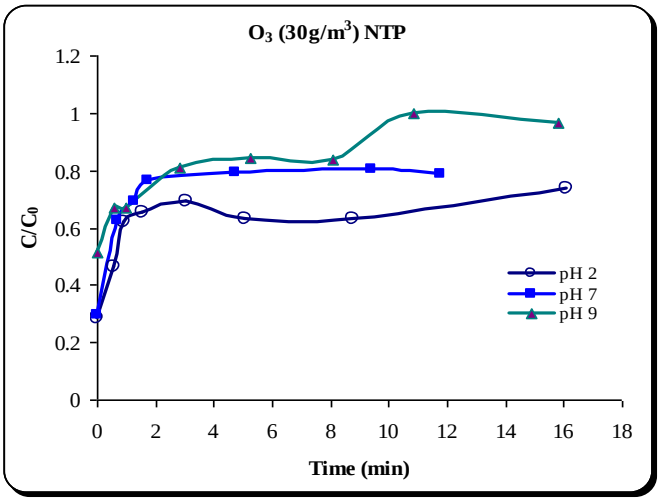

Figure 6.34: Effect of different pH on naphthalene adsorption

Table 6.11: Effect of pH on the lowest exit naphthalene concentration (C_{O3}=30 g/m^3) NTP

pH	q (mg/g)	Lowest exit concentration (mg/L)
2	7.77	27.51
7	8.77	29.55
9	5.71	50.32

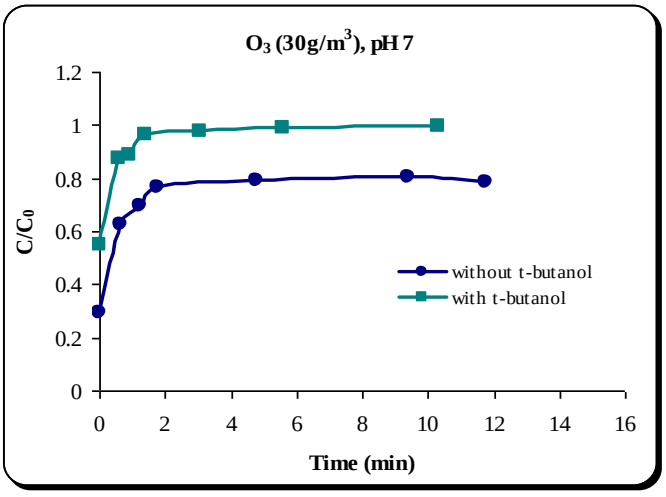

Figure 6.35: Effect of t-butanol on naphthalene degradation

6.4.7. Summary

Adsorption studies of naphthalene on a zeolite material D915 were carried out. It was found that the adsorption of naphthalene followed a Langmuir type isotherm. The removal of naphthalene using the LSO system was found feasible, as long as the

operating conditions are optimised. Under the conditions of the experiments carried out in this work, it was not possible to observe "clear" breakthrough curves but the performance of the system was described by the measurement of the lowest naphthalene exit concentration. In summary, the performance of the LSO system to remove naphthalene is enhanced by increasing the ozone concentration, decreasing the liquid flow rate, decreasing the pH and in the absence of radical scavengers.

6.5. Degradation of Methanol using the LSO System

Methanol degradation was studied using the LSO system. Ozone was adsorbed on the zeolytic material (D915), as described earlier in section 4.6.2.4. In this study, the experiments were performed at room temperature (20 ± 1°C). Experiments were carried out as described in section 4.6.2.5 and the reactor (LSO) contained 6g of D915 rather than 2 g. Methanol at a given concentration (2.5 mol/L) was dissolved in deionised water and the solution was passed through the reactor bed at a flow rate 10 mL/min. Samples at the exit of the LSO reactor were collected at different times. In order to stop the ozone reaction exactly at the collection time, the samples were collected in vials already containing a 0.005 M of a quenching solution of sodium thiosulphate. The concentration of methanol was determined using the GC/FID system described in Section 4.5.4.

6.5.1. Calibration curve for methanol analysis with GC/FID

Six standard solutions of methanol were prepared and injected in the GC/FID system. The operating conditions used in the GC/FID are shown in Table 6.12. Peak areas were correlated to the injected methanol concentration and a plot was obtained as shown in Figure 6.36. The result was a straight line having an equation:

$C_{MeOH\text{-}}(mol/L) = 0.0004 \times (\text{Peak area})$.

Table 6.12: GC conditions for the methanol measurements

Instrument	Detector	Detector temp- °C	Injector temp- °C	Column	Column temp- °C	
					initial	final
GC (PYE UNICAM PU 4500)	FID	250	130	104.PEG 400	95	95

* PEG: Polyethylene glycol.

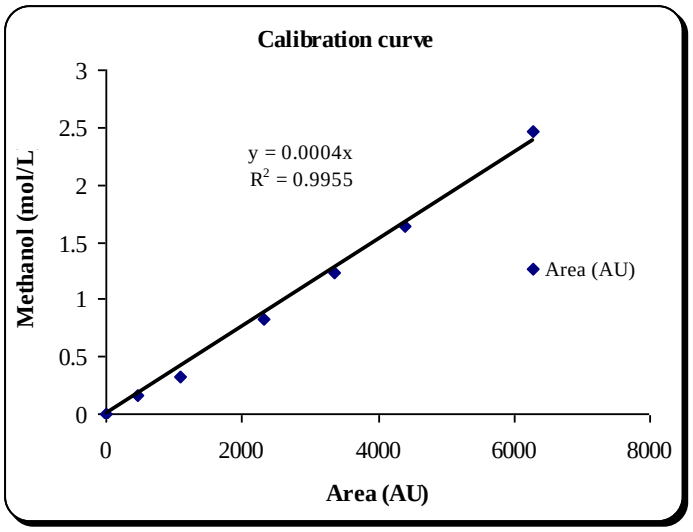

Figure 6.36: Calibration curve of methanol

6.5.2. Adsorption of methanol on zeolite D915

A 50 mL solution of methanol in water at 2.5 mol/L and pH 7 was added to four different masses of zeolite D915 (0.5, 1, 1.5 and 2 g) in a 100 mL glass volumetric flask and mixed well at low speed by a magnetic stirrer over night. The flasks were covered with parafilm to avoid evaporation. The samples were filtered by cellulose 0.45 µm 45 mm using glass syringe 10 mL and the concentration of methanol was measured by GC/FID. The operating conditions for these experiments are shown in Appendix A1.5 Table A1.22. The calculated results of D915 capacity for methanol adsorption are shown here in Table 6.13. (Langmuir and Freudlich) isotherms were also used to model the experimental results. A plot of 1/q = f (1/c) is shown in Figure 6.37 and a plot of ln(q) as function of ln(c) is shown in Figure 6.38. Again here, the Langmuir model was suitable to describe the adsorption isotherm of methanol on D915.

Table 6.13: Results calculation of bed capacity for methanol adsorption

Mass adsorbent (g)	V solution (mL)	C final (mg/L)	q (mg/g)
0	50	9.11	-
0.5	50	6.04	0.31
1	50	5.11	0.20
1.5	50	4.25	0.16
2	50	4.17	0.12

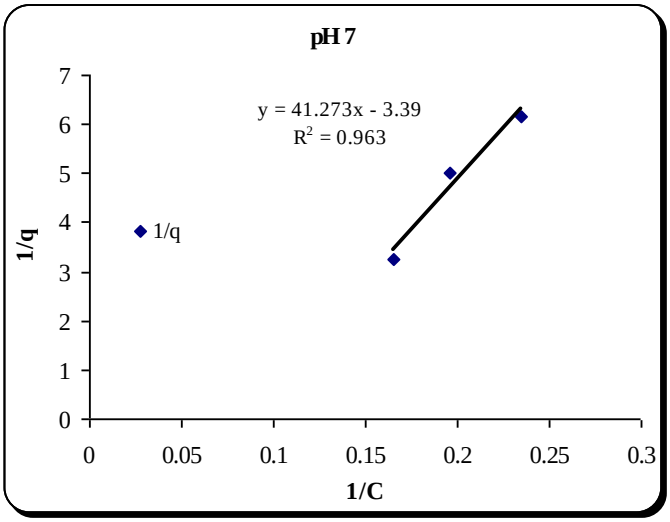

Figure 6.37: Methanol adsorption (model experimental results)

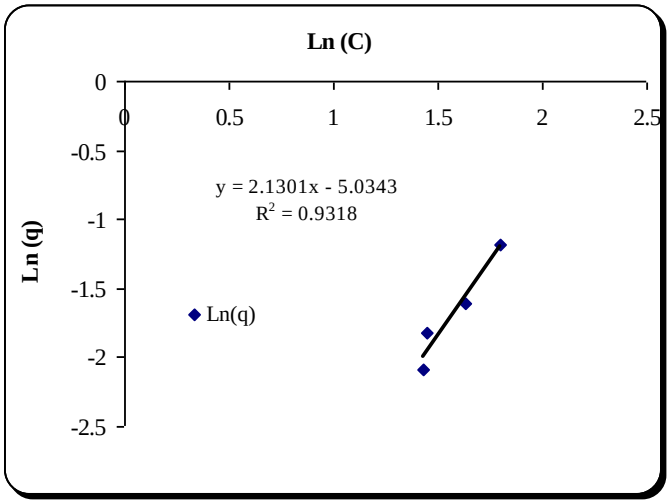

Figure 6.38: Methanol adsorption (model experimental results)

6.5.3. Effect of ozone concentration on methanol removal

The effect of ozone concentration was studied here in a similar way as in previous cases. The experiments were run at pH 7 and at three different ozone gas concentrations of 30, 60 and 80 g/m^3 NTP, using 2.5 mol/L of methanol and a fourth experiment was served as a control run without ozone. The radical scavenger t-butanol was not used in

these experiments. The operating conditions of all experiments are shown in Appendix A1.5 Table A1.24. The results are plotted in Figure 6.39 and the lowest methanol concentrations measured at the outlet of the reactor are shown in Table 6.14. These results show that the removal of methanol increased by increasing the ozone bed capacity (i.e. increased gas concentration). For ozone gas concentrations of 60 and 80 g/m^3 NTP, the exit lowest methanol concentration reached 38 % and 22 % of the inlet concentration respectively before starting to increase almost linearly for about 5.5 minutes, followed by a sudden rapid increase to almost the inlet concentration. The modeling of this behaviour of the LSO system is complex and was not attempted in this work. However, the experimental results show that the LSO system can effectively be used for the removal of methanol if the operating conditions are optimized.

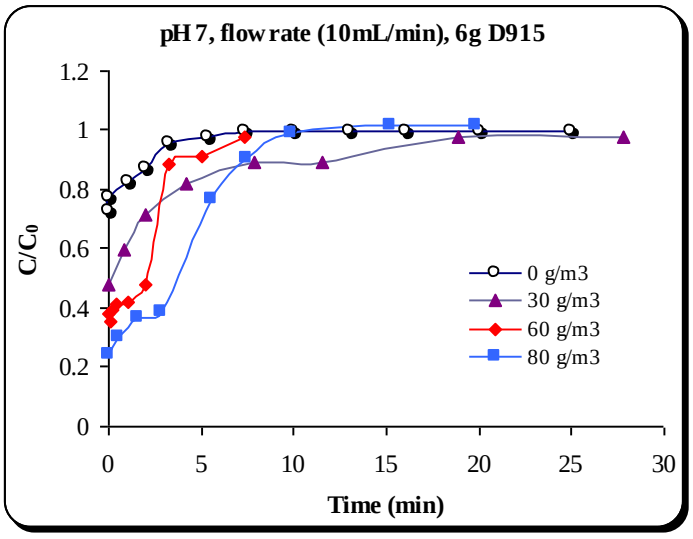

Figure 6.39: Effect of ozone concentration on methanol removal

Table 6.14: Effect of ozone concentration on the lowest exit methanol concentration

C_{O3} (g/m^3) NTP	q_{O3} (mg/g)	Lowest exit concentration (mg/L)
0	0	41
30	27.28	34
60	38.41	26
80	44.29	17

6.5.4. Effect of pH on methanol removal

Experiments were carried out without t-butanol at two different controlled pH values of 2 and 7. The temperature was kept constant at 20±1 ºC. The methanol concentration of the solution was 2.5 mol/L made in water and an ozone concentration of 60 g/m^{3}NTP was used. The water flow rate was 10 mL/min and the adsorbent mass was 6 g D915. Figure 6.40 shows the results of those experiments. It is clear that increasing pH from 2 to 7 did not cause significant effect on the removal of methanol.

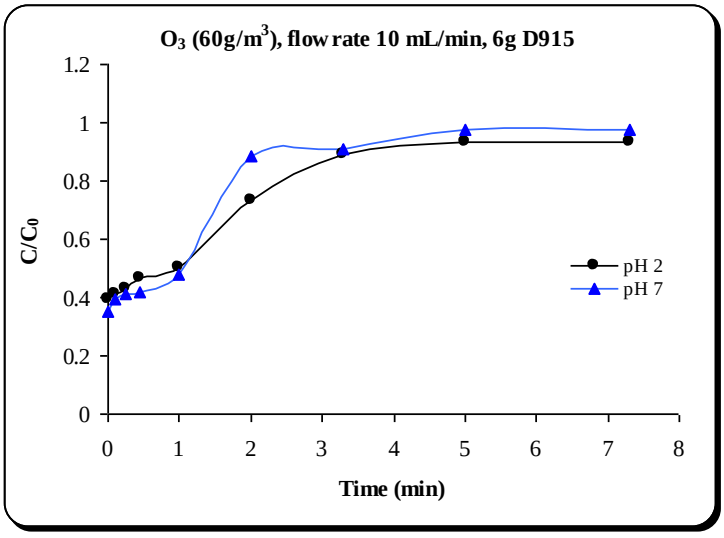

Figure 6.40: Effect of pH on methanol removal

6.5.5. Effect of flow rate on methanol removal

Three different flow rates of 5, 10 and 15 mL/min were used to investigate the effect of flow rate on methanol removal, using 6 g of zeolite D915 at an ozone gas concentration 60 g/m^{3}NTP and pH 7. The operating conditions of all experiments are shown in Appendix A1.5 (Table A1.23) and the results are shown in Figure 6.41. Table 6.15 shows the lowest methanol concentrations measured at the outlet of the reactor as function of liquid flow rate. Again, the results show that the removal of methanol is better at low liquid flow rates. Low liquid flow rates mean high residence times, thus the contact time between ozone and methanol is high, which results in lower exit methanol concentrations at low flow rates. Similarly, as for the naphthalene case, the breakthrough

curves did not reach zero due to the small quantity of adsorbent used and the relatively high solvent flow rate.

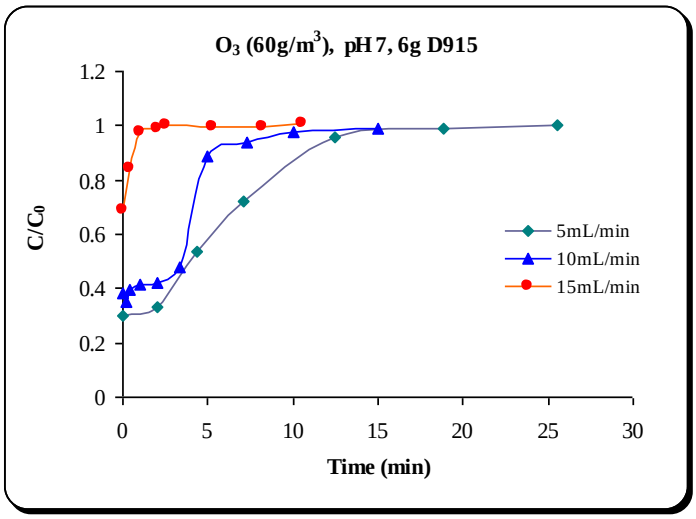

Figure 6.41: Effect of flow rate on methanol removal

Table 6.15: Effect of liquid flow rate on the lowest exit methanol concentration

Q (mL/min)	q_{O3} (mg/g)	Lowest exit concentration (mg/L)
5	32.13	22
10	38.41	26
15	36.75	56

6.5.6. Summary

From methanol experiments in LSO system, the following summary may be made. Adsorption studies of methanol on the zeolite material D915 were carried out and it was found that the adsorption of methanol followed a Langmuir type isotherm. The removal of methanol in the LSO system was improved by increasing the ozone bed capacity and decreasing the liquid flow rate. However, increasing pH from 2 to 7 did not affect significantly the performance of the LSO system. Here again, the LSO system can be used to remove methanol from water, as long as the operating conditions are optimised.

CHAPTER 7: CONCLUSIONS AND FUTURE WORK

7.1. Conclusion

This study concerned the degradation of four organic chemicals (reactive dye RO16, triclocarban, naphthalene and methanol), using the conventional ozone system termed as liquid/gas-ozone (LGO) and tested the feasibility of using a novel ozone-based system, termed as liquid/solid-ozone (LSO), to degrade three of the four organic compounds (reactive dye RO16, naphthalene and methanol). The study involved extensive experimental work and the use of a range of analytical equipment and methods. The main outcome of this work is the presentation of data related to reaction kinetics and mass transfer parameters at different operating conditions such as pH, ozone and the organics concentrations, flow rate and radical scavenger. The data presented in this work is novel and is not available in the open literature. The LSO system was found suitable to degrade the compounds studied here but the conditions have to be optimised in order to fully assess its performance and make adequate conclusions.

Ozone mass transfer parameters have been obtained at different conditions and it was found that the addition of t-butanol (used as radical scavenger) affected the volumetric mass transfer coefficient, k_La, due to changes in the physico-chemical properties of the solution. For example at pH 2, the ozone volumetric mass transfer coefficient (k_La) increased from 4.7×10^{-3} s^{-1} in the absence of t-butanol to 6.3×10^{-3} s^{-1} in the presence of t-butanol at 0.2 M. The application of available data in the literature related to ozone decay and solubility can lead to erroneous results because of the variations in the models used in the literature, which are highly dependent in addition to controlled experimental conditions on the types of water and analytical equipment used. For this reason, studies to determine ozone solubility and its decay rates have been carried out in

this work. It was found that the ozone solubility varied with ozone gas concentration in the form: C_{AL}^{*}(mol/L) = 0.0456× C_{AG} (g/m^3 NTP) at 20 °C. On the other hand, the ozone decomposition was studied at pH values of 2, 5, 7 and 9 in a reactor initially saturated with ozone. At each pH value, the experiment was either carried out in the absence or presence of t-butanol at 0.2 mol/L. Ozone decomposition was found to follow a second order reaction at pH values less than 7, whilst it was first order at pH 9. When the scavenger t-butanol was added, the decomposition of ozone progressed at a lower reaction order of 1.5 for pH values less than 7 and at the same order when without t-butanol at pH 9. Ozone decay was found to increase significantly with pH but t-butanol reduced the decay of ozone. At high pHs, ozone decay increases due to the high concentrations of hydroxide ions, which promote ozone decomposition. In addition, values of the specific surface area (a_L) available in the reactor were determined in the absence and presence of t-butanol (0.2 M). The values of a_L were 2.7 and 3.5 m^2/m^3 in absence and presence of t-butanol respectively. The increase of a_L in the presence of t-butanol was due to reduction in bubble diameters and increase in gas holdup.

The degradation of RO16 studies revealed that an increase in ozone concentration significantly increased the reaction rates. The effectiveness of ozone to degrade the dye was measured by considering the time at which 95 % of the dye has been removed ($t_{0.95}$). A simple equation of the form $t_{0.95} = a \times C_{AGi} \times C_{B0}$ was proposed to give the effect of the inlet ozone concentration C_{AGi} and the initial dye concentration C_{B0} on $t_{0.95}$. During ozonation of RO16, noticeable pH decrease and conductivity increases were observed. The rate constant (k) of the reaction RO16 with ozone in the absence of t-butanol was determined to be 9.1×10^3, 4.4×10^3 and 8.2×10^3 M^{-1}s^{-1} at pHs 2, 7 and 11 respectively, whereas when the t-butanol was added to the solution of RO16, the values of k almost doubled at high pH but remained unchanged at low pH. This result

indicates that molecular ozone reactions prevail the indirect reactions with hydroxyl radicals for the degradation of RO16.

In terms of the degradation of the antiseptic compound triclocarban (TCC), the results from the present laboratory experimental work suggests that triclocarban can be degraded by ozone. From the experiments carried out so far, it was found that pH has a significant effect on the degradation rates of TCC and both direct and indirect reactions contribute to its degradation. Reaction rate constants were in the order of 5.4×10^{4} and 9.3×10^{3} L/mol.s for conditions without and with t-butanol as radical scavenger respectively. The reaction stoichiometry was obtained to have a value of 1.

The degradation of naphthalene using the Liquid/Gas-Ozone (LGO) system was studied. From naphthalene degradation experiments, it can be summarised that the pH had a substantial effect on the degradation rate of naphthalene. Reaction rate constants did not change significantly following the addition of the radical scavenger t-butanol and were in the order of 1.4×10^{5} and 1.6×10^{5} L/mol.s in the absence and presence of t-butanol respectively**.** The reaction stoichiometry was found to have a value of 1mol/mol. Higher pH values decreased the degradation rates, possibly due to competitive reactions between ozone and hydroxide ions. These results show that hydroxyl radicals seem to have limited effect on naphthalene degradation, which has also been observed when a radical scavenger (t-butanol) was used. Reaction rate constants were calculated and were found around 100 times higher than values reported in the literature due to differences in experimental conditions 1.5×10^{3} (Legube et al., 1986) against 1.4×10^{5} $Lmol^{-1}s^{-1}$ (this work).

From the results of the experimental investigation on the degradation of methanol by ozone, it was found that the rate constant (k) of the degradation reaction increased when

the pH increased and the highest value of the rate constant was obtained at pH9**.** The reaction stoichiometry was found to have a value of 1mol/mol.

The two steps of the Liquid/Solid-Ozone (LSO) system were studied. The kinetic data related to ozone adsorption on beds of silica gel and a zeolitic material (D915) were determined and the ozone adsorption process was modeled using models developed in previous studies. It was found that particle rate controls ozone adsorption step but liquid rate controls the water treatment step.

Ozone desorption with pure deionised water was studied at different water flow rates, pHs and t-butanol. A one-parameter exponential model fitted the experimental results well and the parameter was found to change linearly with water flow rate at a given initial bed capacity. The water flow rate was found to accelerate the desorption rates but pH was found to decrease the desorption rates. In contrast, the effect of pH was insignificant in the presence of t-butanol.

Determination of the adsorption isotherms for RO16, naphthalene and methanol revealed that RO16 did not exhibit adsorption on silica gel but both naphthalene and methanol showed adsorption on D915 described by Langmuir model.

The degradation of the three organic compounds with the LSO system was studied. It was found that the LSO system can be used to remove the three compounds studied here as long as the operating conditions are optimised. Under the conditions of the experiments carried out in this work, it was not possible to observe “clear” breakthrough curves for naphthalene and methanol but the performance of the system was described by the measurement of the lowest naphthalene or methanol exit concentration. In contrast, RO16 showed clear breakthrough curves particularly when t-butanol was added to the solution. Overall, it was observed for all three compounds

that the performance of the system is enhanced under lower liquid flow rate and higher initial bed capacity. The effect of pH and t-butanol was compound-dependent.

7.2. Future Work

The thesis described the decomposition of various chemicals in synthetic solutions, including reactive dye RO16, triclocarban, naphthalene and methanol using two ozone-based systems. Future work may explore the removal of these chemicals from contaminated real waste streams which may contain a set of pollutants using the same procedures. When several pollutants are present in the waste water stream the decomposition reaction rate, concentration of the pollutant, temperature and the pressure of the reaction may vary. According to the changes occurring with the various parameters the research scope may change to establish an altered procedure for removal of toxic chemicals from the waste water stream.

The chemistry of decomposition reactions could be followed by the products formed by studying and analysing the reactants and products using HPLC, GC/FID, Ion Chromatography, LC/MS/MS.

Ozonation studies could be expanded to water samples contaminated with pesticides and fertilisers. The effect of the temperature and pressure on the removal of these chemicals could also be studied. Finally, taller columns should be used to study the LSO system.

7.2.1. Effect of temperature and pressure on the degradation of the compounds

More sophisticated equipment could be added to the system such as: control manifold and better thermal bath with heating abilities. The added features would give future researchers more control over two factors: temperature and pressure. In the case that ozone-loaded solids may by utilised in the removal of pollutants, it is advised that a study of the effect of temperature and pressure on the removal of the compounds be

carried out. Mathematical modeling could be studied from the basic literature and the validation of experimental data could be carried out in the future to establish the effect of each parameter on the performance of the system.

7.2.2. HPLC, GC/FID, Ion Chromatography, LC/MS/MS Emissions

As the removal of pollutants with ozone was only monitored by the reduction in colour for the dyes and the UV-absorption peak of TCC, methanol, and naphthalene in the HPLC and GC/FID measurements, further work on the chemistry of decomposition reactions followed by the products formed could be investigated using HPLC, GC/FID, Ion Chromatography, LC/MS/MS. From the present observation low concentration of the pollutant cannot be measured by HPLC and hence sophisticated equipments namely GC/FID could be applied in the future research.

7.2.3. Taller columns

The study of ozone adsorption on (silica gel and zeolite) and the removal of various types of pollutants have brought about some interesting questions, which require further research. As it has been shown that ozone adsorbs favourably on silica gel, further work using high silica content adsorbents may show a greater affinity for ozone adsorption. Recently it has been shown that ozone adsorbs more favourably on HZSM-5 (a zeolite which contains a high silica content) than on silica gel (Tizaoui 1999). Results obtained from the current investigation showed that taller columns and low water flow rates should be used to ascertain the effect of the various parameters.
It is therefore recommended to take this into consideration in a future work.

NOMENCLATURE

A	Ozone (O_3) (g/m^3) NTP
a_L	Specific surface area (m^2m^{-3})
B	Pollutant (RO16 or triclocarban or naphthalene or methanol) (mg/L or mol/L)
C_{AL}*	Ozone concentration saturation in liquid (mg/L)
C_{AG}	Ozone gas concentration (g/m^3) NTP
C_B	Final concentration (mol/L)
C_{B0}	Initial concentration (mol/L)
C_L	Liquid concentration
Conc.	Concentration
D	Diffusivity (m^2s^{-1})
d_p	Average particle diameter (m),
De	Effective ozone diffusivity in silica gel (m^2/s),
D_{O2}	Oxygen diffusivity coefficient (2.5×10^{-9} m^2s^{-1})
D_{O3}	Ozone diffusivity coefficient (1.7×10^{-9} m^2s^{-1})
Ha_1	Hatta number for first-order
k	Rate constant ($M^{-1}s^{-1}$)
k_d	Ozone decomposition rate (s^{-1})
k_La	Mass transfer coefficient (s^{-1})
K_{vp}	Equilibrium constant based on particle volume
L	Total packed bed length (m),
M	Molar concentration (mol/L)
m	Ozone solubility parameter
MeOH	Methanol
N	Mass transfer flux
n	Number of moles
Napht	Naphthalene
NTP	Normal temperature and pressure 1 atm
N_P	Number of particle mass transfer units
O_2	Oxygen
Q_G	Ozone gas flow rate (mL/min)
RO16	Reactive dye (Red Orange)
SG	Silica gel

t	Time (minutes or second)
TCC	Triclocarban or 3, 4, 4-trichlocarbanilide
t-OH	t-butanol
u	Gas interstitial velocity (m/s)
z	Stoichmetric factor, (z)
Greek symbols	
δ	Liquid film thickness (m)
ε	Molar absorbance (M^{-1} cm^{-1})
τ	dimensionless time
β	liquid hold up
Subscripts	
G	gas
Li	liquid
*	Equilibrium
Indices	
Abs	Absorption
Ads	Adsorption
Des	Desorption

REFERENCES

Alder, M.J; Hill, G.R, (1950) Kinetics and Mechanism of Hydroxide Ion catalyzed Ozone Decomposition in an Aqueous Solution, Journal of American Chemical Society, Vol. 72, pp. 1884-1887.

Ardon, M, (1965) Oxygen, New York, W .A. Benjamin, Inc.

Astarita, G. (1967) Mass Transfer with Chemical Reaction, Elsevier, Amsterdam

Atkins, P.W, (1990) Physical Chemistry, 4th ed., Oxford, Oxford University Press.

Avzyanova, E.V; Kabal`nova, N.N; Shereshovats, V.V, (1996) Oxidation of Organic Compounds by Ozone on a Surface 1. Ozonization of Adamantane on Silica gel, Russian Chemical Bulletin, Vol.45, No.2, pp. 360-362.

Bader, H; Hoigne, J, (1982) Determination of Ozone in Water by the Indigo Method: a Submitted Standard Method. Ozone Science and EngineeringVol.4, pp.169-176.

Balcioglu, A. Arslan, L. and M. Scan, (2001) Homogenous and heterogeneous advanced oxidation of two commercial reactive dyes, Environ. Technol, vol. 22, pp. 813–821.

Brink, D.R; Langlais, B; Rechow, D.A, (1991) Ozone in Water Treatment; Application and Engineering", Michigan, Lewis Publishers, Inc.

Brunauer, (1945) Physical Adsorption Princeton University Press, Princeton, N. J.

Bulanin, K.M; Alexeev, A.V; Bystrov, D.S; Lavalley, J.C; Tsyganenko, A.A, (1994) IR Study of Ozone Adsorption on SiO2 Journal of Physical Chemistry, Vol.98, pp.5100-5103.

Bulanin, K.M; Lavalley, J.C; Tsyganenko, A.A, (1995a) IR Spectea of Adsorbed Ozone, Colloids and Surfaces A; Physic-chemical and Engineering Aspects, Vol. 101, part 2-3, pp.153-158.

Bulanin, K.M; Lavalley, J.C; Tsyganenko, A.A, (1995b) Infrared Study of Ozone Adsorption on TiO2 (Antatase), Journal of Physical ChemistryVol. 99, pp. 10294-10298

Bulanin, K.M; Lavalley, J.C; Tsyganenko, A.A, (1997) Infrared Study of Ozone Adsorption on CaO Journal of Physical Chemistry, Vol.101.pp.2917-2922.

Bunce, N. J, (1991) Environmental Chemistry; Winnipeg, Wuerz Publishing Ltd.

Chun-Yu Chiu, Yi-Hung Chen, Yi-Haw Huang, (2007) Removal of naphthalene in Brij 30-containing solution by ozonation using retating packed bed. Journal of Hazardous Materials 147, 732-737.

Coate, Robert, (1997) The Co-Deca-Tech Water/Wastewater Treatment System. Retrieved October 2007, from (http://www.ozonated.com/ptov6-8-.html.date .

Cohen, Z; Keinan, E; Mazur, Y; Varkony, T.H, (1975) Dry Ozonation. A Method for Stereo selective Hydroxylation of Saturated Compounds on Silica Gel, Journal of Organic Chemistry, Vol.40, No.14, pp. 2141-2142.

Cook, G.A; Kiffer, A.D; Klumpp, C.V; Malik, A.H; Spence, L.A (1959) Separation of ozone from oxygen by a Sorption process, Advances in Chemistry Series, pp.44-

Dankckwerts PV (1970) Gas Liquid Reactions, McGraw-Hill New York.

Davis, M.E., (1998) Zeolite-based catalysts for chemical synthesis. Microporous and Mesoporous Materials, 21(4-6):173-182.

Degrémont, (1991a) Water Treatment Handbook, 6th ed., Vol.1, New York, Lavoisier Publishing Inc.,

Degrémont, (1991b) Water Treatment Handbook, 6th ed., Vol.2, New York, Lavoisier Publishing Inc.,

DEL Industries, (1997) Ozone Questions and Answers, Retrieved October 2007, from http://206.190.82.21/qaozn.htm.

Duguet, J.P. ET AL, (1983) Monitoring an Ozone Process Through UV Measurements, 6th Ozone World Congress, IOA, Washington, D.C.

Edgar, J.L; Paneth, F.A, (1941) The Separation of Ozone from other Gases, Journal of the Chemical Society, pp.511-519.

EPA, August (1997), Water Pollution Prevention and Conservation.

EPRI, (1996) Ozone Optimization Turns Tide of Concern about Drinking Water Safety. Retrieved December 2007, from http://www.ozonated.com/ptov6-8-.html.

Fujitah. Et al., (2005) Adsorbed Phase Ozonation of Water Dessolved Organic Pollutants Using High-Silica Zeolites. Adsorption, Volume 11, Supplement 1, pp. 835-839

Gery, N.F. (1994) Drinking water quality Problems and Solution, Trinity College, University of Dublin, Ireland.

Glaze WH, Kang J-W, (1987) The Chemeistery of Water Treatment Processes involving Ozone, Hydrogen Peroxide and Ultraviolet Radiation, Ozone Science & Engineering 9:335-352.

Gmelin, L; (1960) Handbuch der Anorganischen Chemie, Lieferung 4, Weinheim, pp. 1123-1124.

Gordon, G. ET AL, (1987a) A Survey of the Current status of Residual Disinfectant Measurement Methods for All Chlorine Species and Ozone. American Water Works Association Research Foundation, Denver, Colo.

Gordon, G; Rakness, Robson, C.M, (1992) Ozone Concentration Measurement In A Process Gas, International Ozone Association , Pasadena Conference; Ozonation for drinking water treatment, No.20.

Gordon, G., R.D. Gauw, Y. Miyahara, B. WaltersA & B. Bubnis, (2000a.) Using indigo absorbance to calculate the indigo sensitivity coefficient. J. AWWA,92(12):96.

Grasso. D, (1987) Ozonation Dynamics in Water Treatment: Autocatalytic Decomposition, Mass Transfer and Impact on Particle Stability, PhD Dissertation, The University of Michigan, Ann ARBOR, Mich.

Greaves, G.F& Lowndes, M.R, (1987) Ozone use at British Water Treatment Plants, Proc. 2nd Intl. pp 245-265.

Gregg, S.J; Sing, K.S.W, (1982) .Adsorption, Surface Area and Porosity, 2nd ed., London, Academic Press Inc., Ltd.

Gurol, M.D; Singer, P.C, (1982) Kinetics of Ozone Decomposition: A Dynamic Approach, Environmental Science Technology, Vol.16, No.7, pp 377-383.

Halden, R. U. & PaullL, D. H, (2005) Co-occurrence of triclocarban and triclosan in US water resources. Environmental Science & Technology, 39**,** 1420-1426.

Hallmann, M.M, (1996) Photo degradation of Water Pollution., Florida, CRC Press, Inc.,

Hirotaka Fujita, Jun Izum, Masaki Sagehashi, Takao Fujii, and Akiyoshi Sakoda, (2004a). Adsorption and Desorption of Water dissolved ozone on High Silica Zeolite, water Research, 38(1), 159-165.

Hoigne J. et Bader H. (1983), Rate constant of Reactions of ozone with organic and inorganic compounds in water, I. Non dissociating organic compounds. Water Research. 17, 173-183.

Hu, J.X., Li, Y.W., Xiang, H.W., Xu, Y.Y, He, L.M, Gao, M.X., (2001) The Method of Rapidly Synthesizing Small Crystalline ZSM-5 Zeolite with Template Agent. CN00109593.5 (in Chinese).

Hughes, D; Jewell, T; Parpworth, N, (1996) Environmetal Law, 3rd ed., London, Reed Elsevier Ltd.

Hua, Y.M., Hu, W.M, (2001) Synthesis of ethylenediamines over ZSM-5 zeolite. Hua Xue Shi Jie, 42(9):480 (in Chinese).

Ken Rubin, Assistant Professor "Water Pollution, Department of Geology and Geophysics, University of Hawaii, Honolulu, HI 96822.

Kenly, W. J, (1996) Advances in Ozone Monitor Technology , International Ozone Association, Amsterdam Conference, Regional Conference on Ozone, Ultraviolet Light, Advanced Oxidation Processes in Water Treatment, pp.159-174.

Kerc, A; Saatci, A. M (1996) Computerized Continuous Monitoring and Analysis of Ozone in Solution, Ozone Scince and Engineering, Vol. 18, No. 5, pp. 469-476.

Knight, A.G.1951. The Photometric Estimation of Color in Turbidity Waters .J .Inst. Water Eng.5:623.

Kogelschatz, U. (1987) UV Adsorption of Ozone in the Gas Phase, Proc. 8th Ozone World Congress, IOA, Zurich, Switzerland.

Kuo, C.H; Li, K.Y; Win, C.P; Weeks-Jr, J.L (1976) Absorption and Decomposition of Ozone in Aqueous Solutions ALChE Symposium Series, Water-1976: I. Physical, Chemical Wastewater Treatment, Vol. 73, No. 166, pp. 230-241.

Langlais, B. (1985) Ozone Dosage in the Gaseous Phase. Proc. Intel Conf: The Role of Ozone in Water and Wastewater Treatment (R. Perry and r. e. McIntyre, Eds.), Selper Ltd., London, p.33.

Legube, B. Guyon, S. Sugimitsu, H. Dore, M. (1986) Ozonation of naphthalene in aqueous solution. 1. Ozone comsumption and ozonation products, water Res. Vol. 20, No, 2 pp. 197-208.

Legube, B. Sugimitsu, H. Guyon, S. Dore, M. (1986) Ozonation of naphthalene in aqueous solution. 2. Kinetic studies of the initial reaction step, water Res. Vol. 20, No. 2, pp. 209-214.

Lewis, W. K. and Whitman, W. G. (1924), Principles of gas absoption, Ind. & Eng. Chem., 16, 1215-1220.

Lgnasi Sires, Nihal Qturan, Mehmet A. Qturan, Rosa Maria, Jose Antonio, Enric Brillas, (2007) Electro-Fenton degradation of antimicrobials triclosan and triclocarban Electrochimica Act 52 5493-5503

Li, H.Y. Liang, J. Ying, M.L, (1983) Synthesis of ZSM-5 zeolite of high silica/alumina ratio. Cui Hua Xue Bao, 4(3):244-247 (in Chinese).

Liakou, S; Pavlou, S; Lyberatos, G, (1997) Ozonation of Azo Dye Water Scince and Technology, Vol. 35, No. 4, pp. 279-286.

Liu, M., Xiang, S.H, (2001) Studies on the synthesis ofzeolite ZSM-5 with different morphology and crystal size. Shi You Xue Bao (Shi You Jia Gong), 17(2):24-29 (in Chinese).

Lopez, A. Benbelkacem, H. J.-S. Pic and H. Dellefontaine, (2004) Oxidation pathways for ozonation of azo dyes in a semi-batch reactor: a kinetics parameters approach, Environ. Technol, vol. 25 pp. 311–321.

López-López A, Pic JS, Debellefontaine H (2007 Feb). Ozonation of azo dye in a semi-batch reactor: a determination of the molecular and radical contributions. Chemosphere, 66(11):2120-6. Epub 2006 Dec 12.

Magnus, A; Grahling, K, (1929) Uber die Adsorption von Sauerstoff und Ozone an Kieselsauregel, Zeitschrift fur Physikalische Chemie, Vol.145A, pp.27-47.

Maier, D. & Kurzmann, G. E. (1977) The Determination of Higher Ozone Concentrations, Wasser, Luft und Betrieb, 21:125.

Mark J. Hammer, Mark J. Hammer, Jr , Water and Wastewater Technology 4th ed Page 157-159.

Masschelein, W.J, (1982) Ozonization Manual for Water and Wastewater Treatment, Norwich, A Wiley-Interscience publication,

Masschelin, W.J. ET AL, (1989) Determination of Residual Ozone or Chlorine Dioxide in Water with ACVK-An Updated Version. Ozone Sci. Engrg., 11:2:209.

Mauersberger, K. ET AL. (1986) Measurements of the Ozone Adsorption Cross-Section at the 253.7 nm Mercury Line. Geophys. Res. Letters. 13:671.

Molina, L. T.& Molina, M. J, (1986 Absolute Adsorption Cross Section of Ozone in the 185 to 350 nm Wavelength Range. Jour. Geophys. Res., 91:501.

Mumma, A, (1995) Environmental Law: Meeting UK&EC Requirements, Surrey, McGraw-Hill Internaional (UK) Limitied.

Munoz. F. and C. Von Sonntag, (2000).. Determination of Fast Ozone Reaction in Aqueous Solution by Competition Kinetics, J. Chem.Soc., Perkin Trans., 2:661-664

Muthukumar, M., Selvakumar, N., Venkata, J, (2001) Effect of dye structure on decolouration of anionic dyes by using ozone. In: Proceedings of the 15th Ozone World Congress of International ozone Association 2001, London, United Kingdom, pp. 410–421.

O'Donovan, D.C, (1965) Treatment with ozone, Jour, AWWA, 57:9:1167-1194.

Perkowski, J. Kos, L. and Ledakowicz, S. (2000) Advanced oxidation of textile wastewater, Ozone-Sci. Eng. 22 pp. 535–550.

Pohland, F.G. & Bloodgood, D.E. (1963) Laboratory Studies on Mesophilic and Thermopile anaerobic Sludge digestion .J. Water control fed.35:1.

Rakness, K; De Mers, L.D; Blank, B.D, (1996) Gas Phase Ozone Concentration Comparisons From a Commercial UV Meter and KI Wet-Chemistry Tests, Ozone Science and Engineering, Vol.18, No.3, pp231-250.

Raabe, E.W, (1968), Biochemical oxygen demand and degradation of lignin in natural waters. J. Wat. Pollut. Control Feb. 40 (1968), pp. R145–R150.

Rivas, F.J. Beltran, F.J. Carbajo, M. and Gimeno, O. (2003) Homogeneous catalyzed ozone decomposistion in the presence of Co (II), Ozone-Sci. Eng. 25 pp. 261–271

Ruthven, D.M, (1984) Principles of Adsorption and Adsorption Processes, New York, John Wiley and Sons, Inc.,

Sapkota, A., Heldler, J. & Halden, R. U, (2007) Detection of triclocarban and two co-contaminating chlorocarbanilides in US aquatic environments using isotope dilution liquid chromatography tandem mass spectrometry. Environmental Research, 103**,** 21-29.

Slater, M.J., (1991). The Principles of Ion Exchange Technology, (Butterworth-Heinemann: Oxford.

Stephen Brunauer, P. H. Emmett, and Edward Teller, (1938) Adsorption of Gases in Multimolecular Layers J. Am. Chem. Soc., 60 (2), 309-319• DOI: 10.1021/ja01269a023 • Publication Date (Web): 01 May 2002 Downloaded from http://pubs.acs.org on March 4, 2009

Sotelo, J.L; Beltran, F.J; Beltran-Heredia, J, (1989) Henry's Law Constant for the Ozone –Water System, Water Resources, Vol.23, N.10, pp.1239-1246.

Stumm, W, (1958) Ozone as a Disinfectant for Water and Sewage, Journal of the Boston Society of Civil Engineering, Vol. 45, pp. 66-79.

Tchobanoglous, G; Burton, F.L, (1991) Wastewater Engineering –Treatment, Disposal and Reuse, Metcalf and Eddy, Inc., McGraw-Hill, Inc.,

Thomas, K; Hoggan, P.E; Mariey, L; Lamotte, J; Lavalley, J.C, (1997) Experperimental and Theoretical Study of Ozone Adsorption and Alumina, Catalysis Letters, Vol.46, parts 1-2, pp.77-82.

Tizaoui, (1999). Water treatment by ozone loaded adsorbents, Annual Water Meeting for Industrialists and Academics, Bradford.

Tizaoui, Chedly and Slater, M. J, (2003) The design of an industrial waste-water treatment process using adsorbed ozone on silica gel. Process Safety and Environmental Protection, 81**,** 107-113.

Tizaoui, C. and Slater, M. J. (2003). Uses of Ozone in a Three-Phase System for Water Treatment : Ozone Adsorption Ozone Science and Engineering, Vol 25.

Tizaoui, R.I. Bickley, M.J. Slater, W-J. Wang, D.B. Ward, A. Al-Jaberi, (2008) A comparison of navel ozone-based systems photocatalysis for the removal of water pollutants Desalination 227, 57-71.

Tizaoui, Chedly, (2001) Investigation of a new technique for water treatment using adsorbed ozone, Bradford Ph.D, thesis.

Tomiyasu, H; Fukutomi, H; Gordon, G; (1985) Kinetics and Mechanism of Ozone Decomposition in Basic Aqueous Solution, Inorganic Chemistry, Vol. 24, No. 19, pp. 2962-2966.

Trambarulo, R; Ghosh, S.N; Burrus JR., C.A; Gordy, W, (1953) The Molecular Structure, Dipole Moment, and g Factor of Ozone from Its Microwave Spectrum, The Journal of Chemical Physics, Vol.21, No.21, pp. 851-854.

Triclocarban-Wikipedia, (2009,) http://en.wikipedia.org/wiki/Triclocarban,Date of view, 2009.

UK-Environment-Agency, (2008) Naphthalene, URL: http://www.environment-agency.gov.uk/.

U.S. Environmental Protection Agency, (1993) Methods for Determination of Inorganic Substances in Environmental samples

Van Krevelen, D. W.; Hoftijzer, P. J, (1954) Applicability of the Results of Small-Scale Experiments to the Design of Technical Apparatus for Gas Absorption, Trans. Inst. Chem. Eng. 32, p. 60.

Vasmaer, A, (1916) Ozone: Its Manufacture, Properties and Uses, New York, D. Van Nostrand Company.

Water Resources Act, (1991) c.57.

Warren .V, Jr. Mark J.Hammer. - 5th (ed.), (1993) Water Supply And Pollution Control, Harper Collins College Publishers., New York.

Winyall, M.E, (1984) Silica gels: preparation and properties, Applied Industrial Catalysis, Vol.3, pp.43-61.

Wu, J and Wang, T. (2001a) Ozonation of Aqueous Azo Dye in a Semi-batch Reactor, Water. Res. 35; 1093-1099

Zhang, C.L., Kan, Q.B., Wu, Z.Y, (1995) Rapid synthesis and characterization of Fe-ZSM-5 zeolite. Shi You Xue Bao (Shi You Jia Gong), 11(4):20-26 (in Chinese).

Zhu Shiyun, Zheng Xuesong, Li Daotang, (2002), Ozonation of naphthalene sulfonic acid in aqueous solution. Part I: elimination of COD, TOC and increase of their biodegradability, Water Research 36 (2002) 1237-1243.

Zurer, P. S, (1987) Complex Mission Set to Probe Origins of Antaractic Ozone Hole. Chem. Engrg. News, 7.

Yang, R.T, (1987) Gas Separation by Adsorption Processes, Stoneham, Butterworth Publisher,

APPENDICES

Appendix A1: Experimental Conditions

A1.1. Mass transfer Parameters

A1.1.1. Oxygen absorption in deionised water

Oxygen absorption experiments are the experiments numbered from ox1 to ox7, each experiment was carried out with different gas flow rates at 20 ± 1 °C.

Table A1.1. Experimental conditions and calculated results of k_La for CO_2

Exp No	Gas flow rate (mL/min)	pH	Pressure (mbar)	Conduct- (µs/cm)	$k_La(s^{-1})$	C_{AL}^* (mg/L)	C_{AL0} (mg/L)
ox1	100	4.158	171.9	0.85	0.00295	44.0	10.84
ox2	200	4.318	182.2	0.77	0.004049	46.0	11.71
ox3	300	4.35	188.9	0.66	0.008592	47.0	6.16
ox4	400	4.454	186	0.8	0.005762	50.8	7.73
ox5	500	4.252	186.3	0.67	0.006668	47.4	8.67
ox6	600	4.42	181	0.79	0.007472	46.3	7.147
ox7	700	4.132	198.9	0.67	0.014577	50.8	7.73

A1.1.2. Ozone absorption in deionised water

Ozone absorption experiments are the experiments numbered from oz1 to oz8, each experiment was carried out with different ozone concentration at 20 ± 1 °C.

Table A1.2. Experimental operating conditions for ozone absorption

Exp No	Sample (mL)	Gas Flow rate (mL/min)	Ozone conc. inlet (g/m^3)NTP	Ozone conc. out let (g/m^3)NTP	Initial pH	Final pH
oz1	500	400	20	19	5.325	5.114
oz2	500	400	40	38	5.205	5.094
oz3	500	400	60	56.5	5.195	5.022
oz4	500	400	80	78	5.215	5.015
oz5	500	200	20	19.7	4.325	4.114
oz6	500	200	40	39.2	4.205	4.094
oz7	500	200	60	58	4.195	4.022
oz8	500	200	80	77	4.215	4.015

Table A1. 3. Operating conditions for pH and scavenger effect experiments

Exp No	Sample (mL)	Gas Flow rate (mL/min)	Ozone conc. inlet (g/m^3)NTP	t-butanol (mol/L)	Initial pH
Oz9	500	400	80	0.2	2
Oz10	500	400	80	0	2
Oz11	500	400	80	0.2	7
Oz12	500	400	80	0	7
Oz13	500	400	80	0.2	9
Oz14	500	400	80	0	9
Oz15	500	400	20	0.2	2
Oz16	500	400	20	0	2
Oz17	500	400	20	0.2	7
Oz18	500	400	20	0	7
Oz19	500	400	20	0.2	9
Oz20	500	400	20	0	9

A1.1.3.Ozone decay

Table A1.4 shows the operation condition of ozone decay experiments.

Table A1.4. Operating conditions for ozone decay experiments

Exp No	Sample (mL)	Gas flow rate (mL/min)	Ozone conc. (g/m^3)NTP	t-butanol (mol/L)	pH
Od1	500	400	40	0	2
Od2	500	400	40	0.2	2
Od3	500	400	40	0	5
Od4	500	400	40	0.2	5
Od5	500	400	40	0	7
Od6	500	400	40	0.2	7
0d7	500	400	40	0	9
Od8	500	400	40	0.2	9

A1.2. Degradation of Dye RO16

Dye absorption experiments are the experiments numbered from D1 to D31, each experiment was carried out with different concentration of ozone, and concentration of dye RO16 at 20 ± 1 °C.

Table A1.5. Experimental operating conditions for RO16 ozonation

Exp No	Sample (mL)	Flow rate (mL/min)	Ozone conc. Inlet (g/m^3)NTP	Dye conc. (mg/L)	Initial pH	Final pH
D1	500	400	20	25	4.744	3.600
D2	500	400	20	50	4.698	3.489
D3	500	400	20	75	4.717	3.388
D4	500	400	20	100	4.745	3.334

D5	500	400	40	25	4.682	3.664
D6	500	400	40	50	4.726	3.474
D7	500	400	40	75	4.853	3.553
D8	500	400	40	100	4.740	3.330
D9	500	400	60	25	4.720	3.736
D10	500	400	60	50	4.775	3.613
D11	500	400	60	75	4.704	3.447
D12	500	400	60	100	4.712	3.389
D13	500	400	80	25	4.692	3.689
D14	500	400	80	50	4.723	3.584
D15	500	400	80	75	4.698	3.460
D16	500	400	80	100	4.703	3.386

Table A1.6. Experimental operating conditions for dye ozonation: effect of pH and scavenger

Exp No	Sample (mL)	Gas Flow rate (mL/min)	Ozone Conc. Inlet (g/m^3)NTP	Dye Conc. (mg/L)	t-butanol (mol/L)	Initial pH
D17	500	400	20	100	0.2	2
D18	500	400	20	100	0	2
D19	500	400	20	100	0.2	7
D20	500	400	20	100	0	7
D21	500	400	20	100	0.2	11
D22	500	400	20	100	0	11
D23	500	400	80	25	0.2	2
D24	500	400	80	25	0	2
D25	500	400	80	25	0.2	7
D26	500	400	80	25	0	7
D27	500	400	80	25	0.2	11
D28	500	400	80	25	0	11

Table A1.7. operating conditions of all experiments rate constant using competitive method

Exp No	Flow Rate (mL/min)	C_{O3} (g/m^3)NTP	C_{RO16} (mg/L)	C_{Indigo} (mg/L)	$V_{(dye: indigo)}$ (mL) (50:50)%	Rate(k) (s^{-1})
D29	400	20	100	100	500	NA
D30	400	15	100	100	500	NA
D31	400	10	100	100	500	NA

A1.3. Degradation of Triclocarban (TCC)

Table A1.8. Operating conditions of TCC experiments

Exp No	Sample (mL)	Gas Flow rate (mL/min)	Ozone Conc. Inlet (g/m^3)NTP	TCC Conc. (mg/L)	t-butanol (mol/L)	Initial pH
T1	500	400	10	100	0.2	7
T2	500	400	10	100	0	7
T3	500	400	20	100	0.2	7
T4	500	400	20	100	0	7
T5	500	400	60	100	0.2	7
T6	500	400	60	100	0t	7

Table A1.9. Operating conditions of effect of pH on TCC degradation

Exp No	Sample (mL)	Gas Flow rate (mL/min)	Ozone Conc. Inlet (g/m^3)NTP	TCC Conc. (mg/L)	t-butanol (mol/L)	Initial pH
T7	500	400	60	100	0	2
T8	500	400	60	100	0	7
T9	500	400	60	100	0	9

Table A1.10. Operating conditions of effect of temperature on TCC degradation

Exp No	Sample (mL)	Gas Flow Rate (mL/min)	Ozone Conc. Inlet (g/m^3)NTP	TCC Conc. (mg/L)	Temp- (°C)	t-butanol (mol/L)	pH
T10	500	400	20	100	10	0	7
T11	500	400	20	100	10	0.2	7
T12	500	400	20	100	20	0	7
T13	500	400	20	100	20	0.2	7
T14	500	400	20	100	30	0	7
T15	500	400	20	100	30	0.2	7

A1.4. Degradation of Naphthalene

Table A1.11. Operating conditions of naphthalene experiments

Exp No	Sample (mL)	Gas Flow rate (mL/min)	Ozone Conc. Inlet (g/m^3)NTP	Napht- Conc. (mg/L)	t-butanol (mol/L)	pH
N1	200	400	10	100	0.2	7
N2	200	400	10	100	0	7
N3	200	400	40	100	0.2	7
N4	200	400	40	100	0	7

Table A1.12. Operating conditions of effect of pH on naphthalene degradation

Exp No	Sample (mL)	Gas Flow rate (mL/min)	Ozone Conc. Inlet (g/m^3)NTP	Napht- Conc. (mg/L)	t-butanol (mol/L)	pH
N5	200	400	40	100	0	2
N6	200	400	40	100	0	5
N7	200	400	40	100	0	9

Table A1.13. Operating conditions of naphthalene adsorption

D915(g)	Area (AU)	Naphthalene (mg/L)	C/C0
0	43500	79.72582	1
0.5	28261	51.79612	0.649678
1	11364	20.82768	0.261241
1.5	10001	18.32961	0.229908
2	8215	15.05627	0.188851

Table A1.14. Operating conditions of Ozone Adsorption and Desorption on Zeolite D915

Exp No	Sample (mL)	Gas Flow rate (mL/min)	Water flow (mL/min)	Ozone Conc. Inlet (g/m^3)NTP	D915 (g)	pH
Ad1	250	400	10	40	2	7
Ad2	250	400	10	40	2	7
Ad3	250	400	10	40	2	7

Table A1.15. Operating conditions of Effect of Flow Rate on Naphthalene Adsorption

Exp No	Sample (mL)	Gas Flow rate (mL/min)	Water flow (mL/min)	Ozone Conc. Inlet (g/m^3)NTP	D915 (g)	pH
Ad4	250	400	5	40	2	7
Ad5	250	400	10	40	2	7
Ad6	250	400	20	40	2	7

Table A1.16. Operating conditions of Effect of Ozone Gas Concentration on Naphthalene Adsorption

Exp No	Sample (mL)	Gas flow rate (mL/min)	Water flow (mL/min)	Ozone Conc. Inlet (g/m^3)NTP	D915 (g)	pH
Ad7	250	400	10	15	2	7
Ad8	250	400	10	30	2	7
Ad9	250	400	10	60	2	7

Table A1.17. Operating conditions of effect of pH and t-butanol on naphthalene adsorption

Exp No	Sample (mL)	Gas flow rate (mL/min)	Water flow rate (mL/min)	Ozone Conc. Inlet (g/m^3)NTP	D915 (g)	t-butanol (mol/L)	pH
Ad10	250	400	10	30	2	0	2
Ad11	250	400	10	30	2	0.2	2
Ad13	250	400	10	30	2	0	5
Ad14	250	400	10	30	2	0.2	5
Ad15	250	400	10	30	2	0	7
Ad16	250	400	10	30	2	0.2	7

A1.5. Degradation of Methanol

A1.18. Operation condition of methanol calibration curve

V (methanol-mother solution) (mL)	Methanol (mol/L)	Methanol (mg/L)	Area (AU)
0.5	0.123439	3955	326
5	1.234395	39550	7715
10	2.468789	79100	14725
25	6.171973	197750	32715
35	8.640762	276850	45843

Table A1.19. Operating conditions of methanol experiments

Exp No	Sample (mL)	Gas Flow rate (mL/min)	Ozone Conc. Inlet (g/m^3)NTP	Metha- Conc. (%)	t-butanol (mol/L)	pH
Me1	200	400	10	10	0	5
Me2	200	400	30	10	0	5
Me3	200	400	60	10	0	5
Me4	200	400	80	10	0	5

Table A1.20. Operating conditions of effect of pH on methanol degradation

Exp No	Sample (mL)	Gas Flow rate (mL/min)	Ozone Conc. Inlet (g/m^3)NTP	metha- Conc. (%)	t-butanol (mol/L)	pH
Me5	200	400	30	5	0	2
Me6	200	400	30	5	0	5
Me7	200	400	30	5	0.2	5
Me8	200	400	30	5	0	9

Table A1.21. Operation condition of methanol calibration curve

V(methanol-mother solution) (mL)	Methanol (mol/L)	Methanol (mg/L)	Area (AU)
1.5	0.004937	158.1684	493.647
1	0.003291	105.4456	300.78
0.5	0.001646	52.72279	180.624
0.2	0.000658	21.08912	59.359
0.1	0.000329	10.54456	37.723
0.05	0.000165	5.272279	23.556

Table A1.22. Operating conditions of Effect of pH on the reaction rate constant, k of methanol

Exp No	V(reactor) (mL)	V(methanol injected) (mL)	Initial Ozone Conc. (mg/L)	Metha- Conc. (mg/L)	t-butanol (mol/L)	pH
Me9	200	2	13.35	23.237	0	2
Me10	200	2	7.9	21.293	0	7
Me11	200	2	1.68	19.935	0	9

Table A1.23. Operating conditions of methanol adsorption

D915 (g)	V(Methanol) (mL)	Area (AU)	Methanol (mol/L)	Methanol (mg/L)	C/C0
0	50	12029	2.248926	72055.58	1
0.5	50	7976	1.491182	47777.48	0.6630643
1	50	5753	1.075573	34461.36	0.4782609
1.5	50	5615	1.049773	33634.72	0.4667886
2	50	5508	1.029768	32993.78	0.4578934

Table A1.24. Operating conditions of effect of flow rate on methanol adsorption

Exp No	Sample (mL)	Gas Flow rate (mL/min)	Water flow (mL/min)	Ozone Conc. Inlet (g/m^3)NTP	D915 (g)	pH
Me12	500	400	5	60	6	7
Me13	500	400	10	60	6	7
Me14	500	400	15	60	6	7

Table A1.25. Operating conditions of effect of ozone gas concentration on methanol adsorption

Exp No	Sample (mL)	Gas Flow rate (mL/min)	Water flow (mL/min)	Ozone Conc. Inlet (g/m^3)NTP	D915 (g)	pH
Me15	500	400	10	30	6	7
Me16	500	400	10	60	6	7
Me17	500	400	10	80	6	7

Appendix A2: Results

A2.1. Mass transfer

A2.1.1. Oxygen absorption

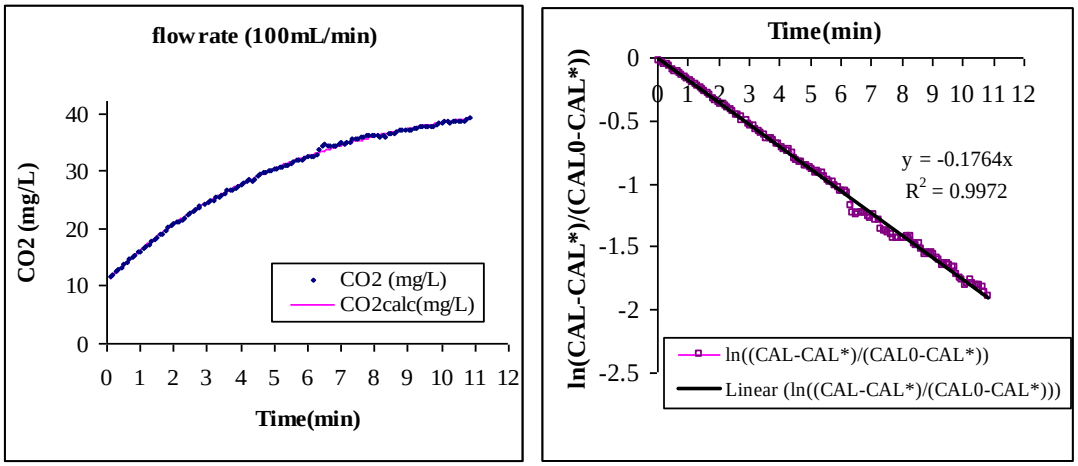

Figure A2.1. Oxygen absorption at 100mL/min

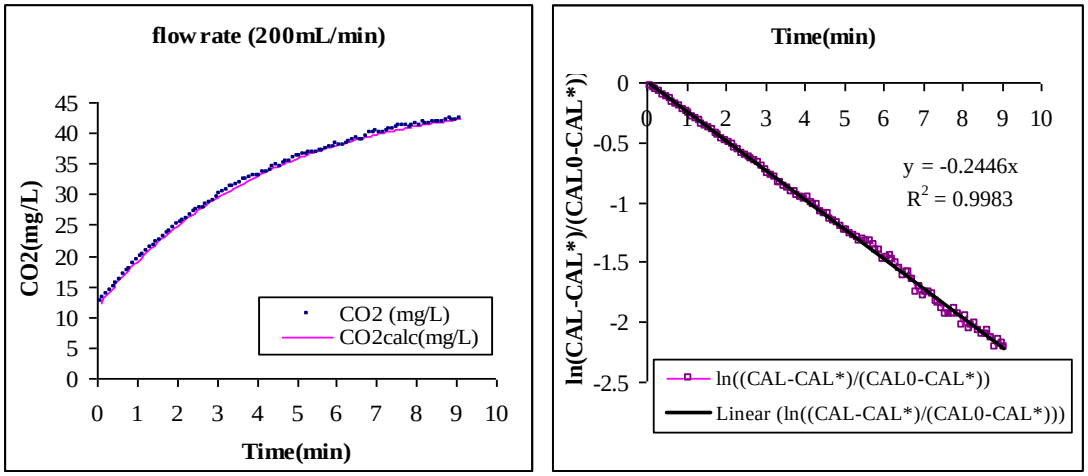

Figure A2.2. Oxygen absorption at 200mL/min

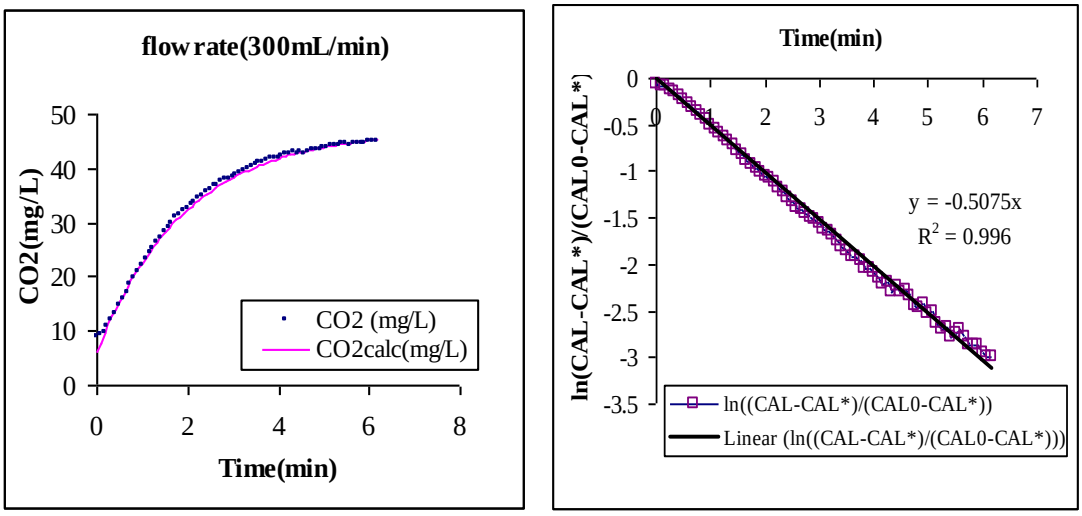

Figure A2.3. Oxygen absorption at 300mL/min

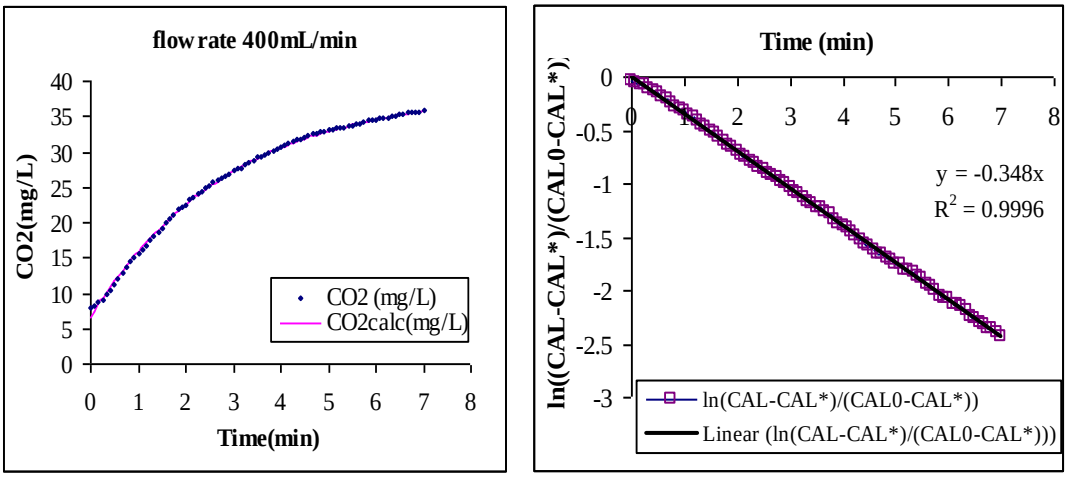

Figure A2.4. Oxygen absorption at 400mL/min

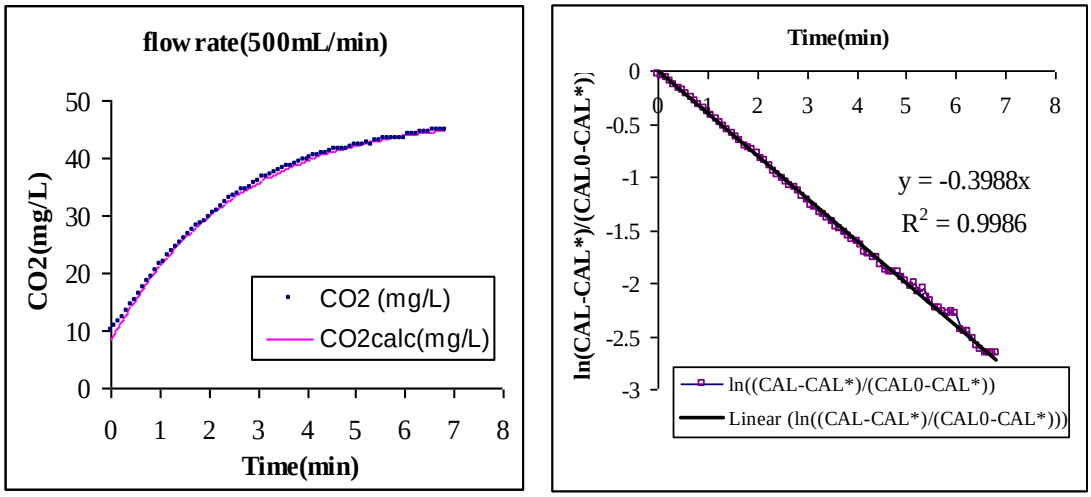

Figure A2.5. Oxygen absorption at 500mL/min

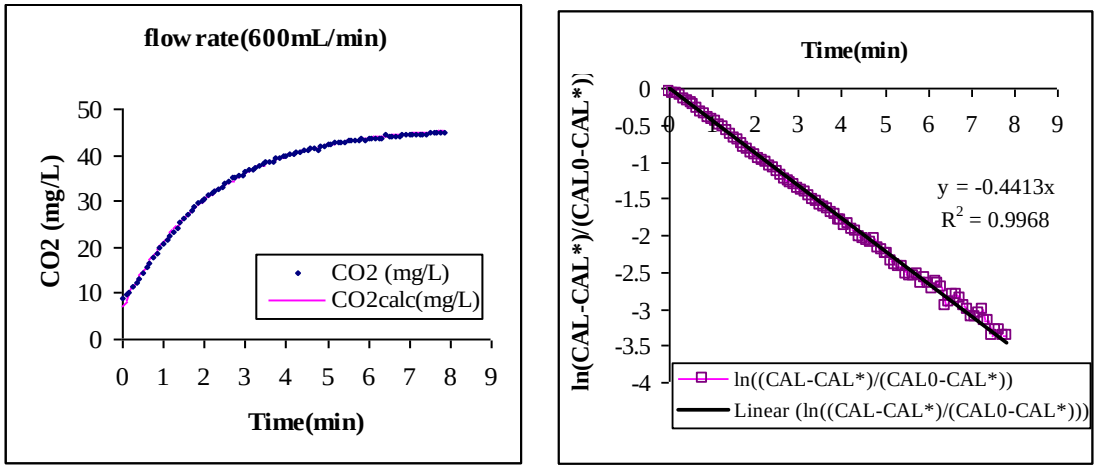

Figure A2.6. Oxygen absorption at 600mL/min

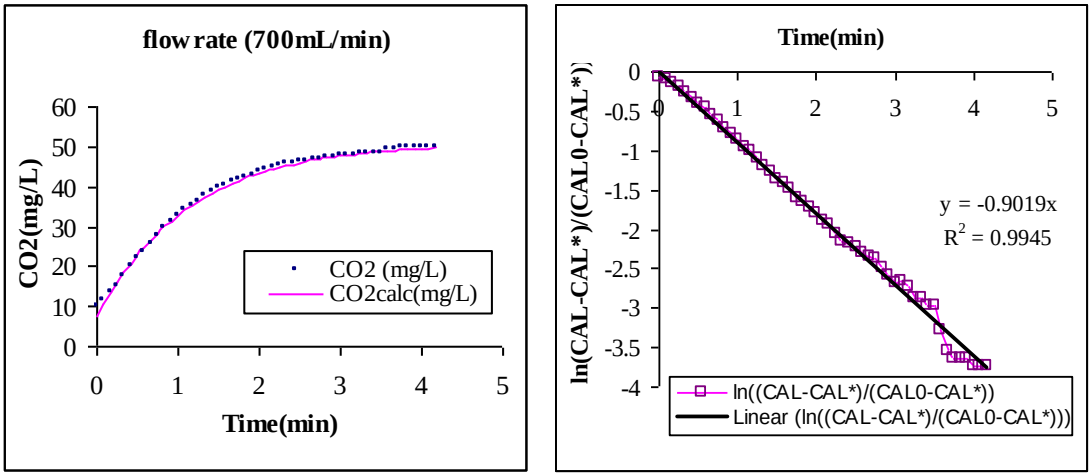

Figure A2.7. Oxygen absorption at 700mL/min

A2.1.2. Ozone absorption

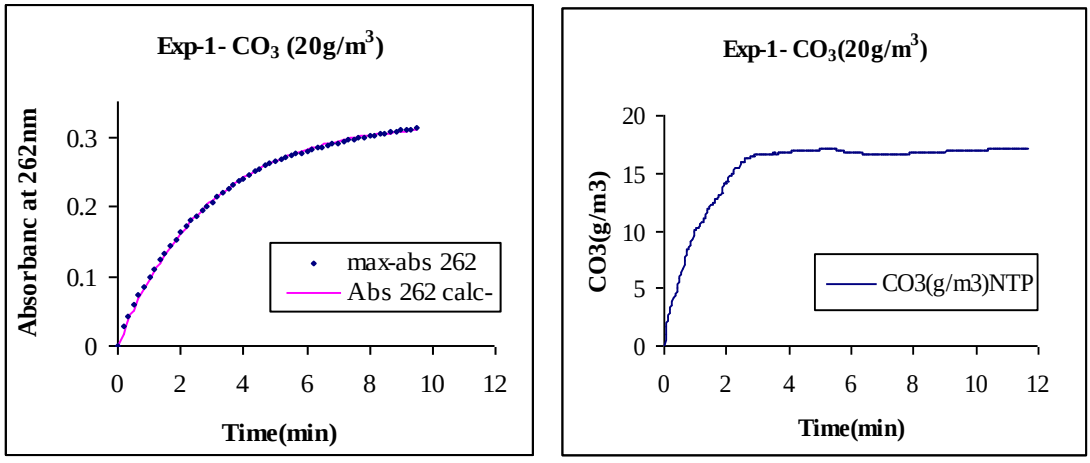

Figure A2.8. Ozone absorption at 20g/m^3

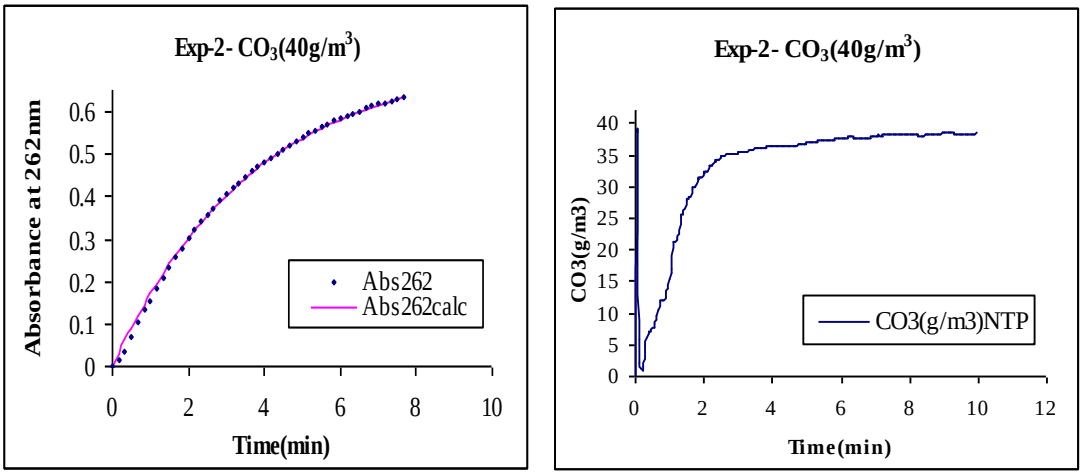

Figure A2.9. Ozone absorption at 40g/m^3

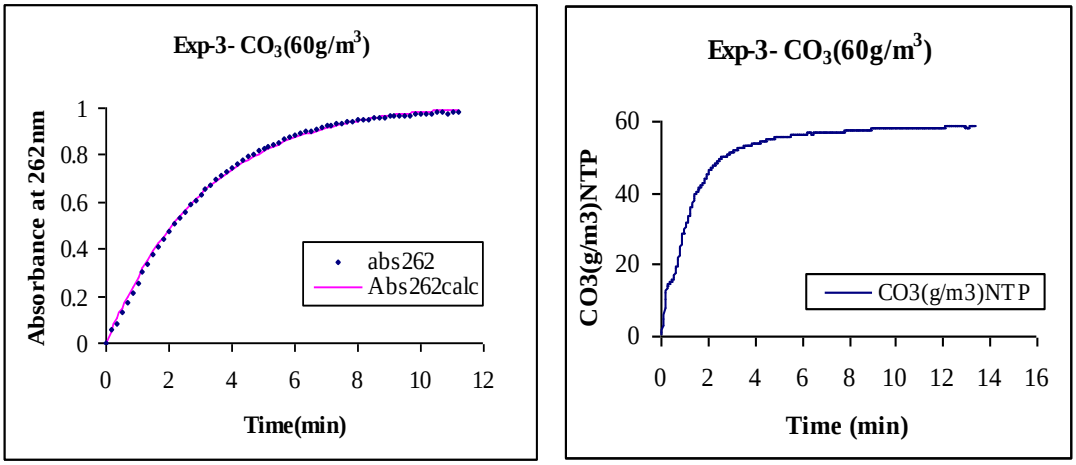

Figure A2.10. Ozone absorption at 60g/m^3

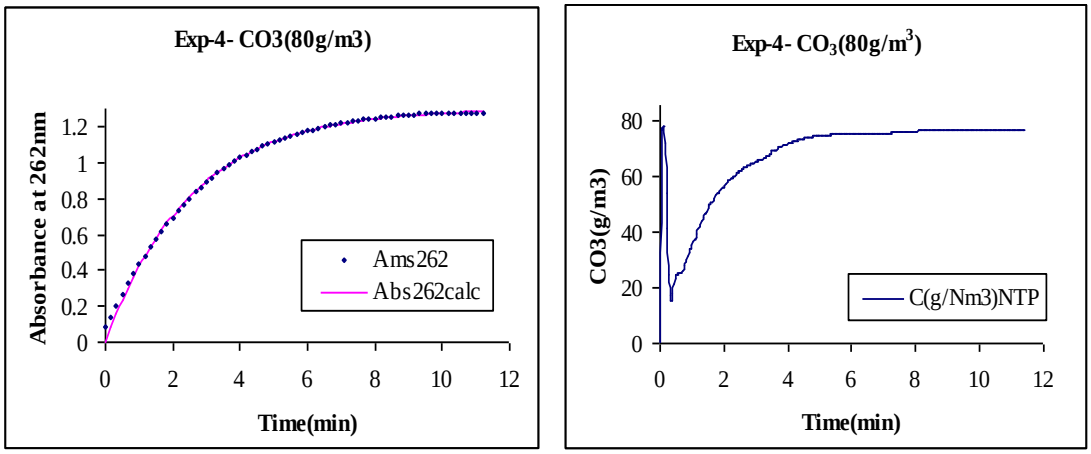

Figure A2.11. Ozone absorption at 80g/m^3

A2.2. Degradation of Dye RO16

A2.2.1. Ozone bubbling in RO16

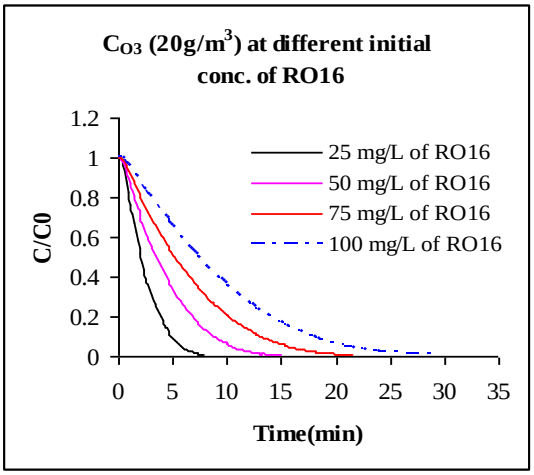

Figure A2.12. Dye decolourisation with 20g/m^3 of ozone at different initial dye concentrations

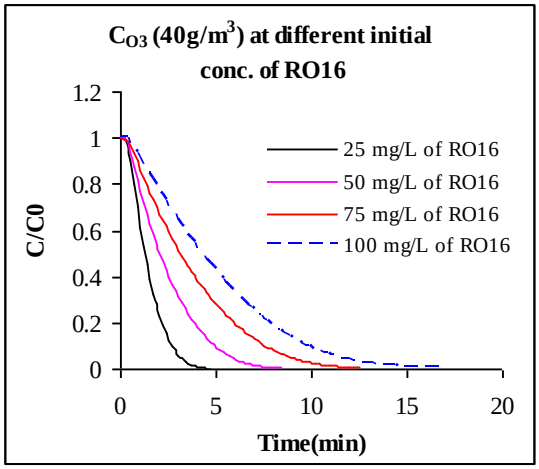

Figure A2.13. Dye decolourisation with 40g/m^3 of ozone at different initial dye concentrations

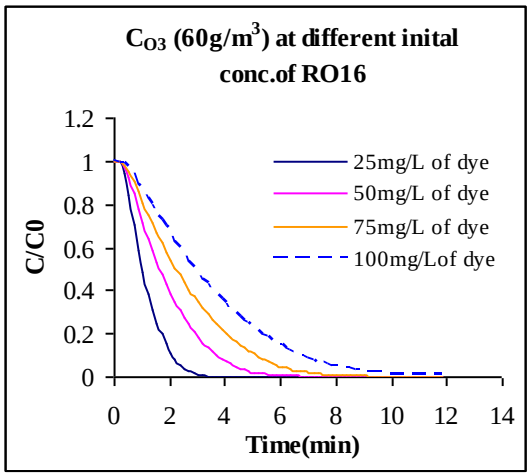

Figure A2.14. Dye decolourisation with 60g/m^3 of ozone at different initial dye concentrations

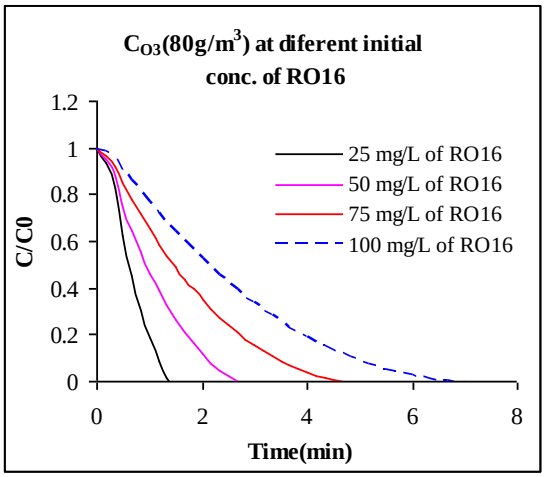

Figure A2.15. Dye decolourisation with 80g/m^3 of ozone at different initial dye concentrations

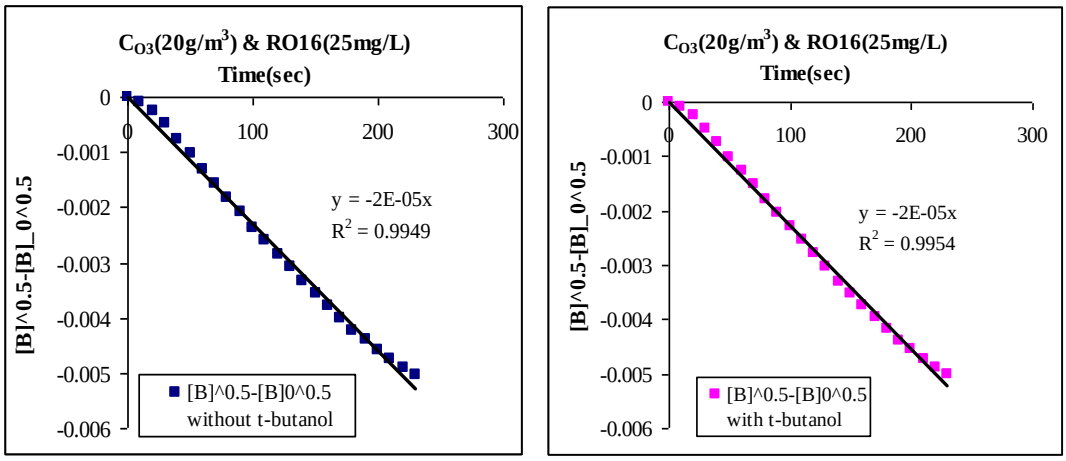

Figure A2.16. [B]^0.5-[B]_0^0.5 versus time (without and with t-butanol) at pH 2

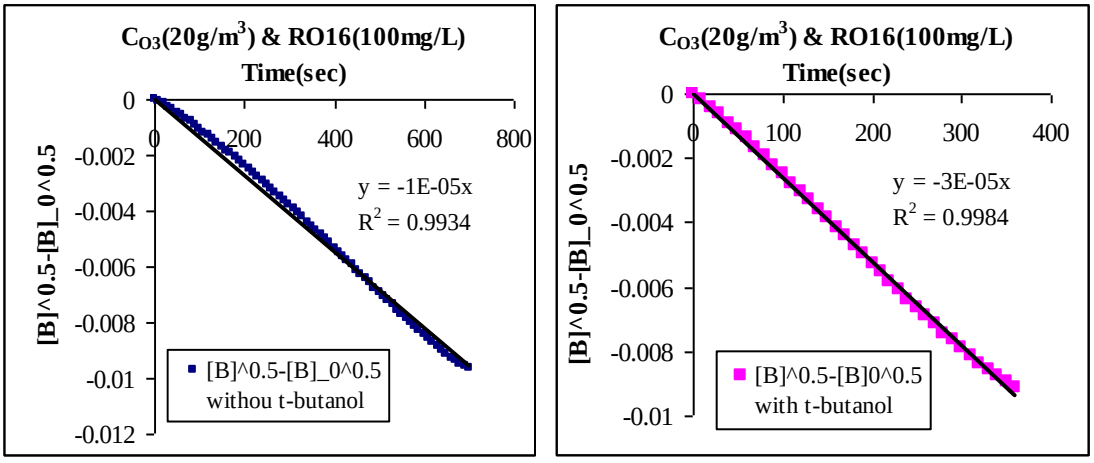

Figure A2.17. [B]^0.5-[B]_0^0.5 versus time (without and with t-butanol) at pH 2

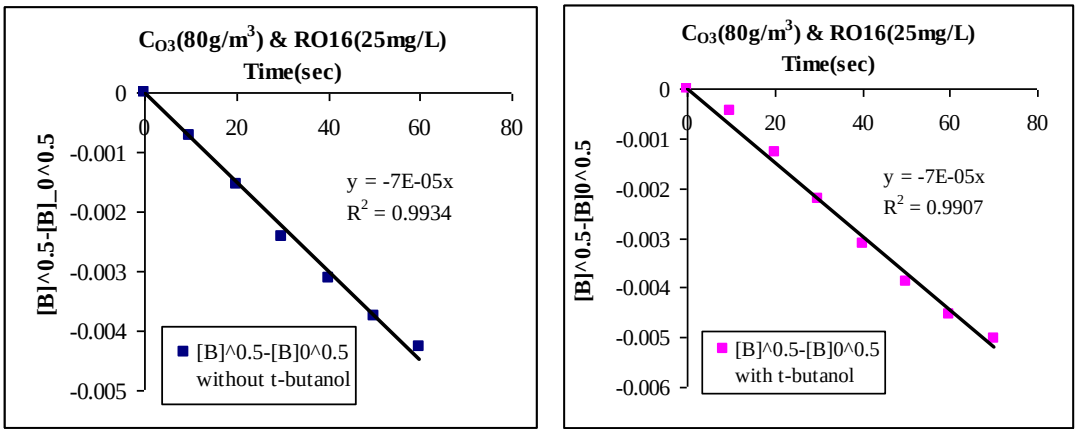

Figure A2.18. [B]^0.5-[B]_0^0.5 versus time (without and with t-butanol) at pH 2

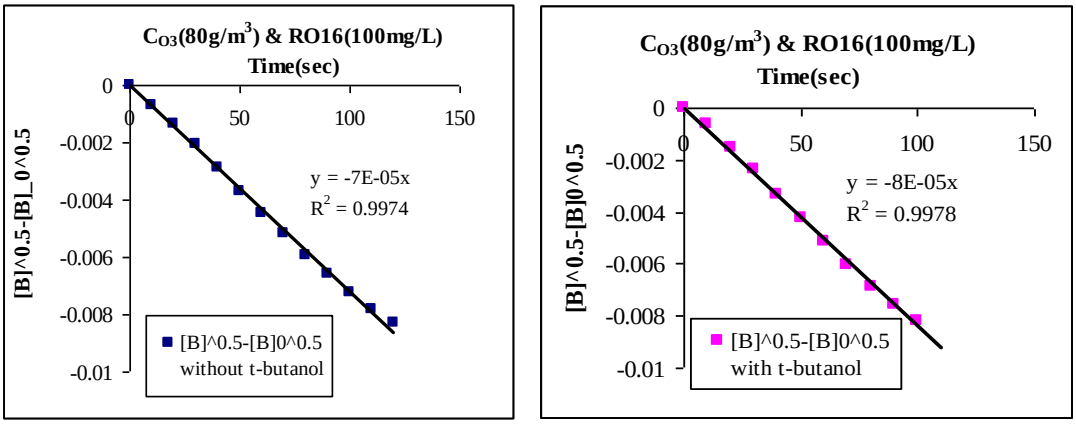

Figure A2.19. [B]^0.5-[B]_0^0.5 versus time (without and with t-butanol) at pH 2

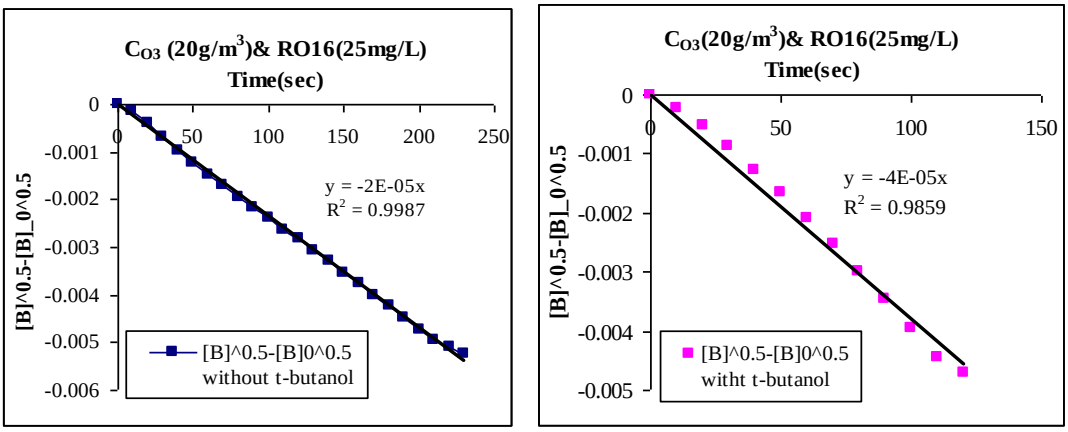

Figure A2.20. [B]^0.5-[B]_0^0.5 versus time (without and with t-butanol) at pH 7

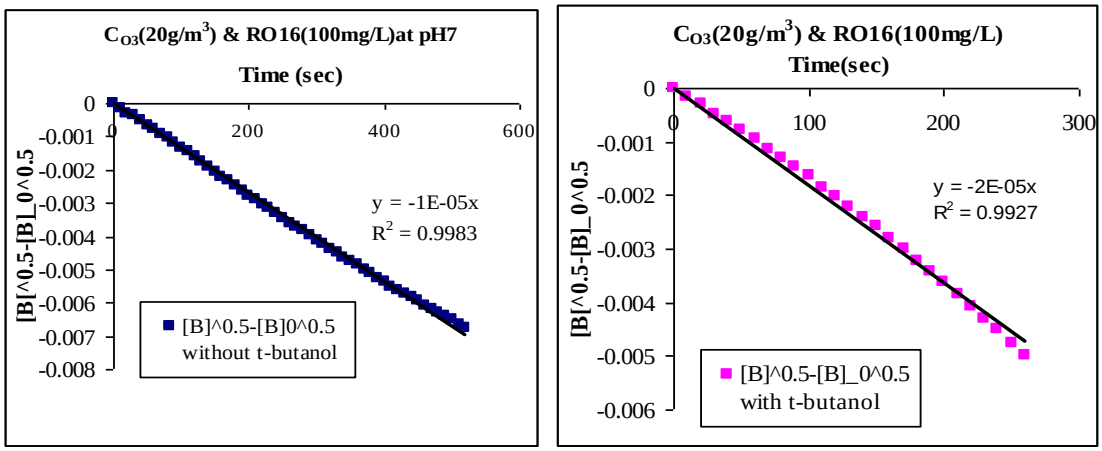

Figure A2.21. [B]^0.5-[B]_0^0.5 versus time (without and with t-butanol) at pH 7

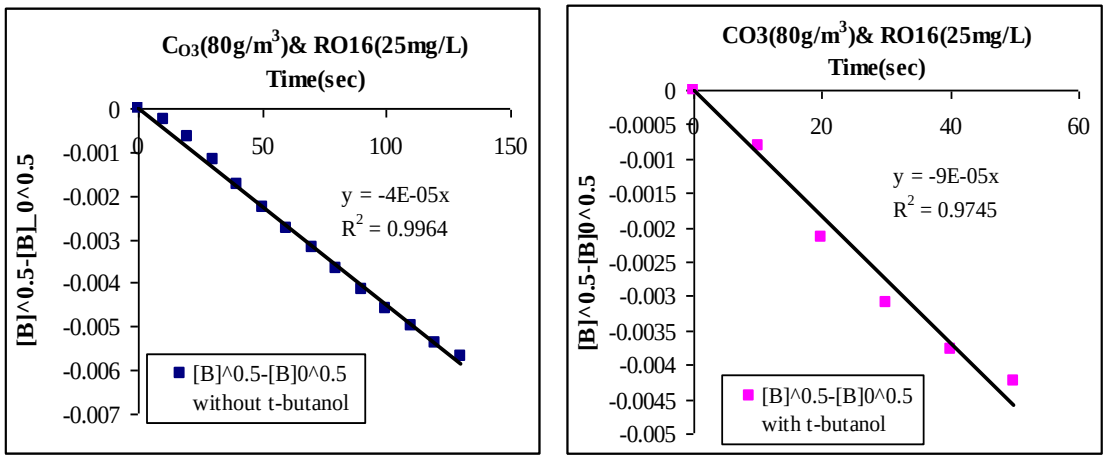

Figure A2.22. [B]^0.5-[B]_0^0.5 versus time (without and with t-butanol) at pH 7

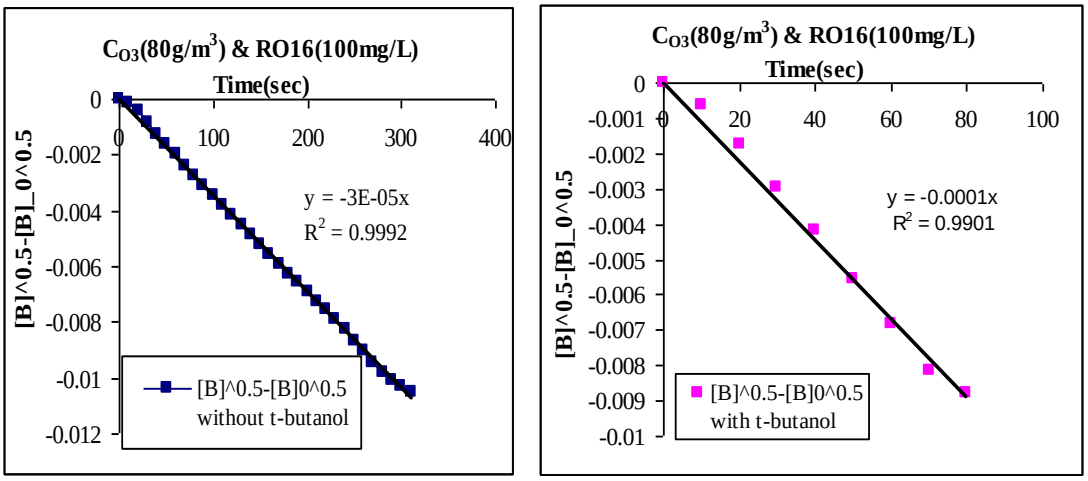

Figure A2.23. [B]^0.5-[B]_0^0.5 versus time (without and with t-butanol) at pH 7

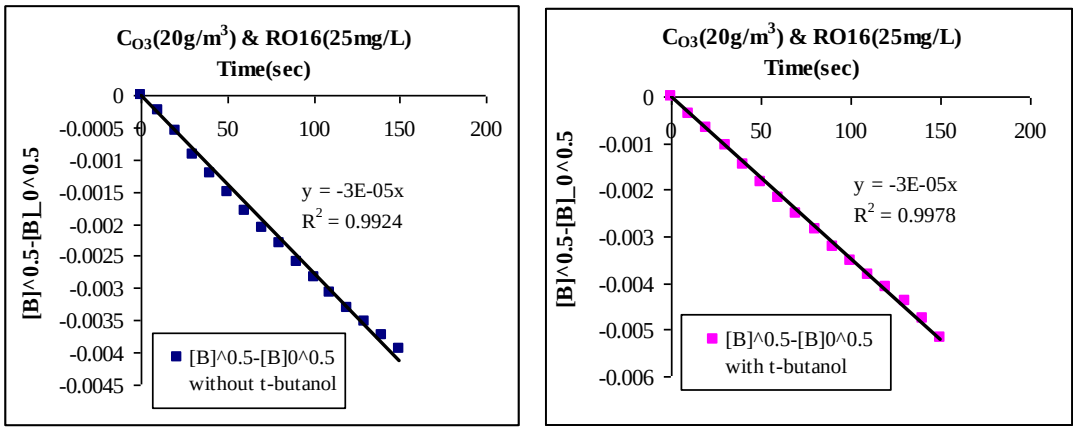

Figure A2.24. [B]^0.5-[B]_0^0.5 versus time (without and with t-butanol) at pH 11

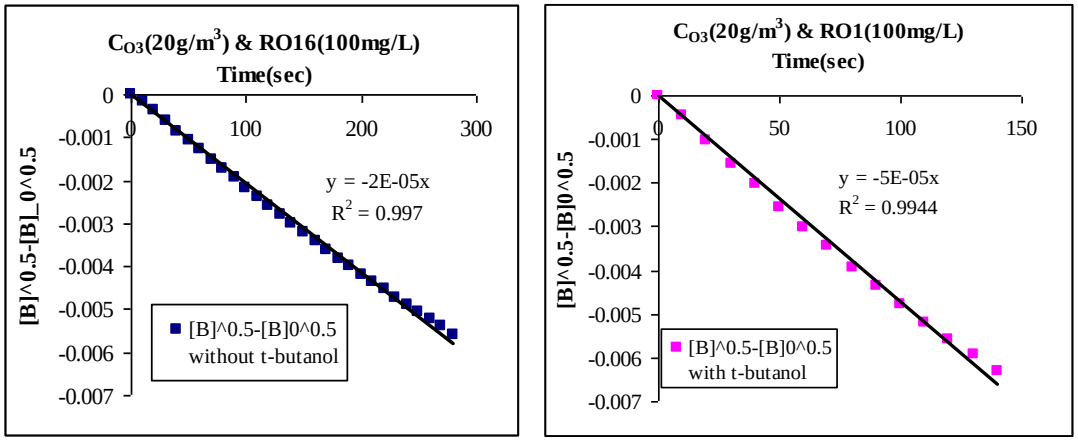

Figure A2.25. [B]^0.5-[B]_0^0.5 versus time (without and with t-butanol) at pH 11

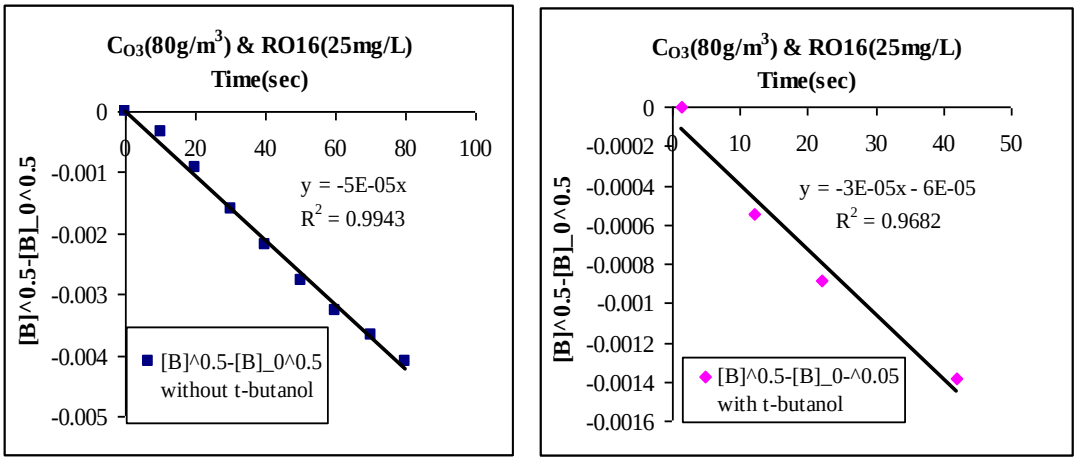

Figure A2.26. [B]^0.5-[B]_0^0.5 versus time (without and with t-butanol) at pH 11

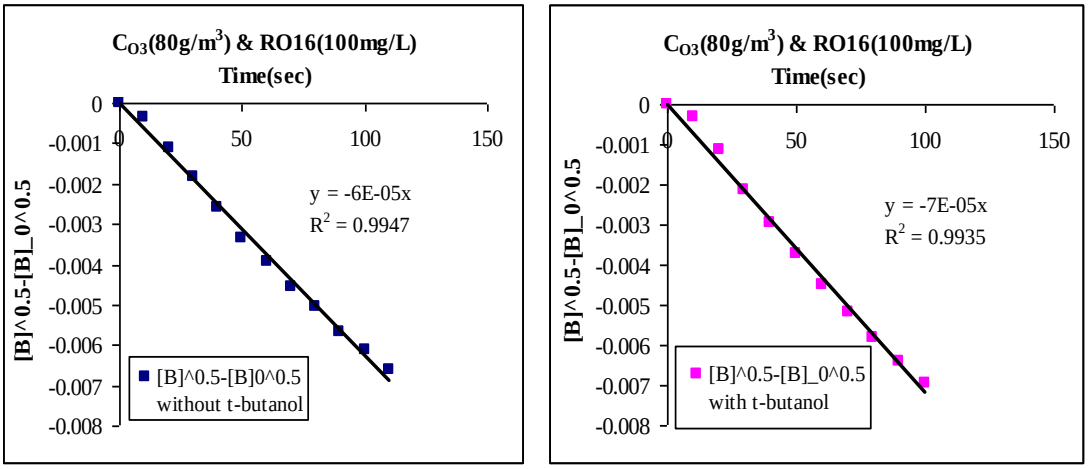

Figure A2.27. [B]^0.5-[B]_0^0.5 versus time (without and with t-butanol) at pH 11

A2.2.2. Heterogeneous competitive kinetics

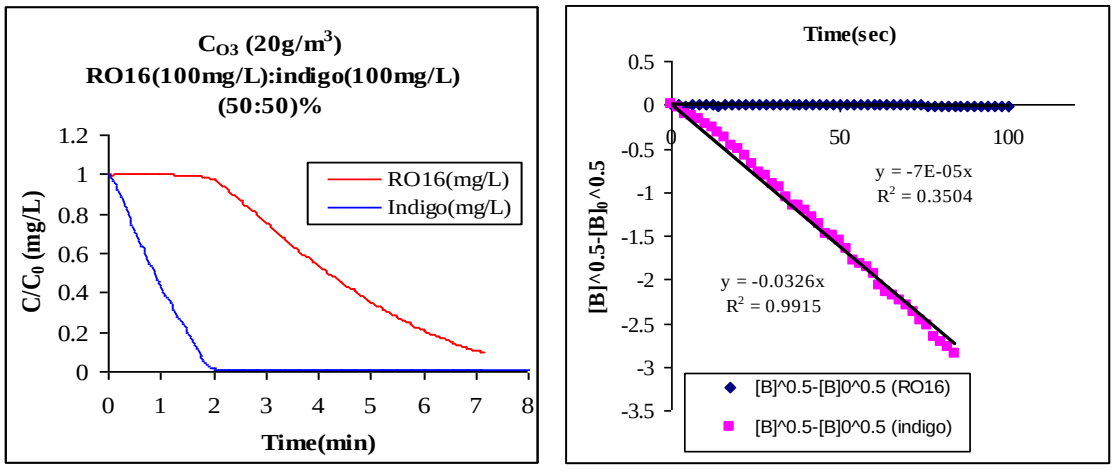

Figure A2.28. Dye decolourization at ozone conc. 20g/m^3 using competitive method

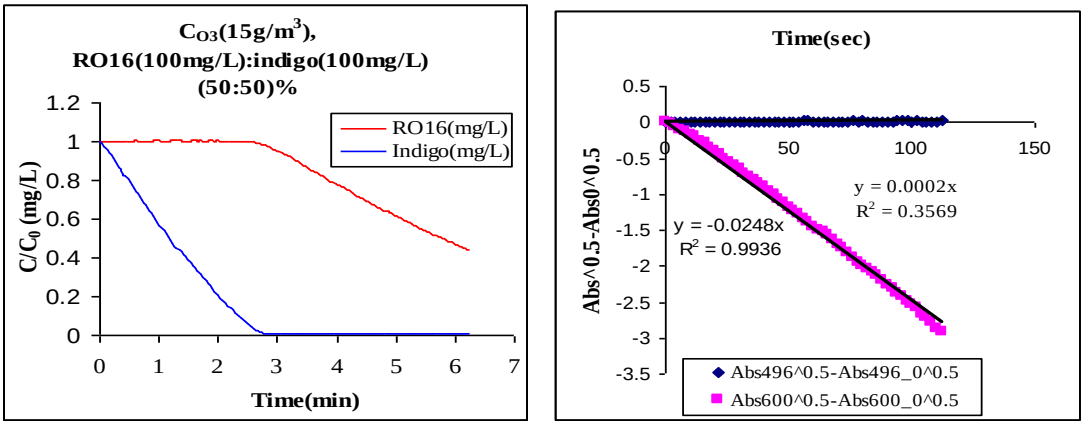

Figure A2.29. Dye decolourization at ozone conc. 15g/m^3 using competitive method

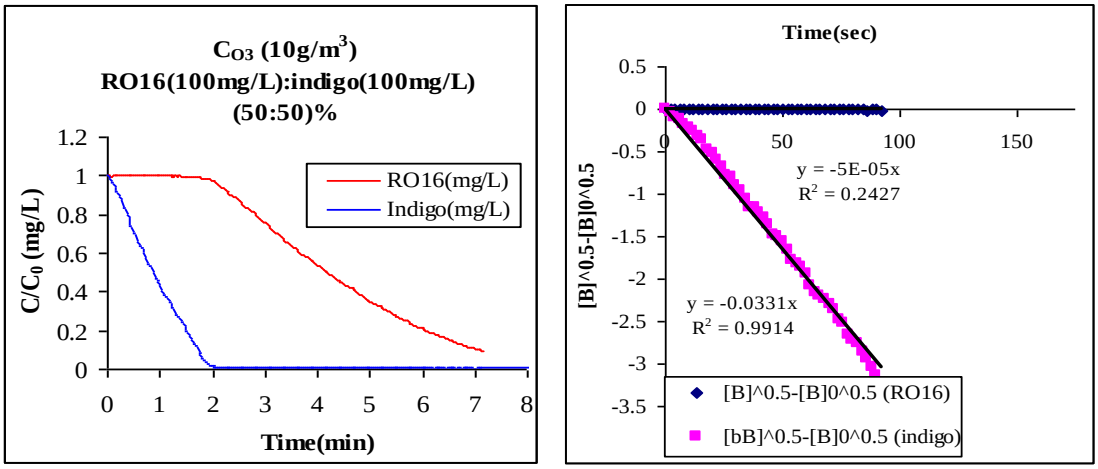

Figure A2.30. Dye decolourization at ozone conc. 10g/m^3 using competitive method

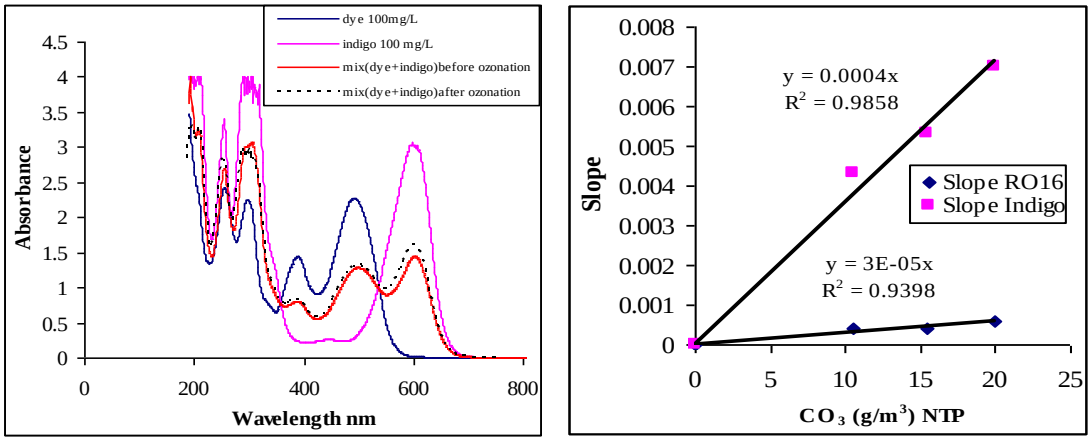

Figure A2.31. Full spectrum of (RO16 + indigo) after ozonation by using competitive method

A2.3. Degradation of Triclocarban (TCC)

A2.3.1. Spectrum of (70%acetonitrile: 30% water) and spectrum of TCC

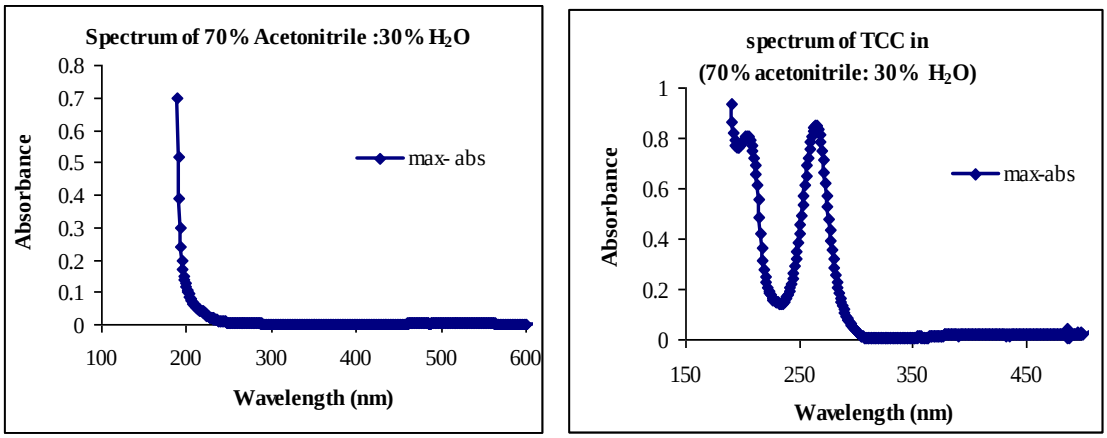

Figure A2.32. Full spectrum of TCC

A2.3.2. Oxygen bubbling in solution (70%ACN: 30%H_2O)

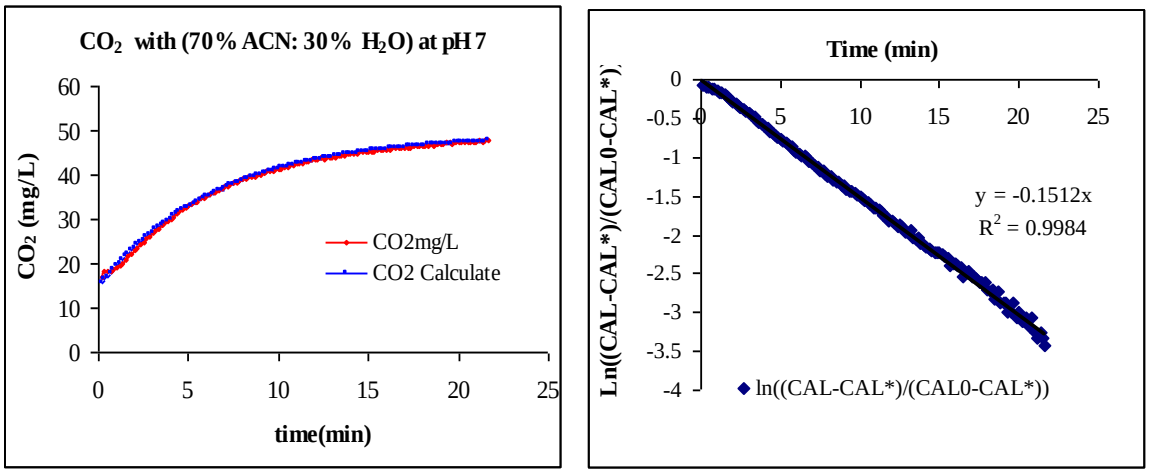

Figure A2.33. Oxygen bubbling in solution of (70%acetonitrile: 30% water)

A2.3.3. Ozone bubbling in solution (70%ACN: 30%H_2O)

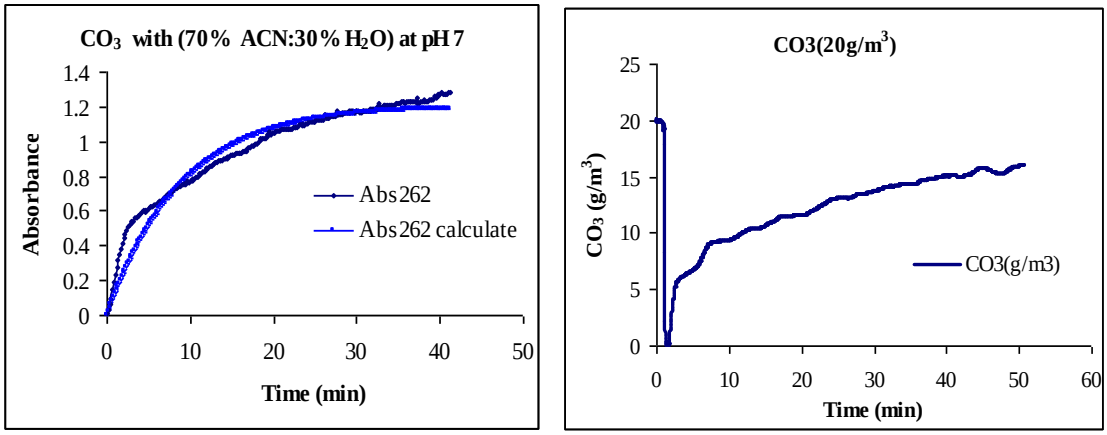

Figure A2.34. Ozone bubbling in solution of (70%acetonitrile: 30% water)

A2.3.4.Ozone bubbling in TCC solution (liquid phase)

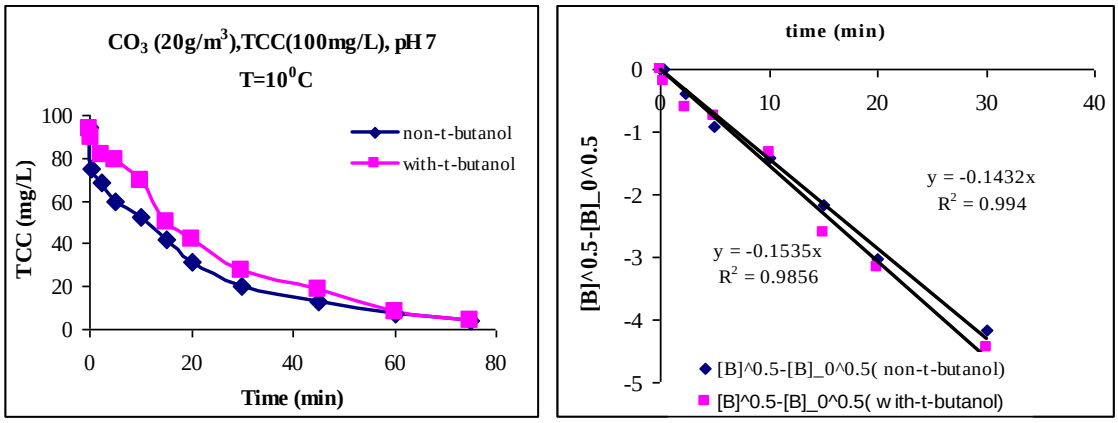

Figure A2.35. Effect of temperature on TCC degradation (liquid phase)

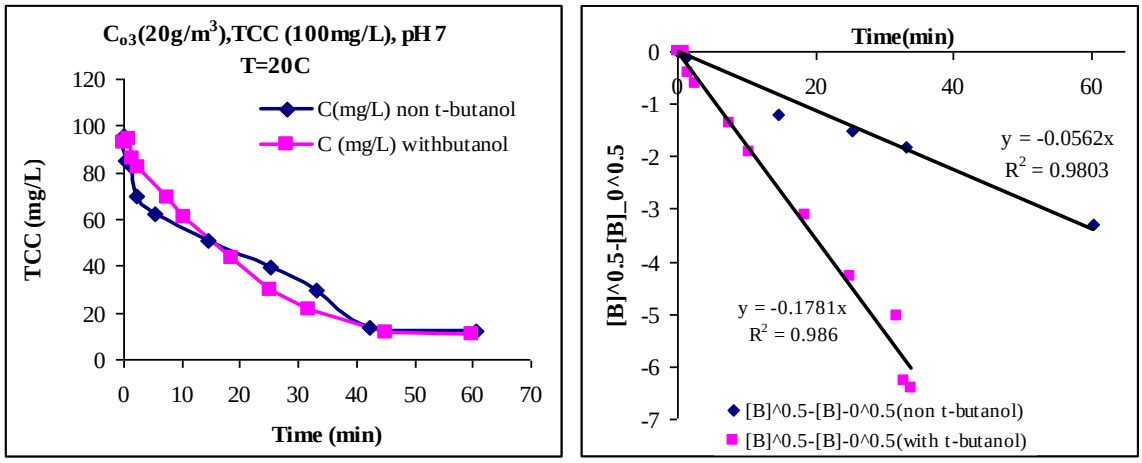

Figure A2.36. Effect of temperature on TCC degradation (liquid phase)

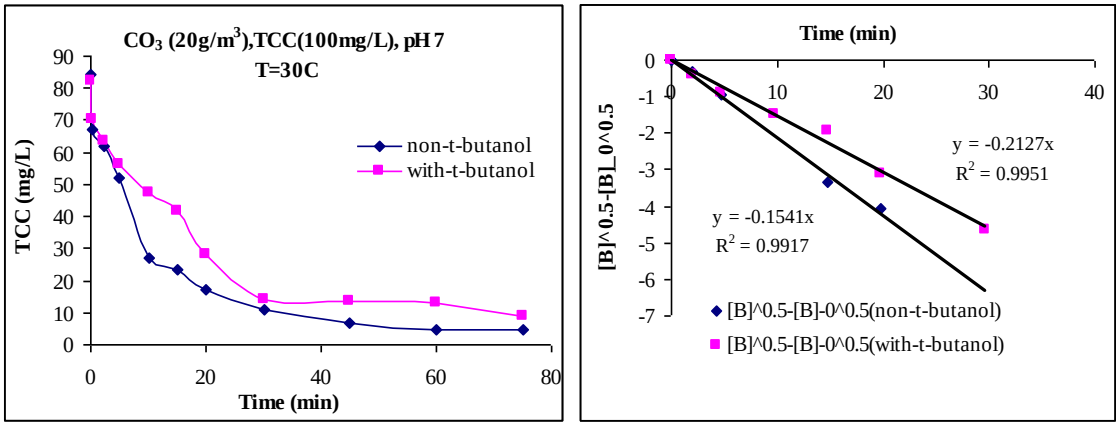

Figure A2.37. Effect of temperature on TCC degradation (liquid phase)

A2.3.5.Ozone bubbling in TCC solution (gas phase)

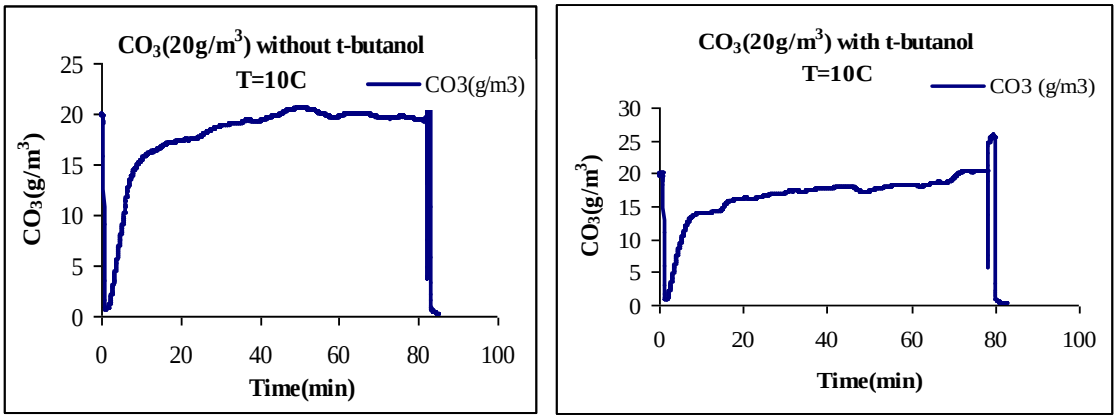

Figure A2.38. Effect of temperature on TCC degradation (gas phase)

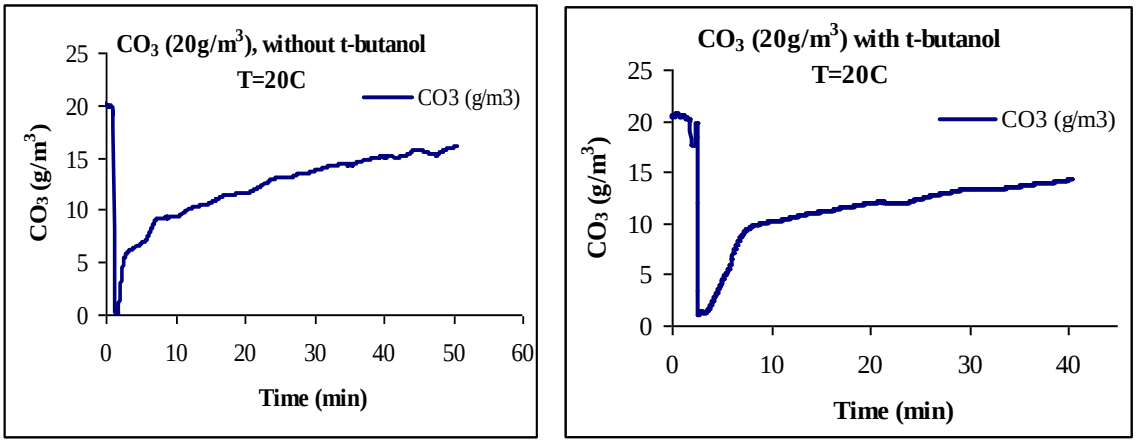

Figure A2.39. Effect of temperature on TCC degradation (gas phase)

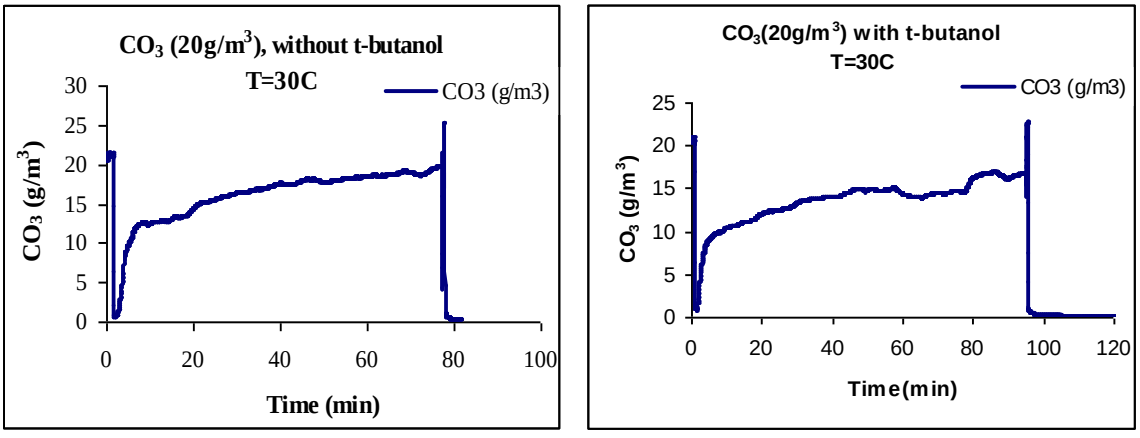

Figure A2.40. Effect of temperature on TCC degradation (gas phase)

Peak areas of Calibration curve of Triclocarban (TCC)

100mg/L

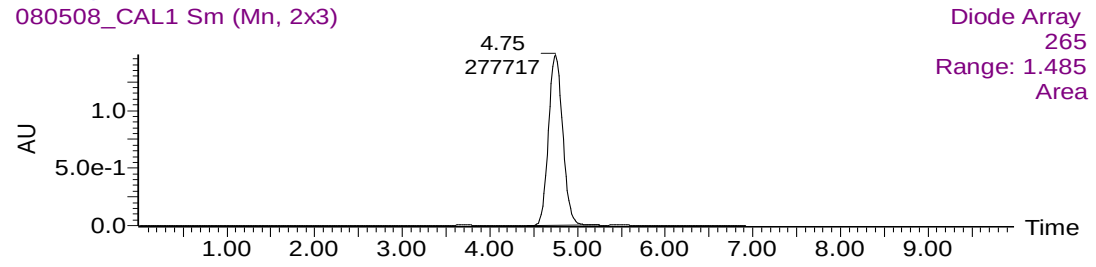

75mg/L

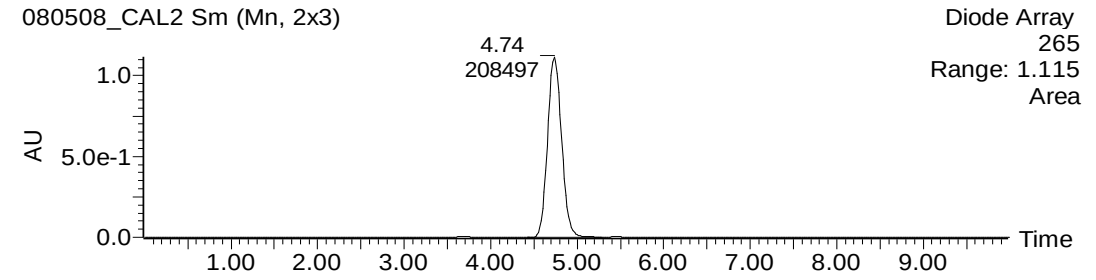

50mg/L

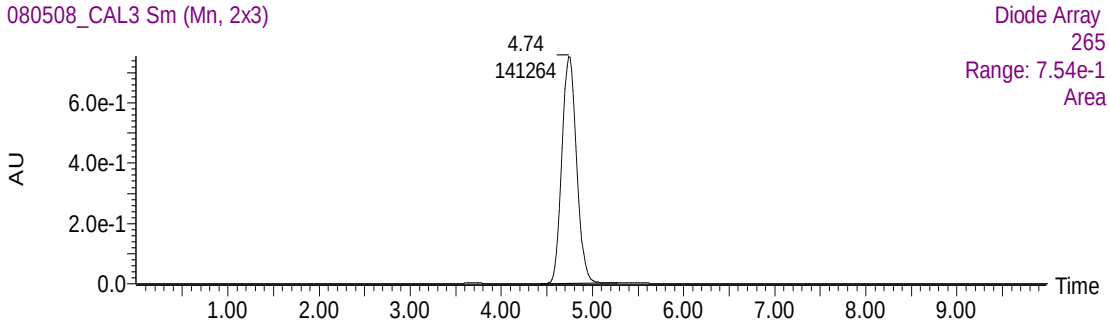

25mg/L

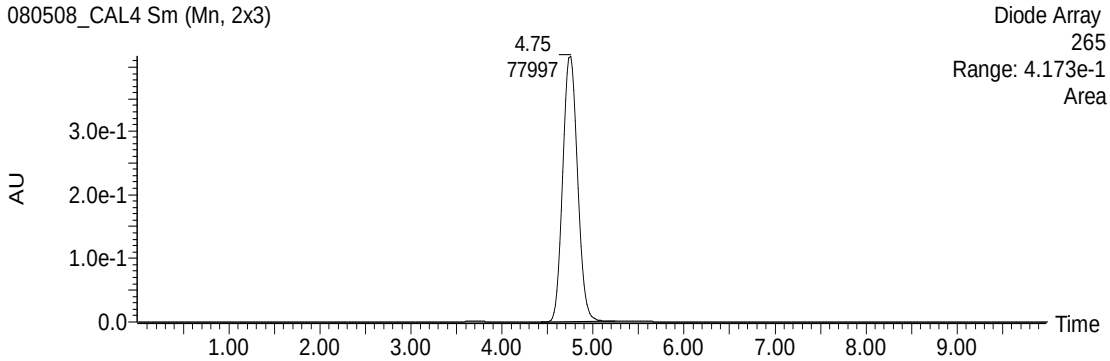

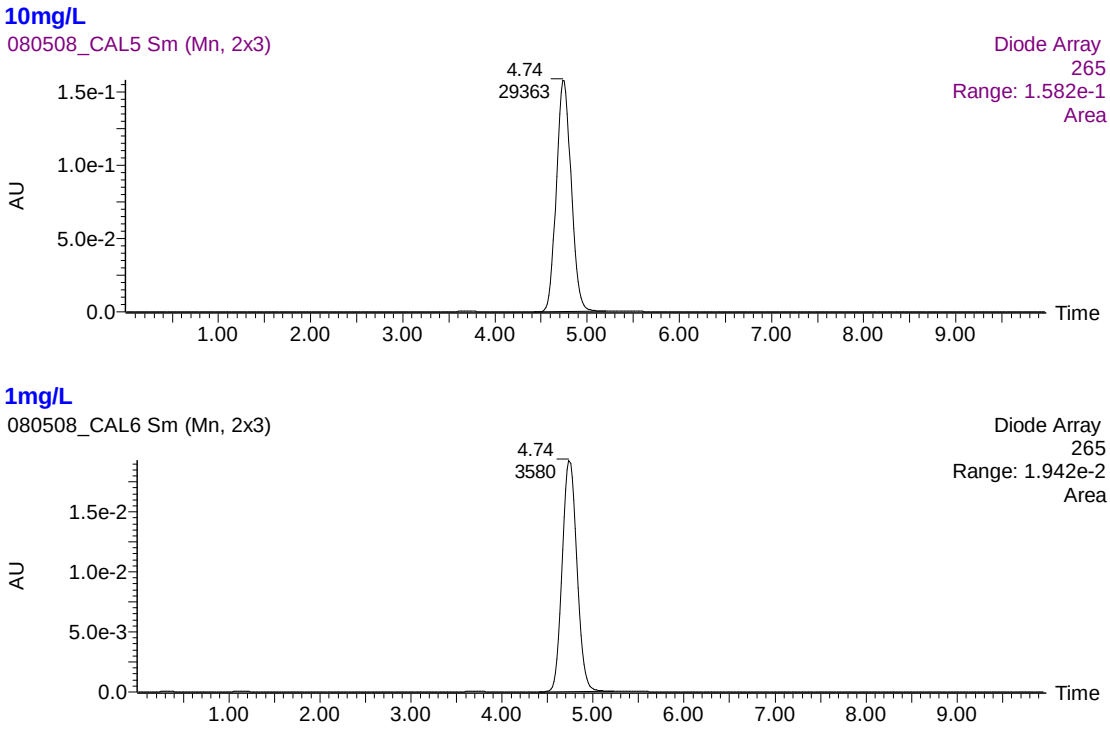

Peak Areas of TCC Degradation by (20g/m^3 of ozone) without t-butanol at pH 2

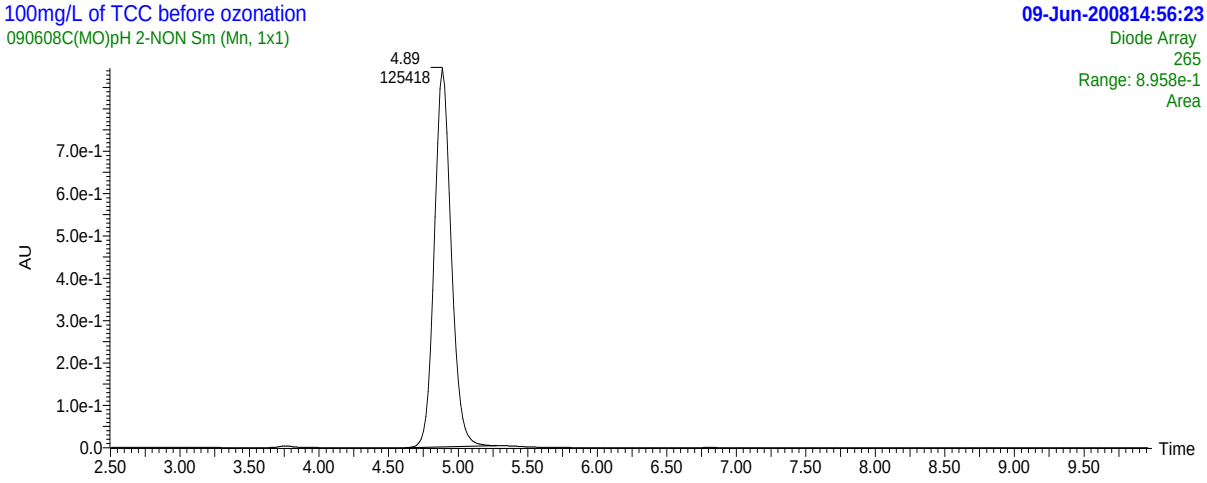

100mg/L of TCC after ozonation
090608C2 Sm (Mn, 1x1)
09-Jun-200815:18:55
Diode Array
265
Range: 2.941e-1
Area

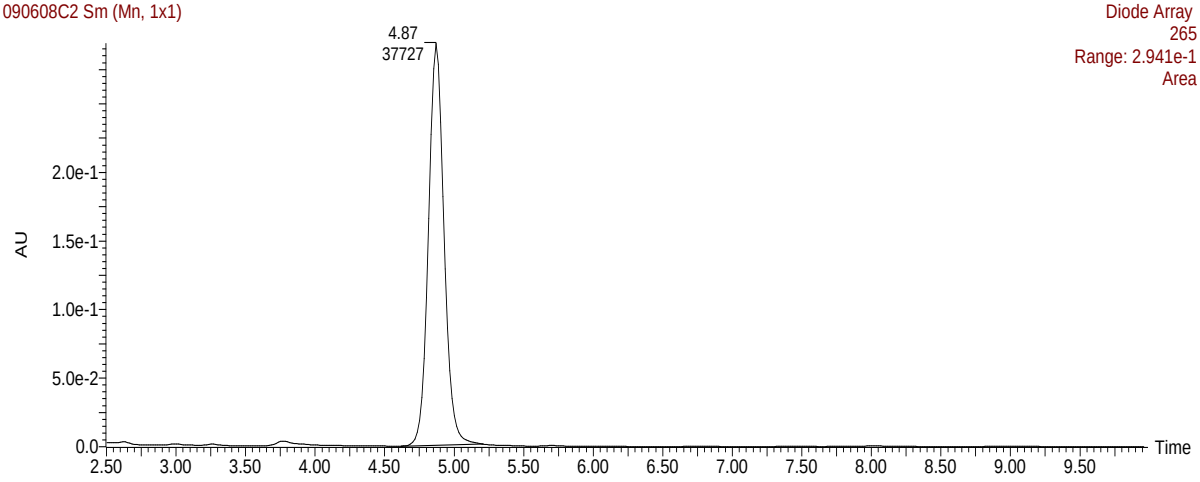

100mg/L of TCC after ozonation
090608C3 Sm (Mn, 1x1)
09-Jun-200815:30:11
Diode Array
265
Range: 2.397e-1
Area

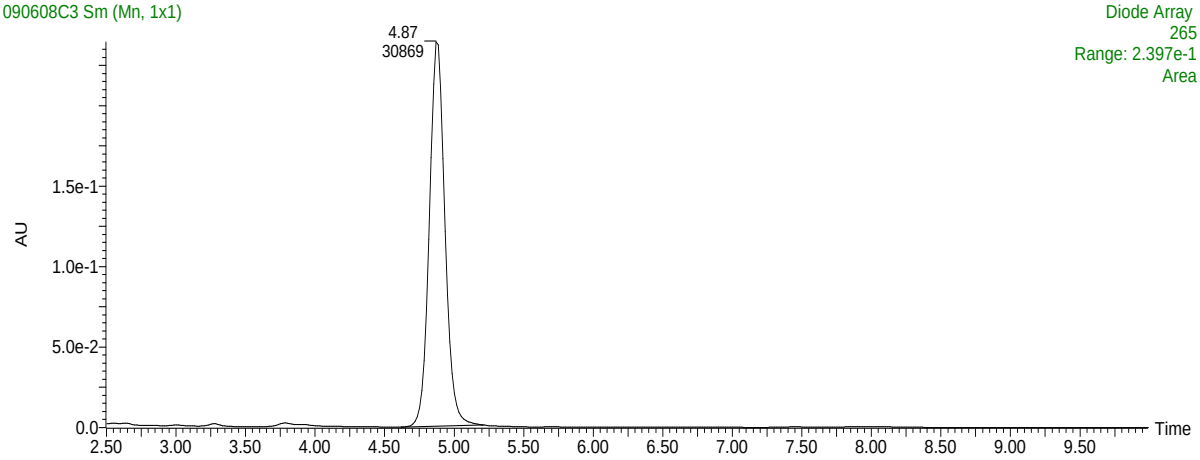

100mg/L of TCC after ozonation
090608C5 Sm (Mn, 1x1)
09-Jun-200815:52:43
Diode Array
265
Range: 1.224e-1
Area

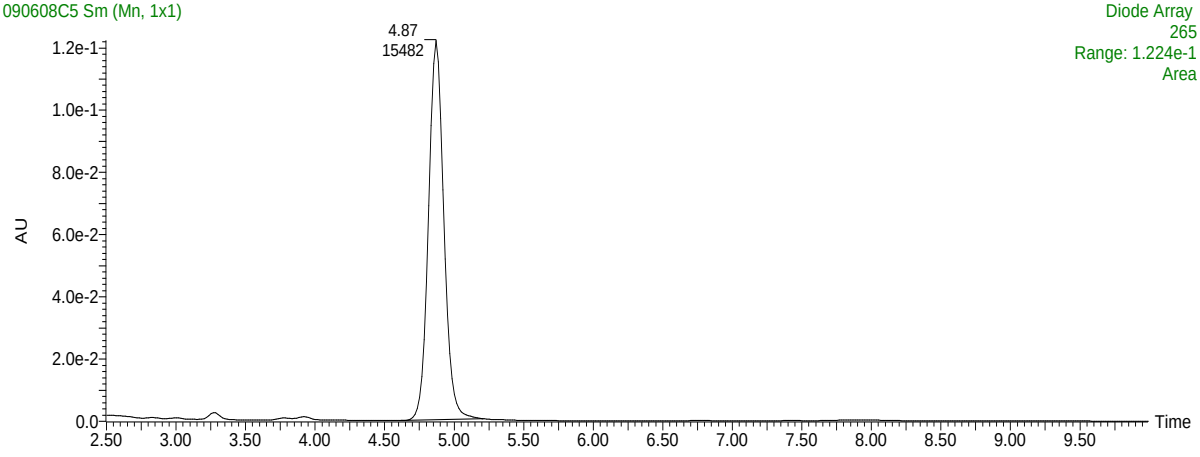

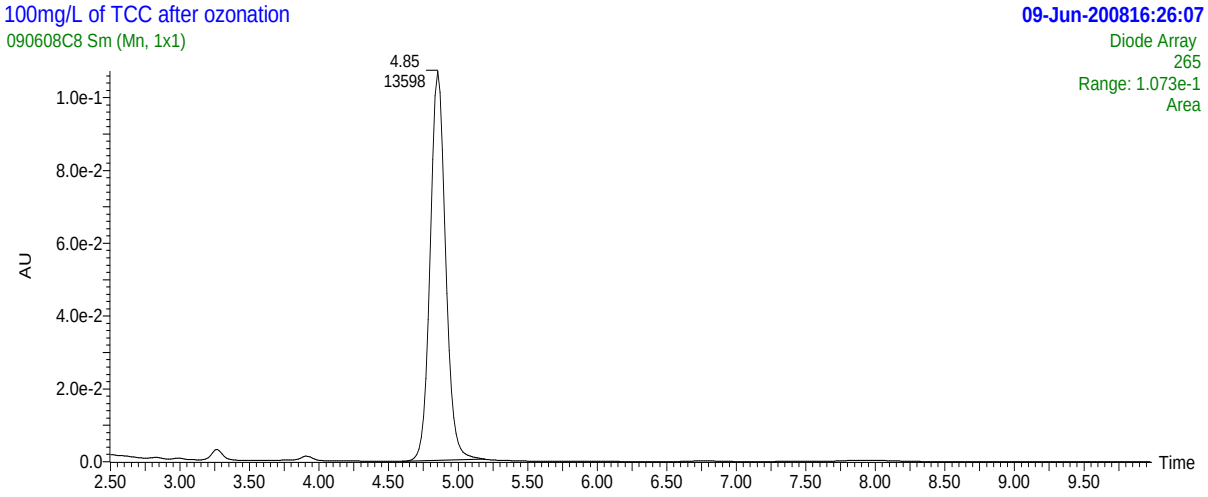

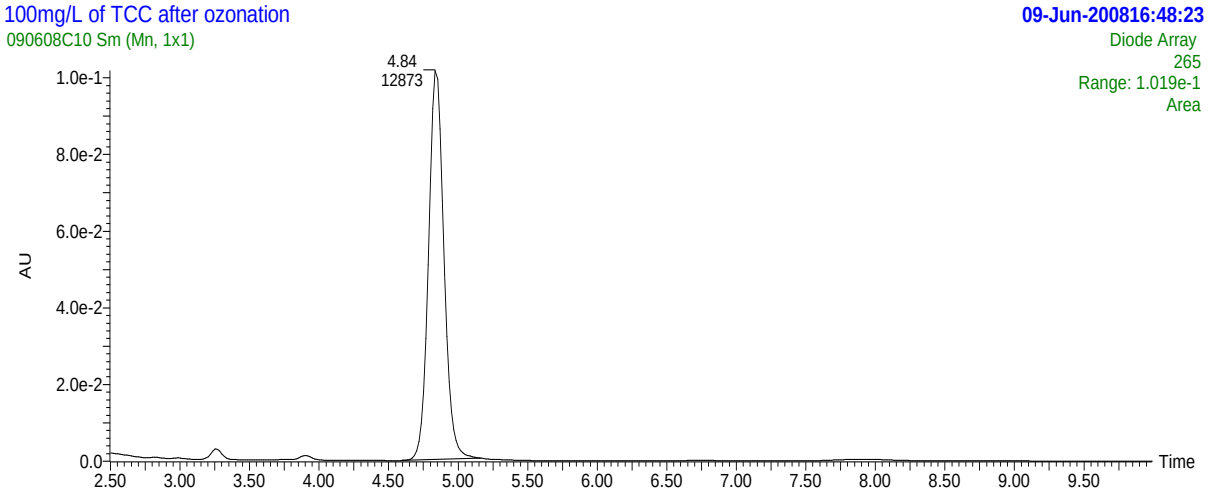

Peak Areas of TCC Degradation by (20g/m^3 of ozone) with t-butanol at pH 2

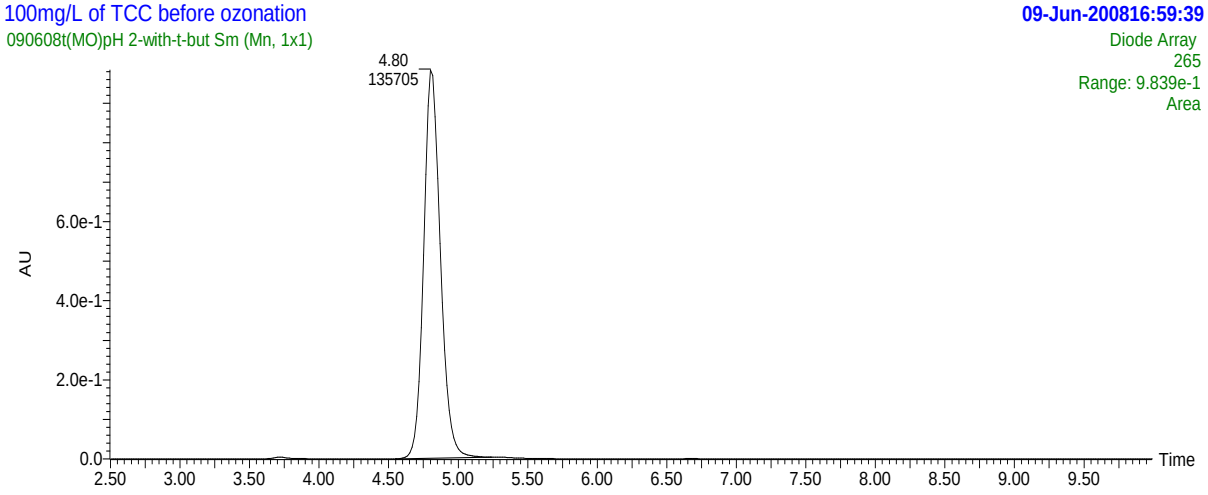

100mg/L of TCC after ozonation
090608t1 Sm (Mn, 1x1)
09-Jun-200817:10:55
Diode Array
265
Range: 2.884e-1
Area

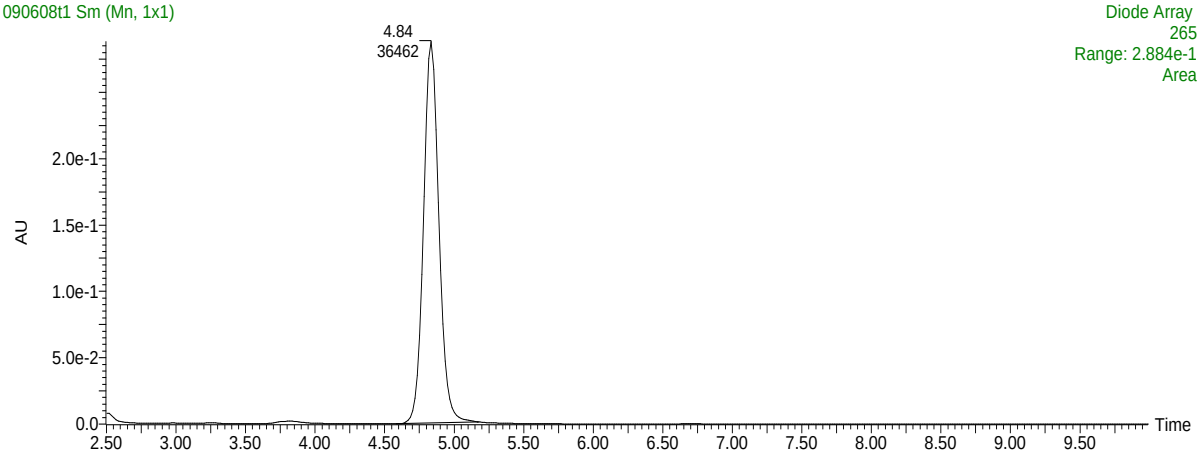

100mg/L of TCC after ozonation
090608t4 Sm (Mn, 1x1)
09-Jun-200817:44:43
Diode Array
265
Range: 2.388e-1
Area

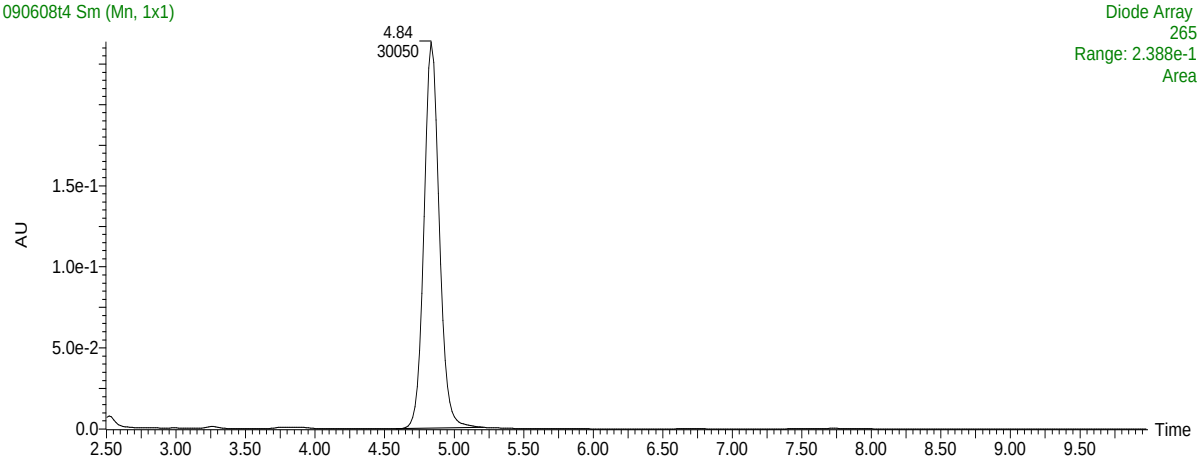

100mg/L of TCC after ozonation
090608t6 Sm (Mn, 1x1)
09-Jun-200818:07:23
Diode Array
265
Range: 1.604e-1
Area

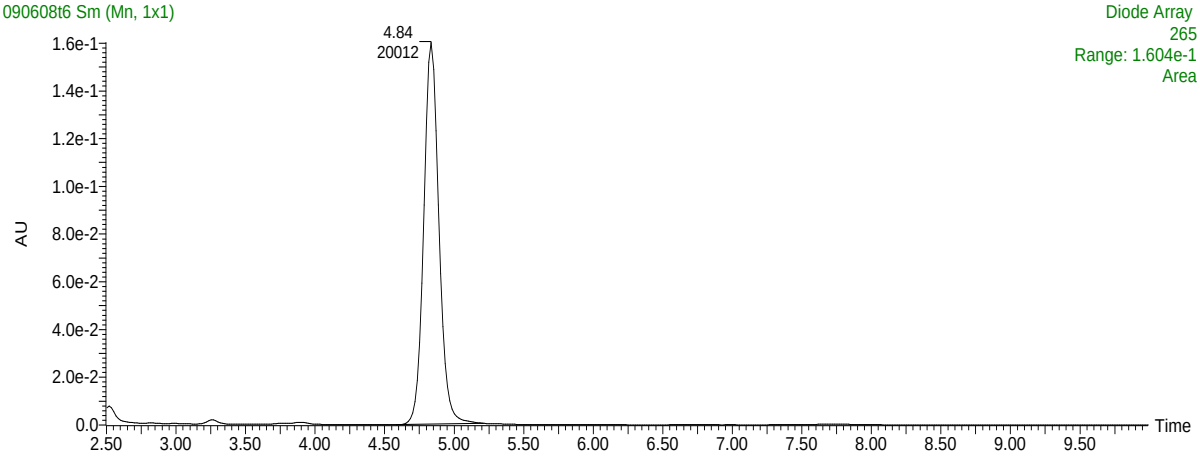

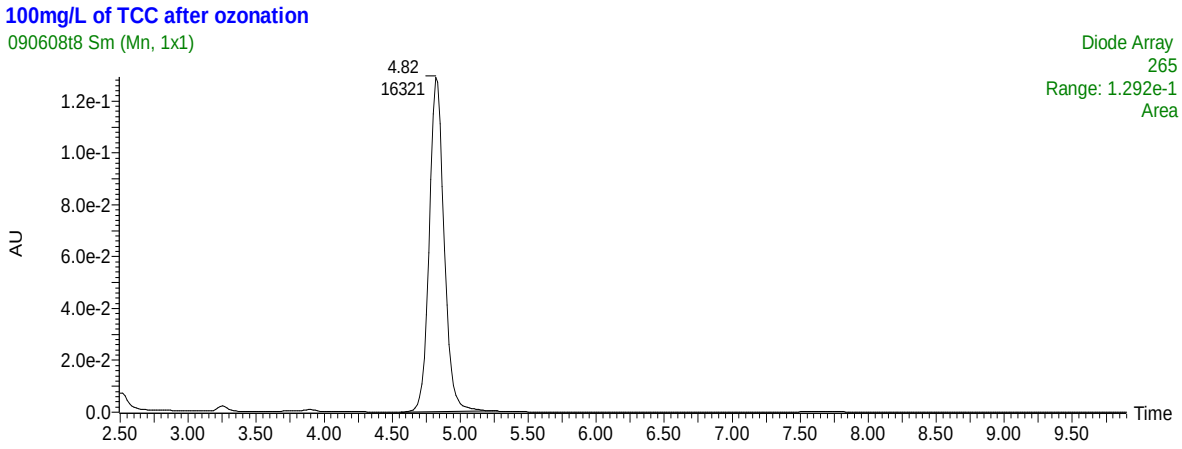

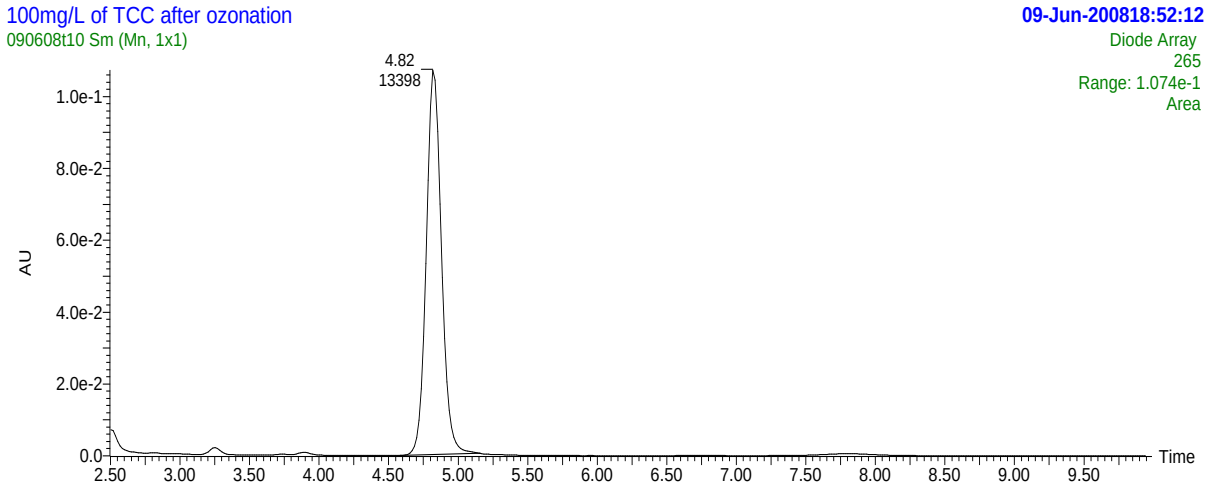

Peak Areas of TCC Degradation by (20g/m^3 of ozone) without t-butanol at pH 5

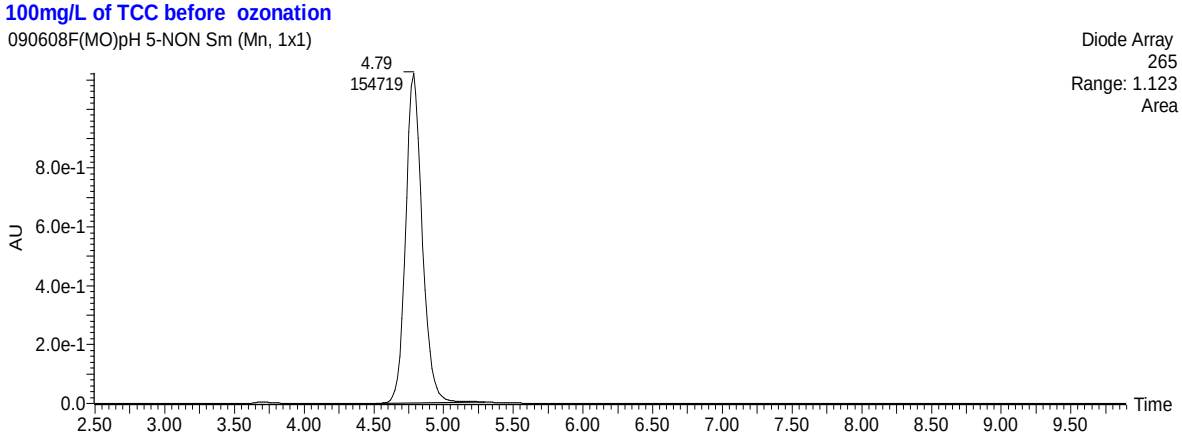

100mg/L of TCC after ozonation

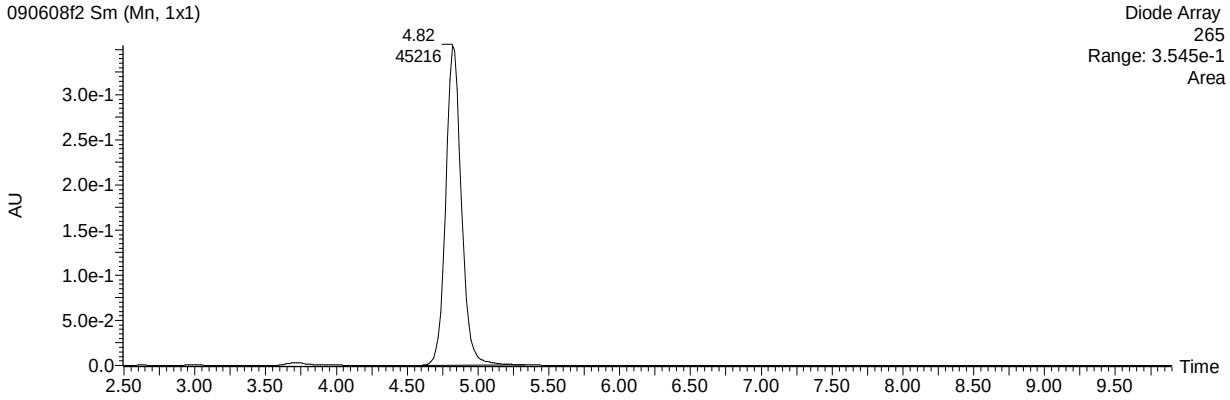

100mg/L of TCC after ozonation

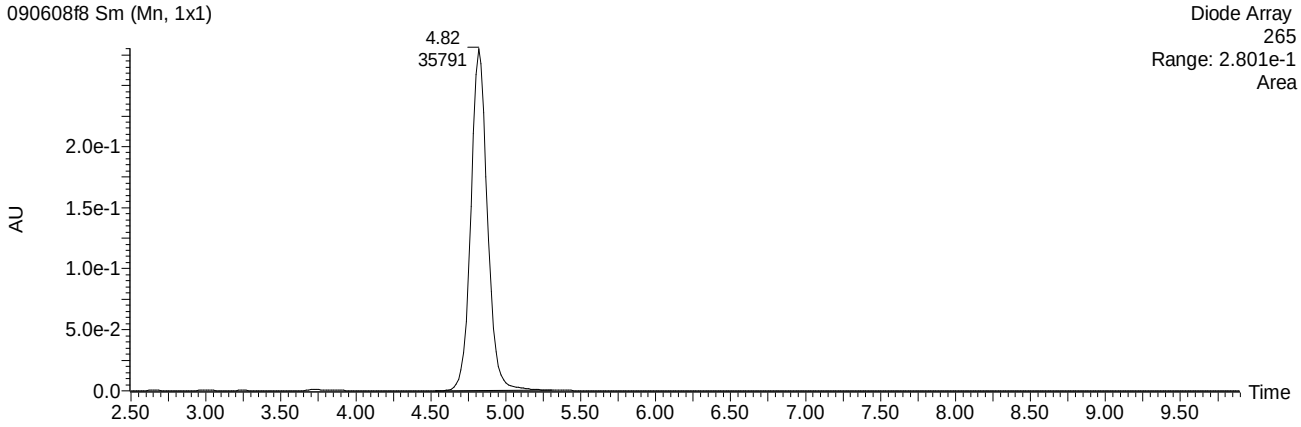

100mg/L of TCC after ozonation

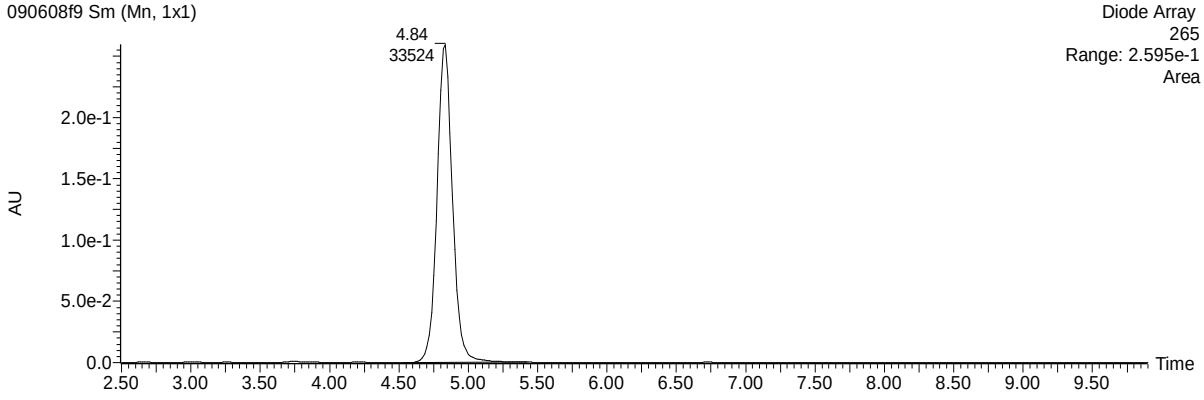

Peak Areas of TCC Degradation by (20g/m^3 of ozone) with t-butanol at pH 5

100mg/L of TCC before ozonation

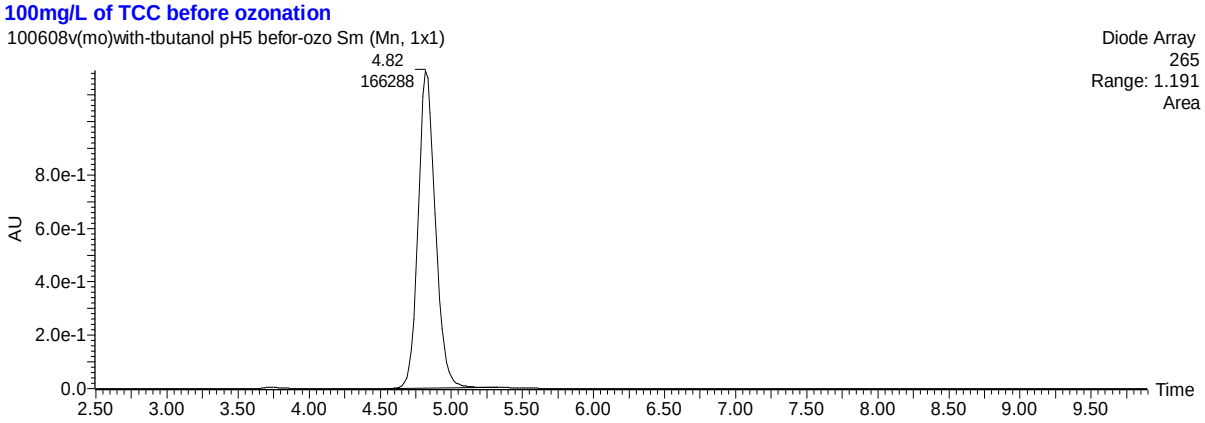

100mg/L of TCC after ozonation

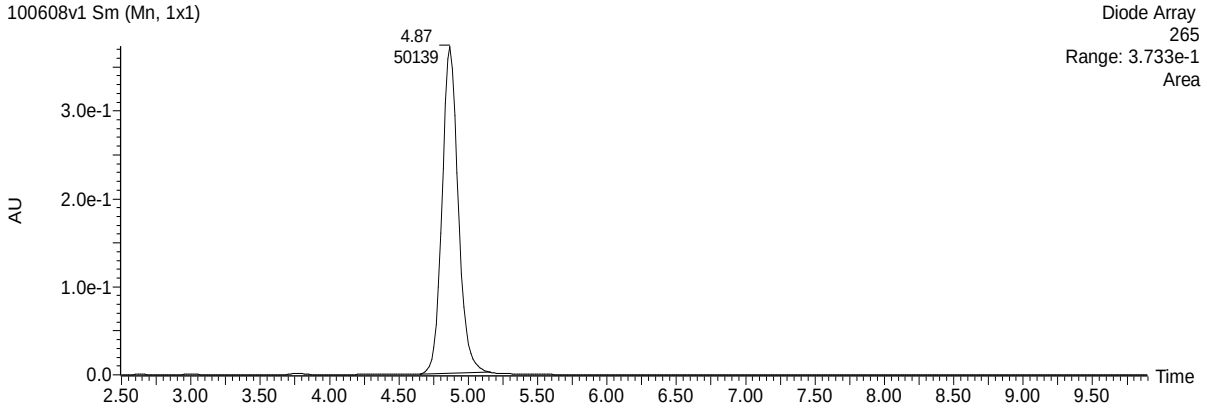

100mg/L of TCC after ozonation

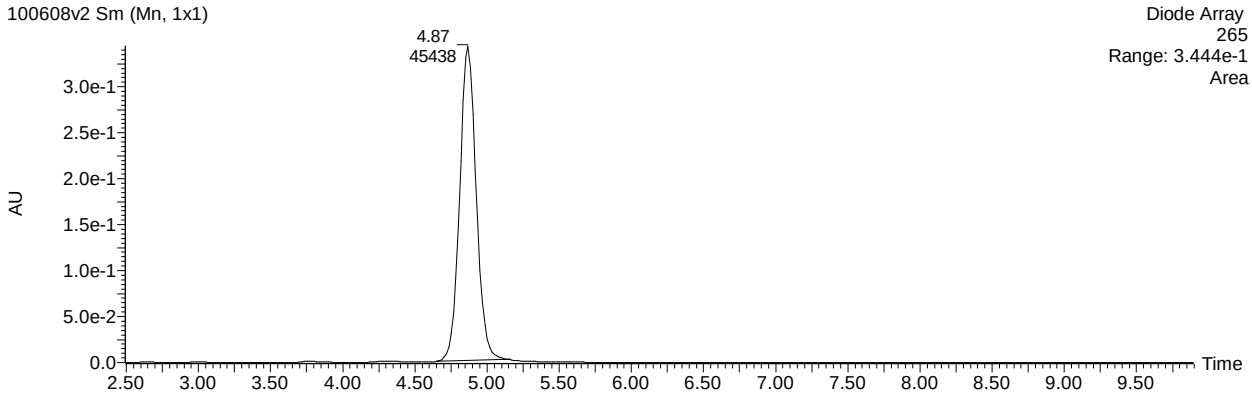

100mg/L of TCC after ozonation

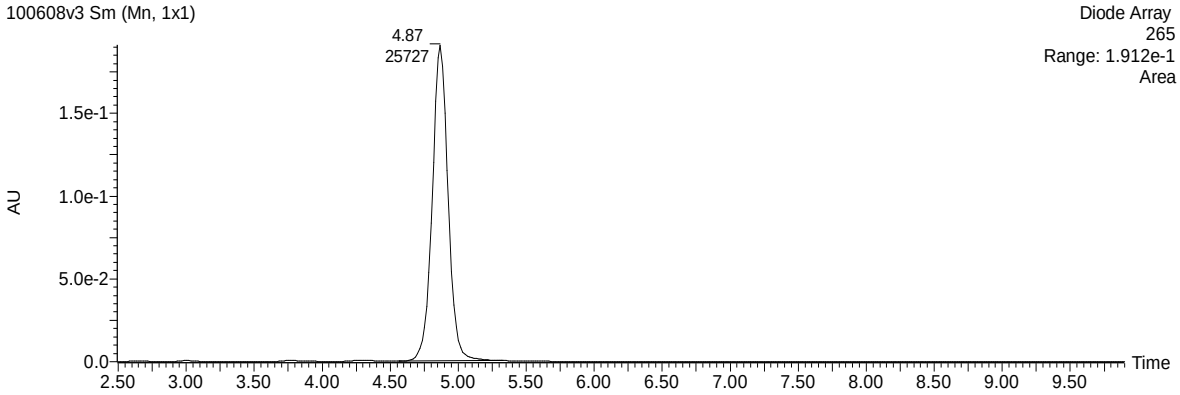

100mg/L of TCC after ozonation

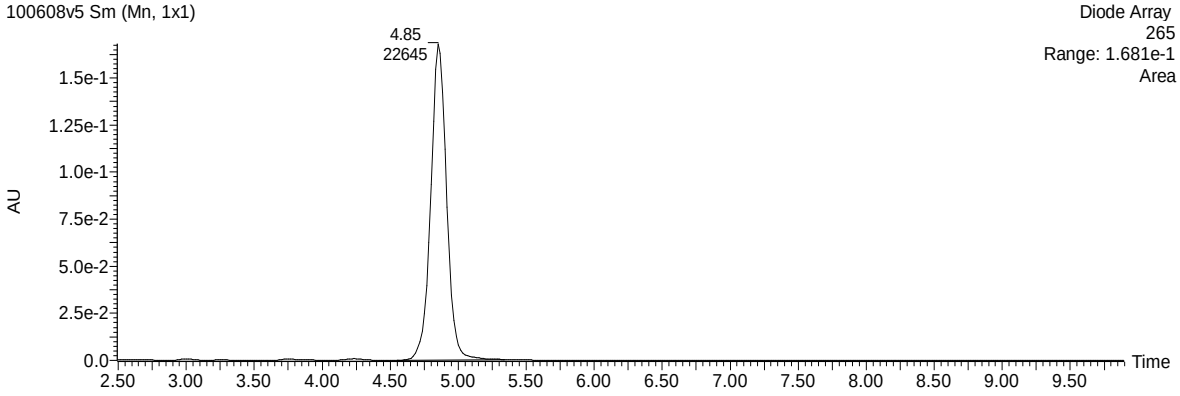

100mg/L of TCC after ozonation

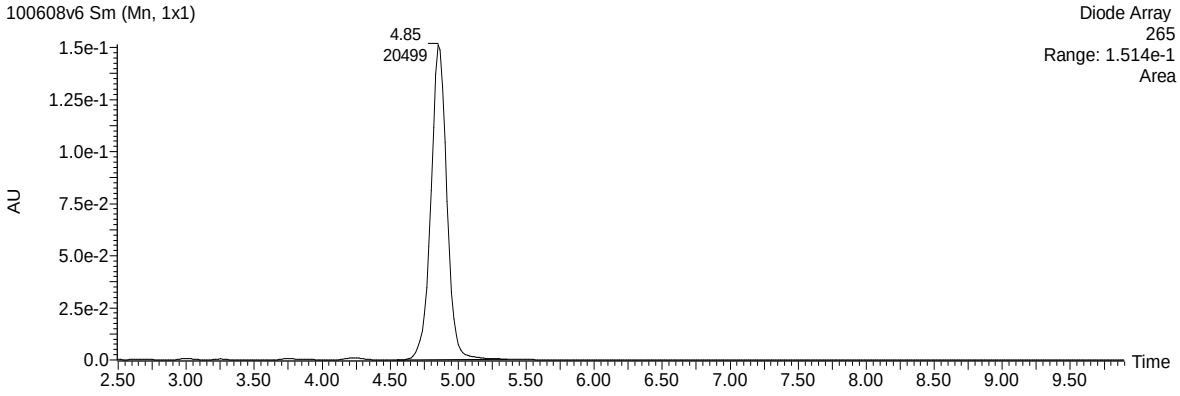

Peak Areas of TCC Degradation by (20g/m^3 of ozone) without t-butanol at pH 7

100mg/L of TCC before ozonation

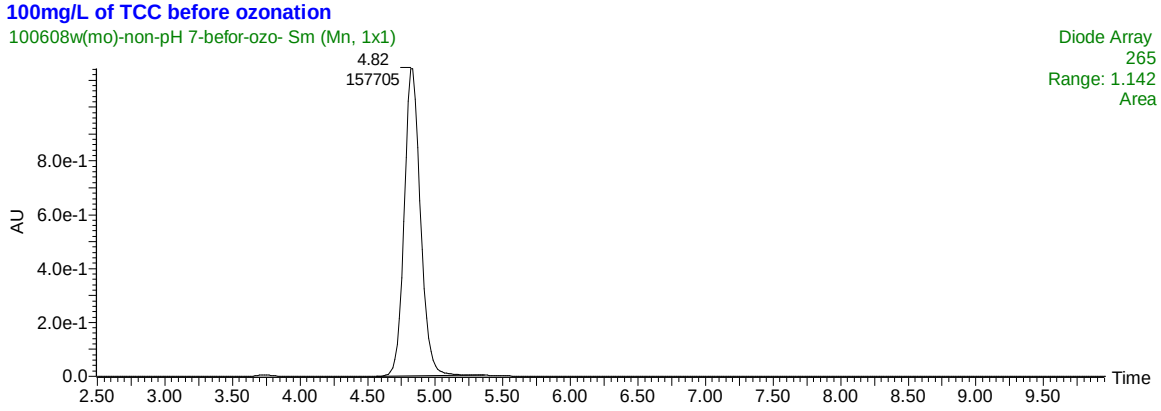

100mg/L of TCC after ozonation

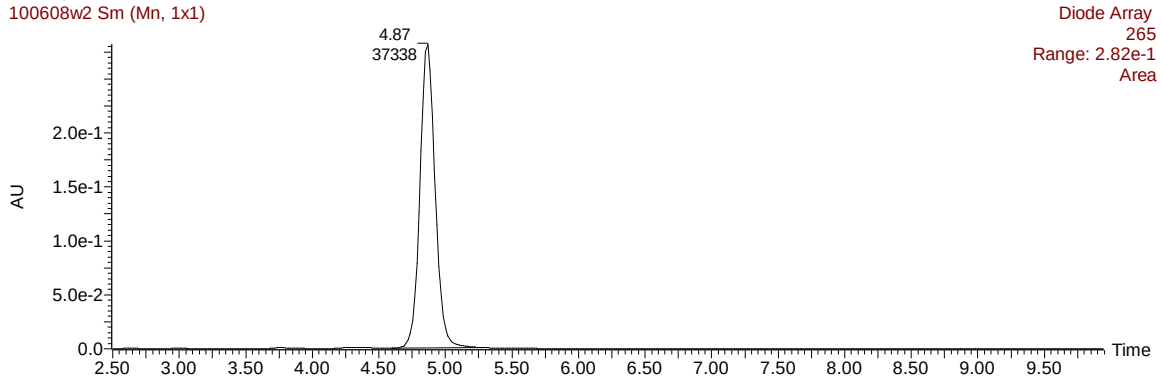

100mg/L of TCC after ozonation

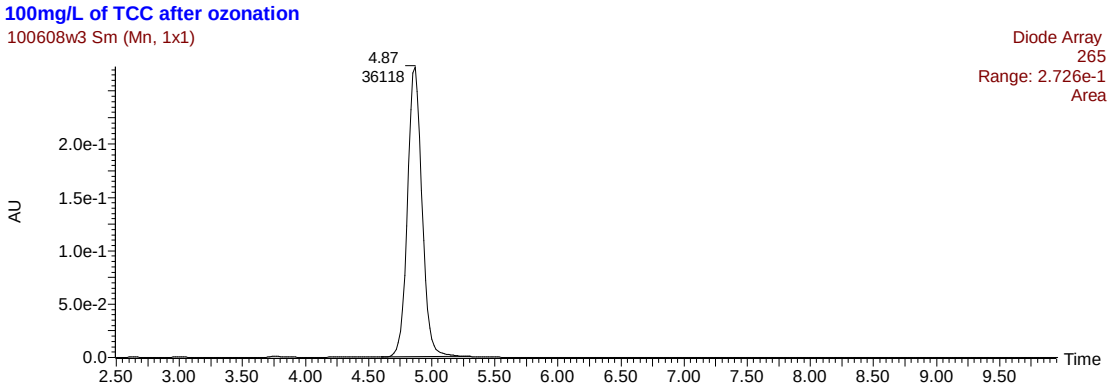

100mg/L of TCC after ozonation

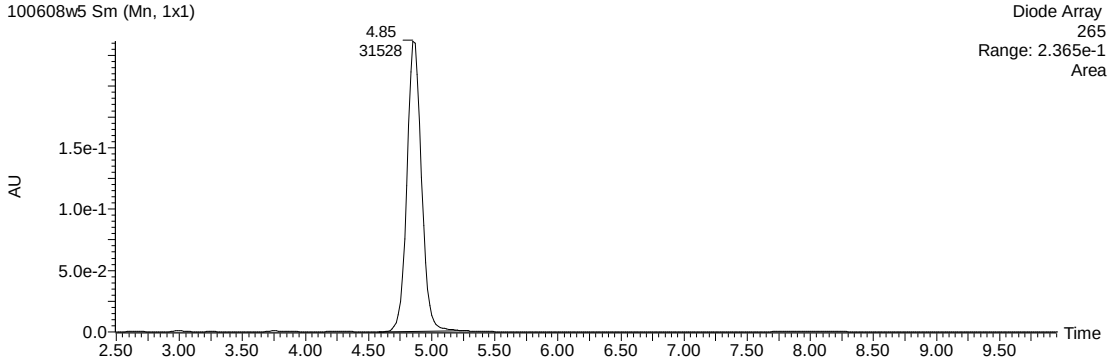

100mg/L of TCC after ozonation

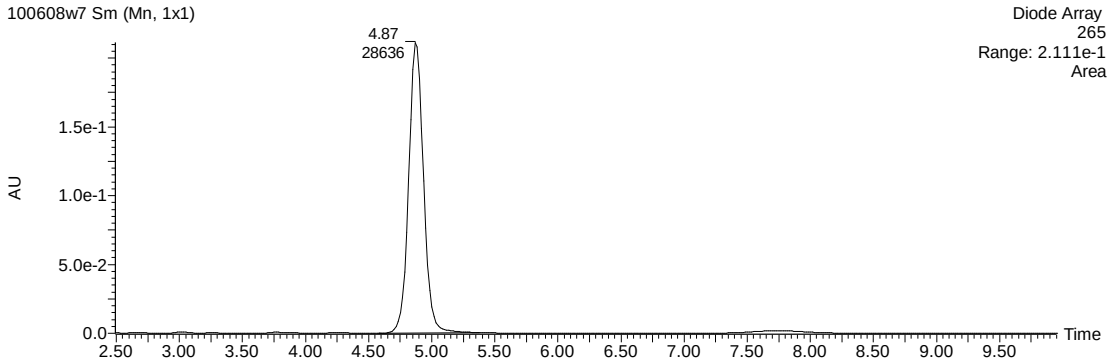

100mg/L of TCC after ozonation

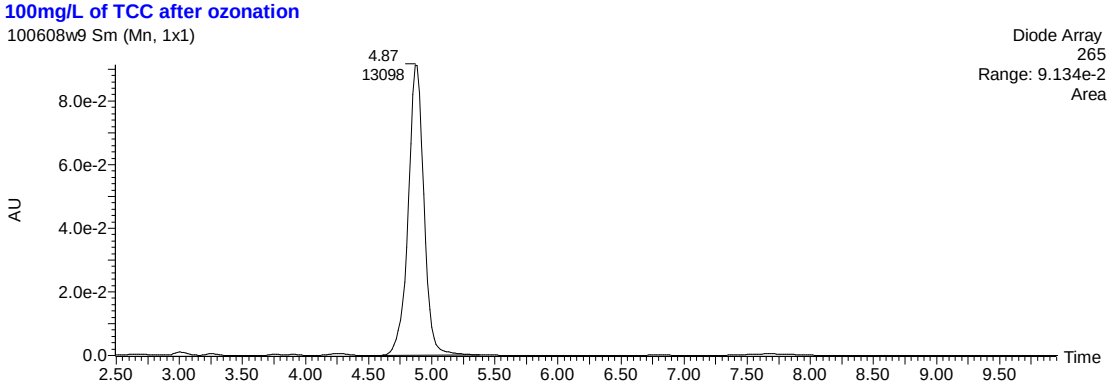

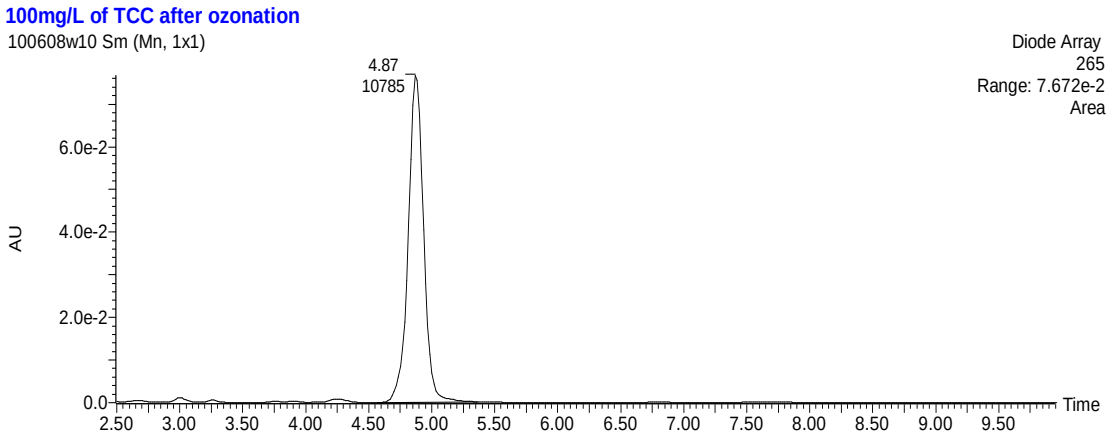

Peak Areas of TCC Degradation by (20g/m^3 of ozone) with t-butanol at pH 7

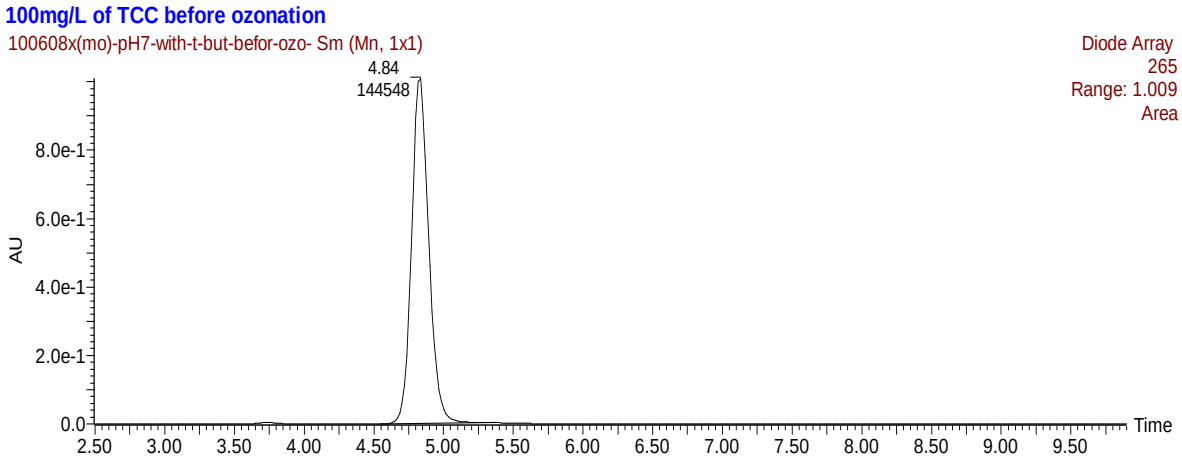

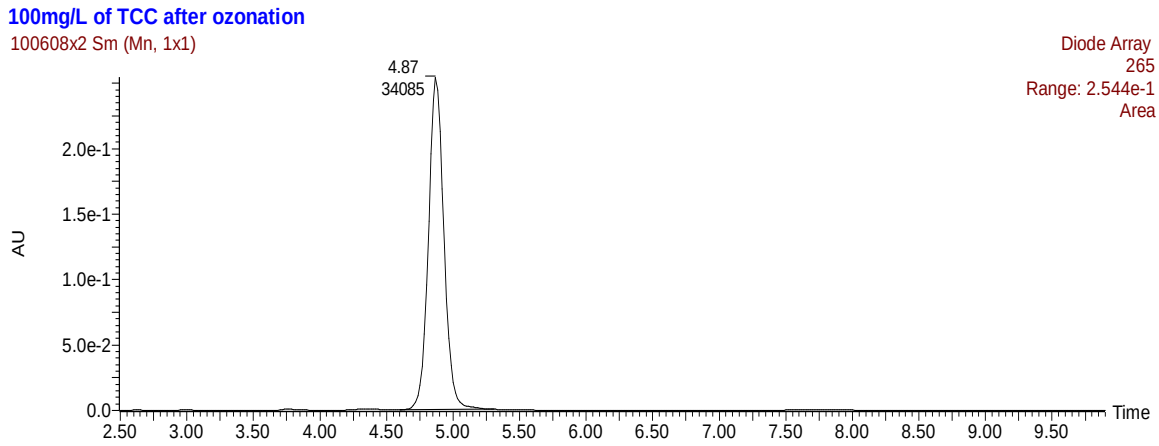

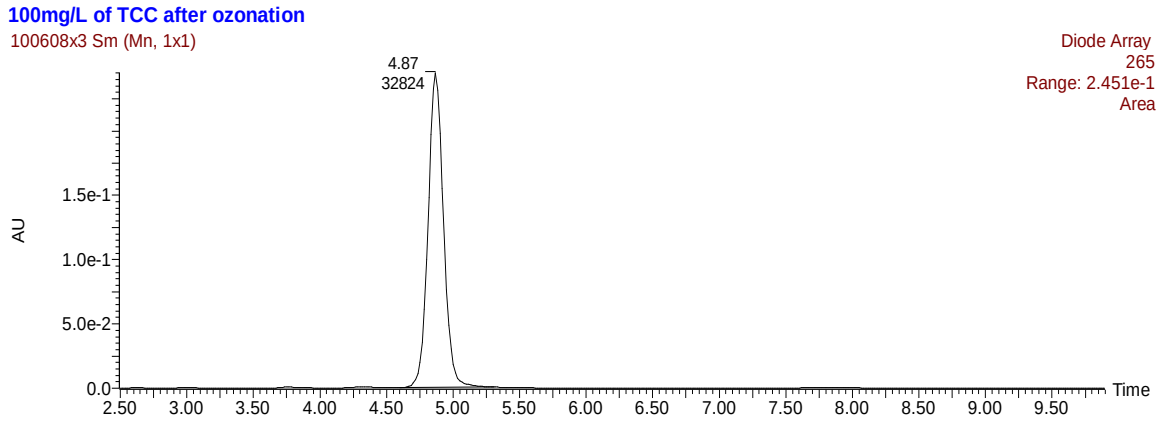
100mg/L of TCC after ozonation
100608x3 Sm (Mn, 1x1)
Diode Array
265
Range: 2.451e-1
Area
4.87
32824
AU
1.5e-1
1.0e-1
5.0e-2
0.0
Time
2.50 3.00 3.50 4.00 4.50 5.00 5.50 6.00 6.50 7.00 7.50 8.00 8.50 9.00 9.50

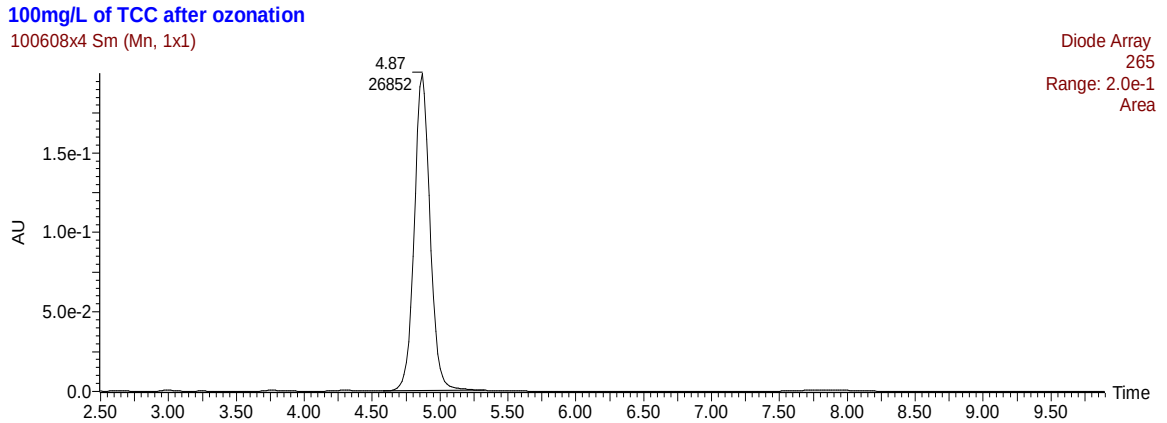
100mg/L of TCC after ozonation
100608x4 Sm (Mn, 1x1)
Diode Array
265
Range: 2.0e-1
Area
4.87
26852
AU
1.5e-1
1.0e-1
5.0e-2
0.0
Time
2.50 3.00 3.50 4.00 4.50 5.00 5.50 6.00 6.50 7.00 7.50 8.00 8.50 9.00 9.50

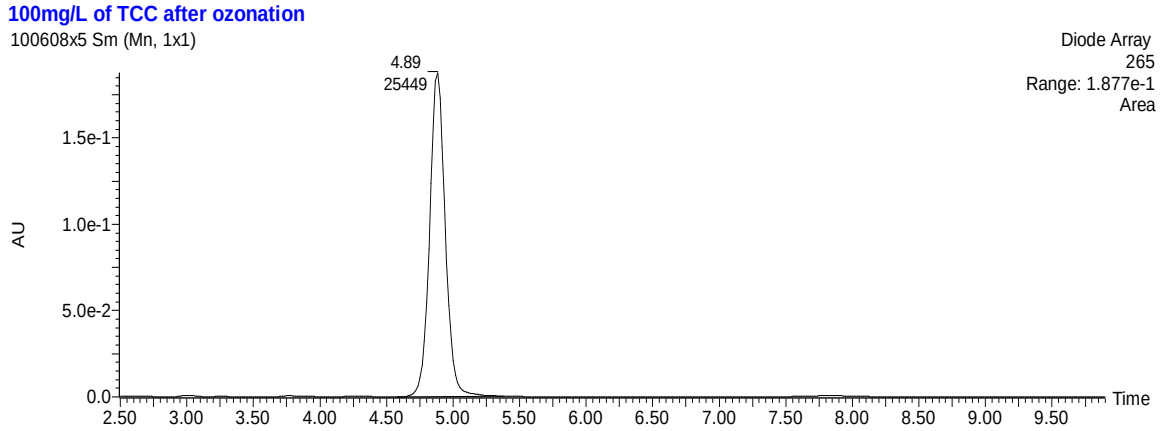
100mg/L of TCC after ozonation
100608x5 Sm (Mn, 1x1)
Diode Array
265
Range: 1.877e-1
Area
4.89
25449
AU
1.5e-1
1.0e-1
5.0e-2
0.0
Time
2.50 3.00 3.50 4.00 4.50 5.00 5.50 6.00 6.50 7.00 7.50 8.00 8.50 9.00 9.50

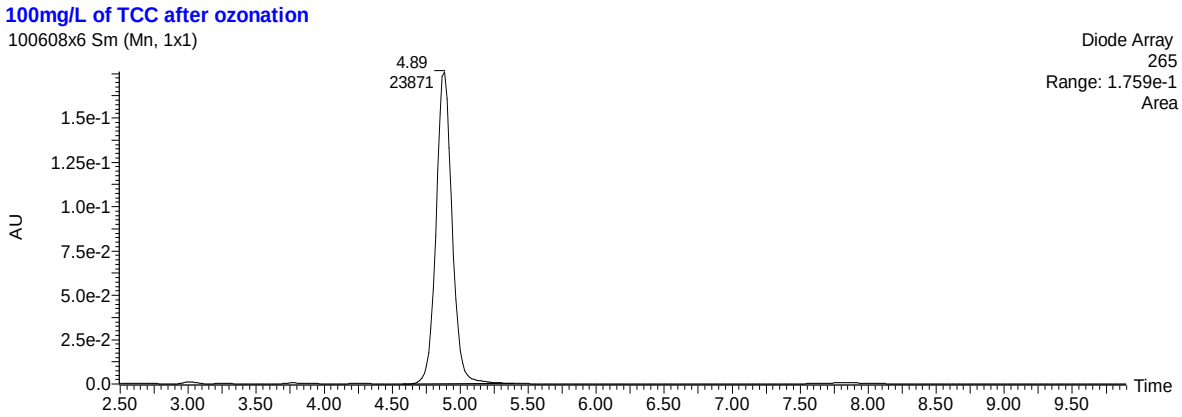

A2.4. Degradation of Naphthalene

A2.4.1. Spectrum of naphthalene and spectrum of 50%methanol: 50% water

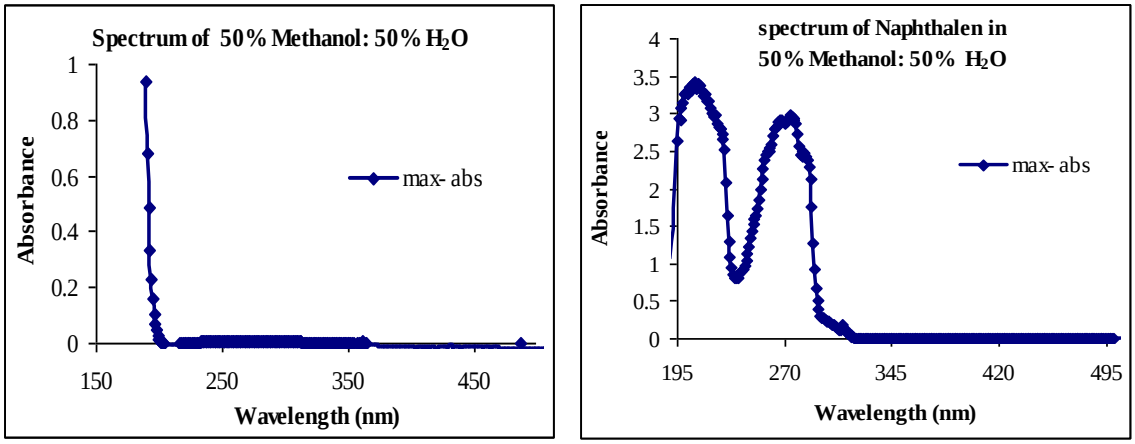

Figure A2.41. Full spectrum of naphthalene

A2.4.2. Ozone bubbling in naphthalene solution (liquid phase)

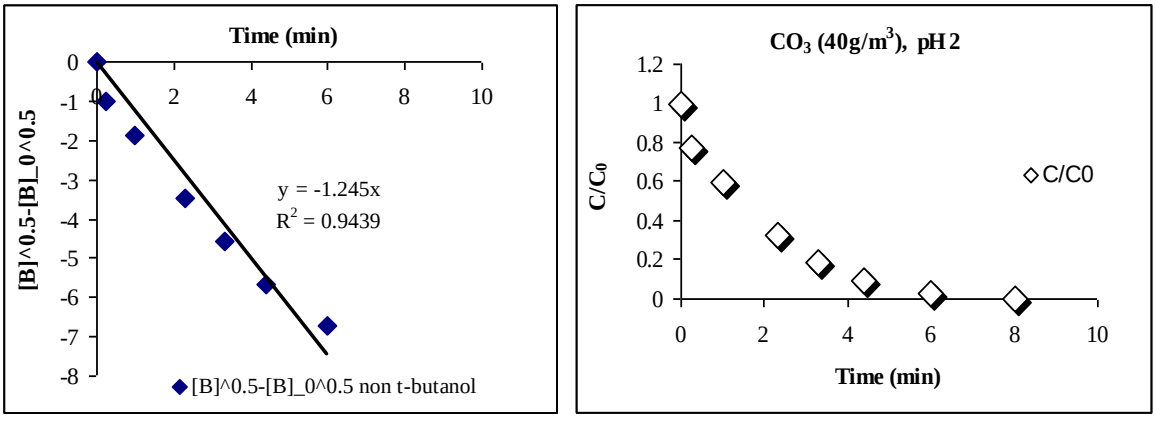

Figure A2.42. Ozone bubbling in naphthalene solution (liquid phase) at pH 2

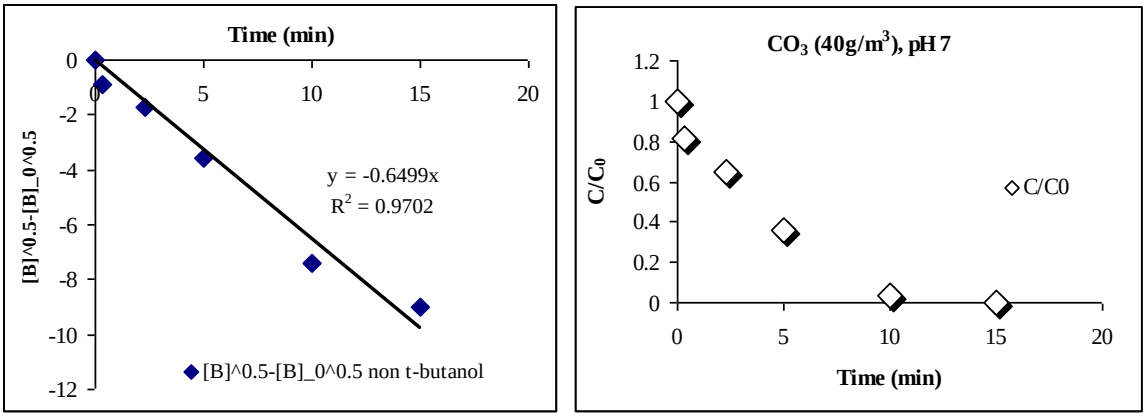

Figure A2.43. Ozone bubbling in naphthalene solution (liquid phase) at pH 7

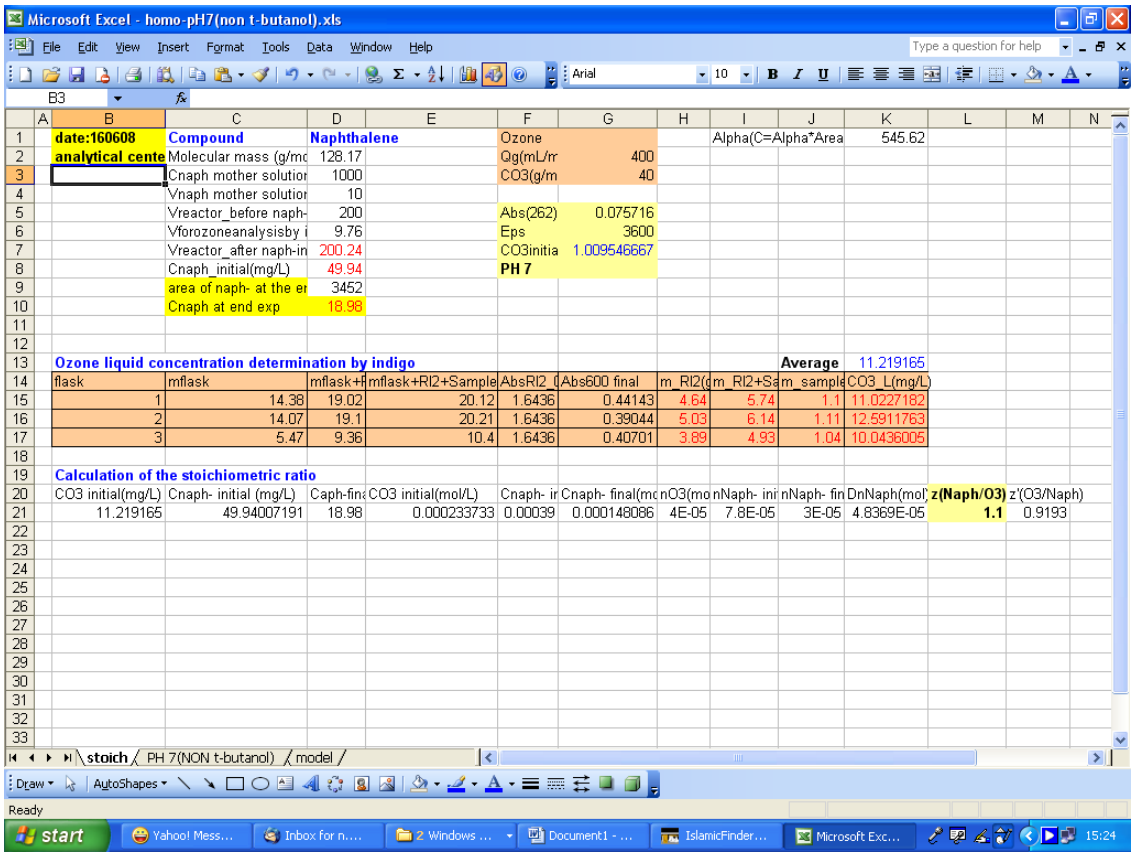

Figure A2. 44. Work sheet of stoichiometric calculation

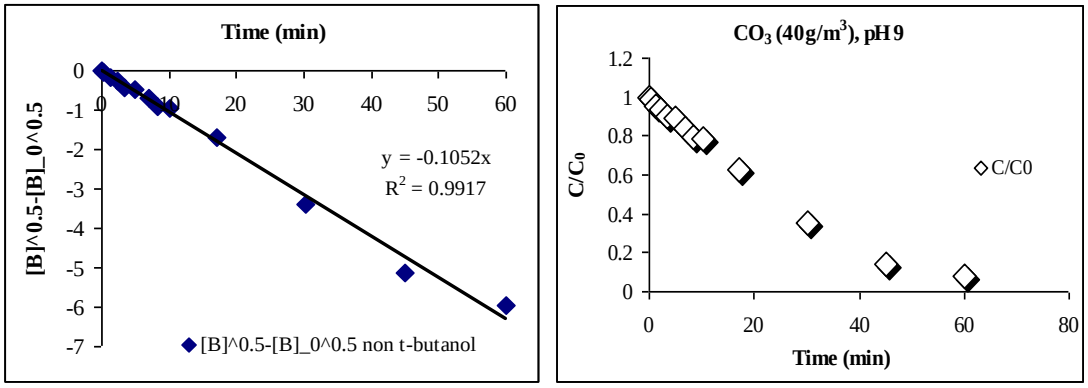

Figure A2.45. Ozone bubbling in naphthalene solution (liquid phase) at pH 9

A2.4.3. Ozone bubbling in naphthalene solution (gas phase)

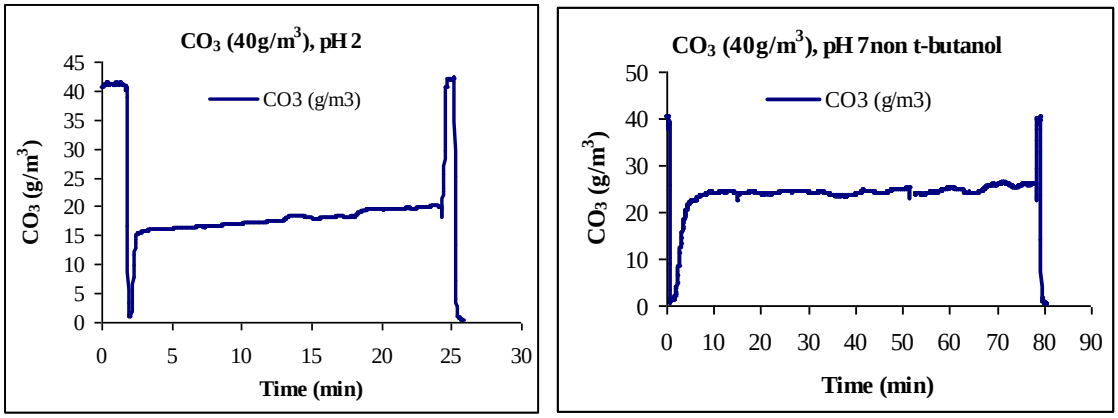

Figure A2.46. Ozone bubbling in naphthalene solution (gas phase) at pH2 and 7

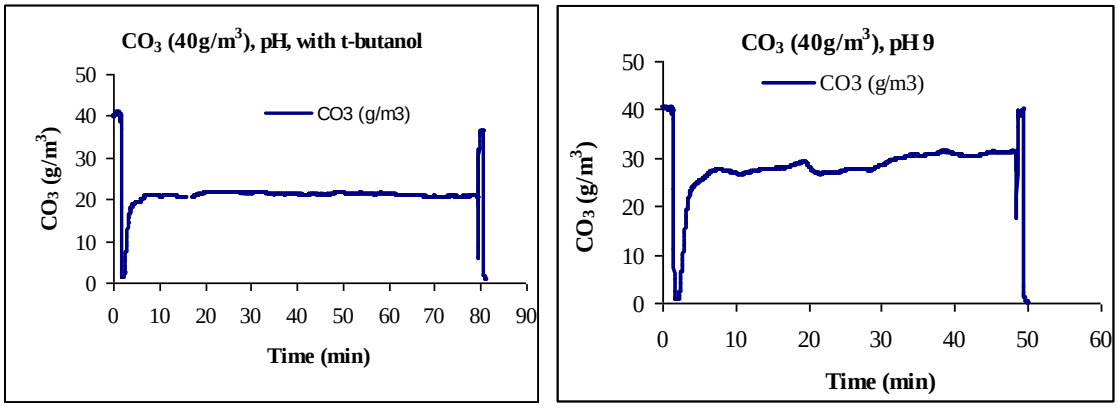

Figure A2.47. Ozone bubbling in naphthalene solution (gas phase) at pH 9

Peak Areas of Calibration Curve of Naphthalene

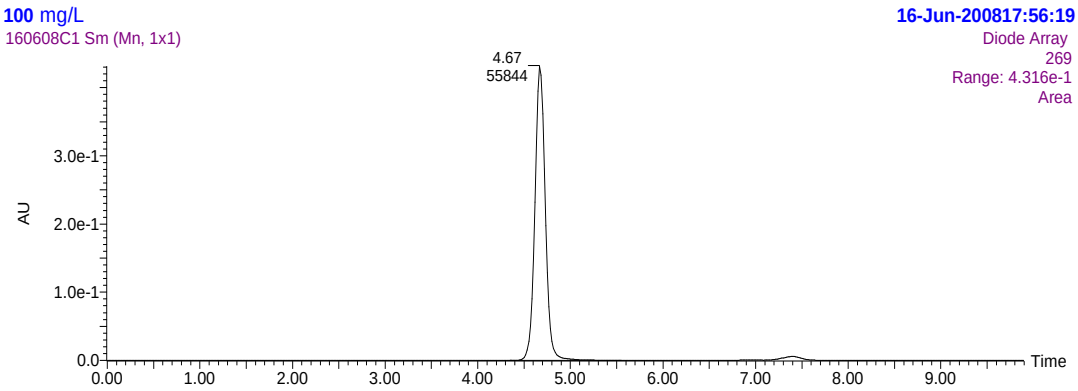

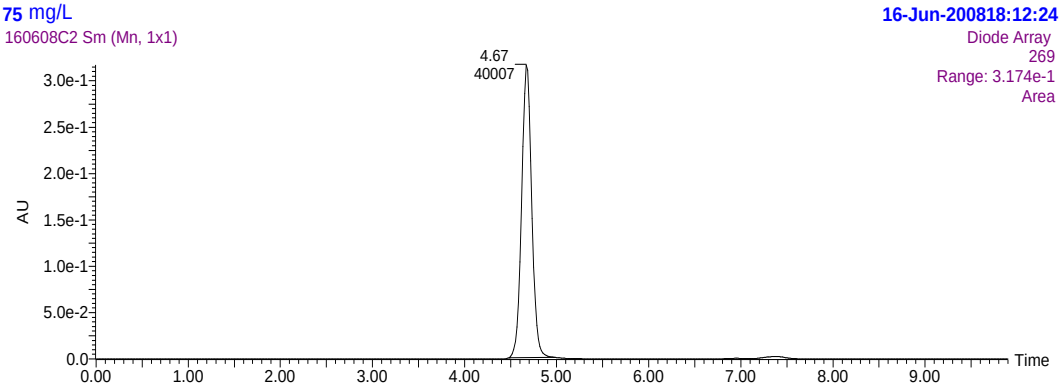

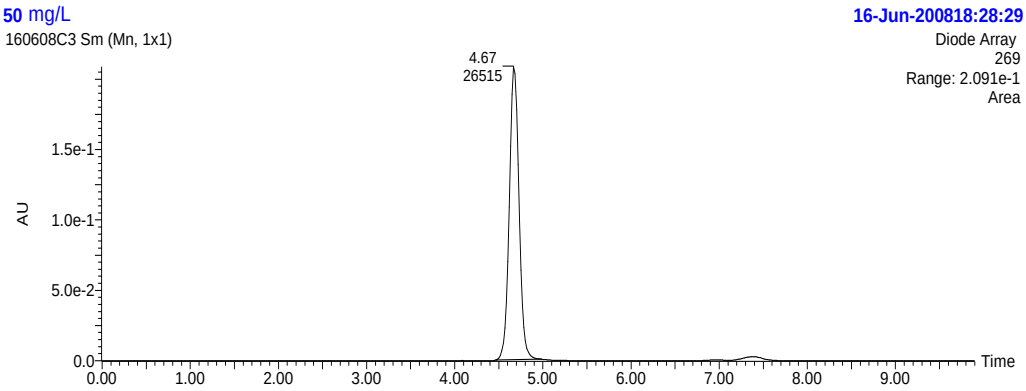

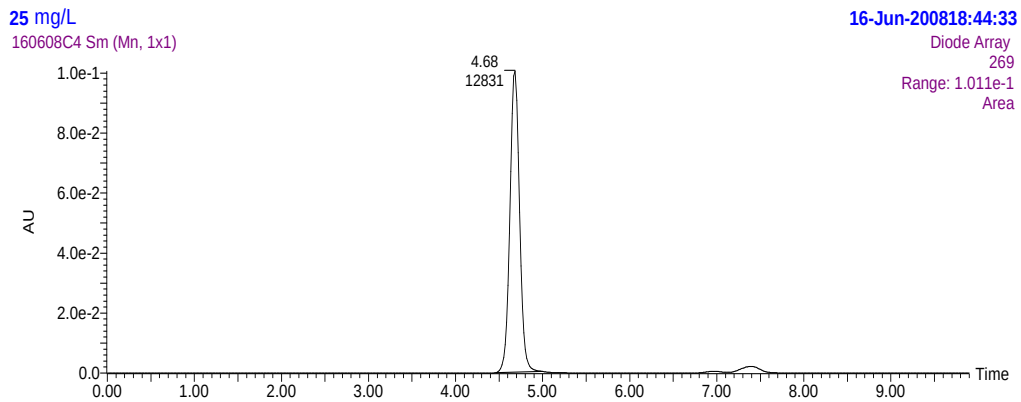

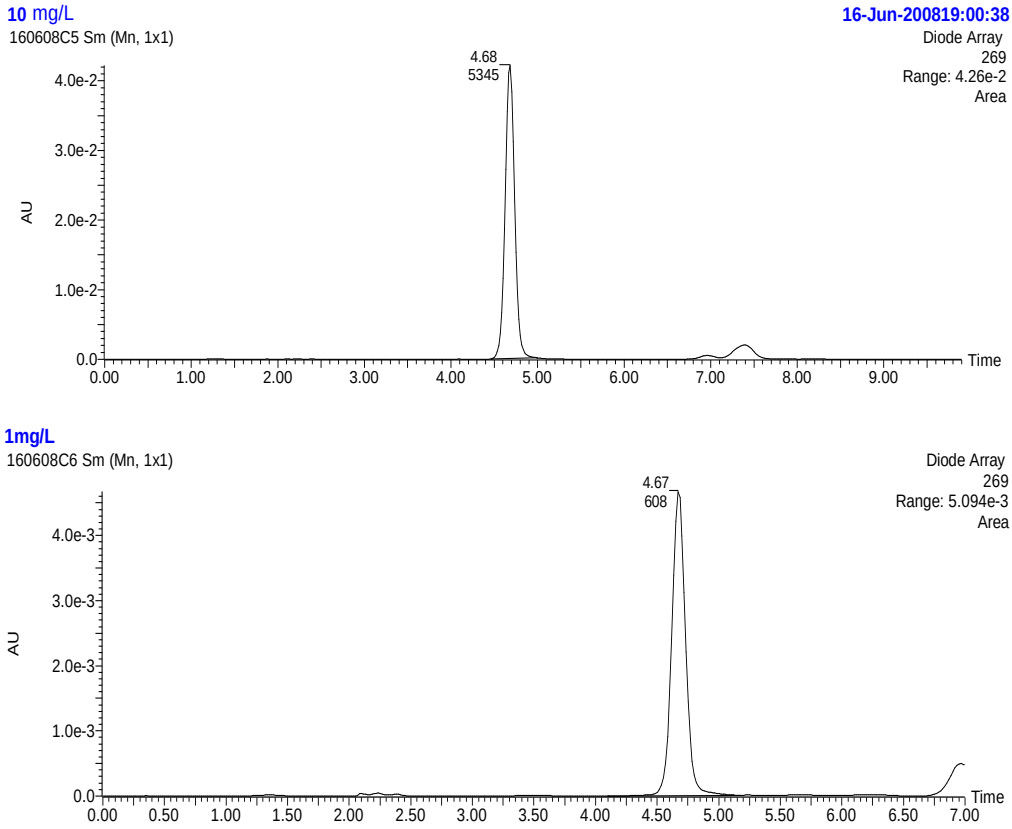

Peak Areas of naphthalene Degradation by ozone (without t-butanol) at pH 7

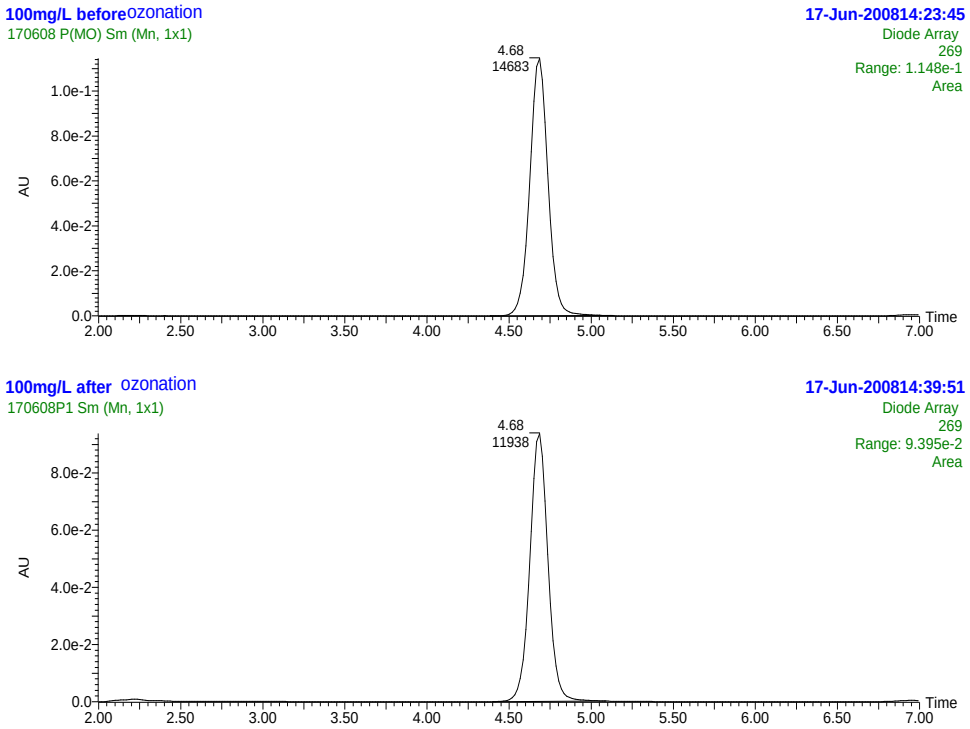

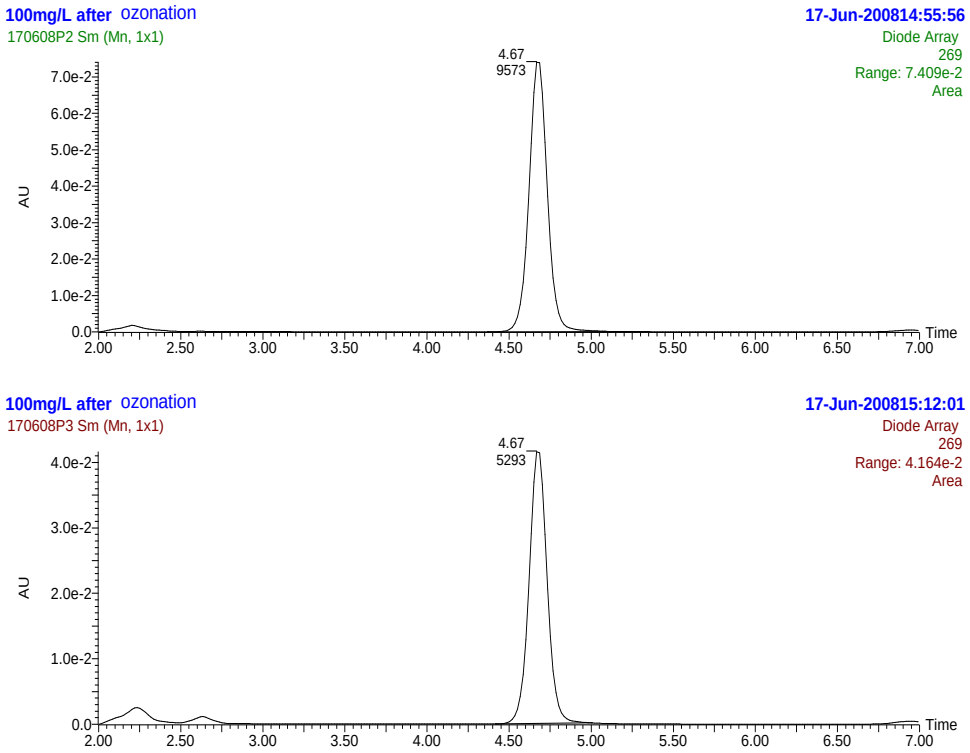

Peak Areas of naphthalene Degradation by ozone (with t-butanol) at pH 7

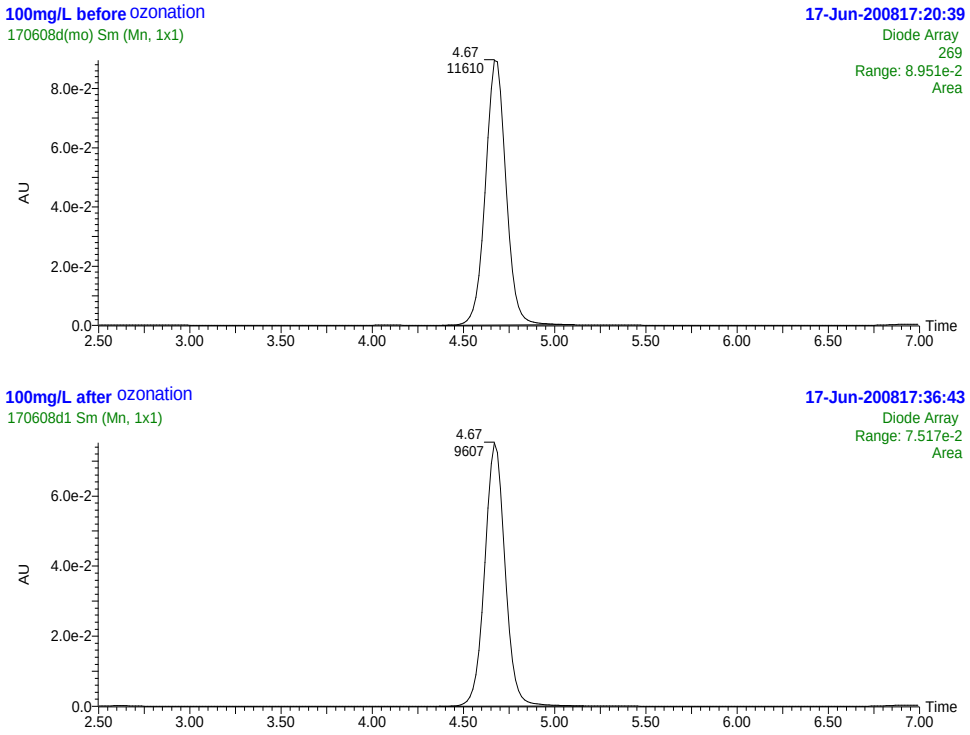

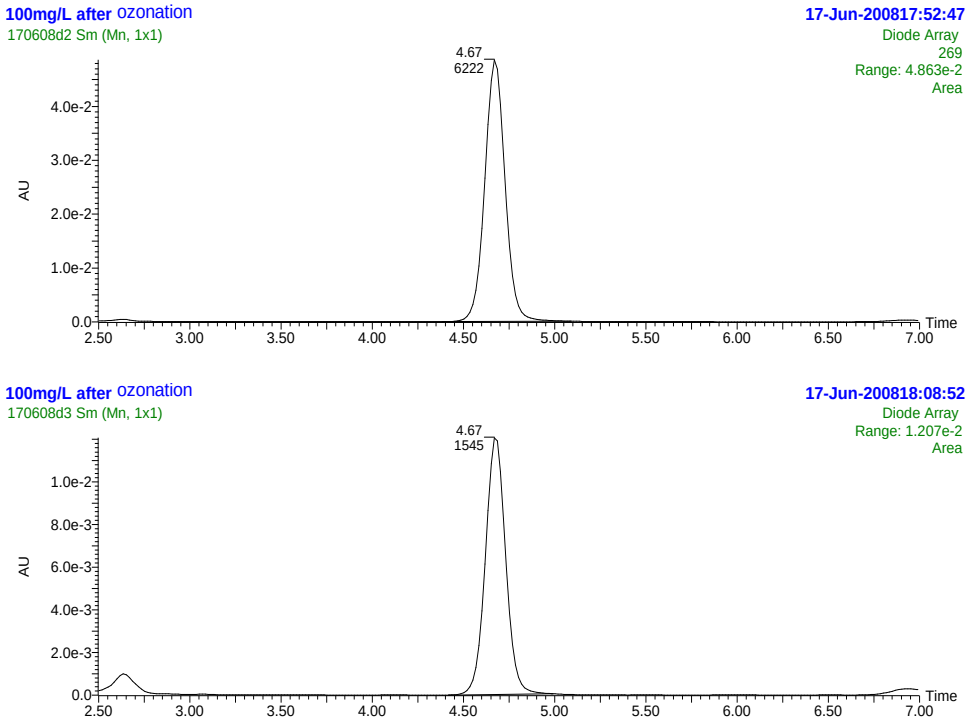

A2.4.4. Naphthalene solution loading on zeolite D915 without ozone

Peak Areas of Naphthalene loading on Zeolite D915 without (ozone and t-butanol) at pH7

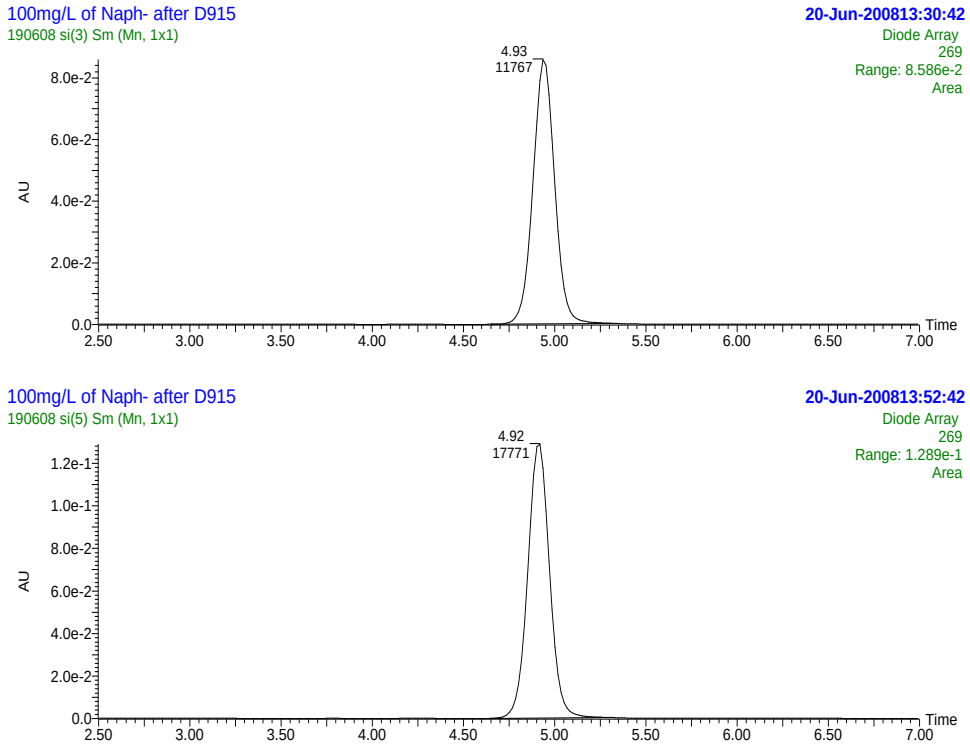

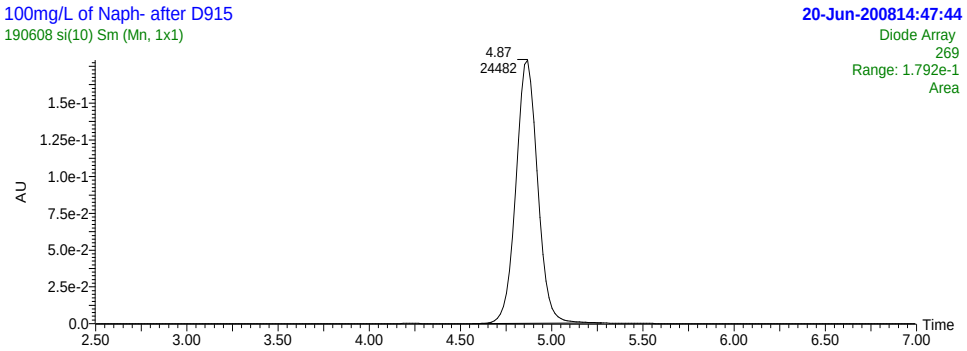

Peak Areas of Naphthalene loading on Zeolite D915 with t-butanol and without ozone at pH 7

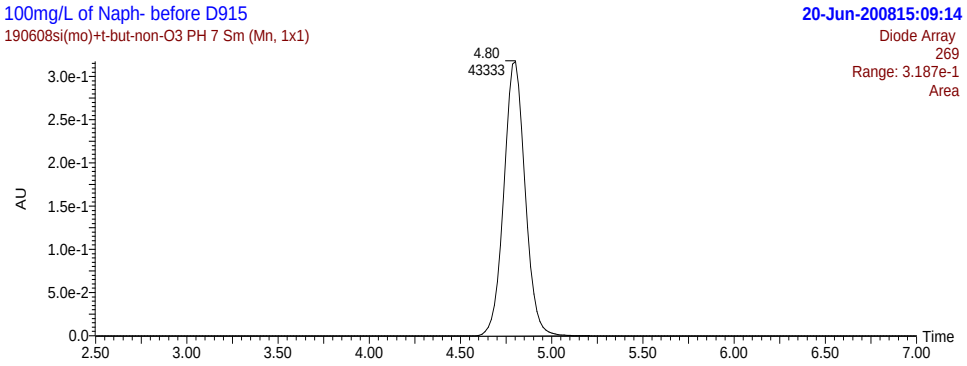

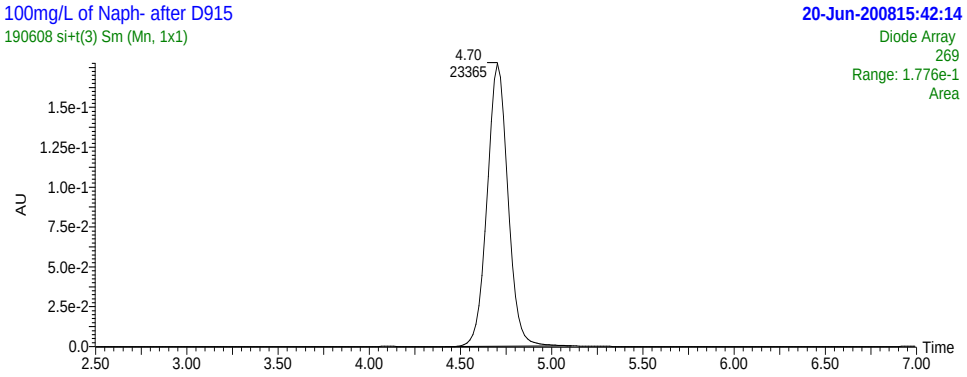

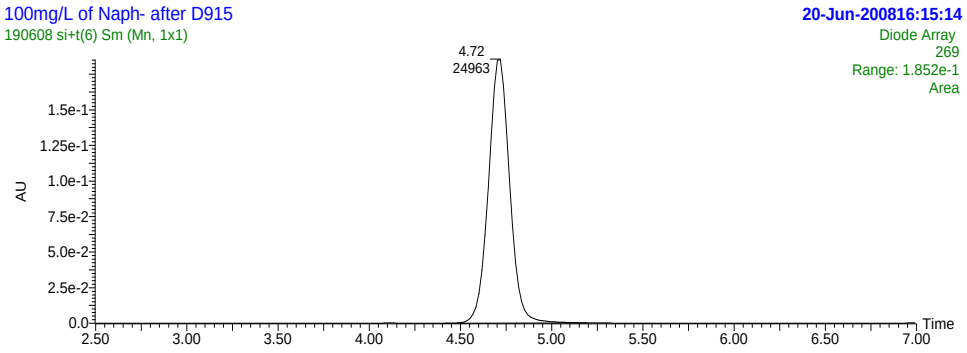

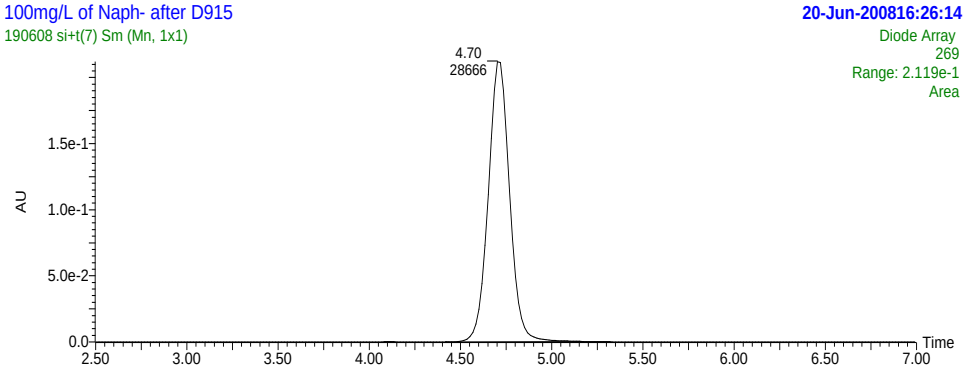

A2.4.5. Naphthalene solution loading on zeolite D915 with ozone

Peak Areas of Naphthalene loading on Zeolite D915 with ozone and without t-butanol at pH 7

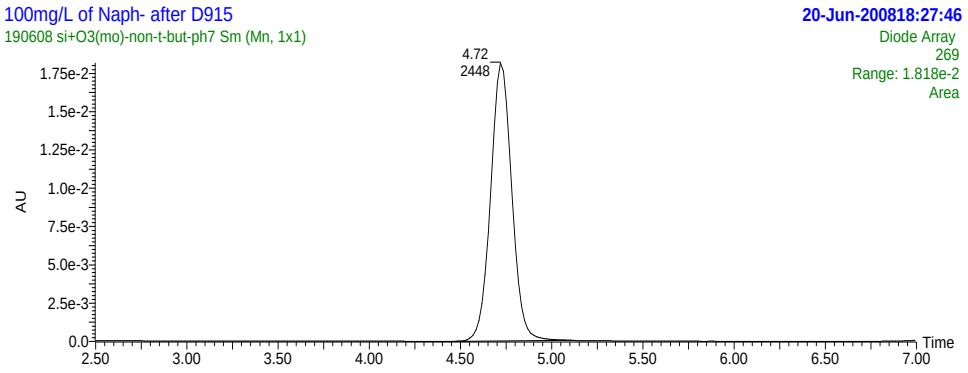

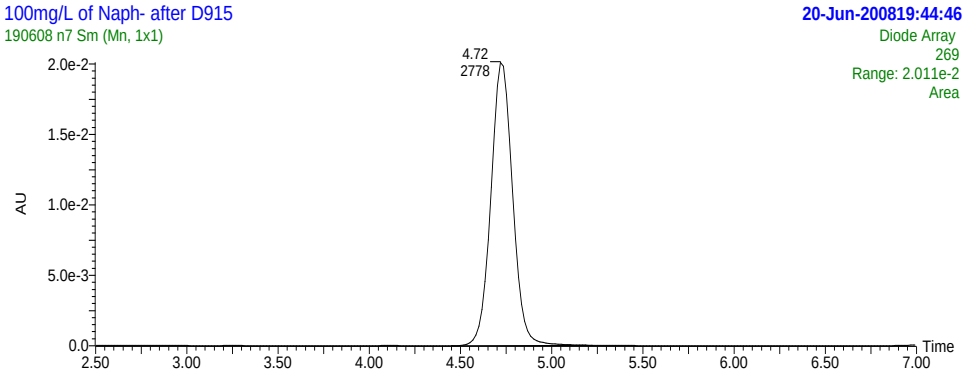

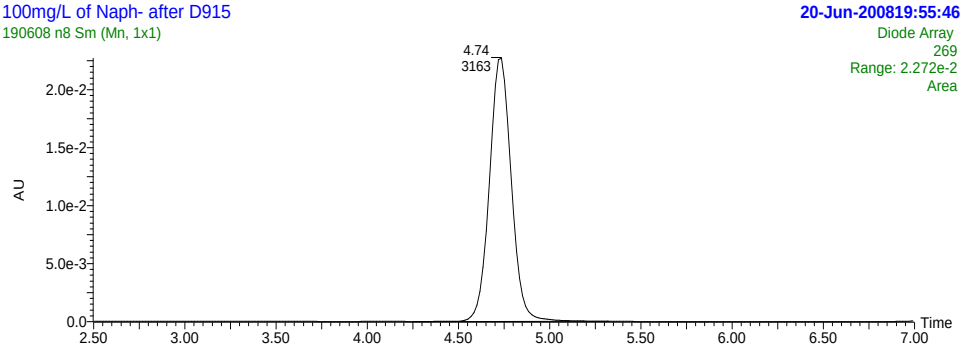

Peak Areas of Naphthalene loading on Zeolite D915 with ozone and t-butanol at pH 7

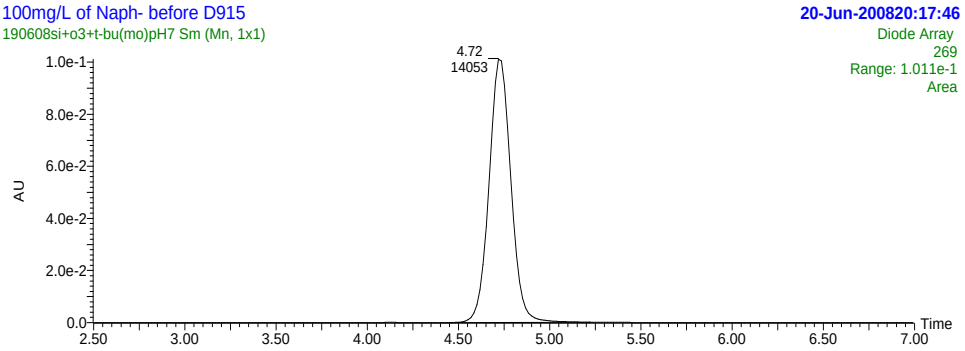

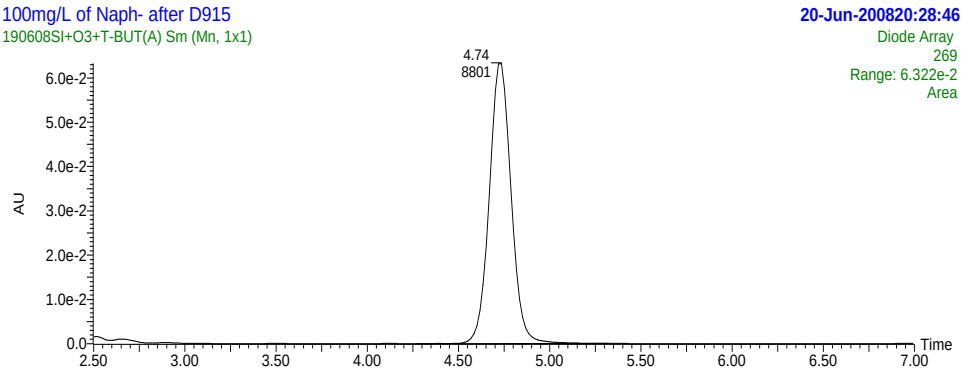

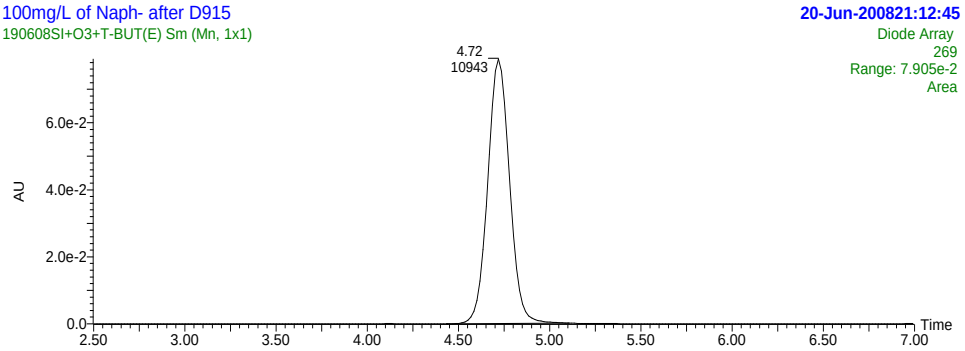

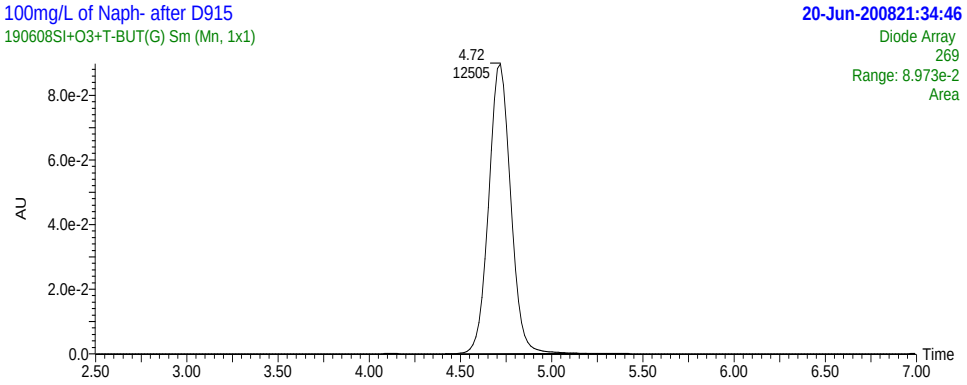

A2.5. Degradation of Methanol

A2.5.1. Liquid / Gas -Ozone (LGO) System

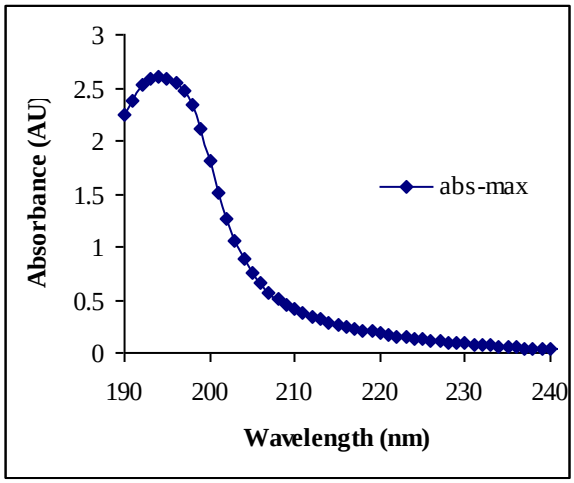

Figure A2.48. Full spectrum of methanol

A2.5.1.1. Effect of ozone concentration

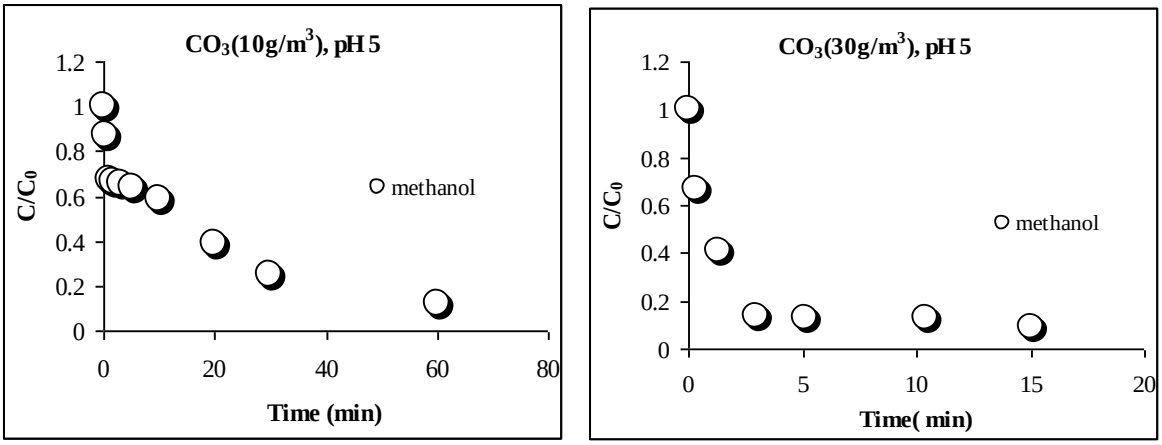

Figure A2.49. Ozone bubbling in methanol solution (liquid phase) at pH 5

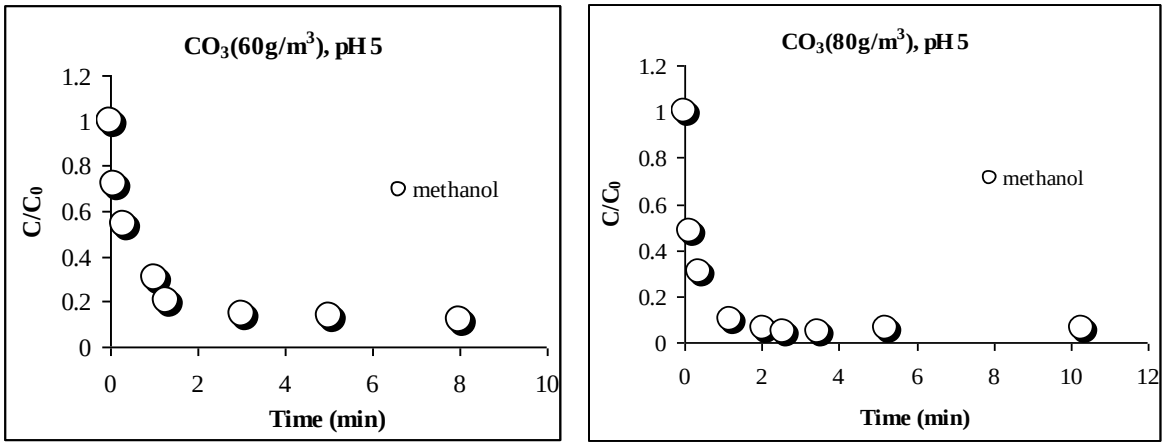

Figure A2.50. Ozone bubbling in methanol solution (liquid phase) at pH 5

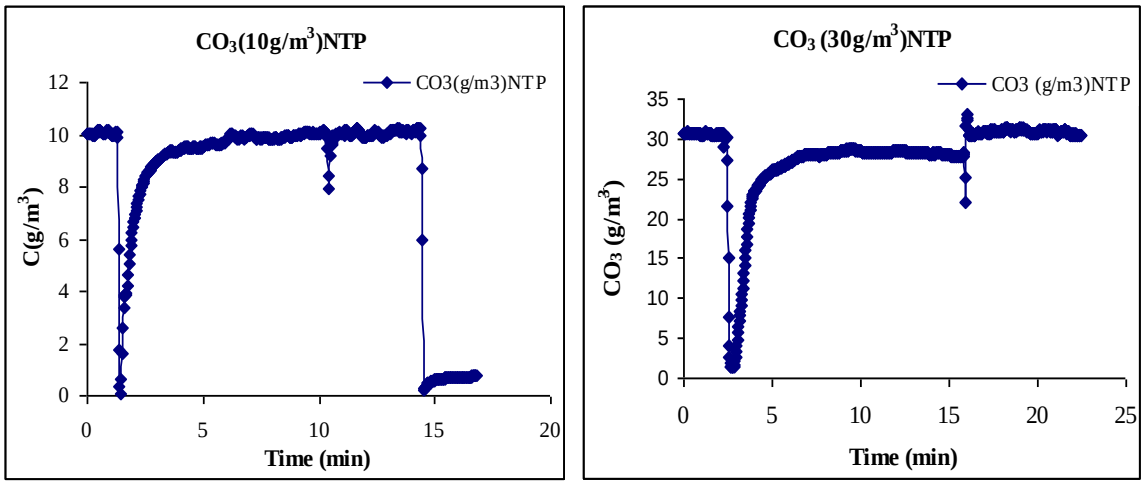

Figure A2.51. Ozone bubbling in methanol solution (gas phase) at pH 5

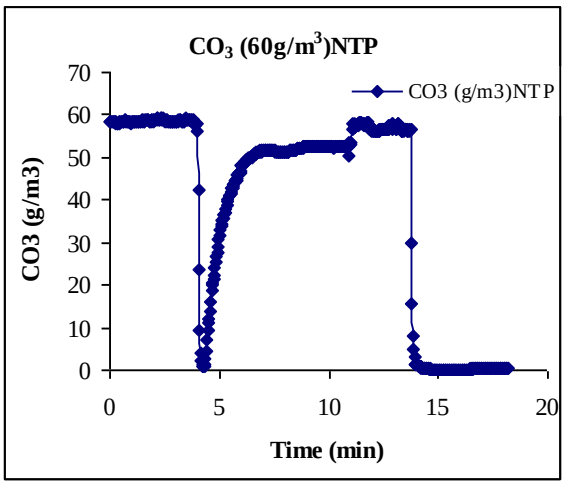

Figure A2.52. Ozone bubbling in methanol solution (gas phase) at pH 5

A2.5.1.2. Effect of t-butanol

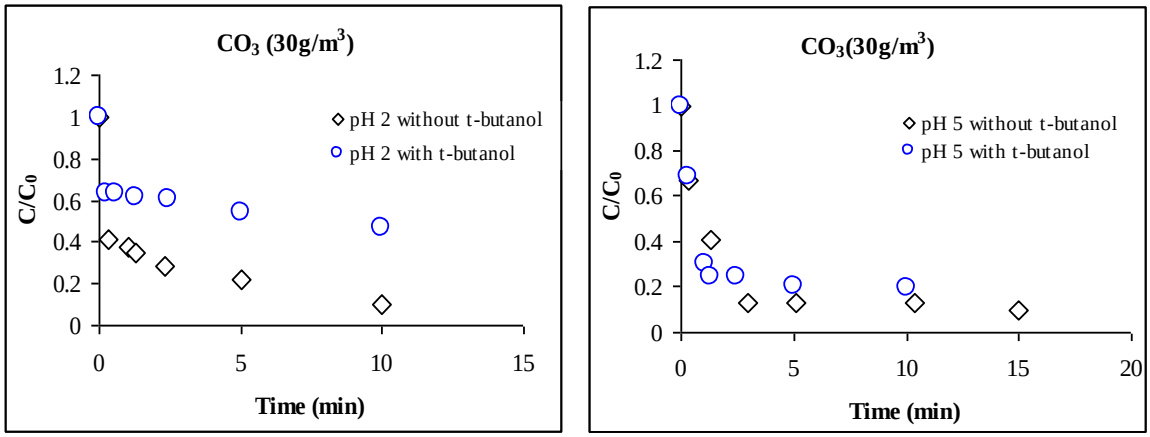

Figure A2.53. Effect of t-butanol on methanol solution at pH (2&5)

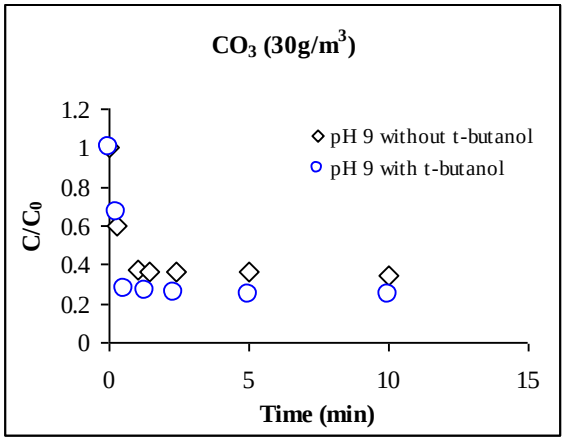

Figure A2.54. Effect of t-butanol on methanol solution at pH 9

A2.5.1.3. Effect of pH

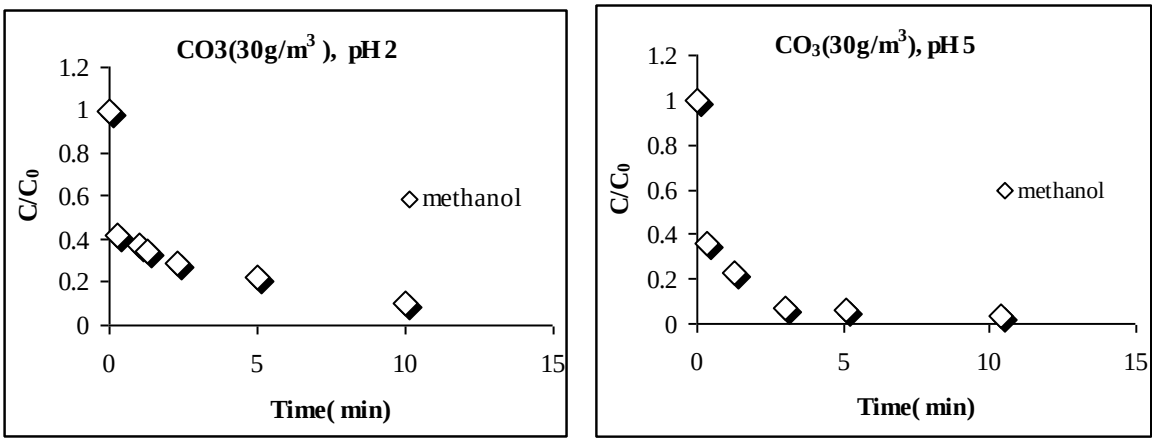

Figure A2.55. Effect of pH on methanol solution

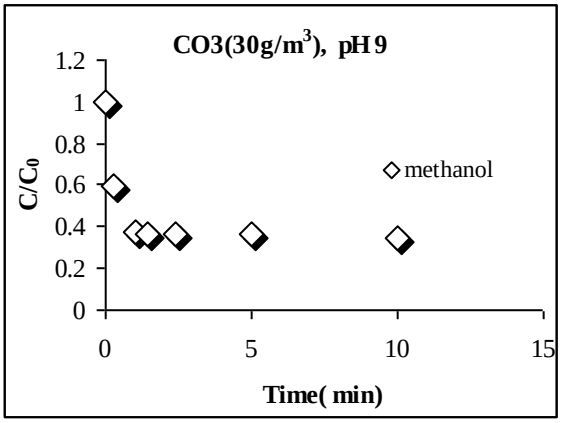

Figure A2.56. Effect of pH on methanol solution

A2.5.2. Liquid/Solid-Ozone (LSO) System

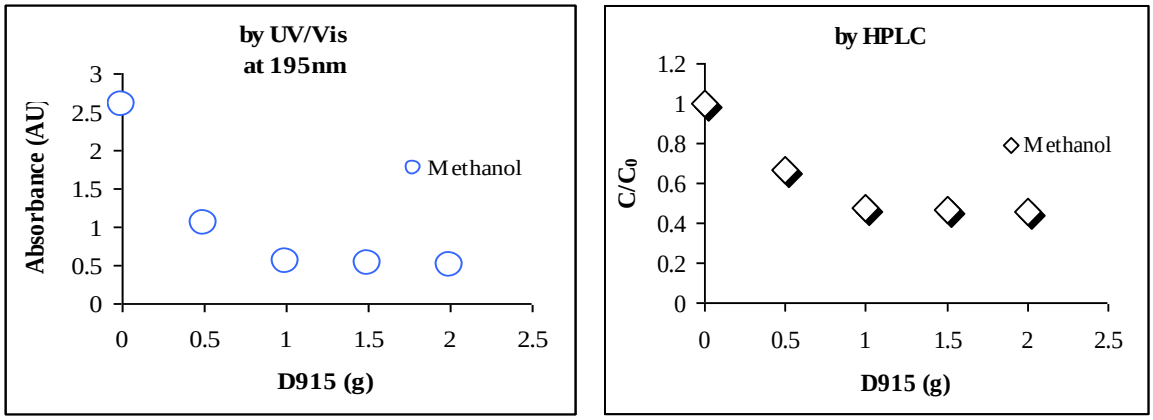

Figure A2.57. Methanol adsorption on D915

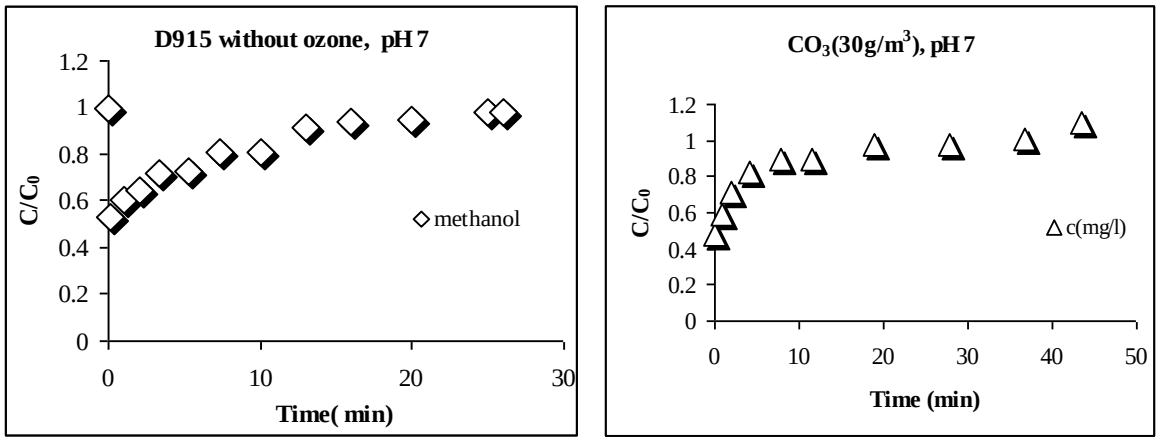

Figure A2.58. Effect of ozone concentration on methanol adsorption on D915

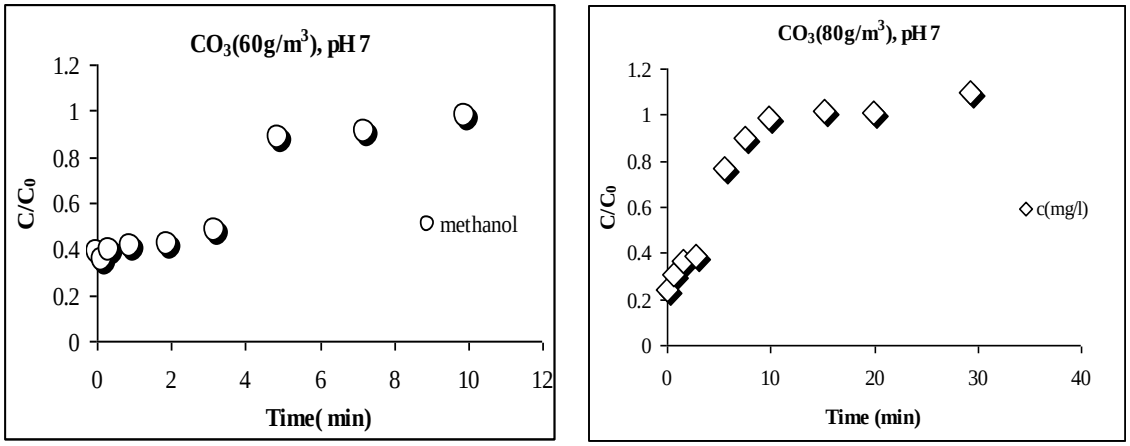

Figure A2.59. Effect of ozone concentration on methanol adsorption on D915

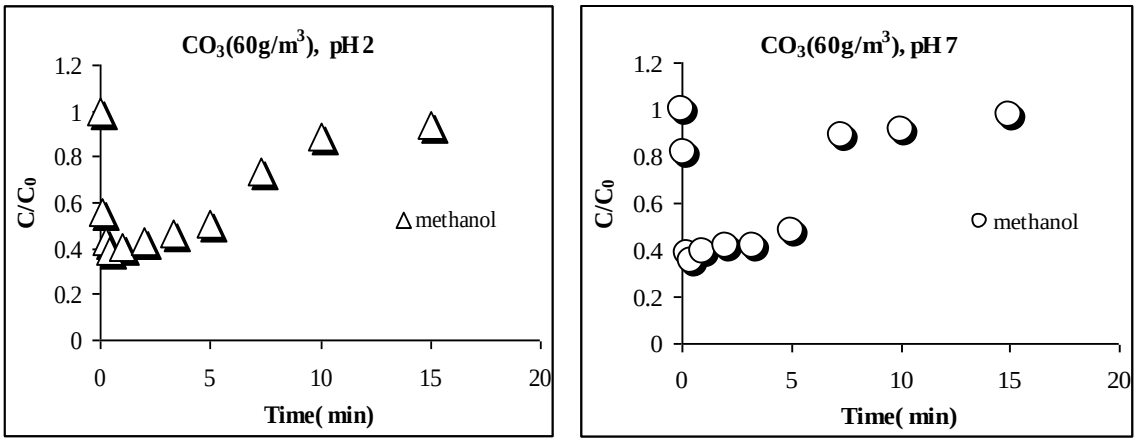

Figure A2.60. Effect of pH on methanol adsorption on D915 with ozone

Appendix A3: EXPERIMANTAL MATREIAL AND TECHNICAL METHOD


Figure 1: System of the ozonation experimental

Figure 2: Ozone generator

Figure 3: Ozone analyser


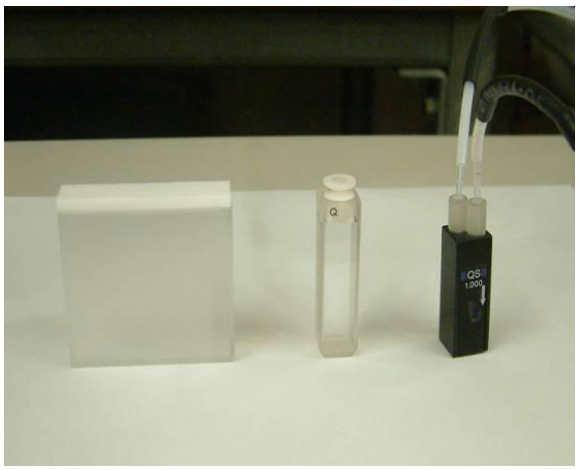

Figure 4: Data software and type of cells

Figure 5: Gas chromatograph (GC/FID)

Figure 6: HPLC

Figure 7: pH meter

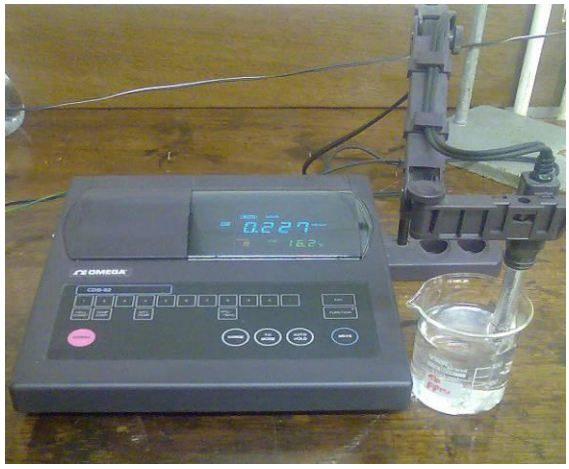

Figure 8: Conductivity meter

Figure 9: Glass ware

Figure 10: Instrument of deionised water

Figure 11: Dye (RO16)

Figure 12: t-butanol

Figure 13: Silica gel

Figure 14: Zeolite D915

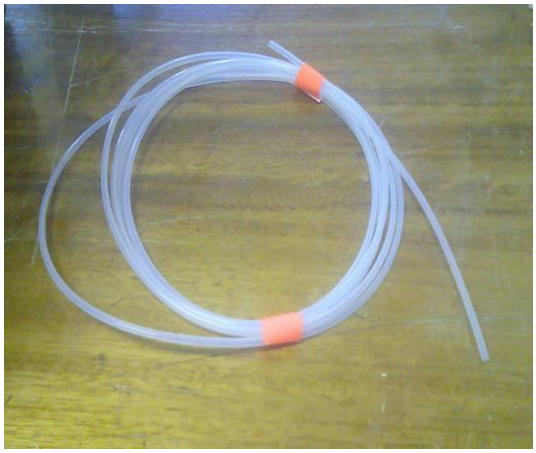

Figure 15: PTFE tube

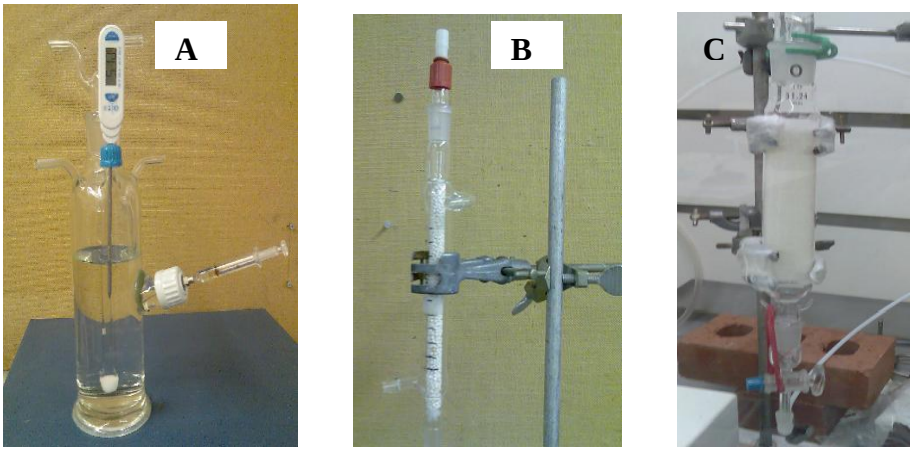

Figure 16: Reactors of ozone experiments

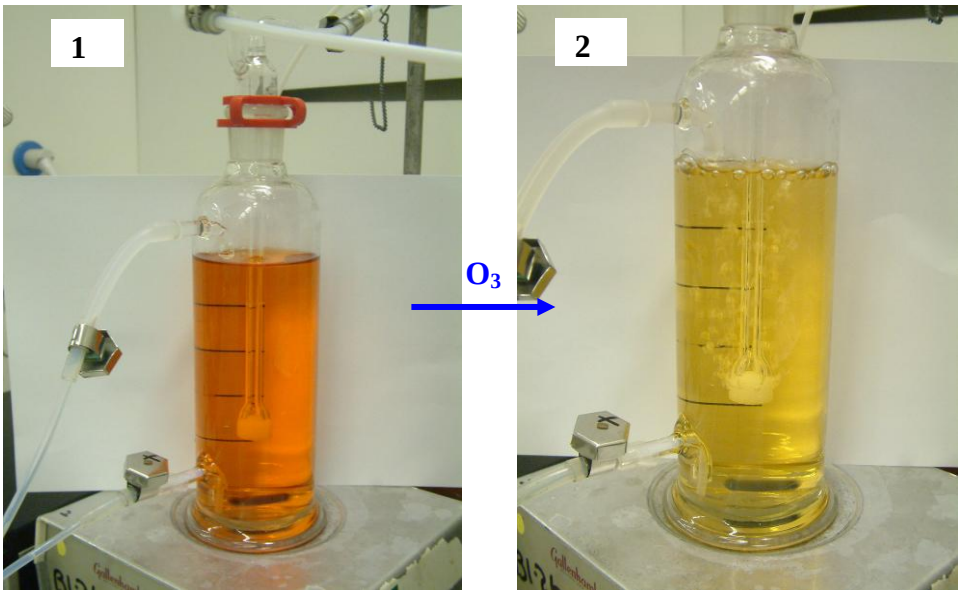

Figure 17: Dye (RO16) during ozonation processe

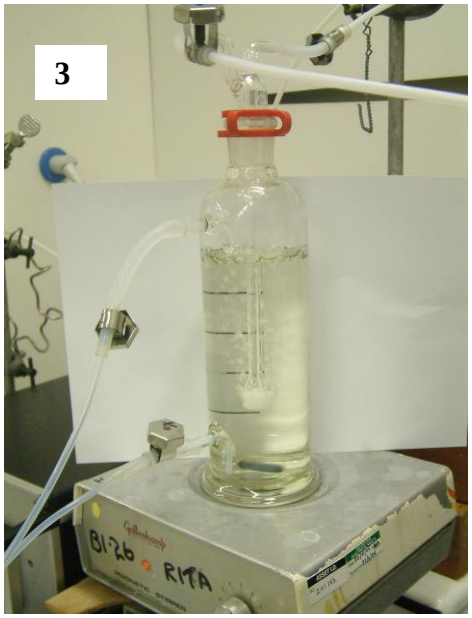

Figure 18: RO16 after ozonation process

Figure 19: Types of gas diffuser

A.3.1. Steps of Indigo Experiment

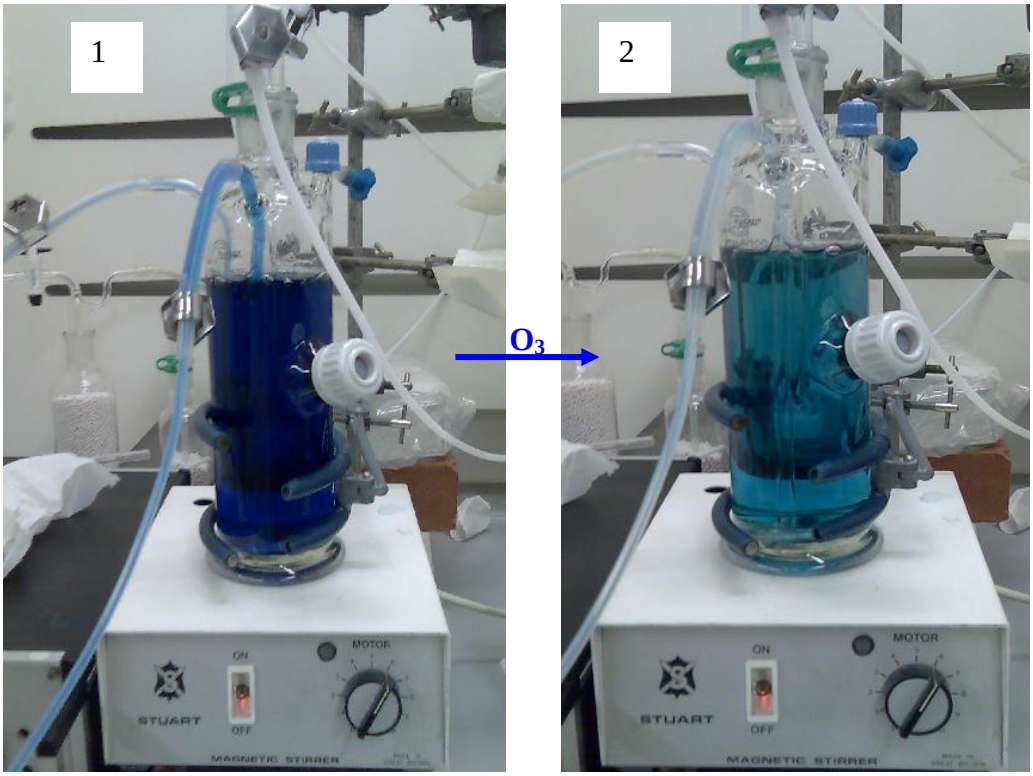

Figure 1: Indigo during ozonation process

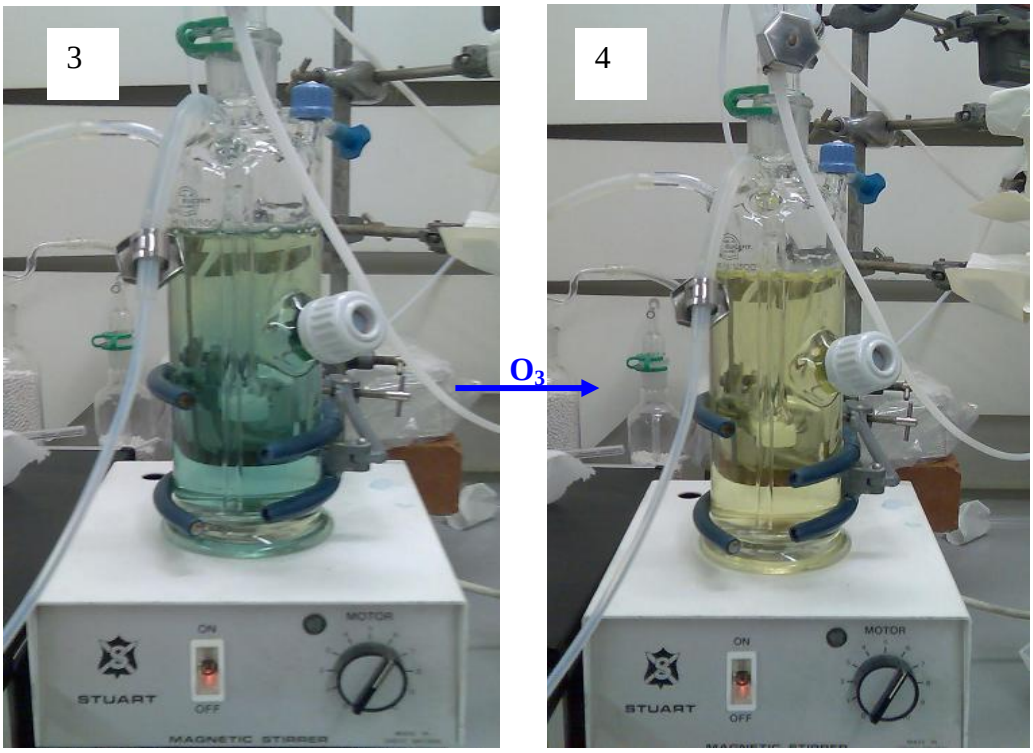

Figure 2: Indigo after ozonation process

A.3.2. Steps of Water Ozonation Experiment with Silica Gel

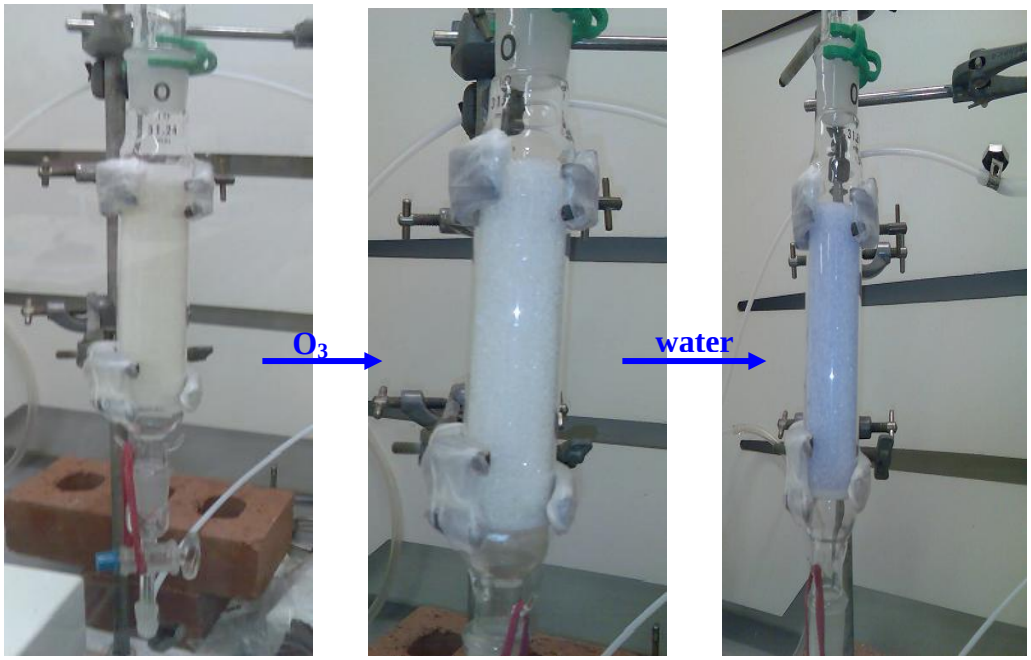

Figure 1: Water ozonation experiment using silica gel

Figure 2: Water ozonation experiment with silica gel

A.3.3. Steps of dye (RO16) Ozonation Experiment with Silica Gel

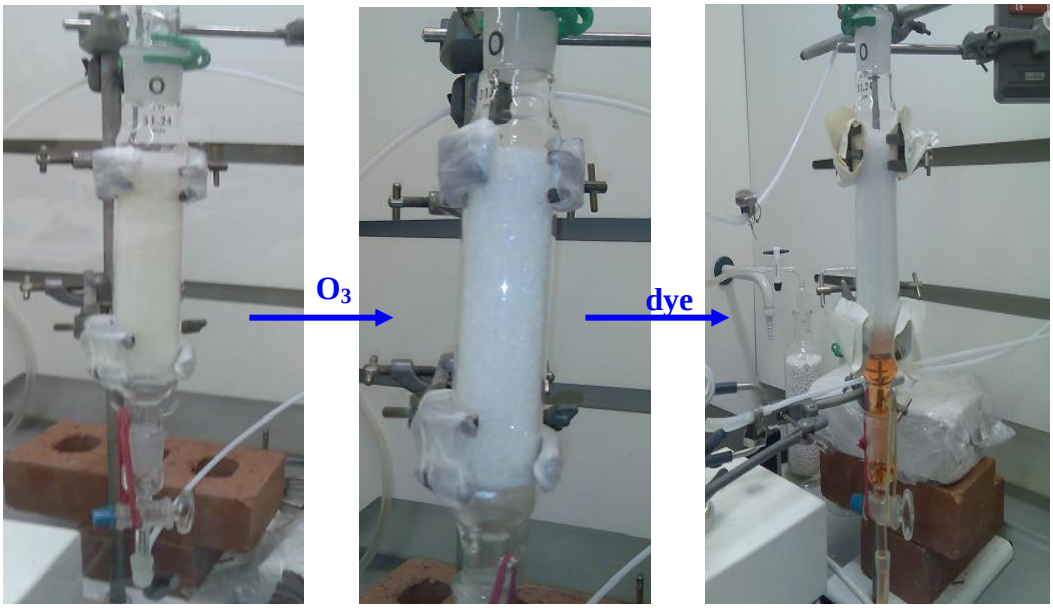

Figure 1: Dye ozonation experiment with silica gel

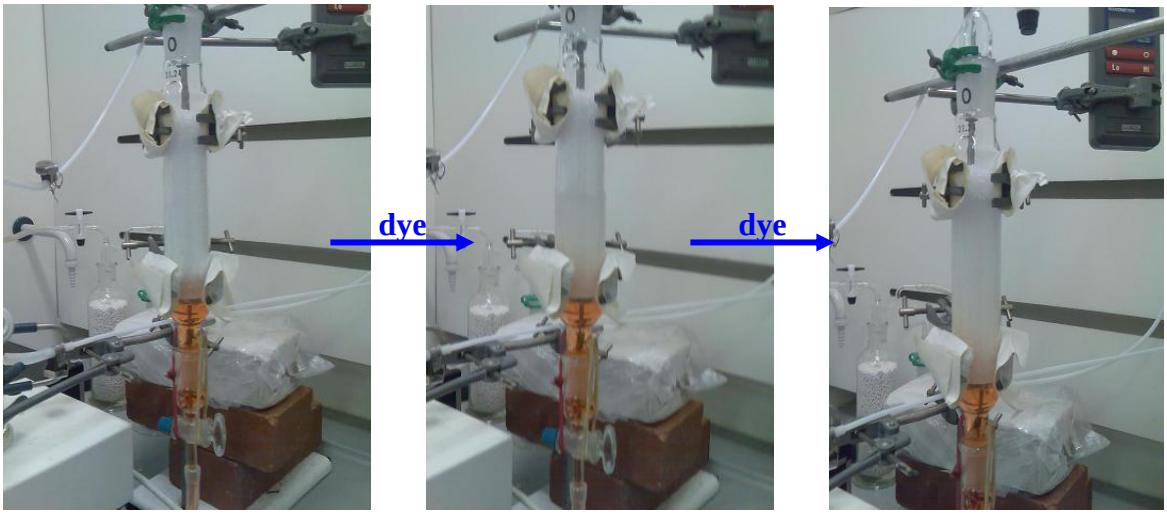

Figure 2: Dye ozonation experiment with silica gel

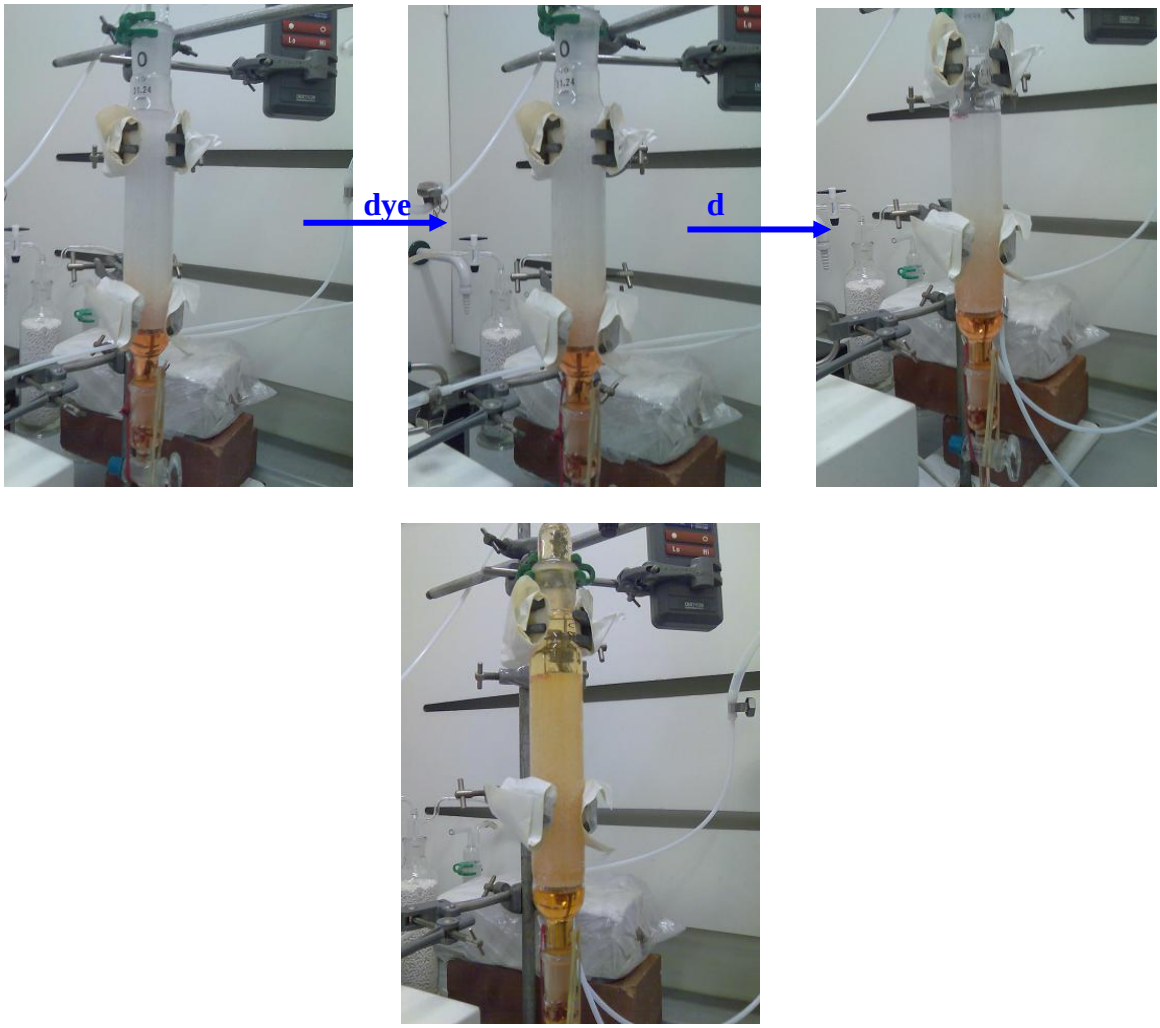

Figure 3: Dye ozonation experiment with silica gel